THE UNIVERSITY
of EDINBURGH

Investigating the recovery of rare earth elements by ionic liquids and bacteria

Jamie Patrick Hunter

Doctor of Philosophy

The University of Edinburgh

2020

Lay Summary

Our reliance on rare earth elements (REEs) in modern technology, clean energy production and medical imaging is continually increasing. In the earth's crust, REEs are present alongside one another and in low concentrations. This, combined with how chemically and physically similar REEs are to one another makes the separation and purification of REEs challenging. Therefore, to meet societies growing demand for REEs, it is crucial that new practices and reagents that can effectively separate and purify REEs are researched.

Industrially, REEs are typically separated using solvent extraction where REEs initially leached (or solubilised) from ores into an aqueous phase are extracted (or transported) into an aqueous-immiscible organic phase by organophosphorus reagents. These organophosphorus reagents are not very selective and poorly discriminate between the often numerous REEs in the aqueous phase.

Therefore, in this work, how an alternative reagent, an ammonium ionic liquid (IL), recovers REEs using solvent extraction is investigated using a large variety of analytical, spectroscopic and computational techniques. By understanding how ammonium ILs stabilise negatively charged, partially hydrated REE-nitrate anions in the organic phase, amido-ammonium ILs containing an amide group were developed for the selective extraction of lighter REEs. Why these amido-ammonium ILs more effectively distinguish between lighter and heavier REEs than standard ammonium ILs and organophosphorus reagents is investigated. The lighter REEs are understood to be stabilised in the organic phase by a hydrogen-bonding network and the structural functionality of the amido-ammonium ILs is found to be key to effective REE separation.

Elevated temperatures and highly acidic solutions are typical choices for the industrial leaching of REEs and can be energy intensive processes. This work indicates that the leaching of REEs from a REE bearing mineral can be achieved using a mildly acidic solution of iron and acid generating bacteria at ambient temperatures. This bacteria assisted leaching process was found to couple well with the selective extraction of the lighter REEs by an amido-ammonium IL, providing an effective, potentially more environmentally friendly REE purification process.

Abstract

The work presented in this thesis focuses on developing and understanding practices and reagents that can be more efficient at rare earth element (REE) recovery and separation than current industrial reagents and practices. With demand for REEs rapidly increasing due to their use in modern technologies and clean energy production, the sustainable supply of these elements has become vitally important for society.

The concepts and difficulties that underpin current REE recovery are introduced in Chapter 2 followed by an appraisal of how an ammonium ionic liquid (IL) transports these elements from an aqueous phase into an immiscible organic phase during solvent extraction. Prior to this work the extraction of REEs using ILs was known but an understanding of the chemical transport mechanisms was limited. A large variety of analytical, spectroscopic and computational techniques have been used: ICP-OES measurements confirmed that REE extraction from nitrate solutions is maximised under low acid, high salt conditions with preferential extraction of the lighter REEs occurring; Karl-Fischer water content measurements confirmed only modest water transport, allowing for (reverse)-micelle formation in the organic phase to be rejected. The combined experimental, analytical and computational data alludes to the transport of REEs through a microhydration mechanism pathway. Organic phase REEs comprising both inner-sphere bound water molecules and nitrate anions are encapsulated and stabilised in the organic phase by multiple lipophilic IL cations through a hydrogen-bonding network.

Chapter 3 builds upon the understanding of REE extraction by ILs gained in Chapter 2. The extraction of REEs using neutral reagents (malonoamides and diglycolamides) is introduced, highlighting their effectiveness but also their tendency to form undesirable precipitates (3rd phase formation). Incorporating chemical characteristics of these reagents such as the amide functional group into an IL results in a stronger extractant with improved selectively for lighter REEs and no solubility issues. The effective separation of lighter REEs (e.g. Ce or Nd) from heavier (e.g. Tb or Dy) REEs using an amide functionalised IL is presented with potential industrial applications discussed. Experimental, analytical and computational work suggests microhydrated REEs are extracted and a more extensive hydrogen-bonding network comprising amides, nitrate anions and water molecules enhances the stability of the formed organic phase assemblies.

Chapter 4 compares the leaching of REEs from eudialyte, a zirconate REE mineral by highly acidic solutions against mildly acidic solutions containing the bacterial strain *Acidithiobacillus thiooxidans*. The percentage of REEs leached using mild conditions is noticeably reduced over highly acidic conditions. Even so, and with no pH adjustment, the leached lighter REEs could be effectively separated from other elements within the leach solutions using an amide functionalised IL, potentially providing a more environmentally friendly REE purification process.

Chapter 5 explores the development of multiple variations of the amide functionalised ILs introduced in Chapter 3, highlighting their similarities and differences. The variants include the incorporation of more amide functionalities and increasing the lipophilicity of the ILs. While initial screening of these reagents did not indicate any improvements over the ILs introduced in Chapter 3, the experimental data collected for these reagents helps to validate the importance of the amido-ammonium function.

Acknowledgements

There are so many people I want to thank for making four years at the University of Edinburgh an absolute joy. While I was initially unsure about setting off on this journey I am delighted to realise I made the right decision.

Firstly thank-you to my principal supervisor Professor Jason Love for his continual enthusiasm, invaluable input and continual support throughout my time at the University of Edinburgh. Even when I was doubtful, you still approached the situation with a calm head and positivity. I want extend my thanks to my co-supervisors Professor Bryne Ngwenya and Professor Carole Morrison. It has been a pleasure working with you both. Your incredible knowledge of fields that were almost beyond me when I started has been invaluable in shaping the work and constructing this thesis. This was made all the more pleasurable by your collective good humour.

Thanks to Euan, for being so welcoming on the day I first arrived, little did I know Mary had only vacated my desk an hour beforehand! Thanks for being a guy of reason, incredible organisation and (bad) humour. Thanks for helping me direct my PhD, settle into Edinburgh and being a solid contact point for anything, although I still almost cry at how bad some of the puns were!

A massive thank-you to Rebecca. Thank-you for always being there to keep me sane, provide positivity and help me with all manner of computational issues, even while you were (frantically?) writing your thesis. Thank-you even more so for the last six months where you have been a voice of reason as I increasingly messaged and moaned about my own thesis. Finally thank-you for all the tasty treats over the years. I think I speak for the ~~office~~ chemistry building on this!

A big thank-you to Innis the absolute trivia mastermind who helped get me started on my computational voyage. I will always remember the humour we had over your university challenge journey and your Captain Innes Carter alter ego.

Many thanks for Andrew for being there in the latter stages of my PhD and being the rationale one within our often ridiculous, lunch break chats. It was a welcome change to lose the 'runner of the office' title!

Thank-you Luke for being there for the second half of my PhD journey and putting up with my increasing grumpiness over the last year. Sorry that I provided you with a range of weird and wonderful ideas although you always took them with much enthusiasm. Many thanks for being so witty and joining in with my and usually Jay's meaningless conversations and rants. Of course, I cannot forget our evening adventures on the PlayStation along with Jay and Craig despite none of us being even remotely decent at it!

While moving from Lab 29 to Lab 201 at the time was a 'mild inconvenience' on reflection it really was not. As of moving, I had the lovely company everyone within the Garden group. Thanks Dr Jenni Garden for hiring such fabulous people and being fabulous herself. Our outings and adventures were always a blast from Pottery painting, to Chemball to Bowling. A specific thanks to Jay who I could always rely on to come climbing with me and be there whenever I needed some positivity. A specific thanks to the Pokemon expert Eszter for showing me that the PhD is a marathon not a sprint. A specific thanks to Weronika for taking up the organisational baton, and going from elated to deflated as many times as I do in one day. A big thanks to Annie for being probably the most energetic person I have met and for being absolute banter. A collective thanks to Yali and Maisarah for always starting the day with huge smiles that have always brightened my day, especially during the writing period.

A big thanks to Liam, Lotte and the other half of the Love group family. Despite me hiding elsewhere in the building, you were always welcoming and willing to help me with any synthetic challenge or my unsuccessful *quest for a crystal! My strictly academic venture to Japan was a real highlight of my PhD and I am delighted I had you (Liam and Lotte) for company.*

Many thanks go to all the amazing people I've had the pleasure of meeting throughout this journey both within chemistry and beyond including Sandy, Rosie, Sofia, Tom, Angelos, Emily, Alexis, Brian, Dylan, Hersch, Phil, the Friday cake squad and lots more for providing me with many enjoyable moments, discussions, pub outings, adventures and running company.

An extra special thanks to Yasmeen and Hannah, my gen. one lab partners, who have been here throughout, sharing both the best parts and worst parts with me. Thanks for helping me get to the end. I really mean it. We have so many fantastic memories I cannot even begin to list them here.

Thank-you Amelia for making my most challenging period a complete joy and then continuing to be a great friend thereafter.

Thank-you my great project students Emily, Thomas, Sara and Kangwei for being so motivated and keen to try whatever ideas I suggested. I hope you all have successful careers. Equally thanks to all the project students who graced the lab and office with their presence but did not have the pleasure of working with me directly. It was a joy to have you around and thanks for being part of the office and lab team.

A big personal thanks to Professor Peter Tasker who with good humour provided support and life advice that I valued very much.

The support staff and technical staff in the School of Chemistry are incredible. Much of the work within the thesis would not have been possible without you. Thank-you so much for assisting unreservedly with any and every challenge I had.

Finally, to my family. Thank-you for being there throughout this journey, your endless unwavering support and total understanding. I would not have reached this point without you.

Publications and conference presentations

Publications

Published:

Chapter 2: Understanding REE recovery using trioctylmethyl ammonium nitrate

"Understanding the Recovery of Rare Earth Elements by Ammonium Salts"

J. P. Hunter, S. Dolezalova, B. T. Ngwenya, C. A. Morrison and J. B. Love, *Metals*, 2018, 8, 13.

In preparation:

Chapter 3: Development of amido-ammonium ILs for REE separation

"Improving light rare earth element extraction through supramolecular scaffold building with an amido-ammonium ionic liquid"

J. P. Hunter, T. Easton, K. Chen, B. T. Ngwenya, C. A. Morrison and J. B. Love

Chapter 5: A brief exploration of amido-ammonium IL modifications for REE extraction

"The effect of structural changes to amido-amine reagents on Rh(III) aquo-chlorido metalate extraction"

R. M. Nicolson, J. P. Hunter, J. B. Love, E. R. Schofield, and C. A. Morrison

Work contained within Chapters 2, 3 and 5 was assisted by Sara Dolezalova, Thomas Easton and Kangwei Chen (final year undergraduate students) while under the supervision of the author.

Presentations

Universities of Scotland inorganic conference 2019, Glasgow, UK – 29th-30th August 2019: Poster presentation (Functionalised ionic liquids for rare earth element separation)

New horizons in chemistry and materials science Workshop 2019, Nagoya, Japan – 1st-3rd July 2019: Poster presentation (Functionalised ionic liquids for rare earth element separation)

5th Annual Joseph Black chemistry conference 2019, Edinburgh, UK – 30th May 2019: Oral presentation (Ammonium amide ionic liquids for selective rare earth element recovery)

Universities of Scotland inorganic conference 2018, Edinburgh, UK – 27th-28th August 2019: Oral presentation (Understanding the recovery of rare earth elements by ammonium salts)

4th Annual IIES science and policy workshop 2018, Edinburgh, UK – 2st-3rd July 2018: Oral presentation (Understanding the recovery of rare earth elements by ammonium salts)

RSC Dalton 2018, Warwick, UK – 3rd-5th April 2018: Poster presentation (Understanding how ionic liquids recover rare-earth elements)

RSC Dalton young member's event 2017, Bath, UK – 7th-8th September 2017: Poster presentation (Understanding how ionic liquids sustainably recover rare earth elements)

Contents

Terms and abbreviations

Δ	change in
δ	chemical shift
°C	degree centigrade
°	degrees
< >	less than, greater than
%	percent
~	approximately
[L]	ligand concentration
[M]	metal concentration
µ	micro
Å	angstrom
aq	aqueous
$CDCl_3$	deuterated chloroform
C_6D_6	deuterated benzene
calc.	calculated
D	distribution coefficient – $[M]_{(org)}/[M]_{(aq}$ The metal content present in the organic phase divided by that present in the aqueous phase
extract, extraction	metal transfer from an aqueous phase to an organic phase
separation factors	the D value of one metal divided by that of another
% recovery	the final % of one metal acquired or obtained following a metallurgical separation process
extractant	A reagent or chemical specifically designed to facilitate the transport (or extraction) of ideally one metal from the aqueous phase to an immiscible organic phase.
d	doublet (NMR)
DCM	dichloromethane
DFT	density functional theory
e.g.	for example
Eq.	equation
ESI	electrospray ionisation (MS)
EXAFS	extended X-ray absorption fine structure
XANES	X-ray absorption near edge structure
FT	fourier transform
g	gram
h	hour
HCl	hydrochloric acid
ICP-OES	inductively coupled plasma optical emission spectroscopy
IR	infrared
K	kilo, kelvin

kJ mol^{-1}	kilojoules per mole
L	litre
m	milli, metre
M	molar
MD	molecular dynamics
Me	methyl
MHz	frequency (NMR)
mg	milligram
min	minute
mL	millilitre
mmol	millimole
mol	mole
MS	mass spectrometry
m/z	mass to charge ratio
NMR	nuclear magnetic resonance
org	organic
PGMs	platinum group metals
pH	$-\log_{10}[H^+]$
pls	pregnant leach solution
ppm	parts per million
T	temperature
^{t}Bu	tertiary butyl
tert	tertiary
THF	tetrahydrofuran
via	by way of
vs.	versus
Z	charge
REE	rare earth element
HNO_3	nitric acid
H_2SO_4	sulfuric acid
TBP	tributyl phosphate
QM	quantum mechanical, quantum mechanics
V	volts
PCM	polarisable continuum model
CSD	Cambridge structural database
s	seconds
+ve	positive
-ve	negative
No.	number
CN	coordination number

List of reagents discussed

Introduced in Chapter 2: Understanding REE recovery using trioctylmethyl ammonium nitrate

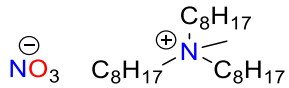

IL0

Introduced in Chapter 3: Development of amido-ammonium ILs for REE separation

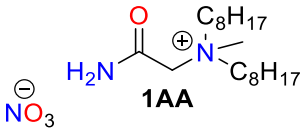

1AA

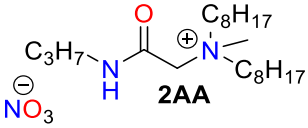

2AA

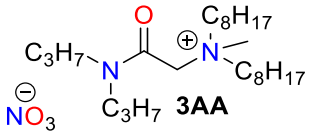

3AA

Introduced in Chapter 5: A brief exploration of amido-ammonium IL modifications for REE extraction

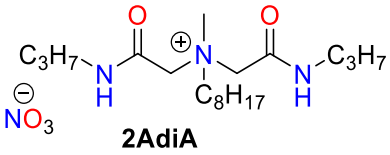

2AdiA

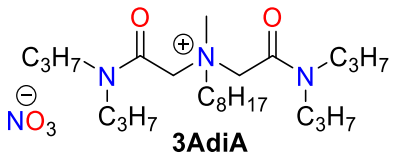

3AdiA

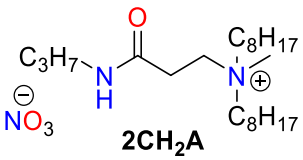

$2CH_2A$

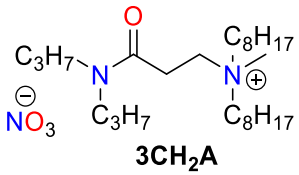

$3CH_2A$

Chapter 1

Introduction

1 Introduction

1.1 The rare earth elements

The rare earth elements (REEs), comprising the lanthanide series, Sc, Y and La, are now crucial to our society and the modern technological world. From electrical equipment to power generation and medical imaging, our dependence on these unique elements is continually increasing.[1, 2]

The elements in the lanthanide series, in addition to *s*, *p* and *d* orbitals, have a total of seven 4*f*-orbitals and these are fz^3; fxz^2; fyz^2; $fxyz$; $fx(x^2-3y^2)$; $fz(x^2-y^2)$; and $fy(3x^2-y^2)$ (Figure 1.1.1).

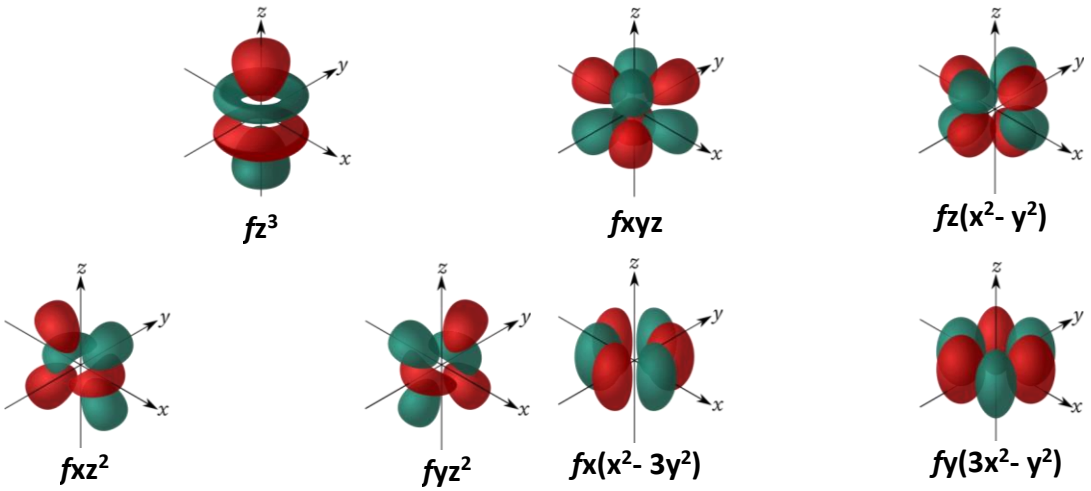

Figure 1.1.1 – The seven *f*-orbitals: fz^3; fxz^2; fyz^2; $fxyz$; $fx(x^2-3y^2)$; $fz(x^2-y^2)$; and $fy(3x^2-y^2)$.

Unlike the *d*-orbitals of transition metals, the *f*-orbitals are typically non-bonding and the splitting of the degenerate *f*-orbitals in crystal fields is small with Δ_{oct} often being only around 1 KJ mol^{-1}. This results in coordination numbers and geometries being dominated by steric effects rather than crystal field stabilisation effects.

The *f*-orbitals of REEs are ineffective at shielding the nuclear charge and this results in a gradual decrease of the ionic radii across the f-block group from La^{3+} (103 pm) to Lu^{3+} (86 pm) and, in doing so, allows for a small variation in the charge density. From left-to-right (La to Lu) the relative Lewis acidity of the element increases.[3] Despite this, the lanthanide series elements (plus Sc, Y and La) all have similar chemical and physical properties. The melting points, boiling points, reactivity, coordination numbers and geometries of REEs are broadly

similar. Additionally, many of the REEs have unique and almost unrivalled magnetic and optical properties resulting in REEs being ideal candidates for numerous roles.[4, 5]

The magnetic coercivity, or the ability to withstand an external magnetic field, of REEs such as Nd is very high resulting in them being ideal candidates for the high strength magnets that are found in MRI scanners, hard disk drives and generators.[6] A Nd based REE magnet is not exclusively Nd, instead being an alloy with Fe (70%) as the main component. About 1% B is present and small quantities of heavier REEs (e.g. Dy) are added to raise the Curie temperature threshold (the temperature at which NdFeB ceases to be permanent magnet).[7, 8] REEs such as Nd substantially enhance magnetic coercivity through "the interaction of their anisotropic (directionality dependant) *f*-electron clouds with the crystal electric field of surrounding charges".[9] Combining this with spin-orbit coupling results in strong REE magnetic moments in a singular direction and a significant amount of energy is required to disrupt this. NdFeB magnets have largely replaced older SmCo magnets due to their competitive price and superior performance but SmCo magnets retain niche uses in high temperature situations as of their greater Curie temperature threshold.

Within medical imaging, specifically MRI, contrasting agents such as the 8-coordinate Gd[DOTA]Na complex (Figure 1.1.2) help to reduce the T_1 relaxation times of protons within water molecules and provide an image of greater resolution. Gd is the only known element (excluding the extremely radioactive Cm) that, as a stable 3+ ion, has 7-unpaired *f*-electrons. This large paramagnetic character reduces the T_1 relaxation time of water molecules during the MRI scan by providing a large fluctuating magnetic field.[10]

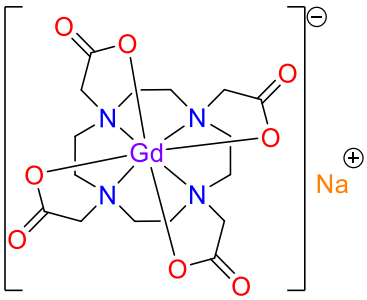

Figure 1.1.2 – Gd[DOTA]Na. A MRI contrast agent.

The optical properties of the REEs and their widespread use in lighting and data transmission is due to their luminescent properties.[11] REE ions often display both fluorescence and phosphorescence, making them particularly suited to the role. Upon absorbing

electromagnetic radiation, an electron is excited from the ground state of the REE into an excited state. These are *f-f* electronic transitions and, due to the 4*f* electrons being generally unaffected by environment, result in sharp bands in the electromagnetic spectrum that are usually independent of complex formation.[3] 4*f*-5*d* electronic transitions are possible but these are much broader and are affected by complexation. While ligands rarely affect *f-f* electronic transitions directly, ligands can absorb electromagnetic radiation and transfer this electromagnetic radiation to the REE ion, and in doing so, can cause emitting excited levels to be populated.[12]

The use of REEs in magnets and phosphors by value totals over two thirds of the market share of REEs with the market demand for REE magnets expected to continue to grow until at least 2035, highlighting the economic importance of these products.[7] The REEs that contribute substantially to these two markets will be the focus of this thesis with other REEs occasionally referenced.

Despite the term 'rare earth' the REEs are not 'rare'. Their total global abundance is estimated at 150 Mt, with most REEs being comparable in abundance to 1st row transition metals such as Co and Ni (Figure 1.1.3).[13, 14]

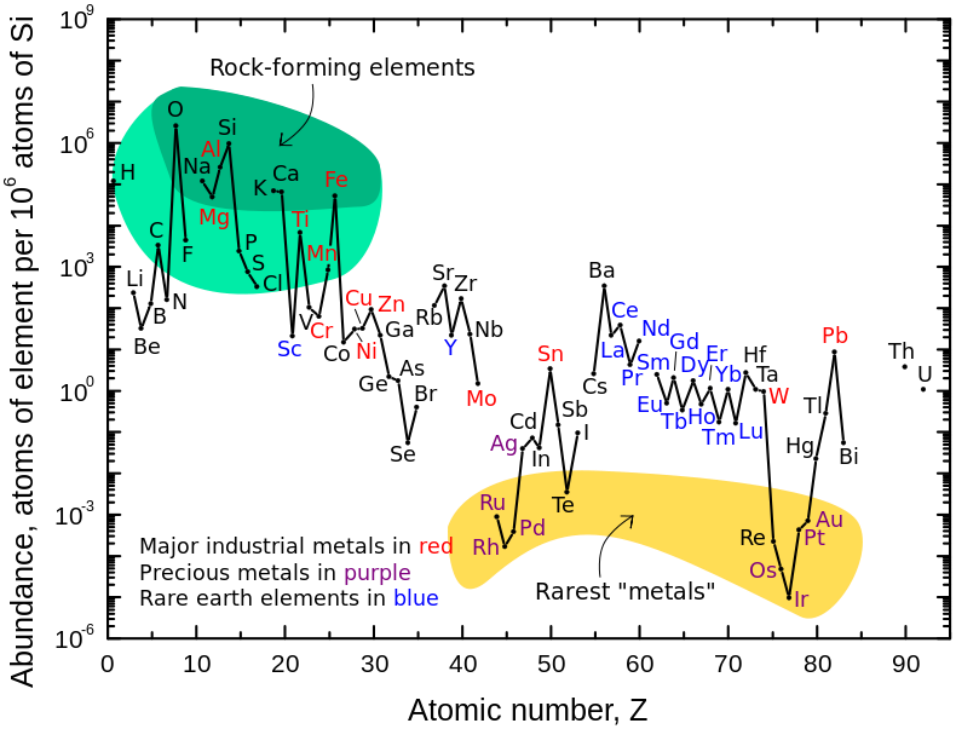

Figure 1.1.3 – The abundance of elements relative to 10^6 atoms of Si. REEs are in blue.[13, 14]

The term ‘rare earth’ has remained due to the low economic viability of many REE ore deposits thus restricting investment into excavation and mining operations. Few locations globally have REE deposits of significant concentrations, with many deposits instead consisting of very low concentrations of ores.[14] Even the most REE-rich ore deposits on average only have an ore grade of 1-3%, with this predominantly comprising lighter REEs (La, Ce, Pr and Nd). This contrasts to traditional base metal mines that in the past had substantial ore grades up to 10% for Cu and up to even 70% for Fe.[15]

Since the early 2000’s China has been the near sole producer of REEs (Figure 1.1.4).[14, 16] In 2019, China produced >130 Kt of REEs and their closest competitor the USA, who recently restarted REE mining operations due to increased economic viability, produced around 26 Kt.[17]

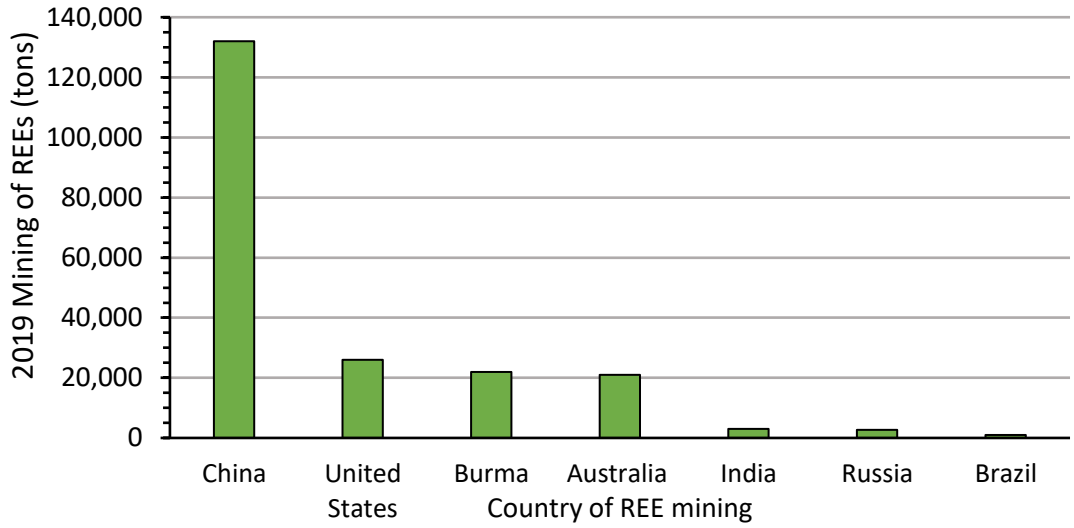

Figure 1.1.4 – The total mining (tons) of REE by country in 2019.[17]

The near total monopoly of supply by one country, in this case China, has resulted in REE dependent industries being exposed to substantial market volatility.[18] In response to the potential risk to supply, and the inherent difficulties in purifying REEs and separating REEs from one another, both the U.S department of energy and the European commission have highlighted their strategic importance.[14] In the medium-term it is feared that the demand for REEs such as Nd, Dy and Tb will outstrip supply (Figure 1.1.5).

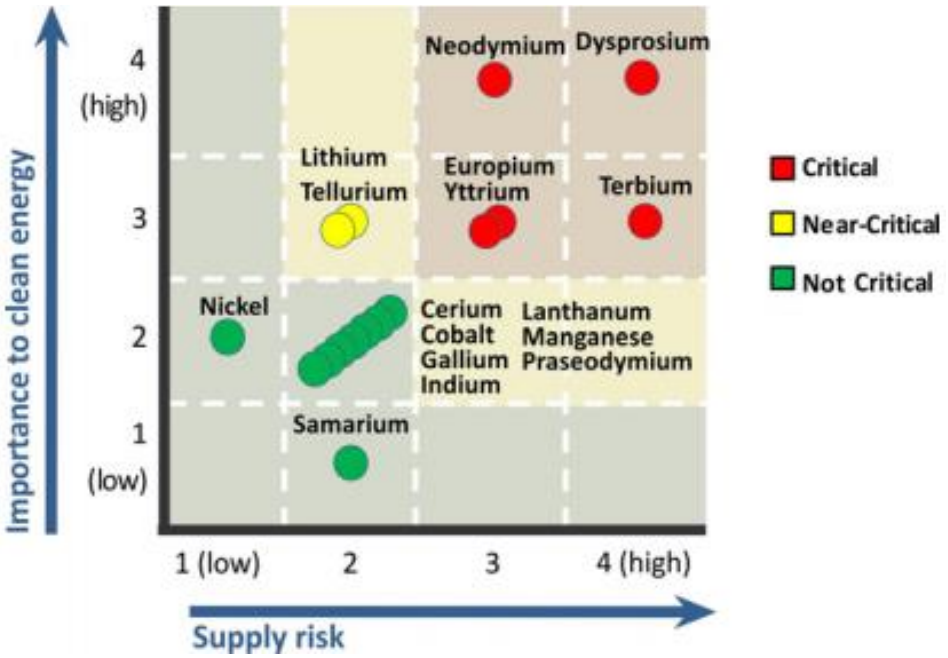

Figure 1.1.5 – The medium-term supply risk for elements in relation to their importance to clean energy.[14]

The very similar chemical and physical properties of the REEs results in many REEs being contained within the same ores and minerals. This makes REEs purification and separation particularly difficult. The techniques currently applied industrially for REE purification and separation will be discussed throughout this thesis.

1.2 Hydrometallurgy overview

Hydrometallurgy is a branch of extractive metallurgy used industrially to recover, purify and separate metals through aqueous processes. This is an alternative to pyrometallurgy that uses elevated temperatures and large amounts of energy while simultaneously generating significant quantities of air pollutants (e.g. SO_2). Furthermore, pyrometallurgical processes require comparatively high initial concentrations of the target metal. Hydrometallurgy is more suited to lower initial metal concentrations and, by recycling and reusing reagents, can achieve lower overall emissions and greater materials balance.[19]

A typical hydrometallurgical (Figure 1.2.1) operation to obtain pure metals from primary sources (e.g. ores) or secondary sources (e.g. scrap metal) consists of several stages.[19]

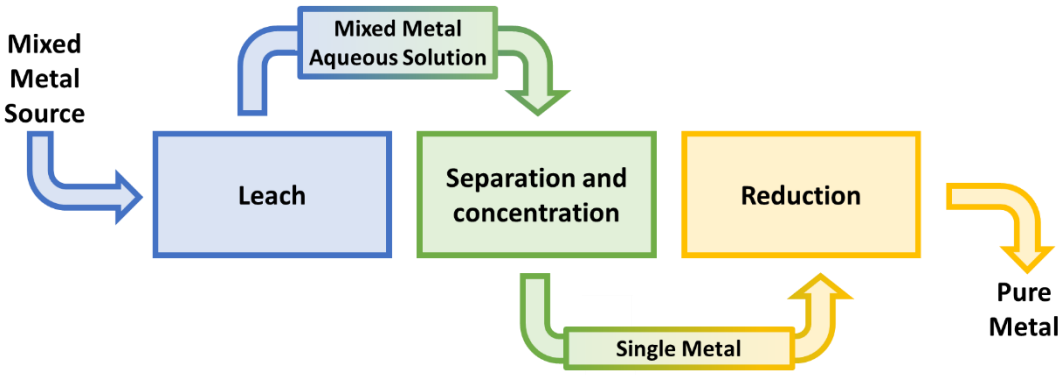

Figure 1.2.1 – A typical hydrometallurgical flowsheet for the purification of a metal from a primary or secondary source.[19]

In most hydrometallurgical processes, metals are initially solubilised (or leached) into an aqueous solution using a strong acid or strong base in the 'leaching stage' (Figure 1.2.1). This results in an aqueous solution containing the leached metals (the pregnant leach solution, or PLS).

As both primary and secondary sources can contain a mixture of different metals at low concentrations, metals must be the separated from one another in order to obtain pure metals. The separation step of a hydrometallurgical flowsheet (Figure 1.2.1) may involve, in a non-exhaustive list, crystallisation, distillation or solvent extraction, either exclusively or sequentially. Separation using solvent extraction will be the focus of this thesis and will be introduced further in section 1.4.

Following a separation step, the reduction of the targeted metal to its zero-oxidation state can be required. A typical industrial choice for this is electrowinning and involves the electrodeposition of metals onto a cathode following the application of a current through a solution containing the target metal. Electrowinning is particularly effective for the separation of Cu from Ni as Cu is electrodeposited while Ni remains in solution. This is as the two electron reduction of Cu^{2+} has a positive reduction potential (+0.34 E°/V) but the two electron reduction of Ni^{2+} has a negative reduction potential (–0.26 E°/V). Once the target metal is as its zero oxidation state it can then be used in further industrial applications.

A typically industrial REE purification and separation flowsheet that incorporates the stages provided in Figure 1.2.1 actually consists of many more stages, with the complete industrial process being particularly complex. Of the stages given in the flowsheet below (Figure 1.2.2)

only those associated with the leaching (section 1.3) and solvent extraction (section 1.4) of REEs will be regularly discussed throughout the thesis. The remaining stages will be occasionally mentioned.[1]

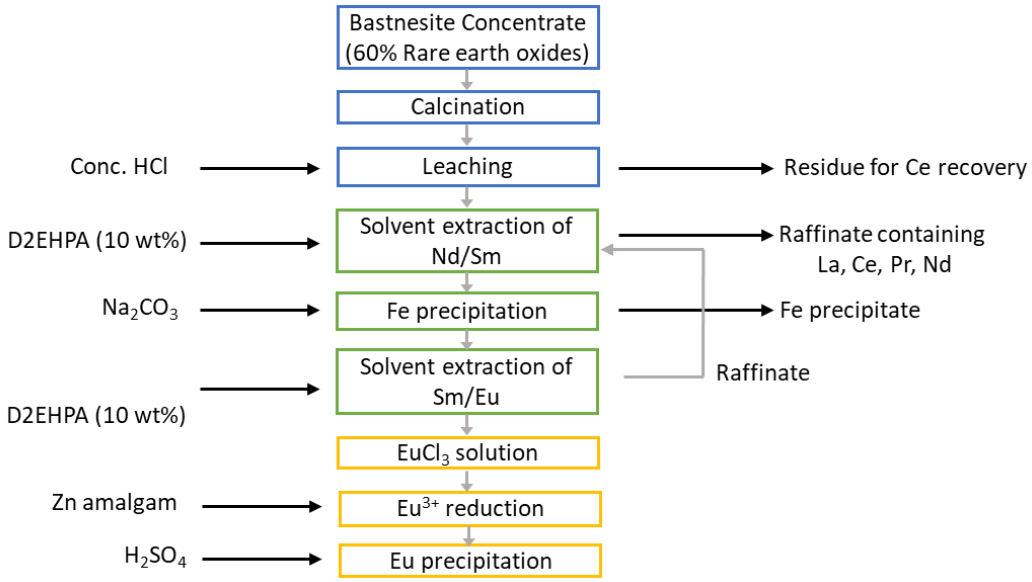

Figure 1.2.2 – A typically industrial REE purification and separation flowsheet. In this flowsheet, Eu is the target REE, starting from bastnaesite a REE fluoride carbonate mineral.[1]

1.3 Leaching and biological leaching

1.3.1 Leaching overview

The leaching of metals requires a source of acid or alkali (section 1.2).[19] The choice of acid or alkali is largely dependent on the target metal and how the metal will be processed in further downstream operations. Leaching with chloride media is generally the industrial choice for precious metals such as Pt and Rh, sulfate media for base metals such as Cu and Ni while alkaline or sulfate media are typical for the REEs.[1, 16, 20-24]

1.3.2 Industrial base metal leaching

Heap leaching (Figure 1.3.2.1) is a common industrial leaching option, especially for base metals, due to a relatively low initial capital cost and minimal subsequent maintenance.[25] In heap leaching, a crushed metal source is first placed on an impermeable surface with a slight gradient and a leach solution is sprayed or drip irrigated.[26] The leach solution then percolates

through the heap, dissolving the target metal and other metals, resulting in a mixed metal solution that is collected by gravity and further processed.

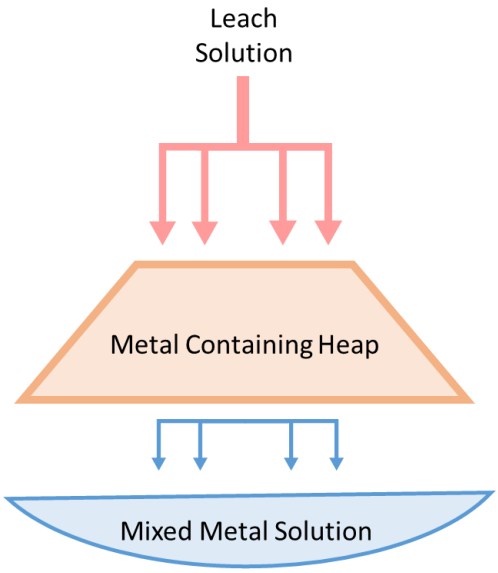

Figure 1.3.2.1 – A highly simplified schematic for the heap leaching of metals from primary or secondary sources.

1.3.3 REE industrial leaching

Industrially heap leaching of REEs is uncommon. Instead, REE sources, such as monazite or xenotime (two REE-phosphate minerals), are often leached using highly concentrated H_2SO_4 (95% w/w) at elevated temperatures (250 °C) (Equations 1.3.3.1 and 1.3.3.2).[27] The process is very quick, with complete leaching being achieved within a few hours. The resulting REE sulfate concentrate is then diluted in water, leaving by-products such as Si and Zr compounds mainly undissolved.

Eq. 1.3.3.1 – $2\ REE(PO_4)_{(s)} + 3\ H_2SO_{4(aq)} \rightarrow REE_2(SO_4)_{3(s)} + 6\ H^+_{(aq)} + 2\ PO_4^{3-}{}_{(aq)}$

Eq. 1.3.3.2 – $REE_2(SO_4)_{3(s)} + n\ H_2O \rightarrow 2\ REE.xH_2O^{3+}{}_{(aq)} + 3\ SO_4^{2-}{}_{(aq)} + (n\text{-}x)\ H_2O$

An alternative industrial operation involves heating REE sources in concentrated NaOH to 150 °C. This results in $REE(OH)_3$ solids that are subsequently dissolved into very dilute H_2SO_4 (Equations 1.3.3.3 and 1.3.3.4).[27]

Eq. 1.3.3.3 – $REE(PO_4)_{(s)} + 3\ NaOH_{(aq)} \rightarrow REE(OH)_{3(s)} + 3\ Na^+_{(aq)} + PO_4^{3-}{}_{(aq)}$

Eq. 1.3.3.4 – $2\ REE(OH)_{3(s)} + 3\ H_2SO_{4\ (aq)} + n\ H_2O \rightarrow 2\ REE.xH_2O^{3+}{}_{(aq)} + 3\ SO_4^{2-}{}_{(aq)} + (n-x+3)\ H_2O$

1.3.4 REE leaching from secondary sources

Currently, there are no substantial industrial scale leaching processes of REEs from secondary resources such as NdFeB magnets, waste fluorescent lighting or Ni-metal hydride batteries. Less than 1% of REEs are currently recycled but the leaching of REEs from secondary resources has been well studied.[2, 28]

The near total dissolution of powdered NdFeB magnets using concentrated H_2SO_4 has been achieved in a process similar to that used for primary REE sources, with >99% of the respective REEs (Nd, Pr, Dy and Gd) leached under optimised conditions.[29] In a proof-of-concept study, NdFeB magnets have been leached using HCl/NH_4Cl (12 and 3.5 M).[30] The non-REE components of NdFeB magnets were removed from the leach solution by contact with an organic phase leaving the REEs in the leach solution. REEs were then precipitated using oxalic acid, regenerating HCl to allow for future magnet leaching. Separation will be discussed in section 1.4.

Red, blue and green phosphor powders within fluorescent lighting contain significant quantities of REEs but highly toxic Hg can be present too. While HCl (0.5 – 4.0 M) readily leached Y, Eu and Gd (up to 99%), up to 90% Hg was co-leached. Replacing HCl with HNO_3 reduced the leaching of Hg to below 25% while maintaining REE leaching (Figure 1.3.4.1).[31] At low acid concentrations, Gd was poorly leached compared with the other REEs (Y, Eu) suggesting a degree of selectivity in the leaching process. The ease of leaching Y and Eu when compared to other REEs is reported in other studies.[32] Y and Eu were readily leached (>95%) from red phosphor powders using HCl (3 M) while almost all Ce and Tb (>90%) remained as an insoluble residue.

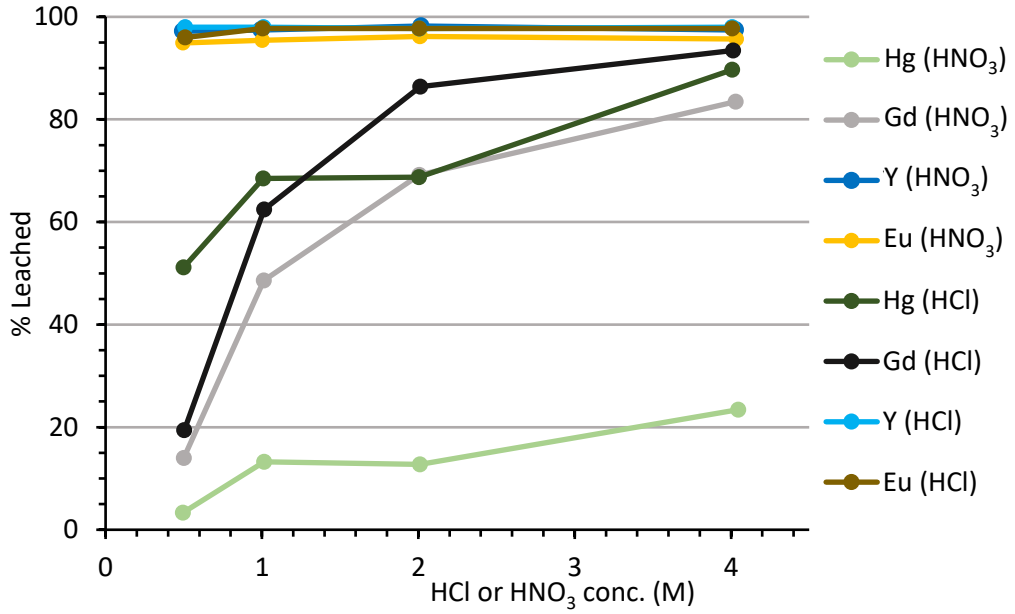

Figure 1.3.4.1 – The leaching of REEs and Hg from fluorescent lamp waste using HCl or HNO_3 (0.5 – 4.0 M).[31]

1.3.5 Bioleaching

The concentrated acid solutions used in industrial leaching processes can result in significant environmental impacts including contamination of the surrounding landscape. Bioleaching (or bacteria assisted leaching) can help to lessen the environmental impacts as the acid concentrations are generally much lower. Bioleaching has been used to leach metals including Au with the bacterium *Chromobacterium violaceum* and Re with the bacterium *Bacillus megaterium*. These are cyanogenic bacteria and produce cyanide that, while very toxic, is an effective leaching reagent for Au and Re. [33, 34]

The greatest commercialisation of bioleaching technology is in the Chilean Cu mining industry, an industry that supplies over a third of the world's Cu.[35] Bioleaching processes are essentially heap leaching processes but due to the lower acid concentrations the timescales are usually an order of magnitude longer.[36] In the Chilean mining landscape, bacteria such as *Acidithiobacillus ferrooxidans* and *Acidithiobacillus thiooxidans* occur naturally. These aerobic bacteria species are autotrophic, producing their own energy using the oxidation of iron and sulfur and thrive under acidic conditions (approx. pH 1-2).[37]

Due to the non-aseptic nature of heap bioleaching in Chilean Cu mining operations there is a diverse composition of active bacteria.[35] Additionally, ore matrices can be complex resulting

in multiple equations and chemical reactions being associated with one heap leaching operation (see equations 1.3.5.1 to 1.3.5.4).[38]

Eq. 1.3.5.1 – $CuFeS_2 + 4\ Fe^{3+} \rightarrow Cu^{2+} + 2\ S + 5\ Fe^{2+}$

Eq. 1.3.5.2 – $2\ Fe^{2+} + 2\ H^+ + ½\ O_2 \rightarrow 2\ Fe^{3+} + H_2O$ *(bacteria-catalysed step)*

Eq. 1.3.5.3 – $2\ S + 3\ O_2 + 2\ H_2O \rightarrow 2\ SO_4^{2-} + 4\ H^+$

Eq. 1.3.5.4 – $CuFeS_2 + 2\ Fe^{3+} + 3.5\ O_2 + H_2O \rightarrow Cu^{2+} + 3\ Fe^{2+} + 2\ H^+ + 2\ SO_4^{2-}$

Acidithiobacillus ferrooxidans bacteria catalyse the leaching of Cu into solution starting from $CuFeS_2$ (chalcopyrite). The specific role of the bacteria is to catalyse the oxidation of Fe^{2+} to Fe^{3+} (eq. 1.3.5.2) and this allows for greater availability of Fe^{3+} to further solubilise $CuFeS_2$.[38] The overall equation (Eq. 1.3.5.4) indicates that the process produces acid and this increases the rate of Cu leaching.

$CuFeS_2$ is the most common deposit of Cu but $CuFeS_2$ is not commonly bioleached due to slow leaching rates that are a result of water insoluble $KFe_3(OH)_6(SO_4)_2$ (jarosite) formation on the $CuFeS_2$ surface when the Fe^{3+} concentration is high.[36, 38] Substantially more operations currently bioleach Cu_2S (chalcocite) that has an average leach reaction rate that is 5x faster, bioleaching 80% of the available Cu within six months under optimised conditions.

1.4 Solvent extraction – separation and concentration

Regardless of how metals are leached into an aqueous phase, a subsequent separation step is usually required in order to remove the target metal from unwanted impurities. This separation can be achieved using solvent extraction (Figure 1.4.1).

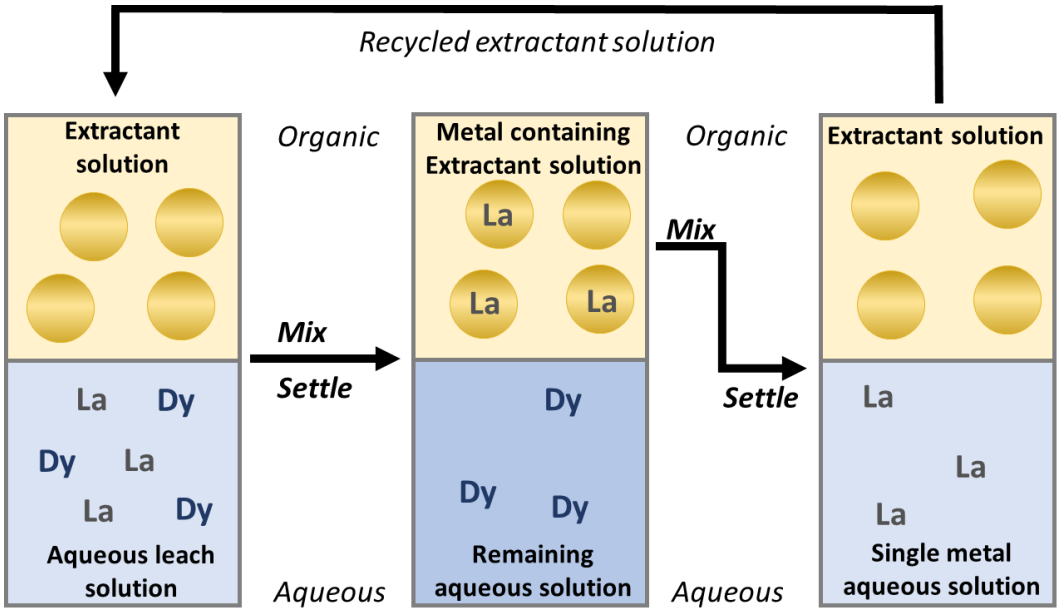

Figure 1.4.1 – A representation of the steps involved in the separation of La using solvent extraction from an aqueous leach solution containing La and Dy.

In a solvent extraction process the aqueous leach solution, often containing many metals and impurities, is contacted with an aqueous-immiscible solvent that contains an extractant. Industrially the immiscible phase is a high boiling, hydrophobic organic solvent such as kerosene.[7, 39] An extractant is a ligand or receptor that ideally targets one metal species, extracting (or transporting) the target metal from the aqueous phase into the organic. When % extraction is mentioned this is the amount, as a %, of the total target metal that has been extracted by the extractant from the aqueous phase into the organic phase.

During extraction the two phases, are thoroughly mixed allowing the extractant to form an organic phase complex or assembly with the target metal, leaving unwanted metals and impurities in the aqueous phase. The phases are physically separated and the target metal-containing organic phase is then treated (usually with a fresh aqueous phase) to return the metal back to the aqueous phase allowing further isolation of the metal e.g. by reduction. This step is named back-extraction or stripping and regenerates the extractant so that the metal recovery and separation process can be repeated and helps provide good materials balance.

For the solvent extraction process to be efficient the extractant must:

- Have aqueous insolubility
    - By introducing lipophilicity into the extractant by addition of branching alkyl 'grease' chains this can be achieved. Too many polar groups in the extractant may result in significant aqueous solubility.
- Target only one metal
    - Through exploiting variations in metal oxidation states, geometries, sizes and overall charges an extractant can be tailored to selectively extract one metal only.
- Be aqueous stable
    - The extractant should be hydrolytically stable during use otherwise degradation can occur resulting in a poor materials balance. Functional groups susceptible to acid or base hydrolysis should be avoided.
- Achieve quick, atom economical loading
    - Following contact with the aqueous phase the organic phase should quickly separate from the aqueous phase. Furthermore, a low concentration of extractant should ideally extract a high concentration of metal.

1.5 Modes of metal extraction

1.5.1 Overview

Industrially, there are several modes of metal extraction and >40 commercial extractants.[40] A metal can be transported from the aqueous phase to the organic phase through cation exchange, metal-salt solvation or anion (metalate) extraction.[19] The mode of extraction depends on the class of extractant used. The extractant chosen is dependent on the aqueous phase composition and the target metal. Differing modes of metal extraction will be introduced in this section and discussed more thoroughly in following chapters.

1.5.2 Metal cation extraction

To extract metals through a cationic exchange pathway, the extractant of choice should be sufficiently acidic to allow for deprotonation into a mildly acidic aqueous phase.[19] Deprotonated extractants then coordinate inner-sphere to the target metal cation resulting in a charge-neutral assembly at the organic-aqueous interface. This complex is then

transported into the organic phase with the proton now residing in the aqueous phase. For M^{2+}, two singly deprotonated extractants (L^-) are required (Eq. 1.5.2.1).

Eq. 1.5.2.1 – $$M^{2+}_{(aq)} + 2\ LH_{(org)} \rightleftharpoons ML_{2(org)} + 2\ H^{+}_{(aq)}$$

This equilibrium is pH dependant. An increasing quantity of metal is transported into the organic phase as the pH is raised. At higher pH, a lower concentration of available H^+ is present resulting in the equilibrium (Eq. 1.5.2.1) shifting to the right promoting the extraction of M^{2+} and loss of H^+.[19] Removing the metal (M^{2+}) from the organic phase requires a fresh aqueous phase of a lower pH (higher H^+ concentration).

Some examples of cation exchange extractants include hydroxy-oximes, carboxylic acids and organophosphorus reagents (section 2.1) (Figure 1.5.2.1).[1, 19, 41]

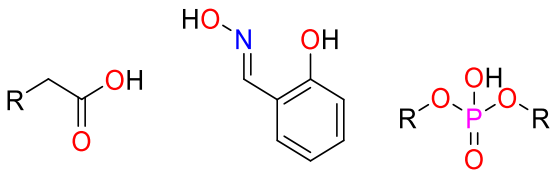

Figure 1.5.2.1 – The general structures of some cationic extractants: (left – right) carboxylic acid; hydroxy-oxime; organophosphorus reagent (R = alkyl chain).

Cation exchange extractants are usually chelating ligands and coordinate through two or more atoms (usually N, O or S). This entropically drives the reaction equilibrium to the right as monodentate binding ligands such a Cl^- or H_2O in the aqueous phase are substituted by bidentate or multidentate ligands. In addition to inner-sphere chelation, outer-sphere interactions can further stabilise the metal-ligand complexes in the organic phase, and in some instances, enhance selectivity.[20]

A prime example of outer-sphere interactions enhancing extraction and selectively is in the extraction of Cu^{2+} with a phenolic oxime (Figure 1.5.2.2), a class of reagent currently used in the production of >25% of the world's Cu supply.[19] Outer-sphere hydrogen-bonding interactions between oximic hydrogens and phenolic oxygens reinforce the square planar geometry with a defined, pseudo-macrocyclic cavity size.[20] As of this, metal cations that adopt square planar geometries (e.g. Cu^{2+}) are selectively transported over those that adopt tetragonal geometries such as Zn^{2+}.

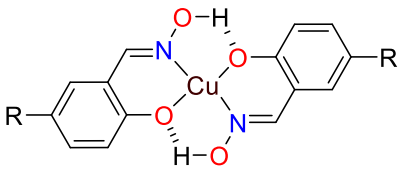

Figure 1.5.2.1 – The pseudo-macrocyclic complex formed between Cu^{2+} and two phenolic oxime ligands (R = alkyl chain).

1.5.3 Anion extraction

Under high anion concentrations some metals, such as platinum group metals (PGMs) (e.g. Pt, Ir and Rh), can form halometalate anions MX_n^{y-} (where X is an anion, n > 1 and y > 0) in the aqueous phase.[24, 42, 43] The 'X' anion is often Cl^-, as a result of HCl leach streams.[24] In the case of PGMs, comparatively slow ligand exchange rates result in kinetically inert metalates. This means PGM extraction by a cation exchange mechanism where inner-sphere ligands are substituted is not practical.[44, 45] Instead, PGM metalates, are transported into the organic phase by a basic extractant (typically an amine or amide) that is protonated by the acidic aqueous phase.[19, 20] For a six coordinate, octahedral 4+ metal (M), the formation of the metalate (MX_6^{2-}) and subsequent extraction by a basic extractant (L) can be expressed by the simplified equations:

Eq. 1.5.3.1 – $$M^{4+}_{(aq)} + 6\ X^-_{(aq)} \rightleftharpoons MX_6^{2-}{}_{(aq)}$$

Eq. 1.5.3.2 – $$MX_6^{2-}{}_{(aq)} + 2\ H^+_{(aq)} + 2\ L_{(org)} \rightleftharpoons (LH)_2MX_{6(org)}$$

The negatively charged metalate must be balanced by protonated extractants to form a neutral assembly that is stable in the organic phase. The protonated extractants associate with a metalate through outer-sphere, supramolecular interactions such as electrostatics and hydrogen-bonding.

Recent advances in anion recognition and the understanding of selective anion receptors within supramolecular chemistry have resulted in the design of ligand systems that discriminate effectively between different anionic species.[46-48] A high level of discrimination is essential given that large excesses of non-metalate anions are required in the aqueous solution (e.g. Cl^-) in order to form the target metalate. An example of this is in the recovery of Pt when starting from high Cl^- solutions. While simple amines are ineffective at discriminating between the $PtCl_6^{2-}$ metalate and Cl^-, an amidoamine ligand provides effective

transportation of Pt.[23] The striking selectivity for Pt arises from the feature of the amidoamine ligands (Figure 1.5.3.1) to protonate at the amine and form intramolecular "proton chelates".[49]

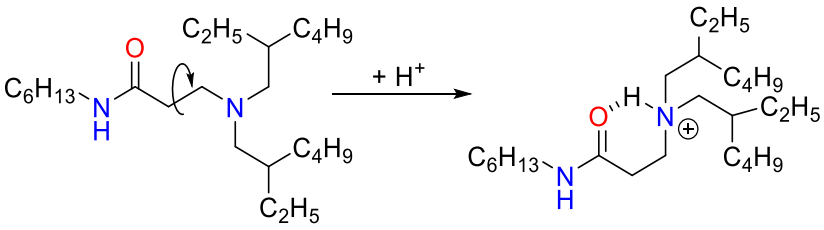

Figure 1.5.3.1 – An unprotonated (left) and protonated (right) amidoamine used for the selective extraction of Pt from chloride media.[24]

This "proton chelation" results in the favourable alignment of an array of C-H groups towards the comparatively 'soft' charge diffuse $PtCl_6^{2-}$ anions rather than towards 'harder' charge dense highly abundant Cl^- anions.[24, 49] While an individual N-H-$PtCl_6^{2-}$ interaction is strong, the multiple weaker, and non-classical C-H-$PtCl_6^{2-}$ interactions provide a significant contribution to the total stability, as determined by DFT calculations. In contrast, DFT calculations indicated that for chloride only a single N-H-Cl^- interaction occurs (Figure 1.5.3.2) resulting in the formation of amidoamine-Pt assemblies being substantially more favourable.

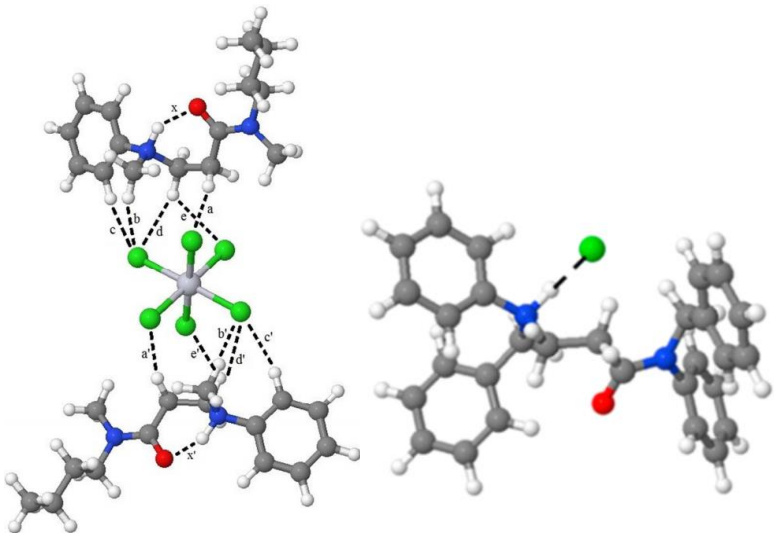

Figure 1.5.3.2 – A comparison of the DFT optimised structures of an amidoamine-$PtCl_6^{2-}$ complex and amidoamine-Cl complex and a visualisation of NH-OC, NH-Cl and CH-Cl interactions.[24] Elements are coloured as C (grey), H (white), O (red), N (blue), Cl (green) and Pt (silver).

1.5.4 Metal salt extraction (solvation)

Metal salt extraction relies on the removal of water molecules from the inner-coordination sphere of metals and their replacement with coordinating neutral ligands or anions present in the aqueous phase. The coordinating ligands can be considered to 'solvate' the metal in the organic phase by creating an organic-soluble complex.[50]

In overall charge neutral macromolecular frameworks, features of both cation and anion extraction are used to allow for discriminatory accommodation of cations and anions. The cations and anions reside in well separated binding pockets suited to their size and chemical properties. The removal of Au as $AuBr_4^-$ along with the counter cation K^+ as $K(H_2O)_6^+$ from an aqueous phase also containing Pt and Pd through the incorporation of $KAuCl_4$ into α-cyclodextrin provides effective separation.[51] The $KAuCl_4$-α-cyclodextrin complexes (Figure 1.5.4.1) instantaneously form and precipitate upon mixing, forming large 'cable-esque' structures with Pt and Pd remaining in solution.

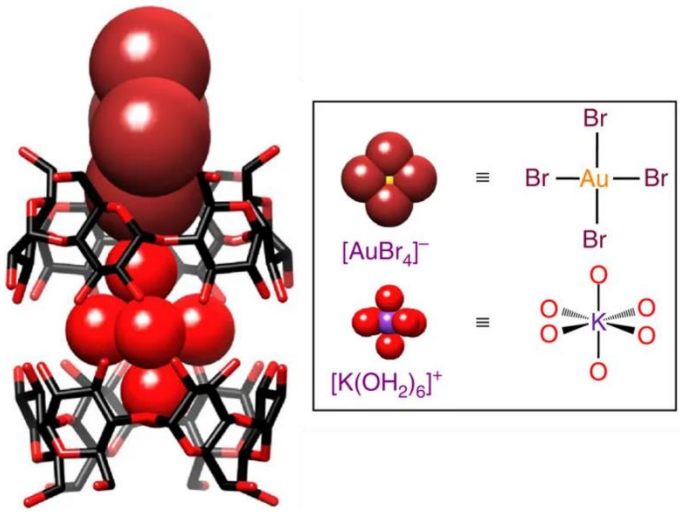

Figure 1.5.4.1 – Side-on-view of the interaction between α-cyclodextrin, $AuBr_4^-$ and $K(H_2O)_6^+$.[51] α-cyclodextrin elements are coloured as C (black) and O (red). Hydrogens are hidden for clarity.

Some reagents that extract metals through a metal salt pathway also transport significant amounts of water into organic phase. These reagents include tributylphosphate and diglycolamides, and the mode of action results in the formation of 'reverse'-micelles.[43, 52, 53] Reverse-micelles often result in poor selectively as the water 'pool' can often accommodate multiple anions and cations with little discrimination, and will be discussed later.

While Cu is often extracted industrially through metal cation exchange (section 1.5.2), slight modifications to phenolic oximes allows for Cu extraction through a metal salt pathway.[19, 20] Using a zwitterionic ligand (Figure 1.5.4.2), where phenolic oxygens are deprotonated and pendant amine groups are protonated, $CuSO_4$ is readily extracted from an acidic aqueous phase.[54, 55] In this case, the Cu^{2+} cations occupy the $N_2O_2^{2-}$ cavity while SO_4^{2-} anions bind through hydrogen-bonding interactions to the two protonated amine groups.

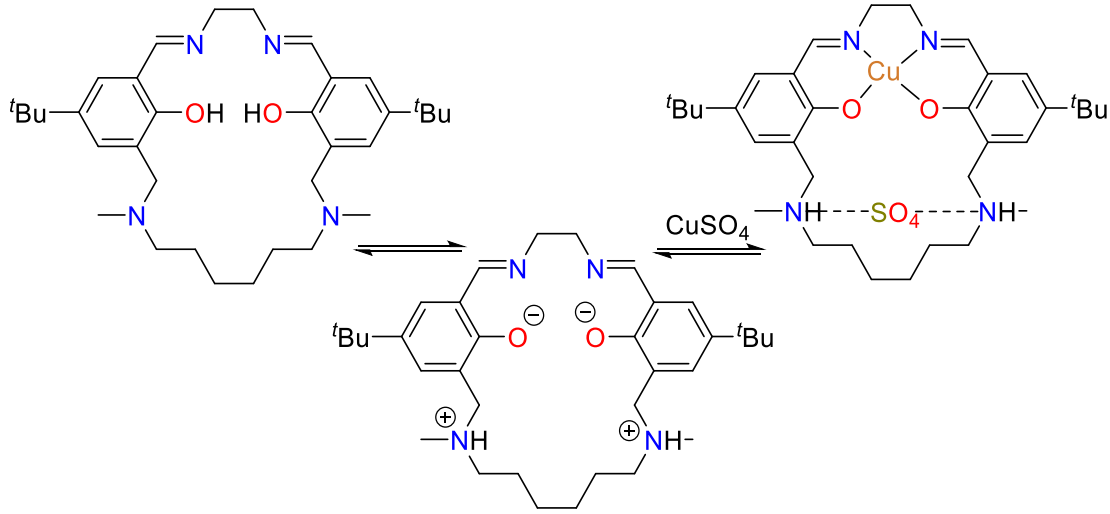

Figure 1.5.4.2 – A phenolic oxime analogue (left), the zwitterionic form (centre) and the zwitteironic-$CuSO_4$ complex (right).[20, 54]

An industrial process that extracts Cu through a metal salt pathway is the CUPREX process. Using a neutral ligand CLX50 (didecyl pyridine-3,5-dicarboxylate), $CuCl_2$ is extracted from chloride solutions resulting in a 4-coordinate $CuCl_2[CLX50]_2$ complex.

Eq. 1.5.4.1 – $$Cu^{2+}_{(aq)} + 2\ Cl^{-}_{(aq)} + 2\ CLX50_{(org)} \rightleftharpoons CuCl_2[CLX50]_{2(org)}$$

One advantage of this process over cation exchange is that protons are not transferred to the aqueous phase over time. This removes the need for pH adjustment during the solvent extraction process.

1.6 Thesis aims and layout

This thesis will explore the recovery and separation of REEs by alternative techniques and reagents to those currently used industrially.

Chapter 2 investigates how an effective, but currently poorly understood, ionic liquid reagent that only contains carbon, hydrogen, oxygen and nitrogen (CHON) atoms extracts REEs from mildly acidic salt solutions. A range of analytical and computational techniques are applied and discussed in order to gain chemical insight into the mode of REE extraction and of the assemblies that form in the organic phase throughout the recovery process.

Chapters 3 and 5 build upon the chemical understanding established in Chapter 2 to develop new ionic liquid reagents that include greater functionality such as amide groups. Some of the modified reagents exhibit strong selectivity for lighter REEs over heavier REEs and nitric acid. A range of techniques are applied to rationalise why the modified reagents display differing chemical behaviour to that of the unfunctionalized ionic liquid in chapter 2. Potential industrial applications are discussed.

Chapter 4 considers the feasibility of leaching REEs from a REE containing mineral (eudialyte) under very mild conditions compared with those used industrially. In this case, an autotrophic bacterium fuelled by aqueous $FeSO_4$ is used to leach the REEs instead of elevated temperatures and concentrated acid. From the resulting leach solution, the separation of the lighter REEs is achieved, demonstrating the feasibility of recovering REEs using milder conditions.

Chapter 2

Understanding REE recovery using trioctylmethyl ammonium nitrate

2 Understanding REE recovery using trioctylmethyl ammonium nitrate

2.1 Current reagents for REE recovery

Rare earth elements (REEs) are predominately extracted during industrial separation and concentration processes by organophosphorus compounds such as di-(2-ethylhexyl)phosphoric acid (D2EHPA) (Figure 2.1.1) that exploit cation exchange mechanisms or Cyanex 925 that is neutral and extracts REEs through solvation.[56, 57]

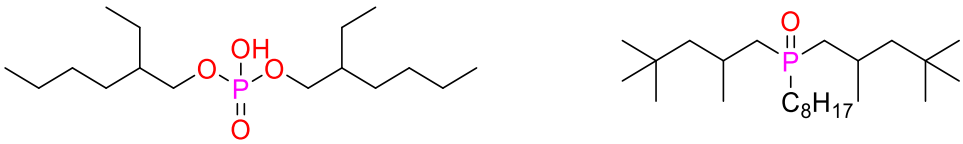

Figure 2.1.1 – Organophosphorus compounds used industrially for the separation and concentration of REEs: D2EHPA (left); Cyanex 925 (right).

The recovery of REEs using D2EHPA is relatively well understood and is known to initially involve the transport of REE^{3+} cations into the organic phase accompanied by the transfer of three protons to the aqueous phase to compensate and charge balance (equation 2.1.1).[58] Following transport into the organic phase by D2EHPA, REE cations have been shown to be fully dehydrated through using time-resolved laser induced fluorescence in combination with IR spectroscopy.[59]

Eq. 2.1.1 – $REE^{3+}_{(aq)} + 3+x(D2EHPA)_{(org)} \rightleftharpoons REE(R_2PO_2)_3(R_2PO_2H)_{x(org)} + 3\ H^+_{(aq)}$

The analysis of the gradient of the line created from plotting log([organic metal]/[aqueous metal] against $log(H^+)$, or 'slope analysis' was originally used to determine the mode of REE extraction.[19] This is complicated by the characteristic of D2EHPA to self-associate to form a stable dimer in non-polar, water-immiscible solvents (Figure 2.1.2).[60] Upon extraction, and if the organophosphorus compound remains in excess, retention of one of the hydrogen bonds can be observed. This results in the organic phase hosting REE complexes of the very general formula $REE(R_2PO_2)_3(R_2PO_2H)_x$ where some hydrogen bonds are retained and others are lost.[39] Generally though, x in the formula $REE(R_2PO_2)_3(R_2PO_2H)_x$ is three.[61, 62]

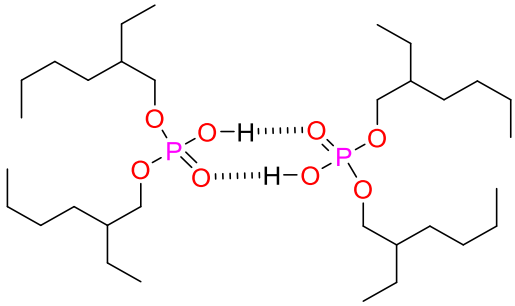

Figure 2.1.2 – Dimeric D2EHPA is commonly observed in non-polar, water-immiscible solvents.

More recently, extended X-ray absorption fine structure (EXAFS) data have helped corroborate preceding experimental evidence and confirmed the presence of three singly deprotonated organophosphorus dimers coordinated to REE^{3+} ions in the organic phase (Figure 2.1.3.).[59, 63]

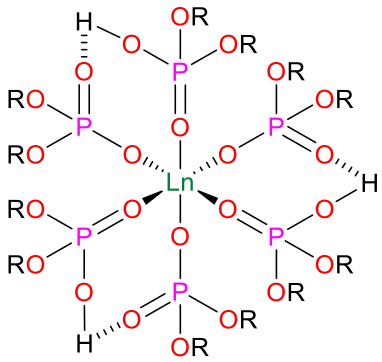

Figure 2.1.3 – A $REE(R_2PO_2)_3(R_2PO_2H)_3$ complex formed in the organic phase following loading of the REE. Determined by EXAFS.[59, 63] The retaining of hydrogen-bonding interactions between organophosphorus compounds upon REE complexation is supported in earlier studies using mass-spectrometry, infrared and UV-vis spectroscopy.[64] R = ethylhexyl carbon chain.

While being only tentatively identifiable by room-temperature EXAFS, an alternative structure where REE-O bonds replace hydrogen bonds and thus create an extended structure is also possible. Organophosphorus-REE organic-phase structures are known to aggregate substantially, forming polymeric structures composed of hundreds of REEs.[65] The formation of $REE(R_2PO_2)_3(R_2PO_2H)_3$ compounds is further supported by ^{31}P nuclear magnetic resonance

(NMR) spectroscopy where experimental integrations agreed well with predicted integrations and by electrospray ionisation - mass spectrometry (ESI-MS) that detected an ion of *m/z* 2070.8 consistent with $La(R_2PO_2)_3(R_2PO_2H)_3H^+$.[59]

As D2EHPA relies on loss of H^+ to the aqueous phase in order to transport REEs to the organic phase, the aqueous phase cannot be excessively acidic otherwise the equilibrium (equation 2.1.1) will lie fully towards the left-hand-side. It will be more favourable for D2EHPA to remain protonated. As such, studies have shown that D2EHPA can sufficiently extract REEs from aqueous solutions down to a minimum of pH 1. One such study reported >99% extraction of Nd at pH 1 from a chloride aqueous phase, another reported >99% extraction of both Gd and Dy at pH 2 (Figure 2.2.4) from a nitrate aqueous phase, while one reported >99% extraction of Eu above pH 2.5.[66-68] D2EHPA preferentially extracts the heavier REEs, with <30% of La extracted under comparable conditions.[67] At pH 1 in another study, <1% of La was extracted from a monazite mineral dissolved in either chloride or nitrate medium, ~2% of Nd was extracted while almost 50% of Dy was extracted, reinforcing the targeting of the heavier REEs such as Dy by D2EHPA.[69]

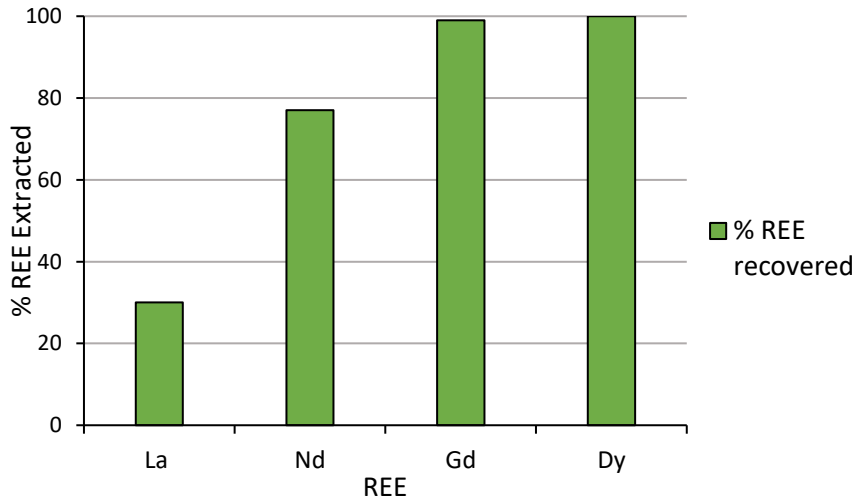

Figure 2.1.4 – The extraction of La, Nd, Gd and Dy from an aqueous nitrate media at pH 2 using D2EHPA (0.05 M) in kerosene.[67]

Despite extensive use industrially, the processes organophosphorus compounds are used within have some fundamental drawbacks, including the tendency for organophosphorus compounds to be lost into the aqueous phase and to be damaging environmental pollutants.[70, 71] A 2012 report highlighted that the REE industry produces >20 million tons of

wastewater annually. Furthermore, some effluents exceed chemical emission levels by up to a hundred times.

The issue is arguably most prevalent in the strip step of the process, with both REEs and organophosphorus compounds transported into the fresh aqueous phase. [70, 72] The acidic conditions used during the stripping process accelerate the compound loss and can lead to acid-catalysed hydrolysis. This hydrolytic decomposition of organophosphorus compounds, and D2EHPA in particular, is additionally reported to occur during periods of prolonged storage. During strip processes, around 1-2% of D2EHPA is reported to be transported into the aqueous phase during each strip.[73] The poor separation of the REEs by D2EHPA and other organophosphorus compounds from an engineering and environmental perspective results in multiple strip cycles, high loss of compound and substantial volumes of organophosphorus contaminated aqueous phases.[7, 74] In the following isolation step, even trace organic impurities can seriously reduce efficiency.[70]

2.2 Metalates and the Hofmiester bias

The purification and recovery of precious metals such as Pt and Au is not affected by organophosphorus compound drawbacks as they are usually extracted from aqueous solutions as halometalates (usually chloridometalates) (Figure 2.2.1).

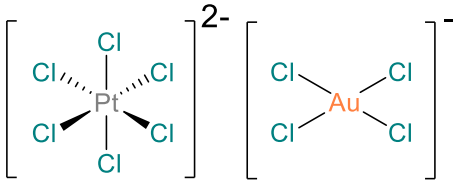

Figure 2.2.1 – The chloridometalate structures of $PtCl_6^{2-}$ (left) and $AuCl_4^-$ (right).

The reagents used industrially are basic and transport a proton (or protons) from the aqueous phase in conjunction with the target metalate, creating an organic-phase assembly. In Au recovery, where Au is present in aqueous chloride as $AuCl_4^-$, methyl isobutyl ketone (MIBK) and dibutyl carbitol (DBC) (Figure 2.2.2) are the extracting reagents of choice.

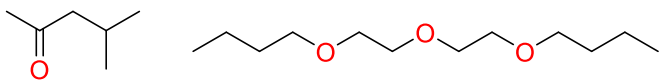

Figure 2.2.2 –Methyl isobutyl ketone (MIBK) (left) and dibutyl carbitol (DBC) (right), reagents used in the recovery of Au.

REEs cannot be recovered through a metalate extraction pathway, with one predominant reason lying with the Hofmeister series.[42, 75, 76] The Hofmeister series was originally applied to the ability of common salts to 'salt-out' of solution egg-white protein but can be more generally applied to how readily cations and anions are transferred from an aqueous phase to an organic phase.[77] Highly hydrated ions 'salt-out' proteins more effectively, and equally are less readily removed from the aqueous phase. The ions have a high enthalpy of hydration that needs to be overcome. Highly hydrated is usually synonymous with the ion being highly charge dense and results in a tightly bound hydration shell where water molecules no longer behave as bulk water.[78, 79] This can be due to the ion being comparatively small, the ion being highly positive/negative or a combination of the two factors. Anions such as sulfate (SO_4^{2-}) or carbonate (CO_3^{2-}) are considered highly hydrated, while ions such as nitrate (NO_3^-) or iodide (I^-) are considered less highly hydrated as per the trend below.[80-82]

$$CO_3^{2-} > SO_4^{2-} > S_2O_3^{2-} > H_2PO_4^- > F^- > Cl^- > Br^- > NO_3^- > I^- > ClO_4^- > SCN^-$$

Extrapolating the series to metalates, $AuCl_4^-$ is straightforwardly extracted by a range of extractants (including Figure 2.2.2) from the aqueous phase as the anion is large and only singly negative; even conventional vacuum pump oil extracts gold given a long enough contact time.[22, 83] The issue during gold extraction is a lack of selectivity. More highly charged PGM chloridometalates such as $PtCl_6^{2-}$, $RhCl_6^{3-}$, and $IrCl_6^{3-}$ are far more difficult to extract from aqueous chloride solutions due to their greater charges with rhodium currently purified industrially through precipitation methods.[84]

In aqueous solution, REEs demand high coordination numbers (≥6) meaning metalates of at least $REE(Cl)_6^{3-}$ or $REE(NO_3)_6^{3-}$ could be expected. In reality REEs do not spontaneously form metalates in the aqueous phase. DFT calculations have indicated that, in the aqueous phase, full hydration of REEs accompanied by an outer-coordination sphere of anions is substantially more energetically favourable (over 200 KJ mol^{-1} difference) than six chloride or six nitrate anions bound in the inner-coordination sphere (Figure 2.2.3.).[42]

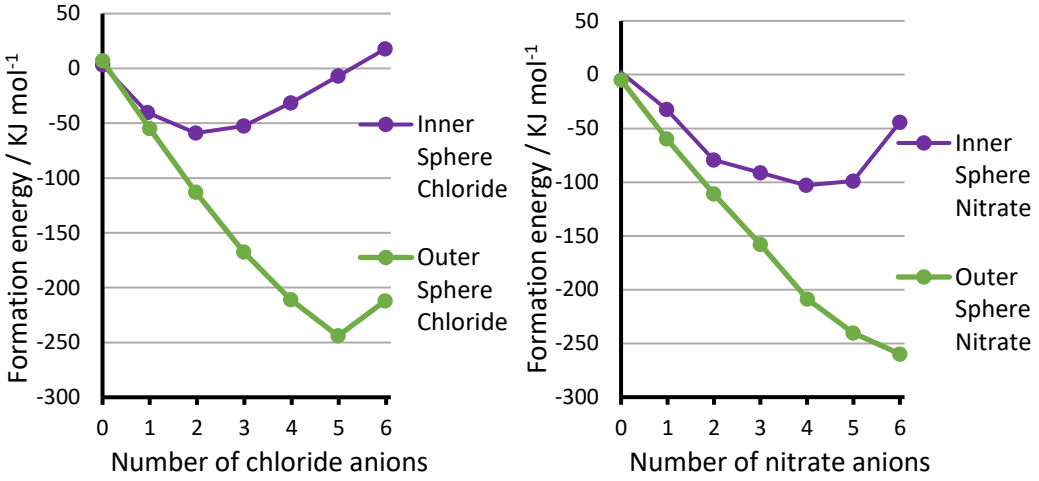

Figure 2.2.3 – Formation energies of La^{3+} inner-sphere complexes and outer-sphere assemblies with varying numbers of chloride (left) or nitrate (right).[42]

The high hydration enthalpies of the REEs have been studied both computationally and experimentally. Their exceptionally high affinity for water greatly exceeds that of 1st row transition metal 2+ cations, with only very charge concentrated ions such as Hf^{4+} and Zr^{4+} having more negative Gibbs energies of hydration ($\Delta_{hyd}G^*$/KJ mol^{-1}).[85] The hydration energy is more negative for the heavier REEs, with -3145 (La) and -3570 (Lu) KJ mol^{-1} reported in one experimental study, while in a computational study values of -3120 (La) and -3520 (Lu) KJ mol^{-1} were found. In both studies, and others, approximately a 400 KJ mol^{-1} graduated difference across the REE series is observed.[86-89] The energetic penalty for transporting water into the organic phase is high meaning in most circumstances hydration energies must be overcome in order to transport a metal into the organic phase. Exceptions to this include metal recovery involving a micellar extraction route. Tributylphosphate (TBP) and diglycolamide ligand systems (Figure 2.2.4) can operate by this pathway, and the formation of micelles will be discussed further in Chapter 3.[43]

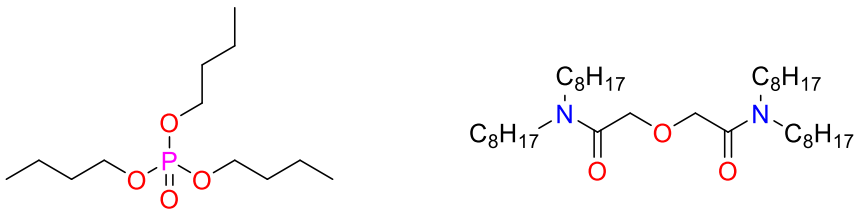

Figure 2.2.4 –Tributylphosphate (TBP), (left) and a diglycolamide (TODGA), (right) are reagents that extract through the formation of micellar aggregates.

2.3 A brief overview of ionic liquids

Ionic liquids (ILs) are salts that are liquid at room temperature. ILs comprise both a permanently positive cation (often ammonium, imidazolium or phosphonium) (Figure 2.3.1) and a counter anion (often chloride, nitrate or bis(triflimide)) to charge balance (Figure 2.3.2).[90]

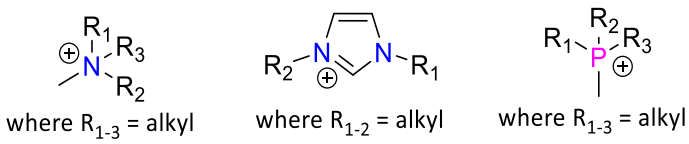

Figure 2.3.1 – Typical cations of ionic liquids: ammonium (left); imidazolium (centre); phosphonium (right).

ILs are now common within both academic and industrial settings with wide applicability due to their desirable chemical properties of low vapour pressure, water immiscibility and relative ease of synthesis.[91] ILs can be designed and tailored to meet specific needs with theoretically 10^{18} unique ILs being possible, in contrast to only around 10^{3} molecular solvents currently in use today.

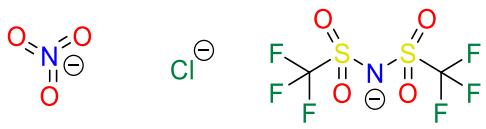

Figure 2.3.2 – Typical anions of ionic liquids: nitrate (left); chloride (centre); bis(triflimide) (right).

The first IL was reported in 1914 following the formation of ethylammonium nitrate (mp 13–14 °C) from the reaction between ethylamine and nitric acid, although no application was documented.[92] By 1961, ILs were applied to the task of lubrication, and then in the subsequent decades applied to a range of tasks and fields including purification, fuel cells and catalysis.[93, 94] Then, in the early 2000's BASF incorporated the IL 1-methylimidazolium chloride into the production of alkoxyphenylphosphines (the BASIL™ process) into what was the largest in terms of scale implementation of an IL into a production process.[91] ILs are now used in a range of pharmaceutical process, such as the use of phosphonium ILs (Figure 2.3.1)

in the Sonogashira reaction (scheme 2.3.3), highlighting their comparatively safe use and versatility. When compared to a conventional solvent (THF) the yield increased fivefold.

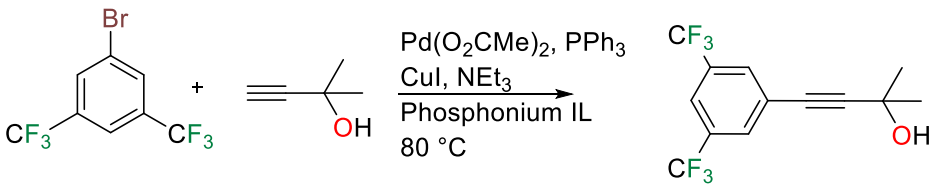

Scheme 2.3.3 – The Sonogashira reaction. A Pd-Cu catalysed reaction of aryl halides and terminal alkyl- or aryl-alkynes. The yield increased fivefold over when THF was replaced by a phosphonium IL as the solvent.[92]

Adogen 464 and Aliquat 336 are commercialised ammonium-based ILs (ABILs) comprising lipophilic quaternary ammonium cations and accompanying chloride counter anions (Figure 2.3.4). The ammonium cations of Adogen 464 and Aliquat 336 are a mixture of isomers with branched alkyl chains lengths between 8-10 carbons, although the main isomer has chain lengths of eight carbons.[95, 96] While Adogen 464 and Aliquat 336 both have methyl trioctylammonium chloride as their main isomer (33 %<), the distribution of isomers totalling the remainder varies slightly and their formulations are therefore not identical.

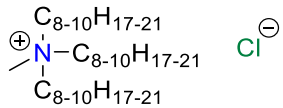

Figure 2.3.4 – The general structures of the commercialised ILs Adogen 464 and Aliquat 336. Adogen 464 contains an ammonium cation of various isomers with varying chains lengths between 8-10 carbons in length.

Adogen 464 and Aliquat 336 have been applied for several decades to the purification of organic compounds and base metals with some very early work exploring the recovery of xylenol orange metal complexes from acid solutions.[97, 98] Recently, the potential to use these ILs as environmentally friendlier replacements for organophosphorus compounds in metal separation and purification has become prominent. Throughout this thesis, ABILs will be predominantly discussed, and imidazolium- and phosphonium-based ILs occasionally referenced.

2.4 Current understanding of REE recovery by ABILs

Studies on how ABILs, herein referred to as ILs, extract REEs from aqueous nitrate medium are arguably sparse and incomplete in the literature and will therefore form the principal discussion within this chapter. Through examining previous published work and current chemical understanding a few hypotheses and observations can be made.

Ammonium cations of ILs cannot bind directly to the inner-sphere of REE but the anions, if perhaps chloride or nitrate, could bind directly. Many stable crystalline REE complexes containing REE-NO_3 or REE-Cl bonds are documented (e.g. CSD codes: QEMJUO, REWQIV, TUMWUT and UFUNER to note a few), but those also containing water are rarer.[99-102] Given the high hydration enthalpies of the REEs as discussed above, retention of some H_2O-REE bonds following extraction can be expected. Some examples of $La(NO_3)_x(H_2O)_y$ complexes include $[La(NO_3)_3(H_2O)_4](C_{10}H_8N_2)_2(H_2O)$ (CSD code: GOZBIG) which contains three bidentate nitrate anions and $[La(NO_3)_2(H_2O)_6](C_6H_{12}N_4)_2(NO_3)(H_2O)_2$ (CSD code: MUQREW) which contains two bidentate nitrate anions (Figure 2.4.1).[103, 104]

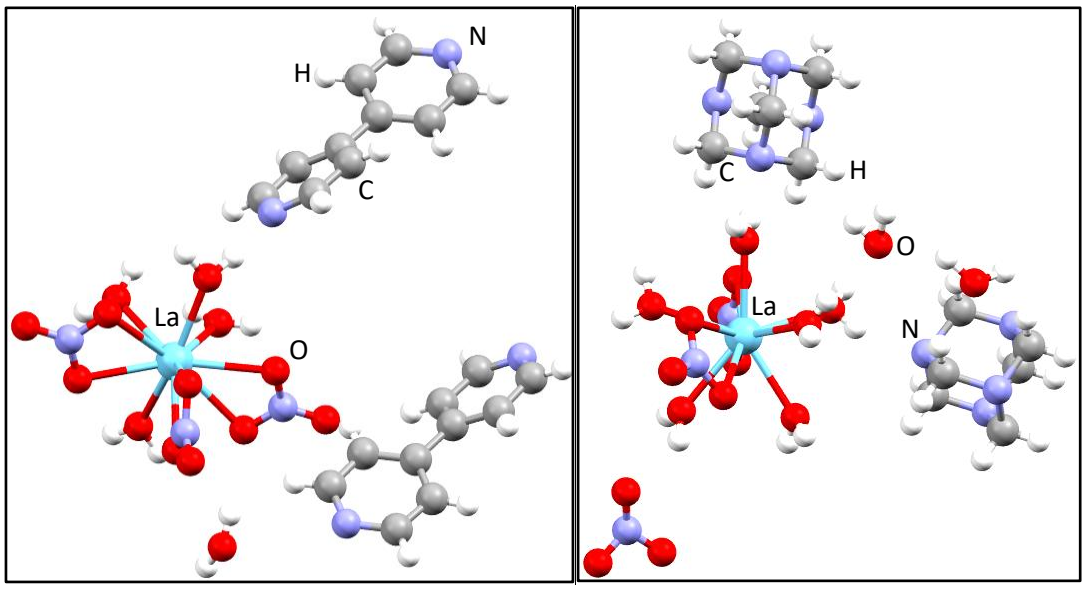

Figure 2.4.1. – Crystalline La compounds containing both nitrate anions and water molecules coordinated to the La centre. The La centre can be considered to be partially dehydrated. $[La(NO_3)_3(H_2O)_4](C_{10}H_8N_2)_2(H_2O)$ (left) (CSD code: GOZBIG)[103] and $[La(NO_3)_2(H_2O)_6](C_6H_{12}N_4)_2(NO_3)(H_2O)_2$ (right) (CSD code: MUQREW)[104]

Direct binding of a sulfate anion to a REE is very rare due to the high hydration energy of the sulfate anion – reported to be almost 800 KJ mol^{-1} more negative than chloride and nitrate in agreement with the Hofmeister bias.[85] Despite this, a few crystalline compounds containing sulfate bound directly to a REE centre are reported in the CSD (Figure 2.4.2).[105, 106] The limited documentation of REE-SO_4 bonds, in combination with very low REE extraction from purely sulfate media using ILs, is supportive of direct REE-anion bonds being required during the extraction process.

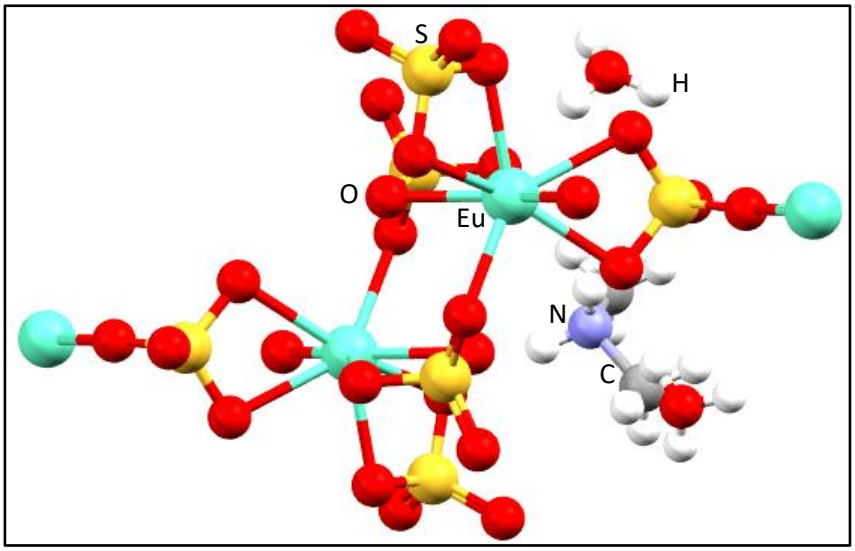

Figure 2.4.2 – A crystalline Eu complex comprising three bidentate sulfate ligands (CSD code: IZAFEV).[106]

When used as both the solvent and the extractant (i.e undiluted, or neat), ILs extract REEs readily from weakly acidic aqueous phases that have a high nitrate salt content. The nitrate salt of Aliquat 336 was found to extract (>99%) Pr from nitrate salt (>4.0 M) solutions.[107] When comparing REE extraction by ILs across the f-block, the light REEs are readily extracted, while heavier REEs beyond Dy are poorly extracted, following the hydration energies trend (section 2.2).[88] Aliquat 336-nitrate (0.1 M) was found to extract almost 60% of La (0.01 M) from a $NaNO_3$/HNO_3 solution (3.5 M/0.1 M), but the separation from Ce was minimal.[108] It should be noted that ILs have been combined with traditional organophosphorus reagents (section 2.1) and most experiments show a positive synergistic effect.[109-112]

The extraction of REEs from nitrate media by ILs is understood to involve the transport of one REE cation and three nitrate anions from the aqueous phase to the organic phase where association with 'x' amount of ILs occurs (Eq. 2.4.1).[113-117]

Eq. 2.4.1 – $REE^{3+}_{(aq)} + 3\ NO_3^-{}_{(aq)} + xIL_{(org)} \rightleftharpoons REE(NO_3)_3(IL)_{x(org)}$

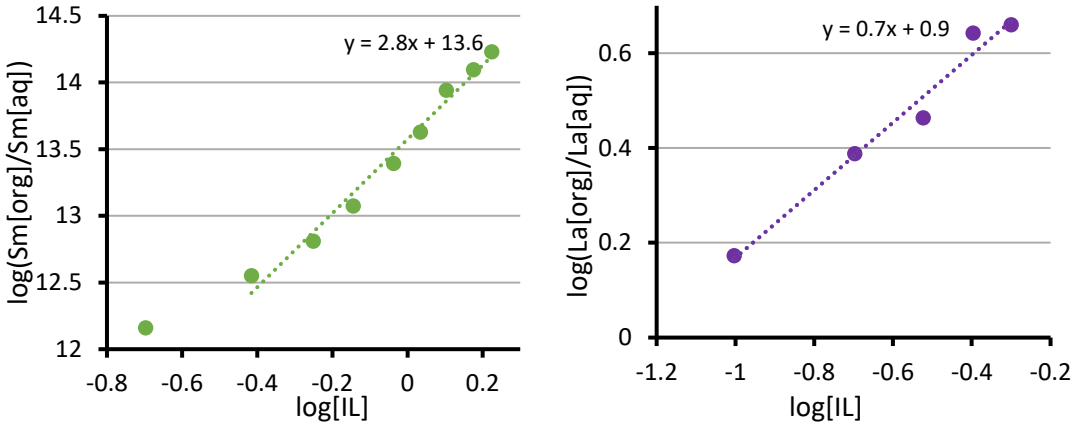

Figure 2.4.3 – Plots of log(Ln[org]/Ln[aq]) vs. log(IL) for the extraction of Sm (left) and La (right) from a NH_4NO_3 (10.0 M) solution, giving a gradient of approximately three at high IL concentrations (>0.7 M or >log[-0.4]) and high Sm loading,[118] and one at lower IL concentrations (<0.7 M or <log[-0.4]) and low La loading.[108]

Interpretation of log/log plots (slope analysis) comparing nitrate concentration against REE transported (Figure 2.4.3) shows a gradient of three at high IL concentrations, suggesting that six nitrate anions interact with the REE and that REEs in the organic phase are present as $REE(NO_3)_6^{3-}$ metalates.[107, 112, 116-118] These metalates would then be stabilised in the organic phase by outer-sphere interactions with the ammonium cations (Figure 2.4.4). At lower IL concentrations or lower metal loading, the REE to IL ratio is more ambiguous and often reported to be smaller – 1:1 or 1:2, implying the formation of $REE(NO_3)_5^{2-}$ or $REE(NO_3)_4^-$ metalates (Figure 2.4.3).[107, 119, 120]

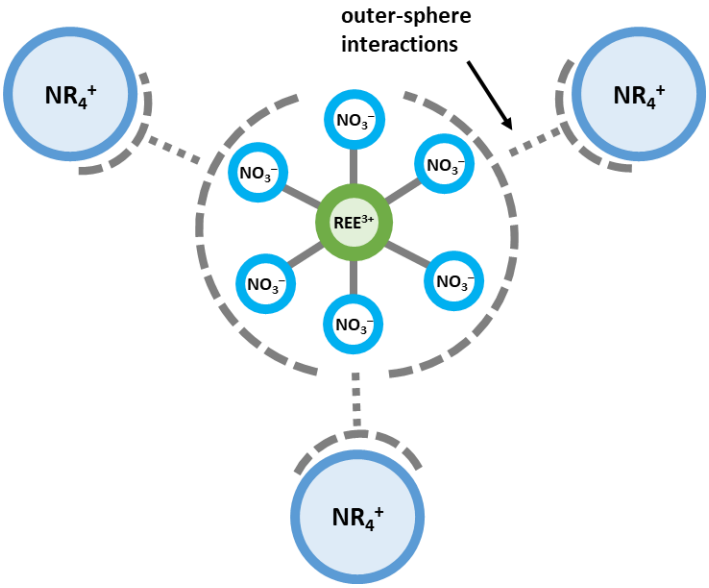

Figure 2.4.4 – A simplified representation of a REE metalate stabilised in the organic phase by outer-sphere interactions with ammonium cations.

As stated above, the formation of REE metalates in the aqueous phase is energetically unfavourable (section 2.2).[42] If REE metalates are to be observed in the organic phase they can be expected to form during transport, such as at the interface, or after REE transport into the organic phase. In the aqueous phase, under forcing conditions of very high chloride or nitrate, partial substitution of water molecules for chloride or nitrate anions at light REE centres has been observed using EXAFS and XANES spectroscopy, resulting in $REE(H_2O)_{9-n}(x)_n^{3-n}$ ions (where n = 1-2 and x is chloride or nitrate, Eq. 2.4.2).[109, 121] Overall charge negative REE species (REE metalates) in the aqueous were not reported in these studies, in agreement with discussed DFT calculations (section 2.2).[42]

Eq. 2.4.2 – $Ce(H_2O)_9^{3+}{}_{(aq)} + 2\ Cl^-_{(aq)} \rightleftharpoons Ce(H_2O)_7Cl_2^+{}_{(aq)}$ [121]

It was reported that strongly acidic aqueous phases (<pH 3) significantly inhibit the transport of REEs to the organic phase by ILs.[107, 111, 114, 118] This initially seems counterintuitive as high acid presence means high anion concentration. Formation of REE metalates in the aqueous phase should be favoured. Metalate formation at high acid concentration is observed with PGMs and leads to their subsequent extraction.[21, 49, 122] At very high acid concentration, competition with the respective anion can occur, especially if the enthalpy of hydration of the anion is only moderate, such as for chloride.[23, 80, 81, 88] This results in reduced extraction

of the target metal, as highlighted in the extraction of $AuCl_4^-$ using a primary amide extractant (Figure 2.4.5).

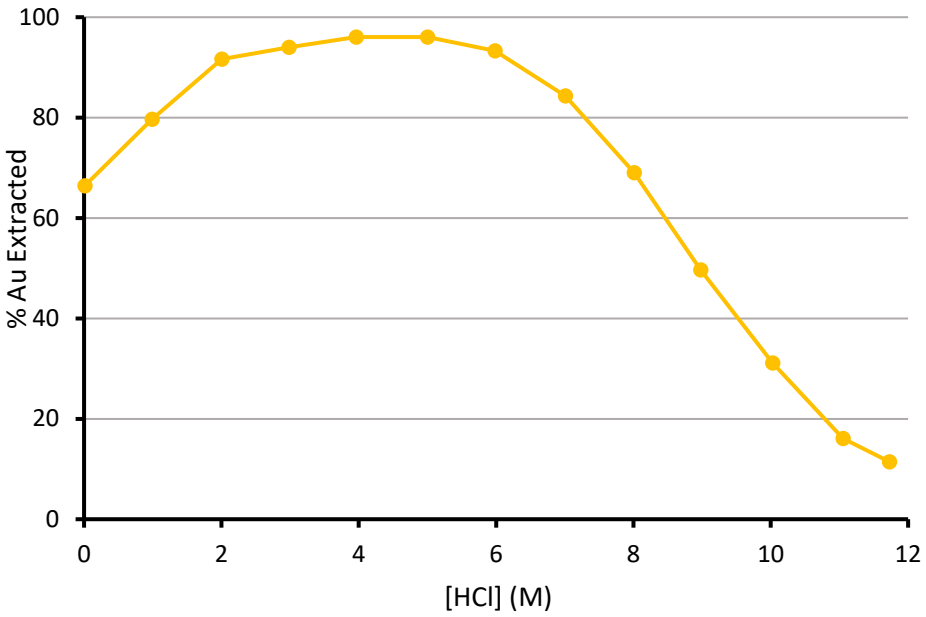

Figure 2.4.5 – The percentage extraction of $AuCl_4^-$ with varying HCl concentration. At high HCl concentrations Cl^- extraction is competing with $AuCl_4^-$ extraction.[21]

Similarly, the up-take of nitric acid by ILs is well documented meaning a competing process is very probable, even at comparatively low concentrations of acid (Eqs. 2.4.3 and 2.4.4).[123] Given a finite concentration of IL, any IL associated with the transport of acid may no longer be available to transport REEs.

Eq. 2.4.3 – $H^+_{(aq)} + NO_3^-{}_{(aq)} + xIL_{(org)} \rightleftharpoons (HNO_3)(IL)_{x(org)}$

Eq. 2.4.4 – $La^{3+}_{(aq)} + 3\ NO_3^-{}_{(aq)} + xIL_{(org)} \rightleftharpoons La(NO_3)_3(IL)_{x(org)}$

To summarise all of the points discussed and before proceeding, the following observations can be noted:

- X-ray crystal structures of REE nitratometalates are reported.[99-102]
- It is energetically unfavourable for REE in the aqueous phase to be present as metalates[42, 109, 121]
- High aqueous acidity supresses REE transport, potentially through competitive anion transport.[21, 42, 123]

- Salt (e.g. $NaNO_3$) addition to the aqueous phase enhances REE extraction rates due to the 'salting-out' effect.[107, 108, 118]
- Lighter REEs are preferentially extracted over heavier REEs possibly due to lower enthalpies of hydration[86, 88]

2.5 IL Synthesis – Trioctylmethylammonium nitrate (IL0)

As commercialised ILs such as Adogen 464 or Aliquat 336 are a blend of compounds these reagents are difficult to characterise by standard chemical techniques such as NMR spectroscopy and mass spectrometry. Therefore, a simple quaternary ammonium IL of standardised alkyl chain lengths is used in the studies described in this chapter.

Following a standard preparation, trioctylmethylammonium nitrate (**IL0**) was synthesised from trioctylamine and its reaction with methyliodide (scheme 2.5.1).[124] Methyliodide was chosen as the methylating agent due to its high reactivity and versatility plus the lability and water solubility of the iodide anion. The resulting ammonium iodide salt was converted to the ammonium nitrate salt by three contacts with a $NaNO_3$ (7.0 M) solution. The removal of iodide was validated through iodine starch testing. Given the high viscosity of **IL0** and therefore the difficulty in accurate weighing, it was stored as a 1.0 M solution in toluene to minimise errors between experiments.

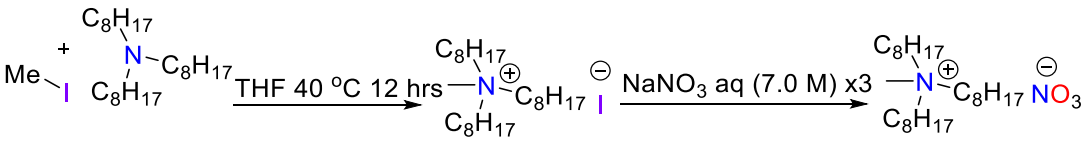

Scheme 2.5.1 – The synthesis of trioctylmethylammonium nitrate (**IL0**) from trioctylamine.

2.6 REE extraction studies

2.6.1 Extraction of REEs from varying $NaNO_3$ solutions

Contacting an aqueous phase containing either La, Nd or Dy (0.01 M) and $NaNO_3$ (1.0 – 7.0 M) with **IL0** (0.10 M) in toluene results in the transport of REEs into the organic phase (Figure 2.6.1). At high $NaNO_3$ concentration (7.0 M), La (99%), Nd (85%), and Dy (52%) are extracted. The percentage extracted decreases substantially as the $NaNO_3$ concentration is lowered, reaching <5% extraction for all REEs tested at 1.0 M $NaNO_3$; this is in accordance with the

'salting-out' effect.[107, 108, 118] Dy was the least readily extracted from the aqueous solution at all $NaNO_3$ concentrations, in agreement with previous research.[88]

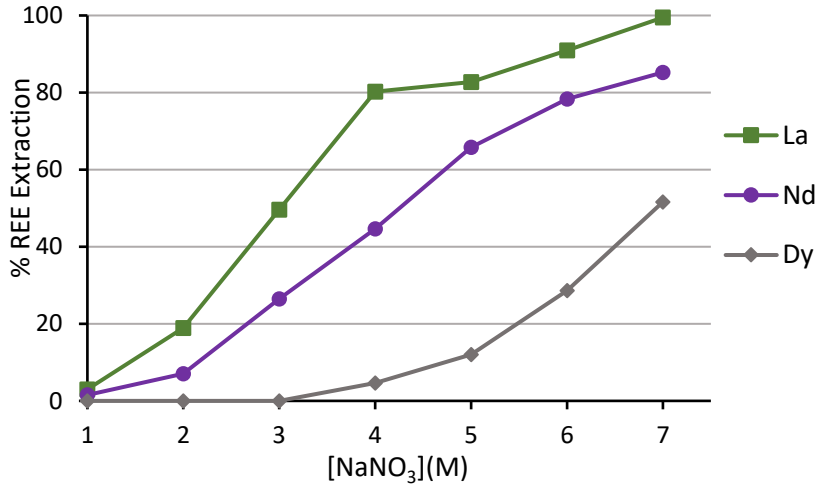

Figure 2.6.1 – The extraction of La, Nd and Dy (0.01 M) using **IL0** (0.10 M) in toluene from aqueous $NaNO_3$ (1.0 – 7.0 M). Interpolation used to aid the eye only.

2.6.2 Extraction of REEs using varying IL0 concentration

Varying the **IL0** concentration (0.01 – 1.00 M) with a constant $NaNO_3$ (7.0 M) concentration results in a similar trend to that above for the transport of La, Nd and Dy from single metal aqueous solutions (Figure 2.6.2). An increasing **IL0** concentration transports an increasing percentage of the REEs into the organic phase with >90% of La, Nd and Dy transported (100%, 98% and 92%) at 1.0 M **IL0**; in contrast, only minimal amounts of La, Nd and Dy (5%, 12% and 13%) are extracted at 0.01 M **IL0**. While increasing **IL0** concentration clearly has a positive effect on the transport of REEs, the percentage of La and Nd transported at 0.1 M **IL0** is not dissimilar to that at 1.0 M **IL0**, with only an 11% (La) and 22% (Nd) improvement observed despite a 10-fold increase in **IL0** concentration.

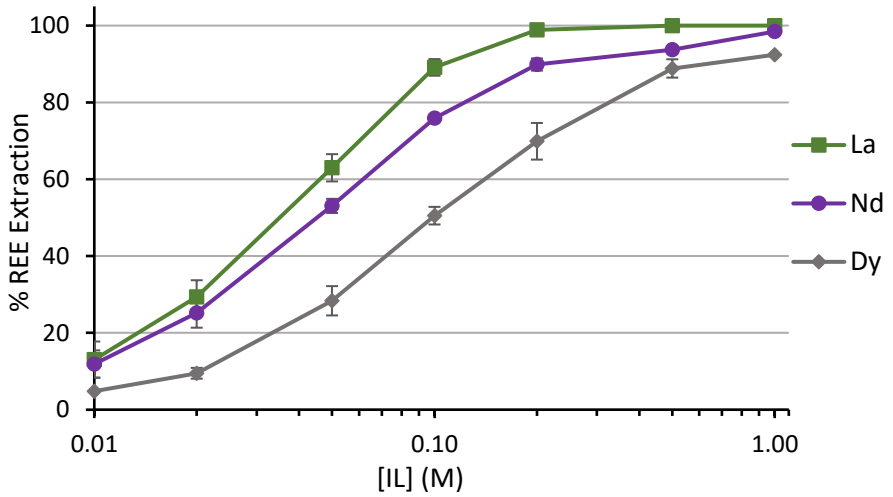

Figure 2.6.2 – The extraction of La, Nd and Dy (0.01 M) using **IL0** (0.01 – 1.00 M) in toluene from aqueous $NaNO_3$ (7.0 M) solution. Interpolation used to aid the eye only.

2.6.3 Time dependant extraction

While the extraction of metals from the aqueous phase with some reagents can take a comparatively long time, the extraction of REEs using **IL0** is almost instantaneous (Figure 2.6.3).[22, 107] Contacting **IL0** (0.1 M) with a $NaNO_3$ (7.0 M) aqueous phase containing La (0.01 M) provides maximum extraction of La (>80%) by 60 seconds of contact. No further increase in % La extraction was observed beyond 60 seconds. For some metals, this rapid transport highlights a rapid rate of formation of the organic stable metal species allied with an outer-sphere complex with inner-sphere bonding interactions absent. REEs display a very rapid rate of ligand exchange (10^{-8} – 10^{-9} s) compared with other metals (e.g. Fe and Al 10^{-1} s) meaning that inner-sphere ligand substitution is rapid and not an inhibiting factor in the rate of phase transport.[44] Therefore, the rate of phase transport provides little information on the mechanism of extraction.

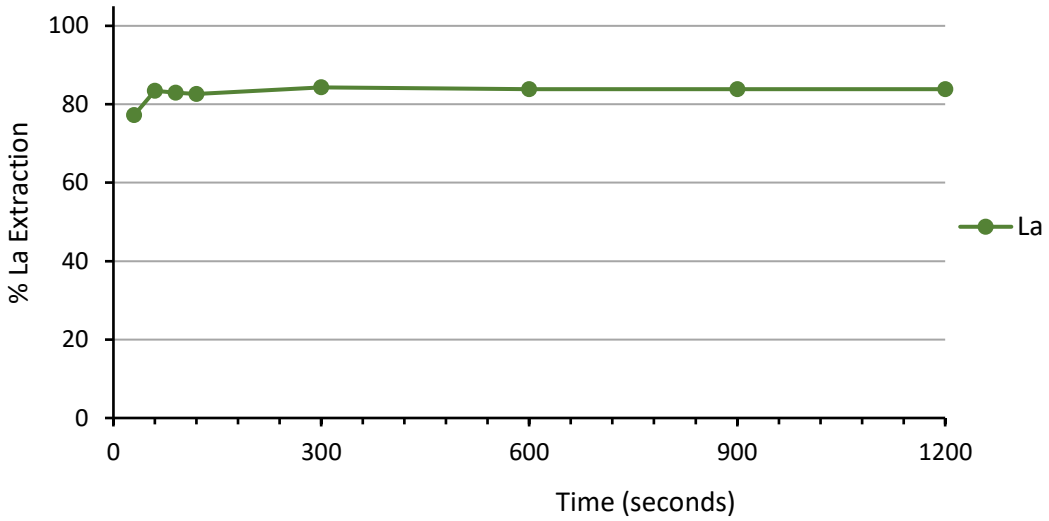

Figure 2.6.3 – The extraction of La (0.01 M) using **IL0** (0.10 M) in toluene from aqueous $NaNO_3$ (7.0 M) solution at various contact times. Interpolation used to aid the eye only.

2.6.4 Extractant Recycling and removal of REEs from the IL0 organic phase

In addition to rapid extraction, the ability to back-extract (or strip) REEs from the organic phase when using **IL0** is competitive when compared to current industrial reagents. Processes using reagents such as D2EHPA can require strong acid to remove REEs from the organic phase and increases the associated complexity and costs, but **IL0** only requires water to achieve total REE stripping from the organic phase.[73, 107, 125, 126] This results in the possibility for **IL0** to be reused multiple times with no noticeable decrease in performance. Indeed, undertaking six solvent extraction experiments (loading and stripping cycles) shows that the extraction of La (0.01 M) from a $NaNO_3$ (7.0 M) aqueous solution using **IL0** (0.10 M) remains roughly constant (68-78%) (Figure 2.6.4). The tendency to degrade or have modest aqueous solubility is one of the main issues associated with many industrial reagents in these processes (section 2.1).[70-73]

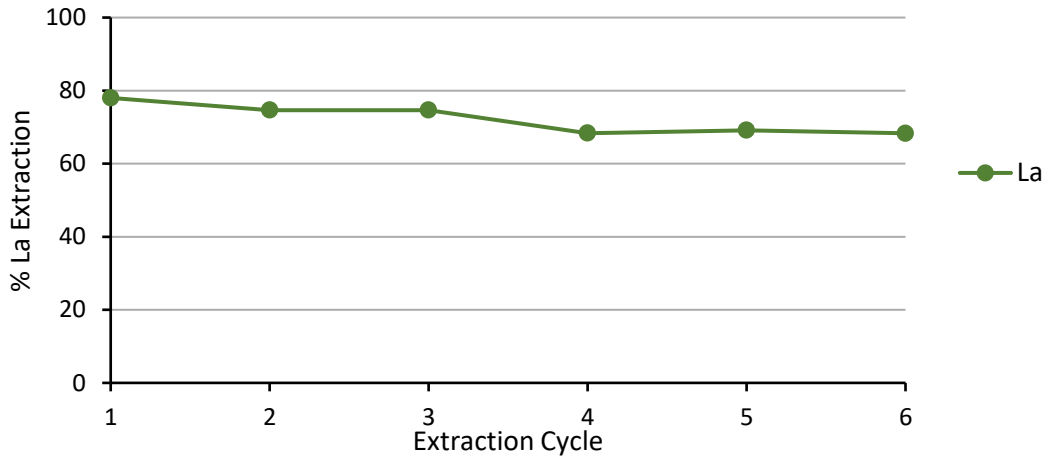

Figure 2.6.4 – The repeated extraction of La (0.01 M) using **IL0** (0.10 M) in toluene from aqueous solution of set $NaNO_3$ concentration (7.0 M).

2.6.5 Extraction of REEs from HNO_3 acid solutions

When acid is present in the aqueous phase the potential of both Aliquat 336 and Adogen 464 to extract REEs from aqueous solution is markedly reduced. **IL0** is equally affected. When **IL0** (0.10 M) was contacted with an acidic aqueous phase of $NaNO_3/HNO_3$ (5.0 M/0.01 – 2.00 M) and La (0.01 M), extraction of La was highest (63%) at low HNO_3 concentrations (0.01 M) (Figure 2.6.5). As HNO_3 concentration is increased beyond HNO_3 (0.10 M), a significant performance decrease was observed and no La extraction (<1%) occurs beyond HNO_3 (1.00 M), presumably due to HNO_3 out competing REEs (section 2.4).

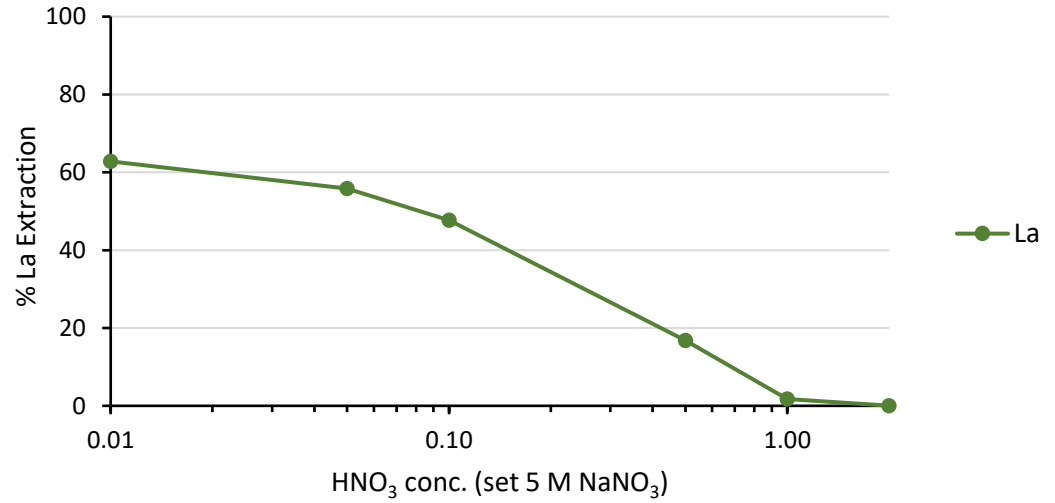

Figure 2.6.5 – The extraction of La (0.01 M) using **IL0** (0.10 M) in toluene from $NaNO_3/HNO_3$ (5.0 M/0.01-2.00 M) aqueous solution. Interpolation used to aid the eye only.

2.6.6 Extraction of REEs into a chloroform IL0 organic phase

If **IL0** (0.1 M) is diluted in chloroform, a more polar solvent than toluene, extraction of REEs from a nitrate solution ($NaNO_3$ 7.0 M) ceases to occur.[127] This indicates that the absence of polarity in the organic diluent is important to the overall recovery process and suggests that polar solvents hinder assembly formation in the organic phase during solvent extraction. When toluene is substituted out for chloroform during a gold recovery process involving amides, the formation of undesirable 3rd phases comprised of complex aggregates of metalate, amide toluene and water is eliminated.[122] In a different system, a Pt precipitate forms following Pt removal from an HCl (6 M) aqueous phase using amidoamines (0.01 – 0.20 M) in toluene. Replacement of toluene with chloroform in this system though completely supresses the removal of Pt from the aqueous phase.[24] This indicates that the disruption of charge neutral assembly formation by polar solvents has precedent.

While **IL0** could perhaps extract REEs more effectively into particularly non-polar diluents such as hexane, its insolubility in these solvents prevented performance testing. Using mesitylene (1, 3, 5-trimethylbenzene), a slightly less polar solvent than toluene, as a diluent, the extraction of La (0.01 M) from $NaNO_3$ (7.0 M) or $NaNO_3/HNO_3$ (5.0 M/0.01 – 2.00 M) aqueous solutions using **IL0** (0.1 M) in mesitylene is comparable to toluene (83% vs 89% and 56% vs 48%) (Figure 2.6.6).

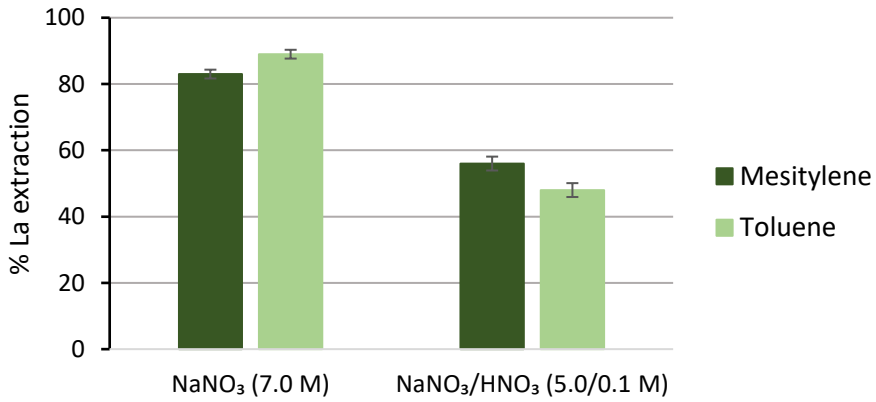

Figure 2.6.6 – La (0.01 M) extraction using IL0 (0.10 M) in mesitylene from $NaNO_3$ (7.0 M) or mixed $NaNO_3/HNO_3$ (5.0 M/0.1 M) aqueous solution. Recorded in triplicate.

2.6.7 Extraction of REEs using IL0 summary

Through varying a range of conditions including $NaNO_3$, **IL0** and HNO_3 concentrations, extraction time and organic diluent, the ability for **IL0** to extract REEs has been explored. In agreement with similar ammonium industrial reagents (Adogen 464/Aliquat 336), **IL0** rapidly extracts lighter REEs preferentially over heavier REEs but its ability to do so is substantially reduced by the presence of acid in the aqueous phase or the use of polar diluents. To understand why these trends are present a range of analytical and spectroscopic techniques were used to characterise the chemical complexes in the organic phase.

2.7 Characterisation of the organic phase assemblies

2.7.1 Karl-Fischer water content measurements

The solvent extraction work supports previous reports that show that the extraction of light REEs using ammonium ILs similar to **IL0** only occurs from low acid and high $NaNO_3$ concentration solutions and with an organic diluent that is comparatively non-polar. Little structural or chemical understanding of the organic phase assemblies or the mode of action by which recovery occurs has been determined from these solvent extraction experiments. Therefore, a series of analytical, spectroscopic, and computational techniques were used to gain a greater understanding of the speciation in the organic phase.

Once cation- and anion-based metal transport mechanisms (due to the absence of ionisable protons within ILs and the difficulty of aqueous phase REE metalate formation) are excluded, metal extraction by reverse-micelle formation is a potential alternative. This mode of action is often characterised by significant water co-transport into the organic phase due to the hydration sphere implicit to reverse-micelle formation (Figure 2.7.1.1).[50, 53] This sphere of water is surrounded by lipophilic, greasy extractant molecules with the overall formation energy of this organic phase stable assembly offsetting the unfavourable transportation of water.

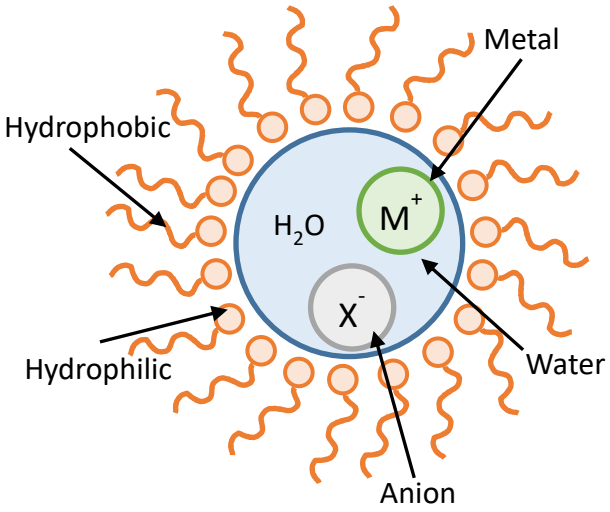

Figure 2.7.1.1 – A simplified representation of a reverse micelle.[53]

Karl-Fischer water content measurements were used to determine the amount of water transported by **IL0**. An increase in water uptake as the organic phase REE concentration increased would suggest reverse-micelle formation.[50]

Aqueous phases comprising $NaNO_3$ (7.0 M) and REE (0.01 M) were contacted with **IL0** (0.01 – 0.50 M) in toluene and the water content of the contacted **IL0** solutions was measured. A linear increase the volume of water transported is observed as **IL0** concentration increased irrespective of the aqueous phase composition (Figure 2.7.1.2). Additionally, the amount of water transported by **IL0** from an aqueous phase of REE (0.01 M) and $NaNO_3$ (7.0 M) was marginally lower than water alone. At 0.01 and 0.1 M **IL0** 713 and 2546 ppm of water, respectively, is transported by **IL0** from water alone, compared to 508 and 1338 ppm of water transported from aqueous La (0.01 M) and $NaNO_3$ (7.0 M).

Contacting an **IL0** (0.25 M) organic phase with an REE-containing aqueous phase ($NaNO_3$ 7.0 M, Nd 0.01-0.50 M) indicates that an increase in metal content results in a modest decrease in water content (Figure 2.7.1.3), decreasing from 2246 ppm at 0.1 M Nd to 1140 ppm at 0.5 M Nd. In contrast, studies using diamides to recover REEs or TBP to recover Pt by micellar modes of action show that the water content of the organic phase increases, linearly in some cases, with increasing metal loading.[43, 50, 53, 128] Given the absence of this occurring in the case of **IL0**, it can be confidently concluded that a reverse-micelle mechanism is not operating.

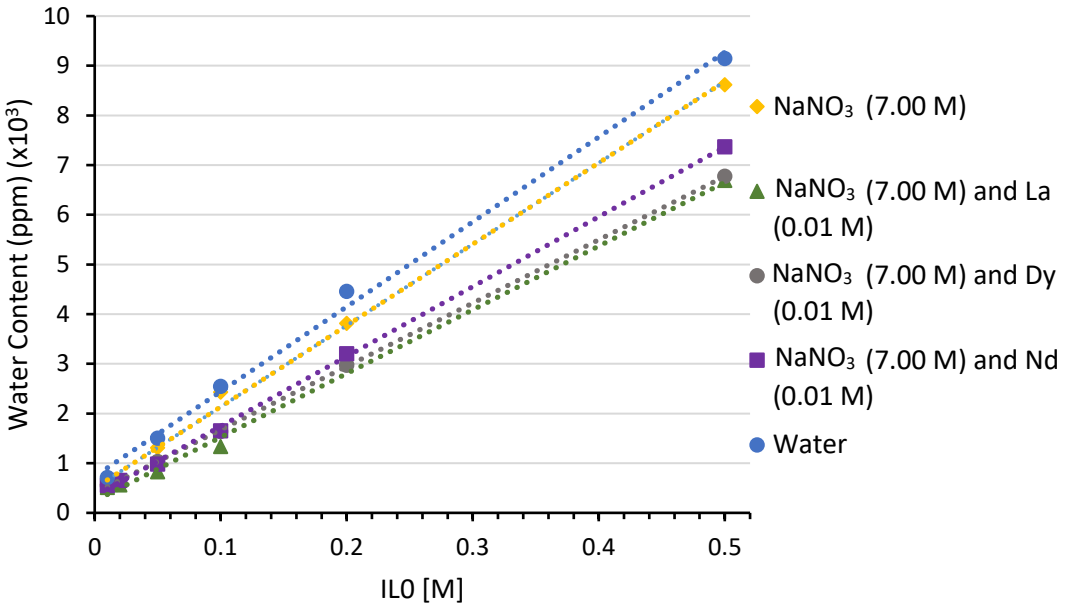

Figure 2.7.1.2 – Karl-Fischer water content measurements of solutions of **IL0** (0.01 - 0.50 M) organic phases after contact with various aqueous phases (water, $NaNO_3$ (7.0 M), REE (0.01 M) and $NaNO_3$ (7.0 M)).

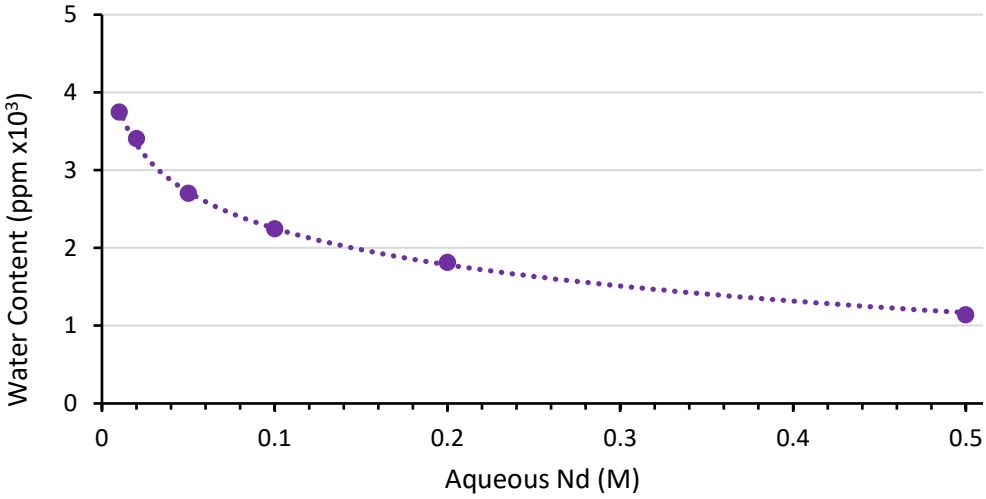

Figure 2.7.1.3 – Karl-Fischer water content measurements of solutions of **IL0** (0.25 M) organic phases after contact with an aqueous phase of varying Nd concentration ($NaNO_3$ 7.0 M, Nd 0.01-0.5 M).

2.7.2 Mass spectrometry of the IL0 organic phase

To gain an insight into the speciation of the REEs following transport into the organic phase, a series of organic phase samples were prepared and analysed by mass spectrometry.

Positive-ion mode electrospray ionisation - mass spectrometry (+ve ESI-MS) of **IL0** alone (0.05 M) and the **IL0** (0.05 M) negative-ion (-ve) mode ESI-MS after multiple contacts with aqueous La, Nd and Dy solutions (0.05 M) were recorded. The +ve ESI-MS of **IL0** alone shows a series of ions of the general formula $(NR_4)(\mathbf{IL0})_n^+$ (where NR_4 is the ammonium cation and n = 0 – 3) (Figure 2.7.2.1). A repeating unit of 430.42 mass units was identified and assigned as the addition of one **IL0**, i.e. comprising an ammonium cation and nitrate anion.

Following REE transport, anions containing a REE cation, ammonium cations and nitrate anions are identified in the -ve ESI-MS of the organic phases (Figure 2.7.2.2), and are assigned the general formula $REE(NO_3)_4(\mathbf{IL0})n^-$ (where n = 0 – 3). A repeating unit of *m*/*z* 430.42 correlating to **IL0** is observed. No ions of more than three **IL0** are seen, but the cone voltage applied during spectrum acquisition, despite being comparatively low in mass-spectrometry terms, could result in higher-order assemblies fragmenting.[129, 130] No assemblies involving water are observed but small ionisable, polar molecules such as water are well documented as being difficult to observe by ESI-MS. Even so, recent studies have begun to elucidate the number of inner-sphere water molecules present within $REE(DOTA)^-$ and $REE(EDTA)^-$ complexes by using variable temperature ESI-MS.[131]

ESI-MS analysis suggests the mode of REE recovery is comparable across the series and occurs through the formation of $REE(NO_3)_3(\mathbf{IL0})_3.xH_2O$ (where $x \geq 0$) aggregates in the organic phase. The limitation of mass spectrometry in this instance though arises from the inability to provide extensive information on the composition of the inner-coordination sphere and that the ions seen may not be representative of the neutral complexes that must reside in the organic phase of a solvent extraction experiment.

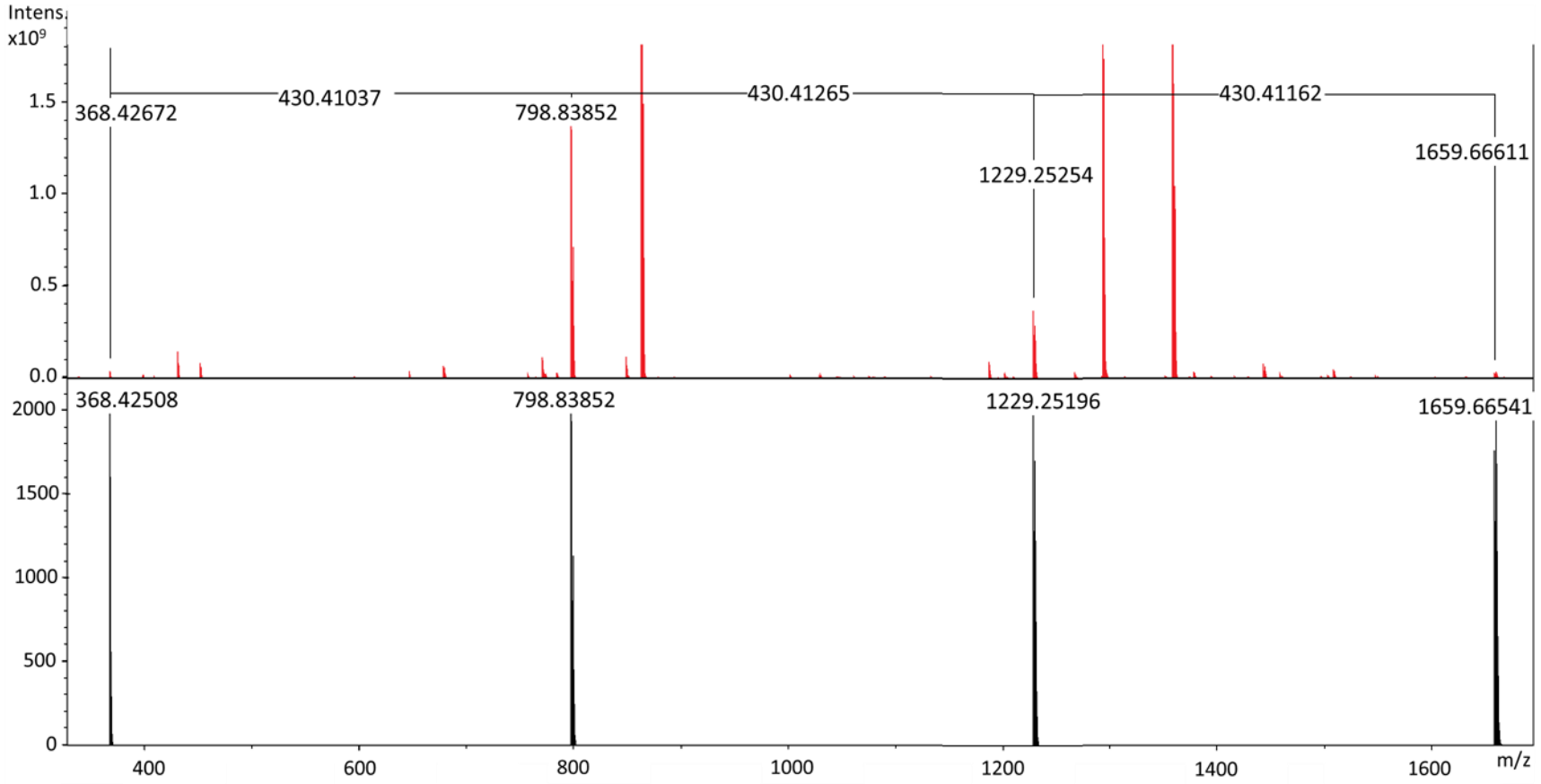

Figure 2.7.2.1 – Positive-ion mode ESI-MS of **IL0** (0.05 M) diluted with methanol (1:25,000). Cations of the general formula NR_4(**IL0**)n^+ with *m/z* ratios of 368.4267 (n = 0, calc. 368.4251), 798.8385 (n = 1, calc. 798.8385), 1229.2525 (n = 2, calc. 1229.2520) and 1659.6661 (n = 3, calc. 1659.6654) are identified.

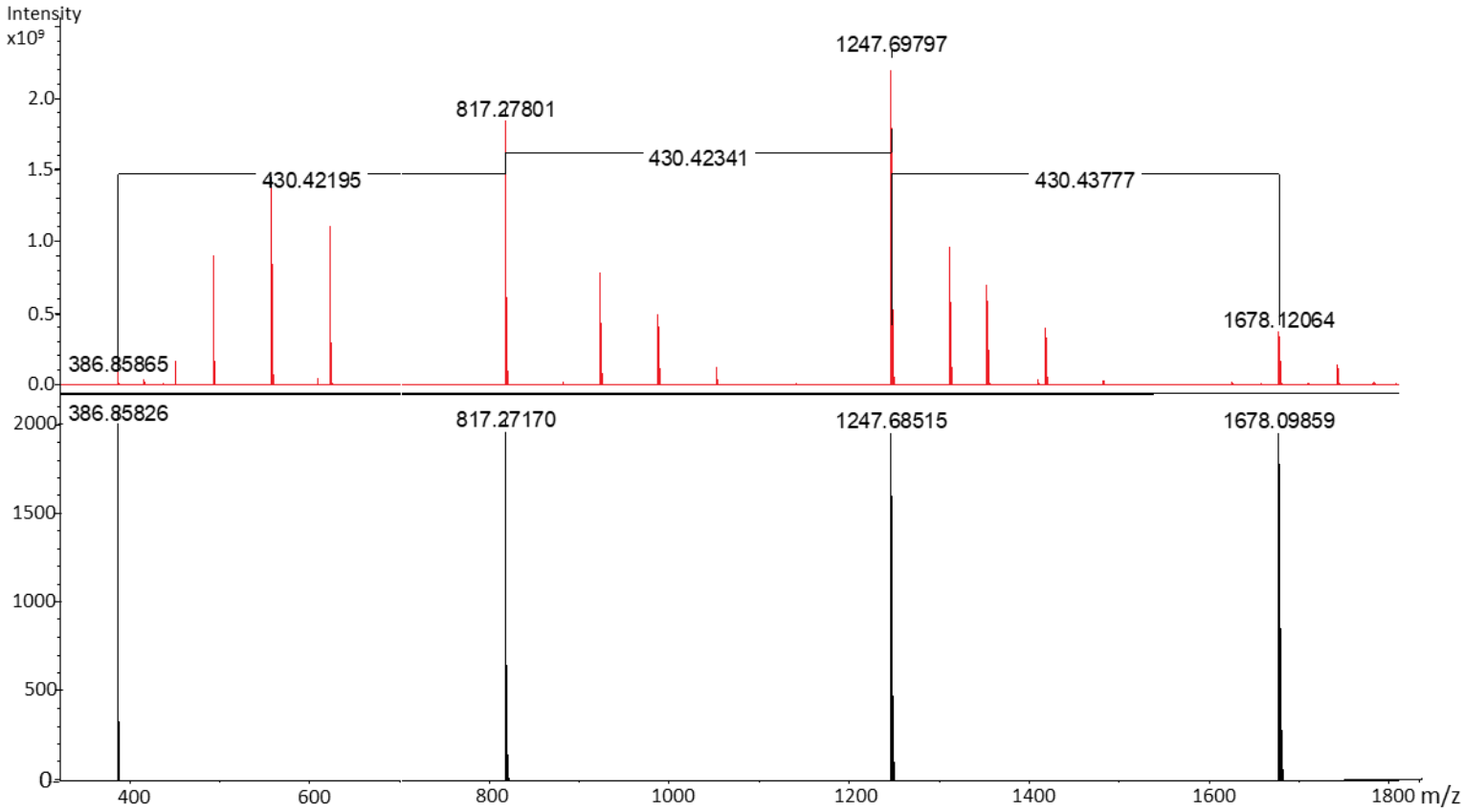

Figure 2.7.2.2 – Negative-ion mode ESI-MS of **IL0** (0.05 M) diluted with methanol (1:25,000) after contact with a $NaNO_3$ (7.0 M) aqueous phase containing La (0.05 M). Anions of the general formula $La(NO_3)_4$(**IL0**)n^- with *m*/*z* ratios of 386.8587 (n = 0, calc. 386.8583), 817.2780 (n = 1, calc. 817.2717) and 1247.6980 (n = 2, calc. 1247.6852) are identified.

2.7.3 ^{1}H, ^{13}C, ^{15}N and ^{139}La NMR studies

Upon ligand complexation to a metal centre, the chemical shift in the NMR spectra of nuclei associated with the ligand can change quite substantially. For example, $^{31}P[^{1}H]$ spectroscopy has been applied previously to understand the speciation of REE-organophosphorus compounds following extraction.[59, 126] The ammonium cation of **IL0** cannot coordinate directly to the REE but a significant change in the chemical shifts of nuclei associated with the ammonium following REE extraction could suggest a strong electrostatic interaction towards an anionic REE nitratometalate. Selective anion binding is extensively reported and NMR spectroscopy is frequently used to quantify and understand the binding interactions.[46-48] For example, the selective uptake of KF rather than CsF from an aqueous solution by a calix[4]-pyrrole-calix[4]crown (Figure 2.7.3.1) ion-pair receptor in nitrobenzene has been studied by NMR spectroscopy.[46] Following KF uptake, the N**H** peaks in the ^{1}H spectrum of the ion-pair receptor shifted by 5.1 ppm and this was concluded to be due to a remarkably strong hydrogen-bonding interaction towards fluoride.

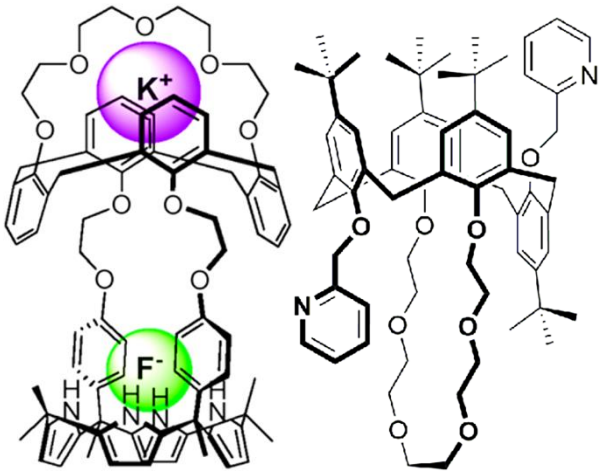

Figure 2.7.3.1 – A calix[4]-pyrrole-calix[4]crown ion-pair receptor for KF (left).[46, 47] A calixcrown system for CsI recovery (right).[132]

In another study, shifts in the ^{1}H NMR spectrum of calixcrown system (Figure 2.7.3.1) were used to determine the selective uptake of CsI into a water immiscible fluorinated solvent over $CsNO_3$, NaI and KI.[47, 132] The Cs^{+} was encapsulated within the crown-ether while, I^{-} ions were confirmed by ^{19}F NMR to be stabilised by halogen bonds to the fluorinated solvent 1,8-diiodoperfluorooctane.

To probe the interaction between **IL0**, water molecules and nitrate anions and REE in the system described earlier, the ^{1}H, ^{13}C and ^{15}N NMR spectra of a solution of **IL0** (0.05 M) in deuterated benzene was recorded before and after contact with an aqueous solution of La (0.01 M) and $NaNO_3$ (7.0 M).

The change in the chemical shifts in the ^{1}H (Table 2.7.3), ^{13}C [^{1}H] and HMBC long-range ^{1}H-^{15}N correlation NMR spectra of **IL0** on contact were minimal, indicating, as expected, only outer-sphere interactions between the ammonium cation and the (potentially hydrated) La nitratometalate species occurs. The largest proton chemical shifts correlated to those situated nearby the nitrogen centre of the ammonium cation; the three methyl $NC\mathbf{H}_3$ protons were shifted from 3.44 ppm to 3.25 ppm and the six $N(C\mathbf{H}_2R)_3$ protons were shifted from 3.39 ppm to 3.16 ppm respectively, indicating minor shielding or a removal of electron density from N^+.

Table 2.7.3 – The change in ^{1}H chemical shifts for **IL0** (0.05 M) following contact with a La (0.05 M), $NaNO_3$ (7.0 M) aqueous phase. NMR recorded in deuterated benzene.

Assigned Proton	^{1}H NMR shift before La (0.05 M) loading (ppm)	^{1}H NMR shift after La (0.05 M) loading (ppm)
$NC\mathbf{H}_3$	*3.44*	*3.25*
$NC\mathbf{H}_2R$	*3.39*	*3.16*
$NCH_2C\mathbf{H}_2R$	*1.63*	*1.58*
$RC\mathbf{H}_3$	*1.08*	*1.11*

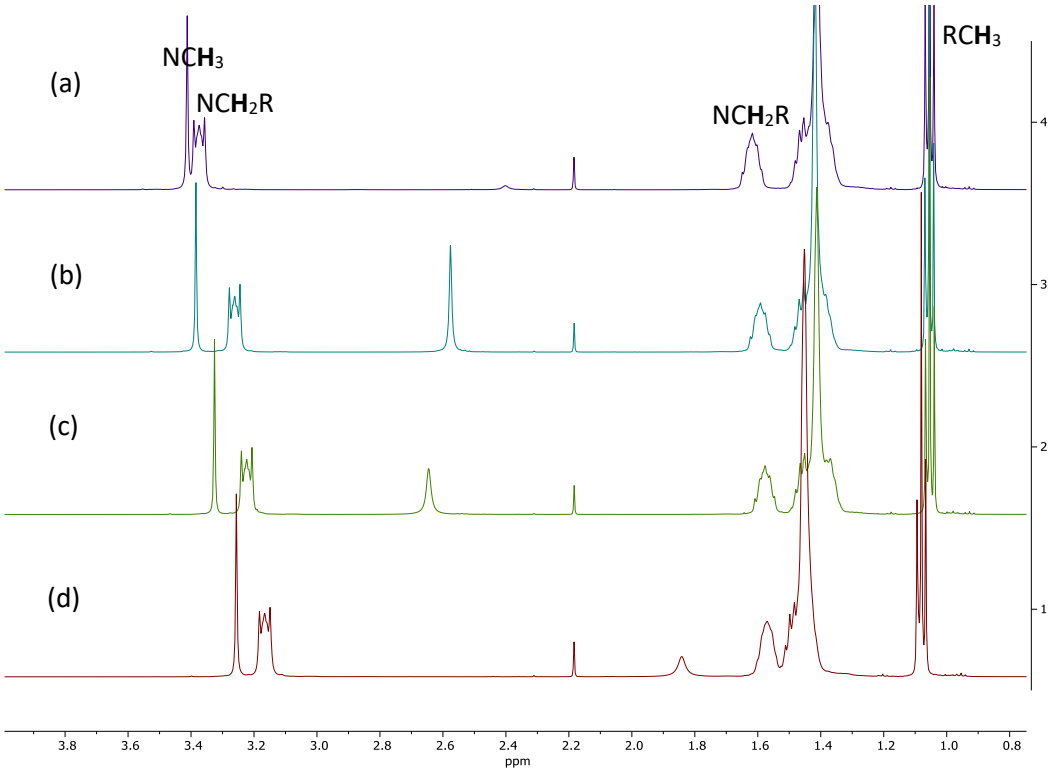

Figure 2.7.3.2 – A comparison of the ^{1}H NMR spectra of **IL0** (0.05 M) in deuterated benzene. From top to bottom: Before contact (a), following contact with water (b), following contact with a $NaNO_3$ (7.0 M) aqueous phase (c) and following contact with a La (0.05 M) and $NaNO_3$ (7.0 M) aqueous phase (d).

Contacting **IL0** (0.05 M) in deuterated benzene with water alone resulted in very minor ^{1}H chemical shifts with the three methyl NC**H**$_3$ protons only shifting from 3.44 ppm to 3.41 ppm suggesting the minor shifts upon La loading correlate to outer-sphere interactions associated with **IL0**-REE metalate aggregation (Figure 2.7.3.2). This is supported by the equally minor chemical shifts observed upon contacting with a $NaNO_3$ (7.0 M) aqueous solution, with the three methyl NC**H**$_3$ protons only shifting from 3.44 ppm to 3.36 ppm.

To probe the inner coordination sphere of the La cation, the ^{139}La spectrum of **IL0** (0.05 M) in toluene after contact with an aqueous phase of $NaNO_3$ (7.0 M) and La (0.05 M) was recorded and compared against the ^{139}La standard of $LaCl_3$ (0.01 M) in D_2O. Despite a poor signal-to-noise ratio, a distinct broad peak at -60 ppm ($w_{1/2}$ -44 to -76 ppm) can be observed in the ^{139}La spectrum (Figure 2.7.3.3). This chemical shift is consistent with the coordination of NO_3^- anions to the La along with dehydration of the REE centre.[133] Additionally, the breadth of

signal suggests that multiple, low symmetry nitrato complexes are present, in agreement with the ESI-MS data above.

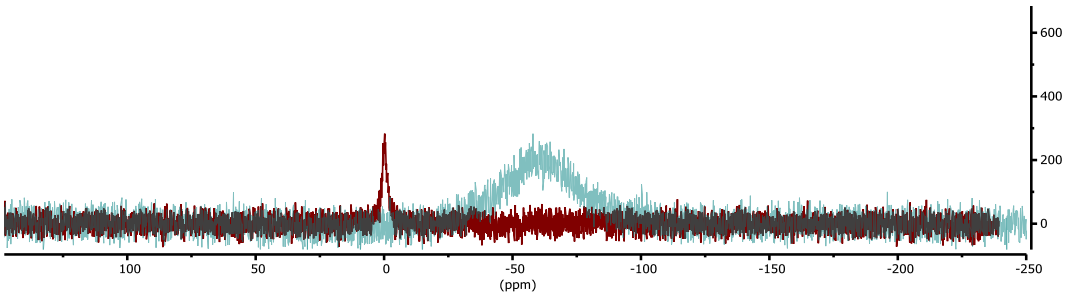

Figure 2.7.3.3 – A comparison of the ^{139}La NMR spectra of **IL0** (0.05 M) in toluene after contact with aqueous $NaNO_3$ (7.0 M) and La (0.01 M) (blue), and the ^{139}La standard of $LaCl_3$ (0.01 M) in D_2O (red).

2.7.4 Nitric acid and sodium nitrate transport

Nitric acid significantly hinders the extraction of REEs from aqueous solution, potentially through competitive extraction given that ILs are known to transport nitric acid from aqueous solution into an organic phase (sections 2.4 and 2.6.5).[123] The amount of nitric acid and sodium nitrate transported from the aqueous to organic phase by **IL0** was quantified by a combination of pH measurements, Na ICP-OES, and ion-chromatography (IC) measurements.

IL0 (0.10 M) in toluene was contacted with aqueous phases of varying concentrations of HNO_3 (0.01 - 1.00 M), $NaNO_3/HNO_3$ (5.0 M/0.01 – 2.00 M) and $NaNO_3/HNO_3$/La (5.0 M/0.01 – 2.00 M/0.01 M). The organic phases were separated and then contacted with water, and the resulting aqueous phases were then analysed. It was found that as the nitric acid concentration of the initial aqueous phase increases (0.01 – 2.00 M), the pH of the final strip solution decreases (3.52, 2.28 and 2.30 to 1.40, 1.38 and 1.44 respectively), meaning an increasing amount of nitric acid is transported into the organic phase by **IL0** (Figure 2.7.4.1). In every case, a lower pH was recorded from samples containing $NaNO_3$ (5.0 M), indicating $NaNO_3$ promotes the transport of HNO_3 from the aqueous phase. This means that the extraction of both HNO_3 and REE $(NO_3)_3$ using **IL0** is increased by the presence of $NaNO_3$ in the aqueous phase. The equilibrium in both Eq 2.7.4.1 (HNO_3 extraction) and 2.7.4.2 (REE $(NO_3)_3$ extraction) moves towards the RHS when $NaNO_3$ is present. This can be attributed to the same ‘salting-out’ affect as observed when the extraction of REEs is increased through

high aqueous salt content but with the replacement of $La(NO_3)_3$ (equation 2.4.1) in the equation with HNO_3 (equation 2.7.4).[107, 108, 118]

Eq. 2.7.4.1 – $H^+_{(aq)} + NO_3^-{}_{(aq)} + x\ IL_{(org)} \rightleftharpoons (HNO_3)(IL)_{x(org)}$

Eq. 2.7.4.2 – $REE^{3+}_{(aq)} + NO_3^-{}_{(aq)} + x\ IL_{(org)} \rightleftharpoons REE(NO_3)_3(IL)_{x(org)}$

There is no discernible difference in pH values upon addition of a REE to the aqueous phase suggesting that the 'salting-out' of nitric acid is almost exclusively from the high sodium nitrate content.

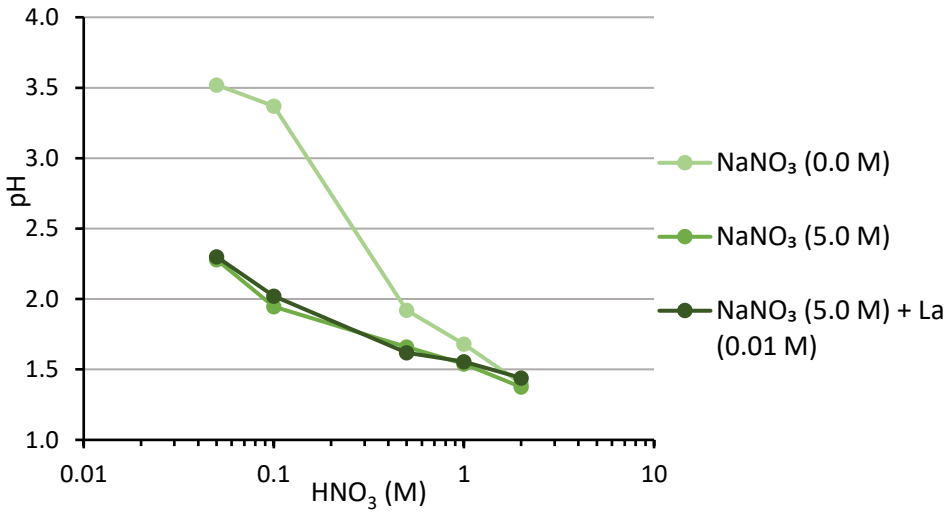

Figure 2.7.4.1 – The pH of aqueous solutions following contact of **IL0** (0.1 M) in toluene with HNO_3 (0.01 – 2.00 M), $HNO_3/NaNO_3$ (0.01 – 2.00 M/5.0 M) and $HNO_3/NaNO_3$/La (0.01 – 2.00 M/5.0 M/0.01 M). Interpolation used to aid the eye only.

IC measurements reveal higher nitrate anion content in the final aqueous strip solutions following **IL0** (0.10 M) contacts with initial $NaNO_3$ (5.0 M) containing aqueous phases than with nitric acid alone (Figure 2.7.4.2). Nitrate anion concentrations of 7.3 mM (HNO_3 0.1 M), 20.9 mM ($NaNO_3/HNO_3$ 5.0 M/0.1 M) and 36.4 mM ($NaNO_3/HNO_3$/La 5.0 M/0.1 M/0.01 M) were found respectively in the final aqueous strip solutions. Additionally, as the nitric acid concentration was increased in the starting aqueous solutions, the nitrate anion concentrations in the final aqueous strip solutions increase, corroborating the pH measurement results.

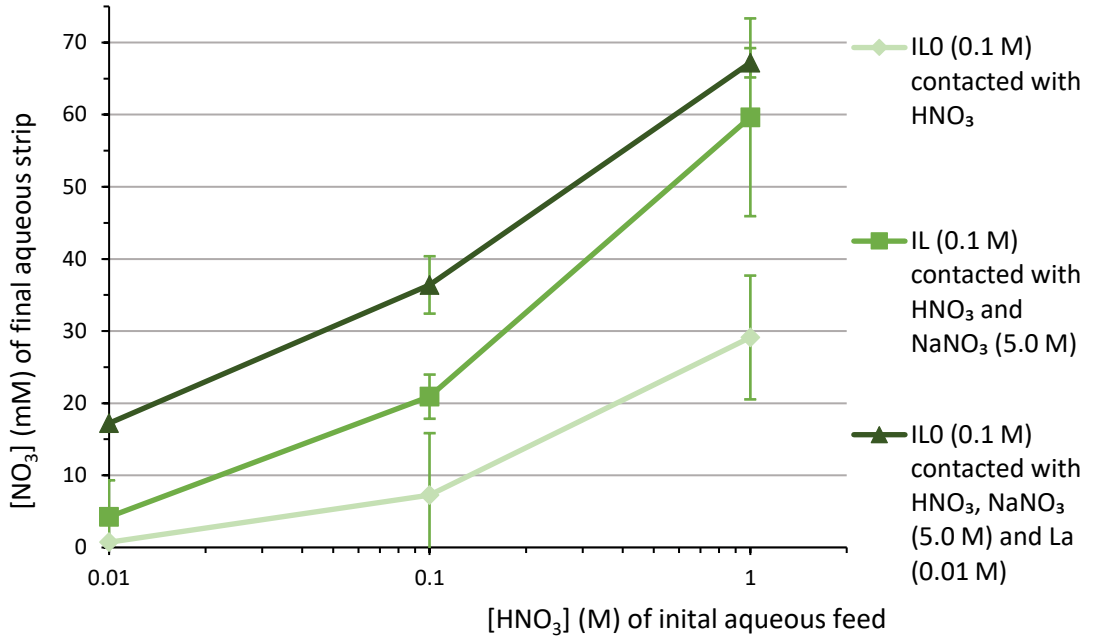

Figure 2.7.4.2 – The nitrate anion content of aqueous solutions following contact of **IL0** (0.1 M) in toluene with HNO_3 (0.01 – 1.00 M), $HNO_3/NaNO_3$ (0.01 – 1.00 M/5.0 M) and $HNO_3/NaNO_3/La$ (0.01 - 1.00 M/5.0 M/0.01 M). Interpolation used to aid the eye only.

IC measurements reveal the amount of nitrate anions transported but provide no information on what the accompanying counter cations are. The nitrate anions may be transported exclusively as HNO_3 or may be transported as a combination of both HNO_3 and $NaNO_3$. Using Na ICP-OES, the percentage of Na and therefore the percentage of $NaNO_3$ transported was quantified. The amount of Na transported is negligible (<1%) (Figure 2.7.4.3), presumably due to the high hydration enthalpy of Na^+, and shows that $NaNO_3$ is not transported by **IL0**.[50, 85]

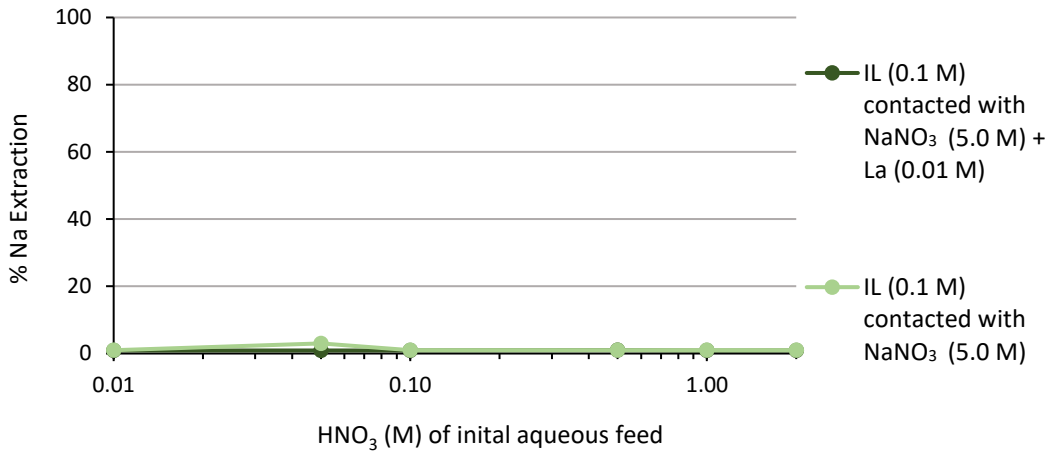

Figure 2.7.4.3 – The extraction of Na from aqueous solutions following contact of **IL0** (0.1 M) in toluene with $HNO_3/NaNO_3$ (0.01 – 1.00 M/5.0 M) and $HNO_3/NaNO_3/La$ (0.01 – 1.00 M/5.0 M/0.01 M).

2.7.5 Infrared spectroscopy

Infrared spectrometry (IR) has been used to confirm inner-sphere binding of D2EHPA to REEs through analysis of the P=O bond stretching frequencies.[59] In our case, IR provided limited characterisation data. The IR spectrum of an **IL0** (0.05 M) organic phase in toluene was initially recorded against a toluene background. Multiple C-H stretches were identified between 2800 – 3000 cm^{-1} while stretches at 1467 and 1341 cm^{-1} were assigned as symmetric and asymmetric N-O bond stretches (Figure 2.7.5). Recording a solution IR spectrum of **IL0** (0.05 M) after $NaNO_3/La$ (7.0 M/ 0.05 M) contact resulted in modest shifts of the N-O stretches to 1435 and 1330 cm^{-1} with no additional new peaks. The modest shifts indicate possible weakening of the N-O bonds that could arise from coordination of nitrate to the La centre.

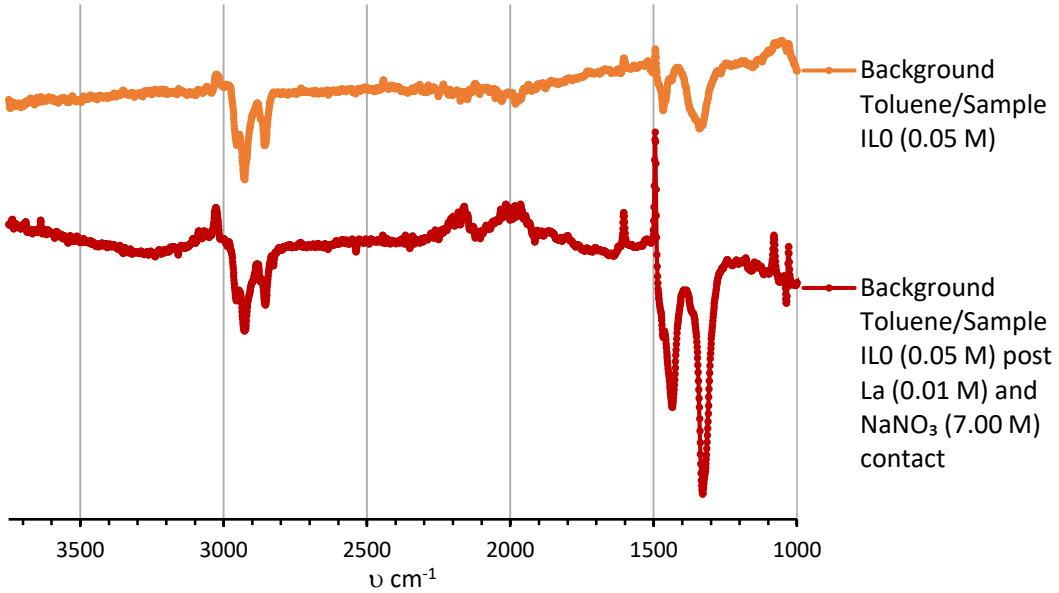

Figure 2.7.5 – The IR spectra of **IL0** (0.05 M), pre and post contact with $NaNO_3$ (7.0 M) plus La (0.05 M) compared against a toluene background.

2.7.6 Summary of spectroscopic techniques

It can be concluded that the extraction of REEs from aqueous solution using **IL0** does not occur through a (reverse) micelle pathway, with instead ESI-MS and NMR data indicating that multiple NO_3^- anions are coordinated in the inner-sphere of a partially dehydrated REE to form a series of anions $REE(NO_3)n(H_2O)x^-$ (where n>3 and x>0) that are stabilised by electrostatic associations with lipophilic NR_4^+ cations. While the ESI-MS and NMR data both provide valuable information, the binding mode of nitrates to REEs and the number of waters present in the inner coordination sphere remain unknown. As such, computational studies were undertaken to further interrogate the structures and bonding in the organic phase.

2.8 Computational modelling of the organic phase assemblies

2.8.1 Overview and introduction

The aggregation of the different components of the organic phase, i.e. **IL0**, nitrate, water and REE, and the interactions between these components, was investigated by computational modelling. In order to maximise the validity of the modelling, the calculations undertaken represent, as closely as possible, the experimental conditions with the well-defined experimental ratios of **IL0**:nitrate:water:REE being used as the basis for these calculations.

The ESI-MS showed that the predominant **IL0**-REE aggregate in the toluene organic phase comprised three **IL0**, three nitrate anions and a single REE. The KF water content measurements indicated on average one water molecule per **IL0**. Therefore, the interactions between three **IL0**, three nitrate anions, three water molecules and one La^{3+} cation were modelled. La was selected due to its comparative ease of extraction using **IL0** and its lack of f-electrons.

Due to computational limitations, simulations modelling the formation of aggregates in the organic phase were run using classical molecular dynamics (MD). The QM optimised structures of the relevant components (ammonium cation, nitrate anion, water and toluene) (Figure 2.8.1) were obtained from geometry optimisation calculations with Gaussian 09 at the B3LYP level of theory with the basis set 6-31+G* applied (section 7.6).

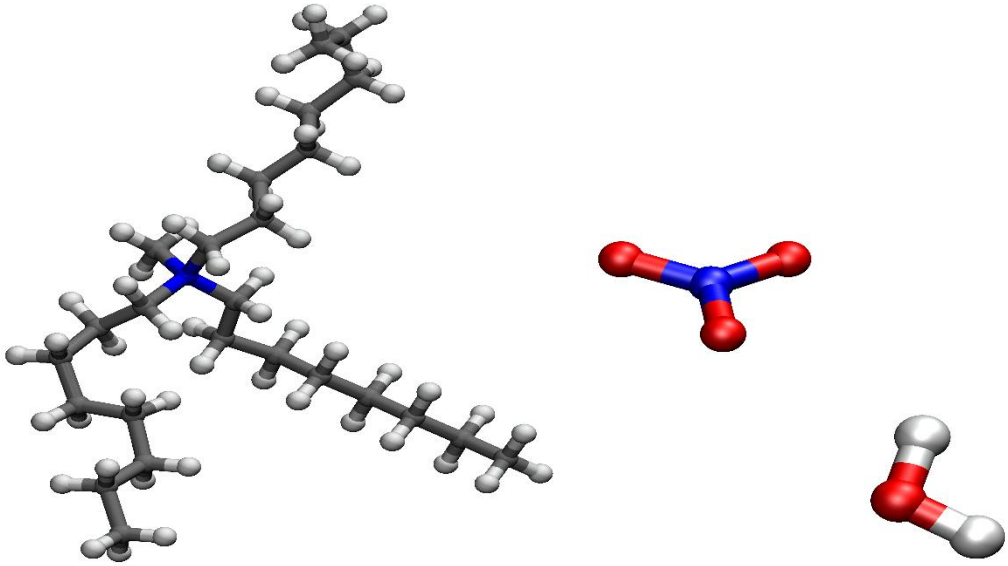

Figure 2.8.1 – The optimised starting geometries for the relevant components. Ammonium cation (left). Nitrate anion (centre). Water molecule (right).

2.8.2 Classical MD simulations with nitrate and REE

Three **IL0** extractants, three nitrate anions, three water molecules and one La^{3+} cation were placed into a 60 $Å^3$ randomly configured toluene solvent box consisting of 1147 toluene molecules and was allowed to proceed under classical MD conditions for a minimum of 10 ns of production run time. All further details are provided in section 7.6. An aggregation of ammonium cations, nitrate anions and water molecules is observed, with multiple nitrate

anions and water molecules closely associated with a partially dehydrated La centre (Figure 2.8.2.1). This MD simulation and all other MD simulations discussed within this section were repeated in triplicate, starting from different starting geometries in each case (section 7.6). In each instance, the same general aggregates were observed.[113]

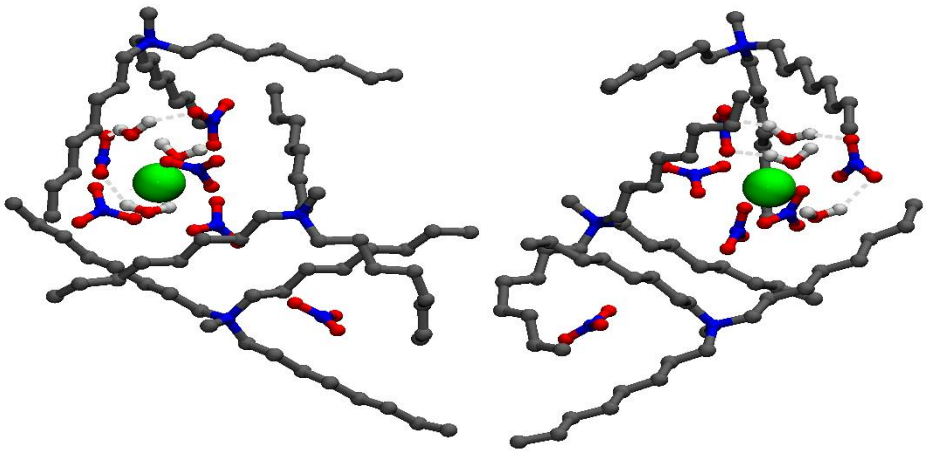

Figure 2.8.2.1 – The formation of a REE-**IL0**-water-nitrate aggregate following a classical MD simulation (left – front, right – reverse). For clarity, hydrogen atoms associated with the ammonium cation are hidden, and hydrogen bonds are made explicit up to an O…H distance of 2.0 Å. These conditions are the case for all future simulation outputs, unless stated.

Closer inspection of the aggregate reveals that its stability is increased through a modest hydrogen-bonding network comprising nitrate anions and water molecules (Figure 2.8.2.1). Structural information about the aggregation and the REEs inner-coordination sphere is determined by analysing the average number of water molecules, nitrate anions and ammonium cations at defined distances from the REE across the simulation (Figure 2.8.2.2). Over the simulation run time, it is seen that five nitrate anions continually associate with the La centre (<3.85 Å), along with three water molecules (<2.85 Å), and three nitrogen atoms from the encapsulating ammonium cations (<9.75 Å). The sixth and final nitrate anion is over 10.0 Å away from the La centre. Thus, overall, the composition of the La centre of the aggregate formed by the interdigitation of three **IL0** ligands comprises three water molecules and five nitrate anions.

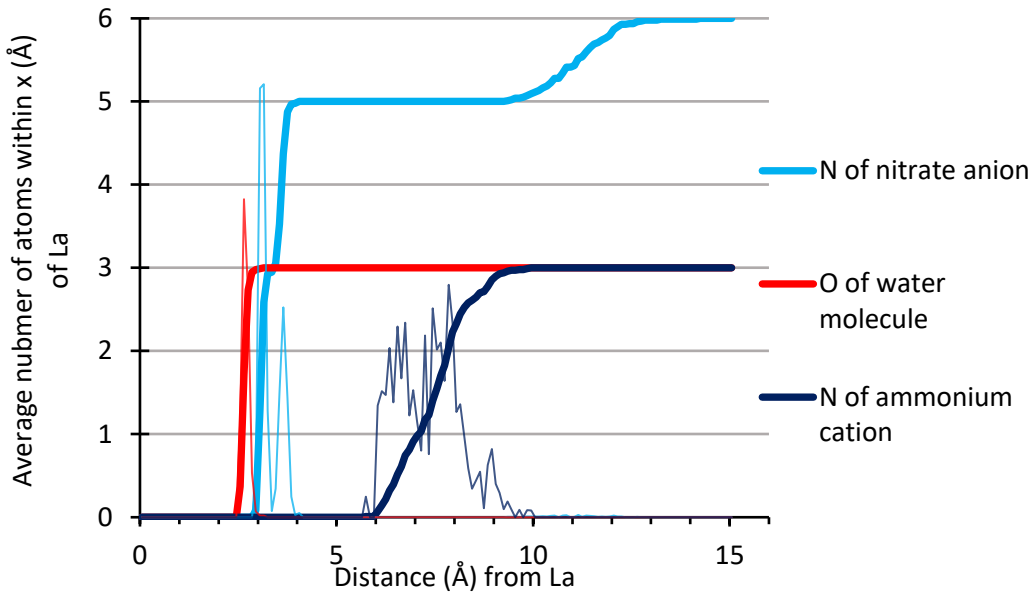

Figure 2.8.2.2 – Integrations obtained from the g(r) output plot from the classical MD simulations, indicating how the average number of IL extractants, water molecules and nitrate anions associated with La increases as a function of distance from La, following the spontaneous formation of a La-containing aggregate. Averaged over 100 simulation frames (1.5 ns).

In the aggregate, the La centre was calculated from 50 simulation frames to be 4.9 ± 0.4% exposed by using a Monte Carlo script (section 7.6.2), where the La centre was defined as the target and a probe sphere was fired 10,000 times from random positions, 20 Å away. This is particularly low when compared to similar tributylphospate and $PtCl_6^{2-}$ systems that have a core exposure value >53%.[43] This suggests that the cavity created by the **IL0**, nitrate anions and water molecules is well suited to accommodate a cation of the radius of La^{3+}, corroborating the experimental data of strong La extraction by **IL0**.[43, 134]

2.8.3 Classical MD simulations with nitrate anions and nitric acid

The experimental results (sections 2.6.5. and 2.7.4.) show a competing process between nitric acid and REE extraction. As such, it is informative to model this former process, using three ammonium cations, four nitrate anions, three water molecules and a hydronium cation under the same conditions and parameters. In this case, the aggregation is similar to that seen for La, but a hydronium cation now occupies the cavity created by the ammonium cations (Figure 2.8.3.1). Three nitrate anions (<3.75 Å) interact with the hydronium cation

through hydrogen-bonding while the fourth nitrate anion is further away (>8.0 Å) (Figures 2.8.3.1 and 2.8.3.2).

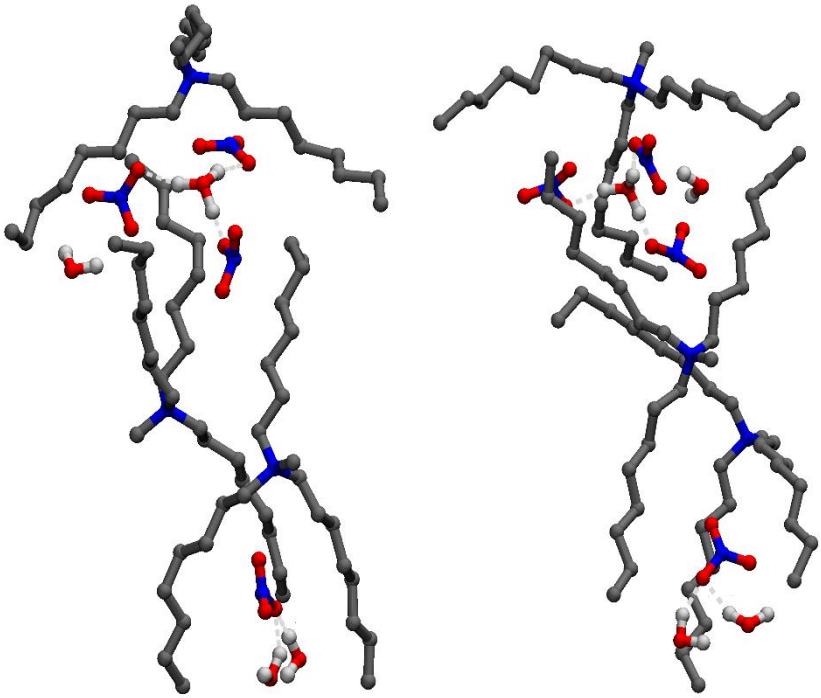

Figure 2.8.3.1 – The formation of a nitric acid-**IL0**-water aggregate following a classical MD simulation (left – front, right – reverse).

The very gradual increase in the average number of water molecules within a defined distance of the hydronium ion suggests that the water molecules are particularly mobile and dynamic, and are not fixed into position by inter-molecular hydrogen-bonding. Comparing hydronium-water distances against time (Figure 2.8.3.3) reveals that one water molecule is generally closer at 4.2 – 7.7 Å while the remaining two are generally further away (>6.8 Å). The three ammonium cations are within 8.75 Å of the hydronium centre vs. 9.75 Å in the La system, suggesting a smaller cavity.

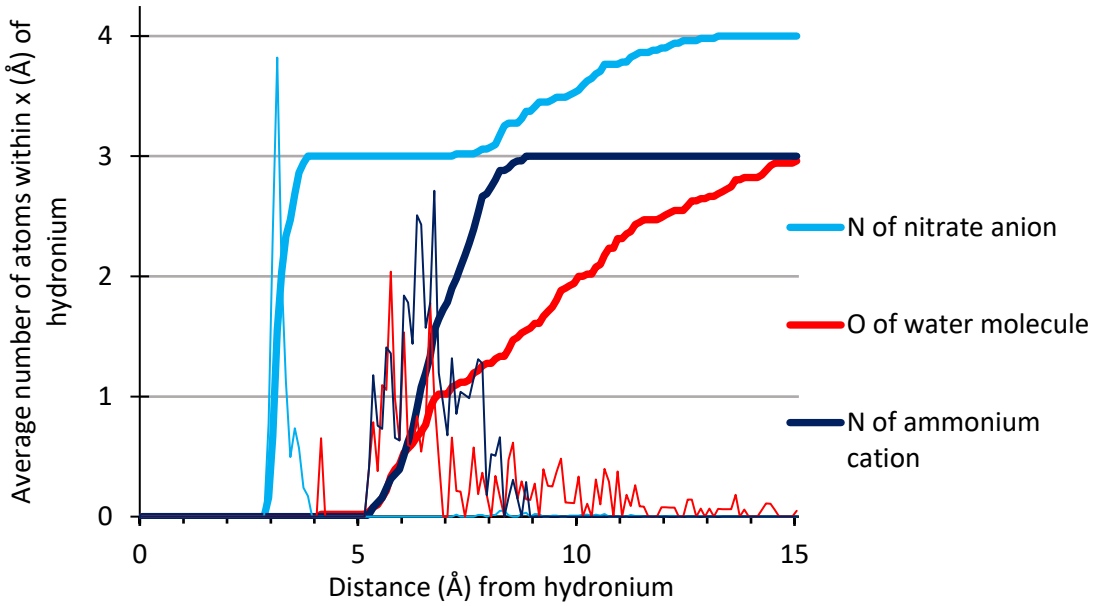

Figure 2.8.3.2 – Integrations obtained from the g(r) output plot from classical MD simulations indicating how the average number of IL extractants, water molecules and nitrate anions associated with a hydronium cation increases as a function of distance from a hydronium cation following the spontaneous formation of a hydronium cation-containing aggregate. Averaged over 50 simulation frames (0.75 ns).

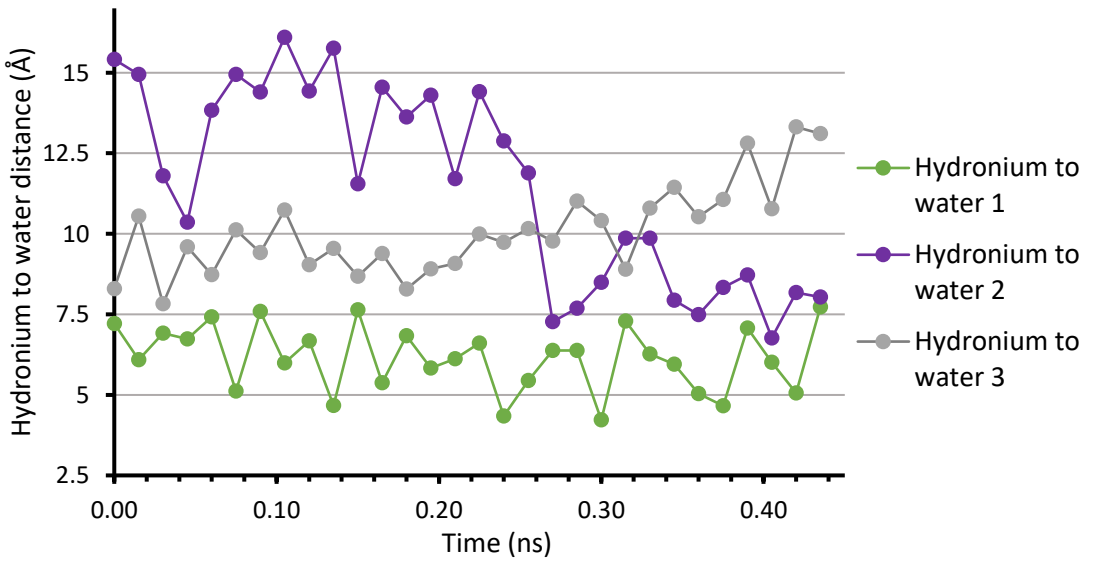

Figure 2.8.3.3 – An output from classical MD simulations showing how hydronium-water distances change as the simulation progresses.

Upon substitution of La for hydronium, the spherical nature of the aggregate appears, visually, to be markedly reduced and more cylindrical, with three lipophilic alkyl arms of the

ammonium encapsulating two water molecules and one nitrate anion disassociated and distant from the hydronium cation (Figure 2.8.3.1). Encapsulating measurements were undertaken with the hydronium cation as the centre point using a Monte Carlo script (section 7.6.2), and show an average exposure across 50 simulation frames of 11.8 ± 5.9 %, suggesting the hydronium cation is more poorly encapsulated than La. The large variance can be attributed to the relatively dynamic nature of the aggregate. The formation of HNO_3 containing aggregates similar to those formed with La, provides some computational evidence as to why competitive extraction between HNO_3 and REEs occurs. As **IL0** can form stable assemblies with both La and HNO_3, a high HNO_3 concentration reduces the concentration of **IL0** available to extract REEs (e.g. La) subsequently lowering the % of REE extracted (Figure 2.6.5).

2.8.4 Classical MD simulations with chloride and REE

The difficulty of recovering REEs with ILs from initial aqueous chloride media due to the inability to form REE chloridometalate anions in the aqueous phase, is well known.[42, 113, 135] To investigate if stable aggregates consisting of **IL0** and REE-chloridometalates can form in the organic phase, the MD simulation undertaken in section 2.8.2 were repeated but with nitrate anions replaced with chloride anions. A stable organic phase aggregate containing a REE-metalate anion still forms, albeit one which has reduced sphericity and, visually, poor encapsulation of the La cation (Figure 2.8.4.1). The La metal centre visually appears to have a coordination number of seven, with five chloride and two water molecules no further than 3.35 Å and 2.85 Å away respectively (Figure 2.8.4.2) .

Work prior to this study suggests nine-coordinate La complexes are typical, meaning the La centre is probably not entirely satisfied in these MD simulations.[42, 63, 86, 88, 109, 121, 136] While a stable aggregate is observed within the MD simulations, the comparatively low number of ligands surrounding the La core may explain why La-chloridometalate anions form less readily in the organic phase when starting from an aqueous La containing chloride media. Furthermore, the absence of any hydrogen-bonding interactions can be expected to reduce the stability of the aggregate.

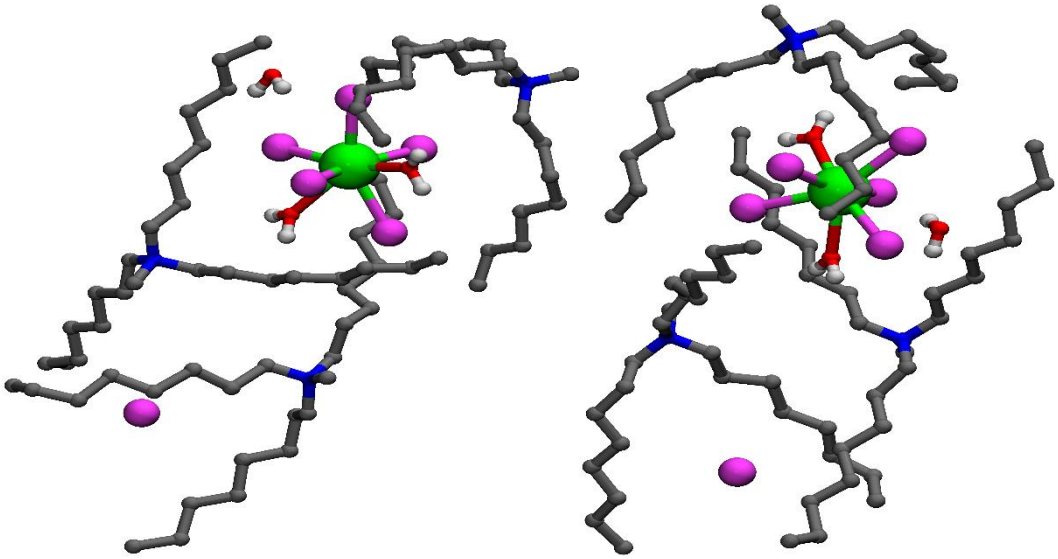

Figure 2.8.4.1 – The formation of a chloride-**IL0**-water-La aggregate following a classical MD simulation (left – front, right – reverse).

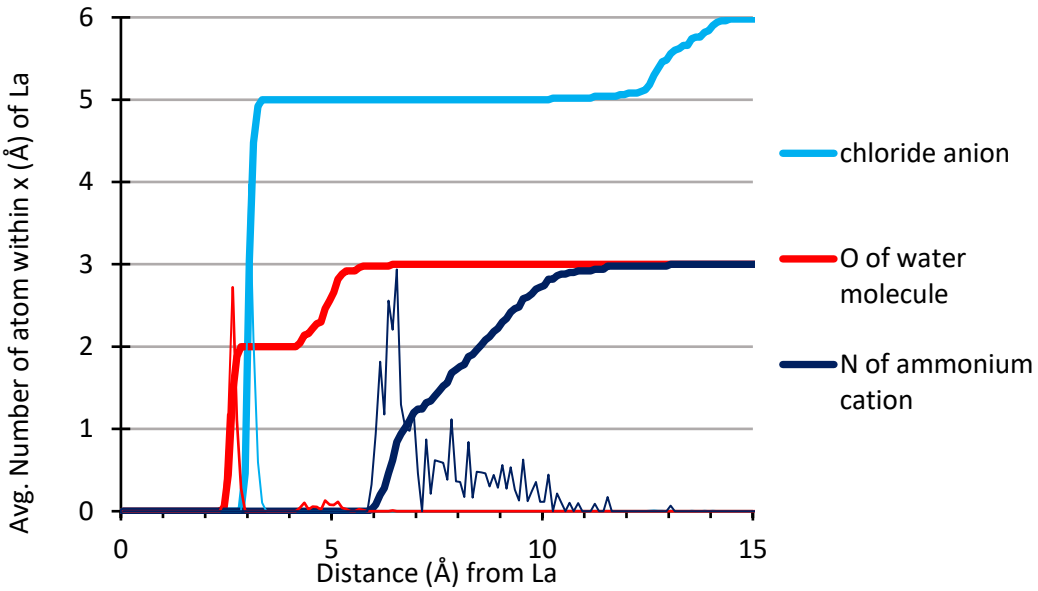

Figure 2.8.4.2 – Integrations obtained from the g(r) output plot from classical MD simulations indicating how the average number of IL extractants, water molecules and chloride anions associated with La increases as a function of distance from La following the spontaneous formation of a La-containing aggregate. Averaged over 100 simulation frames (1.5 ns).

2.8.5 Classical MD simulations with chloroform and REE

The extraction of REEs into more polar organic solvents such as $CHCl_3$ (parameters discussed in 7.6) with **IL0** does not occur (section 2.6.6). When the simulation in toluene is repeated in

chloroform, a far more polar solvent than toluene (0.26 vs. 0.10 relative to water being 1.00), [127, 137] encapsulation of the La centre by lipophilic ammonium cations still occurs. In this case, the La inner-coordination sphere is satisfied by five nitrate anions and two water molecules.

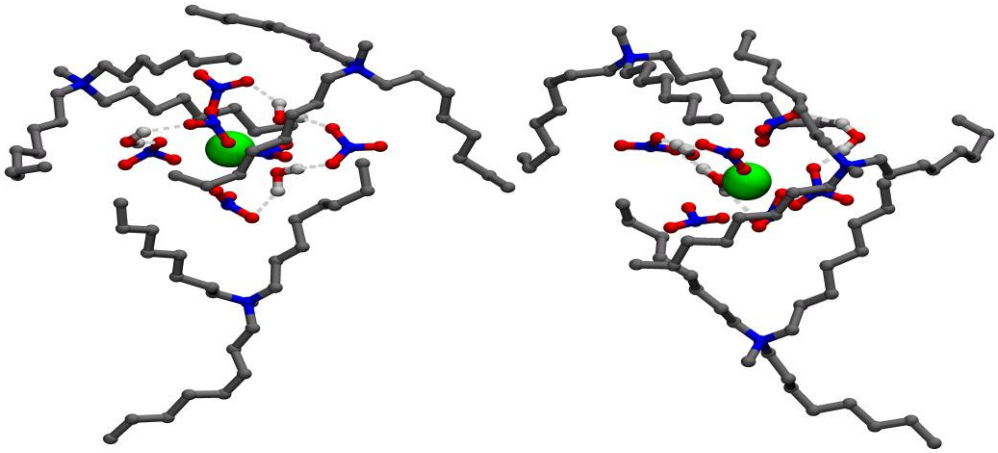

Figure 2.8.5.1 – The formation of a La-**IL0**-water-nitrate aggregate following a classical MD simulation in chloroform (left – front, right – reverse).

The nitrate anions and water molecules appear visually to be closer to the La centre than simulations with toluene as the solvent and is validated by comparing the average number of water molecules, nitrate anions and ammonium cations at defined distances from the REE. All six nitrate anions are within 5.8 Å of the La centre compared with 12.8 Å for toluene (Figure 2.8.5.2). Additionally the La is thoroughly encapsulated by the alkylammonium cation, with the exposure calculated to be just 2.4 ± 0.2 % and is perhaps due to the additional nitrate anion residing closer to the La than in other simulations. The formation of a stable aggregate is unexpected as experimentally the formation of REE-**IL0** aggregates in chloroform does not occur.

As the classical MD simulations yield stable aggregates within chloroform in contrast to the absence of stable aggregates experimentally, it can be concluded that classical MD simulations have some limitations in their ability to define how ILs extract REEs. These limitations presumably stem from the force field parameters only poorly representing the modelled interactions between molecules and ions. Minor discrepancies between computational parameters and their true values may be sufficient to promote the formation of stable aggregates. Therefore, MD simulations should be used only as a guide and be supported by experimental evidence and quantum mechanical calculations (section 2.8.6).

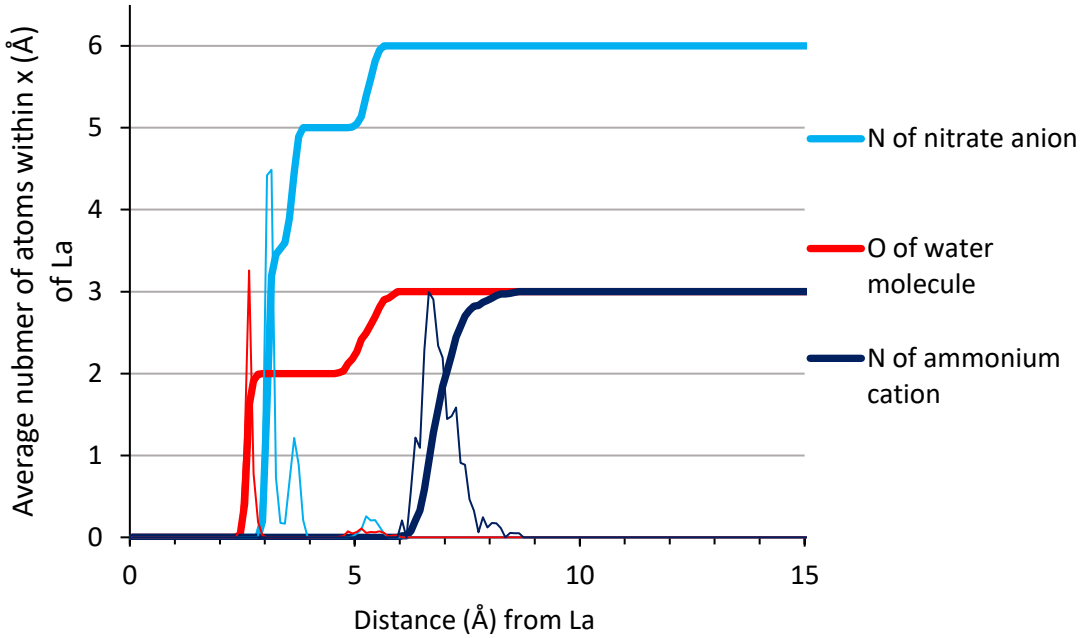

Figure 2.8.5.2 – Integrations obtained from the g(r) output plot from the classical MD simulations, indicating how the average number of IL extractants, water molecules and nitrate anions associated with La increases as a function of distance from La, following the spontaneous formation of a La-containing aggregate. Averaged over 100 simulation frames (1.5 ns).

2.8.6 Quantum mechanical geometry optimisations - DFT studies

While MD simulations are useful in analysing the aggregation of individual components from a multi-component system, they do not define the precise bonding interactions within the aggregation. Therefore, the stable aggregate from the MD calculations was used as an input geometry for QM geometry optimisation calculations to determine the composition of the inner-coordination sphere of the La centre, in particular to deduce the monodentate or bidentate coordination modes of the nitrate anions (Figure 2.8.2.2) (section 7.6.3). From these calculations, the geometry optimised structure contains a La centre with an inner coordination number of eleven (Figure 2.8.6.1). The QM details are provided in section 7.6.

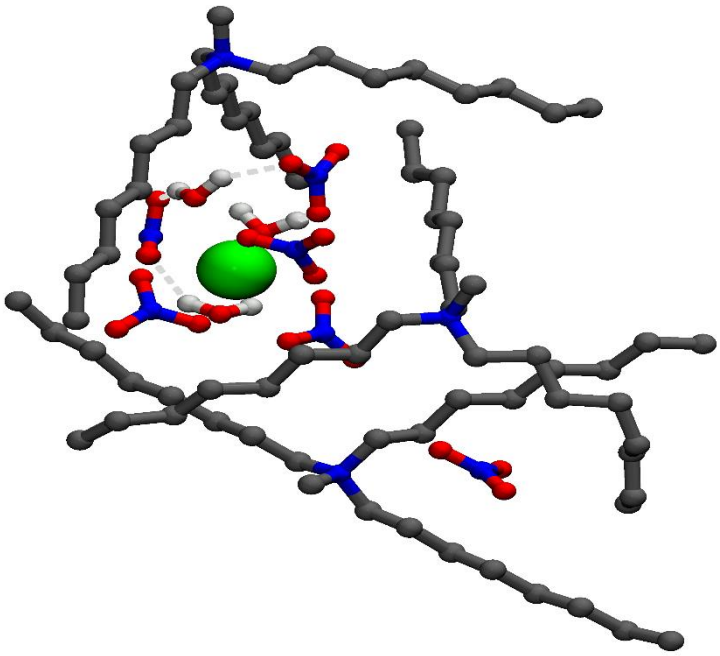

Figure 2.8.6.1 – A DFT optimised structure of the terminus configuration of a La-containing aggregate from an MD simulation comprising one La, three nitrate anions, three **IL0** and three water molecules.

Close inspection of the coordination of the La centre shows three bidentate nitrate anions, two monodentate nitrate anions, and three water molecules. The average La-O bond distances for water molecules and nitrate anions at 2.7 Å is comparable to previously reported La-O distances.[103, 104] The modest hydrogen-bonding array seen in the MD calculations remains intact (Figure 2.8.6.2).

Monte Carlo encapsulation measurements undertaken on the DFT optimised structure with the La as the centre point show an exposure of 1% suggesting that the La nitratometalate is well suited for the cavity created by the alkylammonium cations.

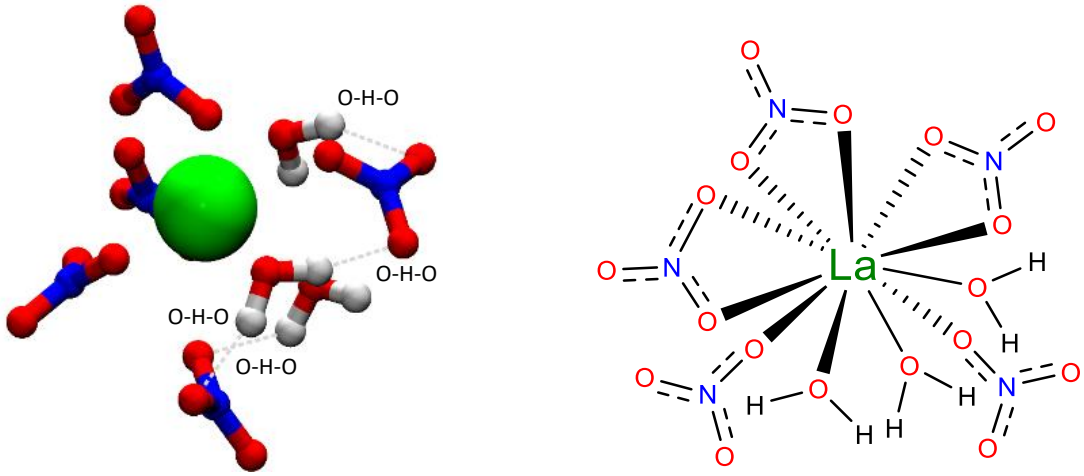

Figure 2.8.6.2 – The DFT optimised inner coordination sphere of a La-containing aggregate (left). A ChemDraw representation of the inner coordination sphere (right).

The formation of the La-**IL0** assembly was determined to be thermodynamically favourable with a formation energy (ΔU_f) (section 7.6.3) of −37 KJ mol^{-1} calculated from the internal energies of the individual components (reactants) and of the La-**IL0** assembly (products) (Eq. 2.8.6.1).

Eq. 2.8.6.1 – $\Sigma\, U(\text{products}) - \Sigma\, U(\text{reactants})$

A formation energy of this value compares favourably with formation energies for other supramolecular assemblies formed during metal recovery processes.[24] The negative formation energy supports the earlier hypothesis (section 2.8.2) that the La is well suited to accommodate the cavity created by **IL0**, nitrate anions and water molecules and supports the experimental data (section 2.6). The nitrate anions and water molecules acting as charge mediating bridges and as molecular scaffolds undoubtedly contribute to the favourable formation of the assembly.

2.9 Conclusions

The ionic liquid **IL0** can transport REEs from aqueous solutions into an organic phase if the conditions are tailored suitably, e.g. low acid concentrations, high nitrate salt content, and a low-polarity organic solvent. The ability of **IL0** to selectively target one REE is limited, highlighted by the extraction of La (99%), Nd (85%) and Dy (52%) from single metal aqueous feeds of $NaNO_3$ (7.0 M) when using **IL0** (0.1 M). The ability for **IL0** to target specific REEs is not a significant improvement over traditional industrial reagents such as D2EHPA that poorly

distinguish between adjacent REEs.[7, 74] Despite poor REE selectivity, **IL0** does have remarkable stability, negligible aqueous solubility and can be readily stripped with water. This suggests a process incorporating **IL0** would have environmentally friendly credentials. The targeting of specific REE using ILs will be explored within chapter 3.

While previous work has highlighted the inability of REEs to form chloride and nitrato metalates in the aqueous phase, the analytical and computational evidence gathered here strongly indicates that REE nitratometalates of the general formula $REE(NO_3)_5(H_2O)_x^{2-}$ (where x>0) do form in the organic phase, stabilised and encapsulated by the lipophilic alkylammonium cations.[42, 109, 121, 138] The REEs are not entirely dehydrated upon transport into the organic phase and instead remain partially hydrated – or microhydrated. There is a large energy penalty associated with the complete dehydration of a REE cationic centre (a $\Delta_{hyd}G^*$ of -3145 KJ mol^{-1} for La).[85] Therefore, the extraction of partly, rather than entirely, dehydrated REE may result in the lowest energetic cost overall.

The presence of modest hydrogen-bonding networks in the organic phase aggregates is shown by computational modelling and could be essential to organic phase stabilisation. If the hydrogen-bonding network can be expanded, through inclusion of hydrogen donors and acceptors into the ammonium cation, the stability of the REE aggregates could be enhanced. This will be the focus of chapters 3 and 5.

Chapter 3

Development of amido-ammonium ILs for REE separation

3 Development of amido-ammonium ILs for REE separation

3.1 REE separation – industrial reagents

Organophosphorus compounds such as di-(2-ethylhexyl)phosphoric acid (D2EHPA) poorly separate adjacent REEs. Numerous studies report that D2EHPA only achieves separation factors of around 2 for adjacent REEs.[67, 69] Separation factors can be calculated by measuring the quantity of one REE the aqueous and organic phases and dividing by the same measurement of another REE. It is the distribution (D) value of one REE divided by the D value of another REE.

Eq. 3.1.1 – $([REE(b)]_{org}/[REE(b)]_{aq})/([REE(a)]_{org}/[REE(a)]_{aq})$

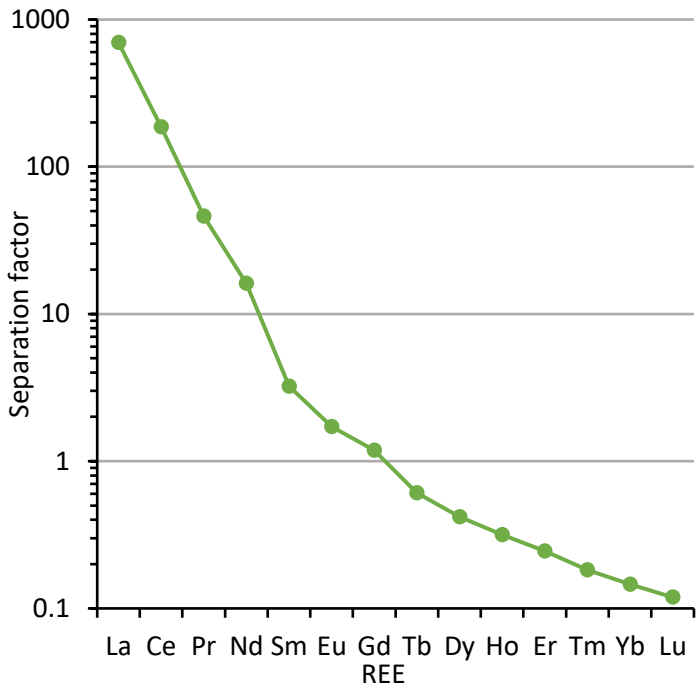

Figure 3.1.1 – An example of REE separation factors relative to Y using tributyl phosphate (1.0 M) in dodecane. The target REE was extracted from a solution also containing Y.[74]

As highlighted above (Figure 3.1.1), organophosphorus compounds can discriminate well between lighter, less Lewis acidic REEs (e.g. La, Ce, Pr, Nd) and a heavier, more Lewis acidic REE (e.g. Y) but poorly between REEs of similar Lewis acidity such as Y, Gd, Tb and Dy.[74]

In one study, D2EHPA (0.05 M) in kerosene extracted minimal Sm (6%) from an aqueous HNO_3 solution, but significant amounts of Lu (72%) with a gradual increase in extraction percentage observed across the f-block (Table 3.1.1).[69] The separation factors for adjacent REEs averaged 1.46 and are corroborated by more recent studies.[139-143]

Table 3.1.1 – The percentage extraction and separation factors of REEs from an aqueous HNO_3 solution with D2EHPA (0.05 M) in kerosene.[69] Tm was not analysed in this study.

REE	% REE extraction	REE(b)/REE(a)	Separation Factor
Sm	*5.5*		
Eu	*10.1*	*Eu/Sm*	*1.84*
Gd	*12.4*	*Gd/Eu*	*1.23*
Tb	*22.6*	*Tb/Gd*	*1.82*
Dy	*34.3*	*Dy/Tb*	*1.52*
Ho	*42.5*	*Ho/Dy*	*1.24*
Er	*64.9*	*Er/Ho*	*1.53*
Tm			
Yb	*68.1*		
Lu	*71.8*	*Lu/Yb*	*1.05*

D2EHPA (0.60 M) in kerosene extracted REEs (La-Er) (0.002 – 0.57 g/L) from a H_2SO_4 (1.0 M) apatite ore leach solution with an average separation factor between adjacent REEs of 3.31.[139] A very low percentage (<5%) of the lighter REEs (La–Nd) were extracted allowing for modest separation of heavier REEs from lighter REEs. Rather than transport the lighter REEs into kerosene, lighter REEs were recovered by precipitation using oxalic acid (0.08 M) thus separating the lighter REEs from the apatite impurities – determined to be predominantly Ca, P and Al.

Organophosphorus compounds form $REE(R_2PO_2)_3(R_2PO_2H)_3$ complexes with REEs in the organic phase with six PO–REE bonds satisfying the REE inner coordination sphere with outer–sphere hydrogen–bonding interactions providing additional stability (section 2.1).[59, 63] The predominant factors defining the stability of the complexes is the strength of these bonds. As the relative charge density of the REE cation increases, the oxygen donor atoms bind more strongly to the REE cation, causing a contraction in the PO–REE bond distances.

The REE-P distances in REE–D2EHPA complexes are calculated computationally to decrease from 2.75 Å (Ho) to 2.71 Å (Lu) with, on average, a 0.01 Å distance difference when comparing adjacent REEs (Figure 3.1.2).[41]

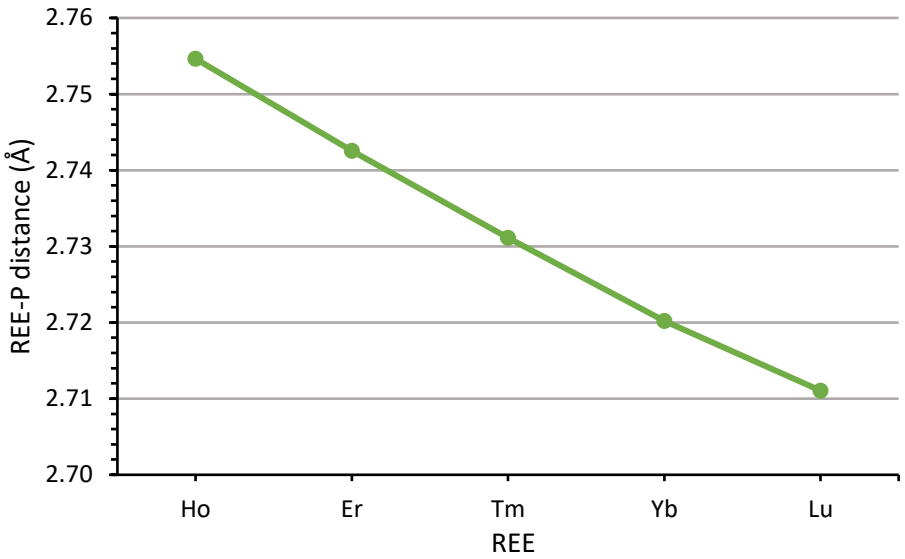

Figure 3.1.2 – The computationally modelled distances (Å) between REE cations and the P atom of D2EHPA.[41]

The REE–O distances were found to be 2.14 Å (Ho) and 2.09 Å (Lu). The modest selectivity of D2EHPA, and analogues, can be attributed to the minor contraction in these bond lengths. While no REE-D2EHPA compounds are currently reported in the Cambridge Structural Database (CSD) it should be noted that these REE-O calculated bond lengths are shorter than those reported for solid state structures such as a bis(cyclohexaphosphato)–Nd complex (CSD code: TIJKUT) or a tris(tetraphenylimidodiphosphinato-O,O')–La (CSD code: FOPJOJ) complex that both have average REE-O bond lengths of 2.45 Å.[144, 145]

As discussed above, REE recovery can be achieved using precipitation.[139] Using discriminatory precipitation and inorganic chemical recognition with a methoxy-substituted tripodal hydroxylamine ligand ($H_3TriNOx^{OMe}$) (Figure 3.1.3), a separation factor of almost 300 has been achieved for Nd and Dy.[146] To a starting mixture of $REE[N(SiMe_3)_2]_3$ silylamido compounds in benzene, $H_3TriNOx$ in benzene was subsequently added. A precipitate formed and was determined to be almost exclusively (>95%) $Dy(TriNOx^{OMe})$ while the remnant solution contained less than 10% $Dy(TriNOx^{OMe})$ but over 90% of the Nd analogue. The high separation factors were understood to arise from the greater propensity for Nd over Dy to form the

more soluble dimeric complex [REE(TriNOx$_{OMe}$)]$_2$.[147] Reactions of REECl$_3$ with boric acid at elevated temperatures have been shown to produce different REE–borate crystallisation products that are dependent on the REE.[148] From a binary Nd and Dy mixture, judicious control of reaction kinetics achieved quantitative recovery of Nd and Dy as $Nd_2B_{12}O_{18}Cl_2(OH)_4(H_2O)_4.nH_2O$ and $Dy_4B_{24}O_{36}(OH)_{12}(H_2O)$ with the two crystalline compounds then separated using a flotation method.

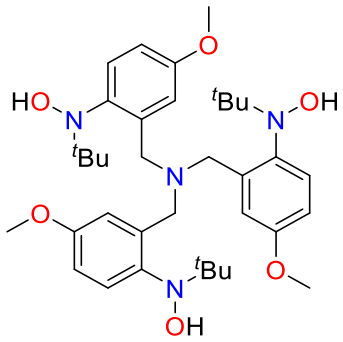

Figure 3.1.3 – A methoxy-substituted tripodal hydroxylamine ligand ($H_3TriNOx^{OMe}$) used for selective REE precipitation.[146, 147]

3.2 Amides for REE recovery

Lipophilic amides such as diglycolamides and malonamides (Figure 3.2.1), under appropriate conditions, readily extract REEs.[52, 149-151]

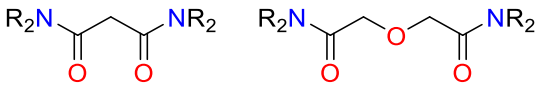

Figure 3.2.1 – A malonamide (left) and a diglycolamide (right). Reagents used during REE recovery.

A malonamide **(MA)**, where nitrogen atoms of tertiary amides are bonded to methyl and benzyl substituents, extracts REEs from aqueous solution.[149] Contacting an HNO_3 (4.0 M) aqueous phase with **MA** (0.2 M) in chloroform resulted in preferential extraction of earlier REEs. High symmetry Ln$(NO_3)_3$(**MA**)x complexes were identified in the organic phase using UV-Vis spectroscopy and FT-IR spectroscopy; in the IR spectra, two C=O stretches at 1647 and 1671 cm^{-1} for **MA** converged into one stretch at 1647 cm^{-1} on contact with a Lu containing aqueous phase, with no other stretches identified in the carbonyl region, suggesting that only

one conformation is present.[152] These data were corroborated in later studies and expanded upon such as the confirmation of nitrate bound directly to the REE cation.[52, 152] Furthermore, luminescence emission data of Eu-**MA** complexes indicated a noticeable change in the $^5D_0 \rightarrow {}^7F_2$ (around 610 – 630 nm) transition, a transition known to be highly sensitive to inner-sphere coordination changes.[152] EXAFS spectroscopy at low Eu^{3+} concentrations revealed that the number of malonamides, nitrates and water molecules around a Eu^{3+} cation is three, three and one respectively. This fitting model alluded to a combination of monodentate and bidentate binding for malonamide and nitrate ligands which is abetted by classical molecular dynamics (MD) simulations (Figure 3.2.2).[52]

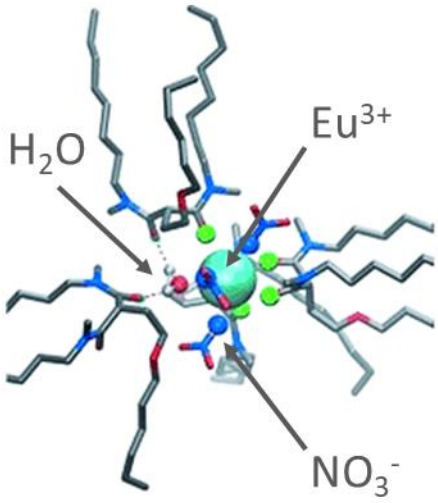

Figure 3.2.2 – The formation of a Eu-malonamide-nitrate-water aggregate following a classical molecular dynamics simulation where Eu (cyan), is coordinated by malonamide carbonyls (green spheres), nitrate oxygen's (blue spheres) and water oxygen's (red spheres).[52]

At low concentrations of malonamides (and diglycolamides) inner-sphere coordination behaviour to REEs is exhibited, but as the concentration of REE and malonamide is increased, the complexes and structures change significantly.[52] During the extraction process a 'third-phase', a phase that is immiscible with both the aqueous and organic phases, forms at elevated REE and malonamide concentrations, resulting in a triphasic system. The third–phase is comparatively dense due to the high concentration of REE and malonamide ligand within it and this compares well with other reported 'third-phase' formations resulting from metal recovery processes.[52, 122, 128] Using a highly aliphatic malonamide (0.5 M) in dodecane,

Ce removal from the aqueous phase occurs at all Ce concentrations (0.01 – 0.10 M) but once above 0.05 M Ce, most Ce resides in the 'third–phase' (Figure 3.2.3).

Small angle X-ray scattering (SAXS) spectroscopy in conjunction with a series of Ce extraction experiments concluded that the 'third–phase' comprised reverse micelle structures. Aggregations comprising four malonamides, one $Ce(NO_3)_3$ complex and one water molecule were present and HNO_3 in the aqueous phase was suggested to facilitate the aggregation.[128]

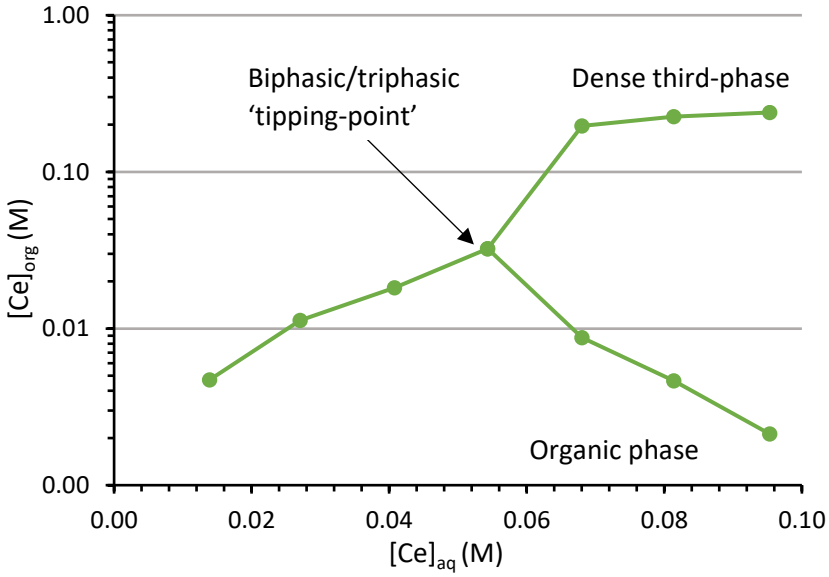

Figure 3.2.3 – The extraction of Ce (0.01 – 0.10 M) using an aliphatic malonamide (0.50 M) in dodecane. When the Ce concentrations exceeds 0.05 M, a dense Ce and malonamide containing 'third-phase' forms.[128] Interpolation used to aid the eye only.

As the REE concentration in the organic phase increases, the REE-malonamide complexes reconfigure from discrete $REE(NO_3)_3(H_2O)$–malonamide complexes into REE reverse micelles where REE centres are bridged by nitrate anions.[52] Through a combination of classical MD simulations (Figure 3.2.4) and SAXS spectroscopy, the repulsive nature of Eu-Eu interactions were determined to be circumvented through hydrogen–bonding interactions between malonamides and outer-sphere water molecules. Water molecules acted as mediators to bring nearby aggregates closer, creating larger supramolecular structures containing up to seven Eu cations.

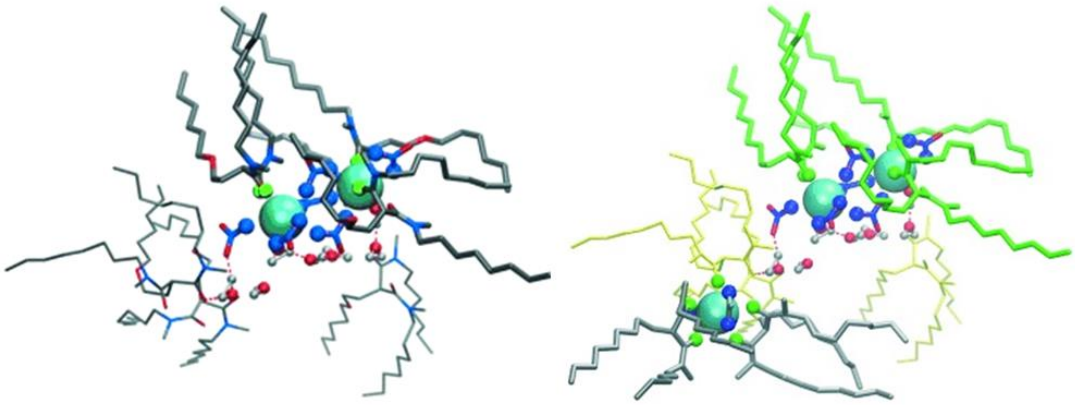

Figure 3.2.4 – The formation of Eu–malonamide–nitrate–water supramolecular aggregates following classical MD simulations. Eu (cyan), malonamide carbonyls (green), nitrate nitrogens (blue) and water oxygen's (red).[52]

The complex behaviour of malonamides would result in great difficulties if implemented into an industrial REE recovery process. These issues also pertain to diglycolamide reagents that are stronger REE extractants than malonamides, but due to the presence of the central ether oxygen display reverse selectivity, extracting heavier REEs over lighter REEs (Figure 3.2.5).[50, 149, 153] TODGA (Figure 2.2.4), a diglycolamide, separates adjacent lighter REEs effectively but discriminates very poorly between heavier REEs. TODGA forms 3:1 L:M complexes with REEs, providing a coordination number of nine when extracting from a $NaNO_3$ aqueous phase.[154, 155] The amount of water transported into the organic phase, despite not coordinated to the REE, increases linearly from around three per REE (La) to around five per REE (Gd, Dy, Tm).

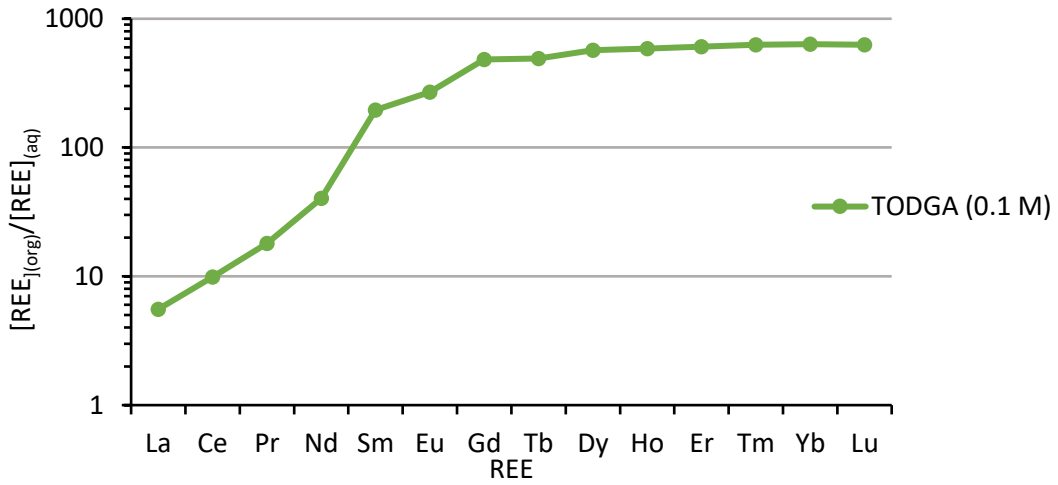

Figure 3.2.5 – Extraction of REEs using TODGA (0.1 M) in dodecane from HNO_3 (1.0 M).[50, 156] Interpolation used to aid the eye only.

Using density functional theory (DFT) calculations, the REE–O (diglycolamide ether) bond distances were found to gradually decrease from 2.59 Å (La) to 2.40 Å (Yb) (Figure 3.2.6). The REE-O (diglycolamide ether) bond distance contractions caused a gradual increase in the steric crowding around the REE resulting in the REE–O (nitrate anion) distances gradually increasing from 4.67 Å (La) to 4.95 Å (Gd). The plateauing of % water and % REE transported beyond Gd can is rationalised by the coordination shell stabilisation beyond Gd.[50]

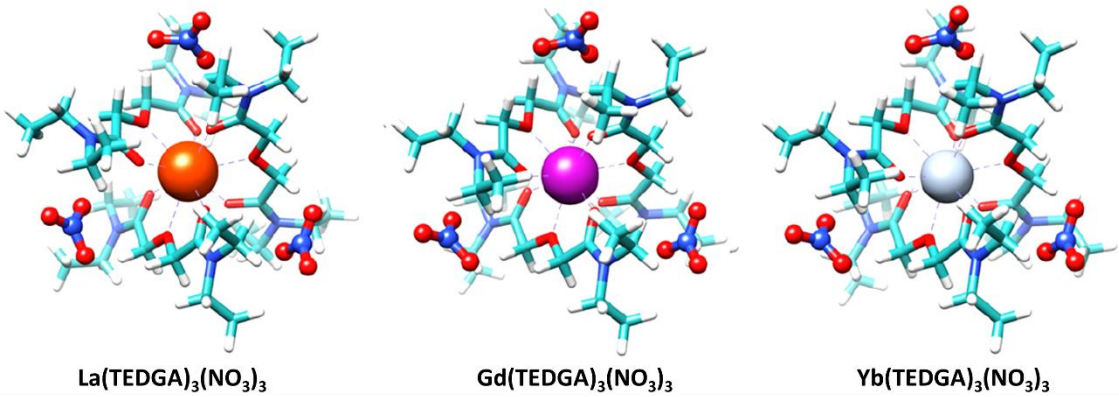

Figure 3.2.6 – DFT optimised structures of REE(TEDGA)$_3$(NO$_3$)$_3$ complexes. The octyl substituents of TODGA have been shortened to ethyl due to computational limitations.[50] Elements are coloured as La (orange), Gd (purple), Yb (grey), O (red), N (blue), H (white) and C (green).

The decreases in REE–O (diglycolamide ether) bond distances observed computationally agree with previously reported crystallographic data for [REE(TEDGA)$_3$](NO$_3$)$_3$.4H$_2$O compounds (e.g. CSD code: POLRIT) where TEDGA is an short alkyl chain TODGA analogue.[157] While solid phase crystallographic data is not representative of solution phase, hydrogen-bonding interactions between nitrate anion, TEDGA and co-crystallised water molecules were evident.

In summary, the striking separation of the lighter REEs (La–Gd) with diglycolamides is a result of the substantial change in the coordination shells. Once the coordination shells stabilise beyond Gd, REE extraction is very high and selectively ceases. At low ligand and metal concentration, discrete REE-diglycolamide ions are observed but as concentrations are increased large problematic poly-nuclear micellar aggregates form.

3.3 Functionalised ILs

The incorporation of functional groups into ILs that can coordinate the REE such as organic acids, diglycolamides, and acetylacetones has been explored.[158, 159]

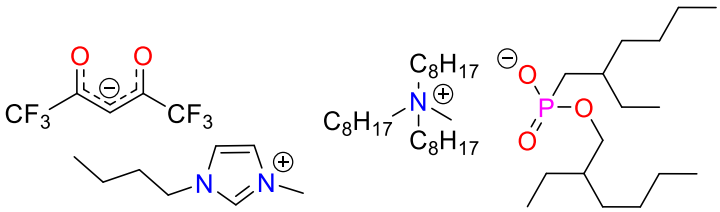

Figure 3.3.1 – Examples of functionalised ILs. An imidazolium acetylacetonate IL (left).[158] A phosphinic acid ammonium IL (right).[159]

When the anionic bidentate hexafluoroacetylacetonate is used as the anion component in an IL with a non-coordinating imidazolium cation, REEs are extracted from aqueous phases. Discrete REE complexes comprising four bidentate acetylacetonates charged balanced by one imidazolium cation were formed in the water immiscible organic phase.[158] This was supported by the solid-state structure (Figure 3.3.1), from which hydrogen-bonding interactions between acetylacetonate carbonyls and imidazolium hydrogens were also identified.

Incorporation of a phosphine oxide functionality into the imidazolium cation of the anion-functionalised IL resulted in the formation of a nine coordinate REE centre (Figure 3.3.2).[160] In this case, four negative bidentate acetylacetonates remain present but now the imidazolium additionally coordinates through the phosphine oxide. Using $^{31}P[^{1}H]$ NMR spectroscopy and crystallographic data, the formal bonding interaction between the anionic and cationic components, rather than a hydrogen-bond, was verified in both the solution and solid phases.

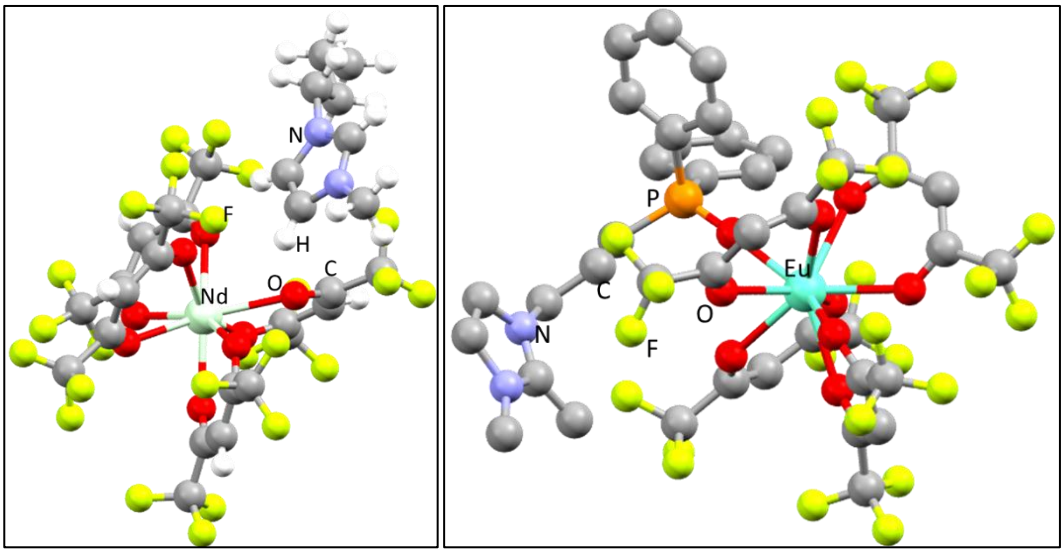

Figure 3.3.2 – (left) Crystal structure of an Nd–acetylacetonate-imidazolium complex (CSD code: PURLAQ) obtained following contact of an aqueous solution containing Nd with an IL phase.[158] (right) The crystal structure of an Eu-acetylacetone–imidazolium complex (CSD code: REBCOS) obtained following contact of an aqueous solution containing Eu.[160] Elements are coloured as H (white), C (grey), N (blue), O (red), F (yellow), P (orange) and Nd/Eu (green). Some H atoms are hidden for clarity.

While the unfunctionalized IL, **IL0** (chapter 2) preferentially extracts lighter REEs, replacement of the nitrate anion with a deprotonated phosphinic acid (Figure 3.3.1) reverses the selectivity to favour the heavier REEs.[159] The IL (Figure 3.3.1) (3 mM) extracted minimal intermediate REEs (0.5 mM) (Gd–Er) but a much greater percentage of very heavy REEs (Tm–Lu) from a chloride aqueous phase. The energetic favourability associated with phosphinic acid coordination to a charge–dense heavy REE centre, as determined by IR spectroscopy, outweighs the energetic penalty of dehydrating the more highly hydrated heavier REE centres (section 2.2).[86-89]

For actinide separation, the non-coordinating anion bis(triflimide) (Figure 2.3.2) used in conjunction with an amide functionalised ammonium IL cation (Figure 3.3.4) selectively extracts Pu over U and Am from nitric acid (1 – 8 M) with separation factors of 10^5 obtained.[161] Aggregates containing Pu, nitrate anions and ammonium cations form in the organic phase, suggesting an anion-exchange mechanism with transfer of bis(triflimide) to the aqueous phase. Dynamic light scattering (DLS) measurements determined the radius of

the organic phase aggregate formed increased from a radius of 7 nm to an average of 123 nm upon Pu extraction.

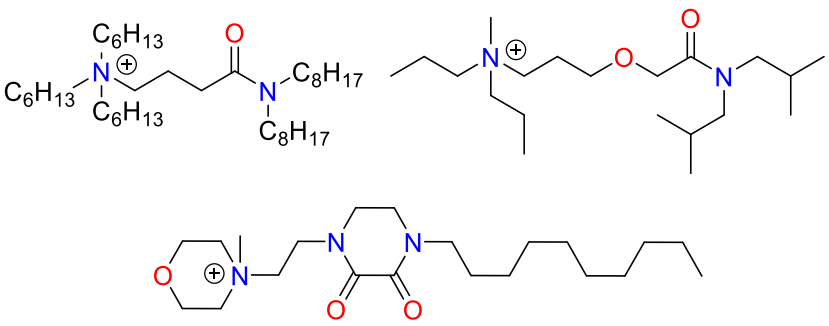

Figure 3.3.4 – An amido-ammonium cation (left), a diglycolamido-ammonium cation (right) and a diamide-ammonium cation (bottom).[161-163]

Replacement of the amido-ammonium cation with a diglycolamido-ammonium cation allowed for Eu extraction from aqueous nitric acid (0.01 – 1.00 M) solutions.[162] Using IL (34 mM), full extraction (>99%) of Eu (1 µM) was observed from HNO_3 (0.01 M) but at HNO_3 (1.00 M) minimal Eu extraction (<5%) occurred. As the nitric acid concentration was increased, the transport of nitric acid in absolute terms increased, suggesting competition between REE and nitric acid transport as discussed earlier (section 2.4 and 2.7.4).

The combination of a diamide–ammonium cation (Figure 3.3.4) and a bis(triflimide) anion provides effective separation of heavier REEs (Sm, Lu) from base metals (Zn, Ni, Co) from acidic chloride media.[163] The efficient separation was attributed to the absence of any amine donor ligands. IR spectroscopy measurements identified a strong interaction between amide carbonyl and REE ions as the carbonyl stretching frequency shifted to lower wavenumbers, from 1672 cm^{-1} to 1648 cm^{-1}. This interaction was further supported by $^{13}C[^{1}H]$ NMR spectroscopy studies that showed a minor down-field shift (approx. 2 ppm) of the two carbonyl carbons by upon contact with the aqueous phase containing the REE.

To gain structural information on the inner coordination sphere of the REE, DFT calculations were undertaken and the optimised structure comprised an eight coordinate REE centre with three bidentate diamide–ammonium cations and one bidentate bis(triflimide) anion (Figure 3.3.5).[163] It should be noted that this structure is surprising, given the tendency for bis(triflimide) anions to remain non-coordinating and that the overall charge of this cation is +5. It can be assumed that a combination of bis(triflimide) and chloride anions would be

associated in the outer-coordination sphere to provide charge balance and maintain organic phase solubility.

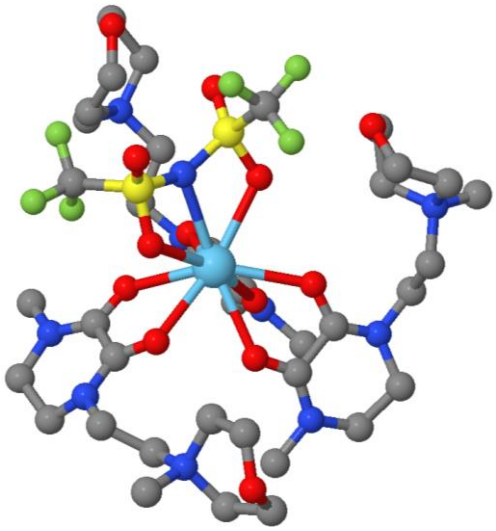

Figure 3.3.5 – DFT optimised structure of a REE–IL complex consisting of La, bis(triflimide) anions and diamide-ammonium cations.[163] Elements are coloured as C (grey), N (dark blue), O (red), S (yellow), La (light blue) and F (green). H are hidden for clarity.

It is evident that functionalised IL reagents display significant advantages such as selective REE extraction and minimal 'third-phase' formation over both traditional organophosphorus reagents and neutral amide reagents. Unfortunately, the ILs currently reported to effectively separate REEs often involve small-scale multi-step synthetic procedures, or are used within complex multi-cation multi-anion systems where the speciation of REE complexes in the organic phase is not known. In view of this, the prime focuses within this chapter will be the development and synthesis of functionalised ammonium IL reagents using simple synthetic procedures and understanding how and why their performance with respect to REE separation and recovery varies from that of unfunctionalized **IL0**.

3.4 Amido-ammonium (AA) IL synthesis

Primary (1°), secondary (2°) and tertiary (3°) amido-ammonium ILs were synthesised straightforwardly from 2-chloroacetyl chloride (Figure 3.4.1). The acid chloride is converted to the amide by reaction with ammonia (1°), propylamine (2°) or dipropylamine (3°) with liberation of HCl. The resulting 2-chloro acetamides are then reacted with dioctylamine to yield amido–amine intermediates, again with HCl liberated. The resulting amido–amine

intermediates are then methylated using methyliodide (section 2.5), and the iodide exchanged for nitrate to yield the primary, secondary, and tertiary amido-ammonium nitrate compounds, herein referred to as **1AA**, **2AA** and **3AA**.[124, 134]

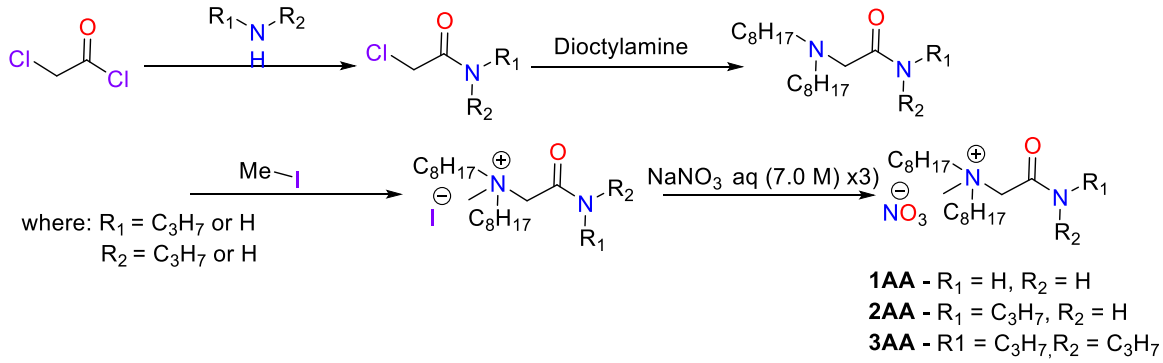

Scheme 3.4.1 – The synthesis of the 1° (**1AA**), 2° (**2AA**) and 3° (**3AA**) amide-ammonium ILs starting from 2-chloroacetyl chloride.[124, 134]

3.5 REE extraction and separation studies

3.5.1 Initial REE extraction tests

To assess the performance of **1AA**, **2AA** and **3AA** against **IL0**, a series of initial REE extraction tests were undertaken. Organic solutions of **1AA**, **2AA** and **3AA** (0.1 M) were all contacted with a series of aqueous phases containing La (0.01 M). The different compositions of the aqueous phases were: $NaNO_3$ (7.0 M); $HNO_3/NaNO_3$ (0.1 M/5.0 M); HNO_3 (2.0 M).

No REE extraction (<1%) is achieved from water alone using **1AA**, **2AA** or **3AA** in accordance with the 'salting-out' effect and mirrors **IL0** (Figure 3.5.1.1).[107, 108, 118] The extraction of La from $NaNO_3$ (7.0 M) is more successful with 39% (**1AA**), 83% (**2AA**) and 72% (**3AA**) extracted respectively. **2AA** and **3AA** are comparable in REE extraction performance to **IL0** (91%) but **1AA** is significantly worse. This is observed again in the extraction of La from $HNO_3/NaNO_3$ (0.1 M/5.0 M), with 52% (**IL0**), 18% (**1AA**), 62% (**2AA**) and 36% (**3AA**) La extraction respectively. The comparisons to **IL0** deviate with the extraction of La from HNO_3 (2.0 M) as **IL0** (0.1 M) does not extract La from acid only aqueous phases but **2AA** and **3AA** do extract modest amounts (14%) and (4%) from HNO_3 (2.0 M).

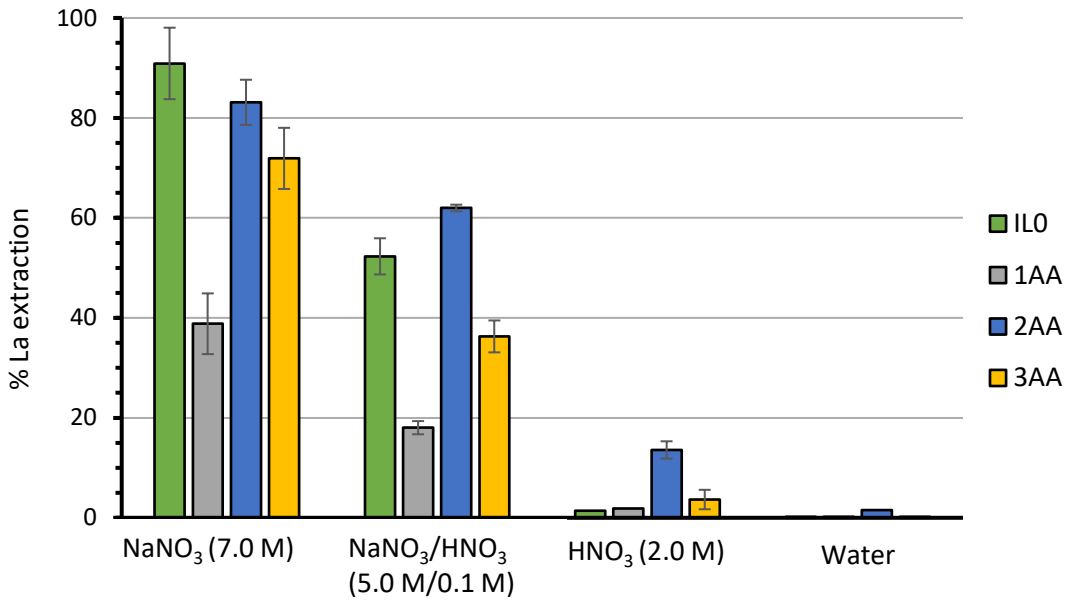

Figure 3.5.1.1 – Preliminary performance tests for La (0.01 M) extraction using **1AA**, **2AA** and **3AA** in toluene from water, $NaNO_3$ (7.0 M), $HNO_3/NaNO_3$ (0.1 M/5.0 M) and HNO_3 (2.0 M), compared against **IL0**.

1AA under the conditions tested is evidently a poor reagent for La extraction. **1AA** is presumably the least lipophilic IL studied and may exhibit significant solubility in aqueous solutions which would reduce the concentration of **1AA** in the organic phase and result in a reduction in the quantity of La extracted. Therefore, using NMR spectroscopy, the solubility of **1AA** in aqueous solutions was investigated. The ^{1}H NMR spectra of a solution of **1AA** (0.1 M) in deuterated benzene was recorded before and after contact with an aqueous solution of water of La (0.01 M) and $NaNO_3$ (7.0 M) (Figure 3.5.1.2). Dioxane (4% v/v) was used as an internal standard. The integrations of the C**H**$_2$ proton chemical shifts for the internal standard dioxane and the NC**H**$_2$ proton chemical shifts of **1AA** were then compared.

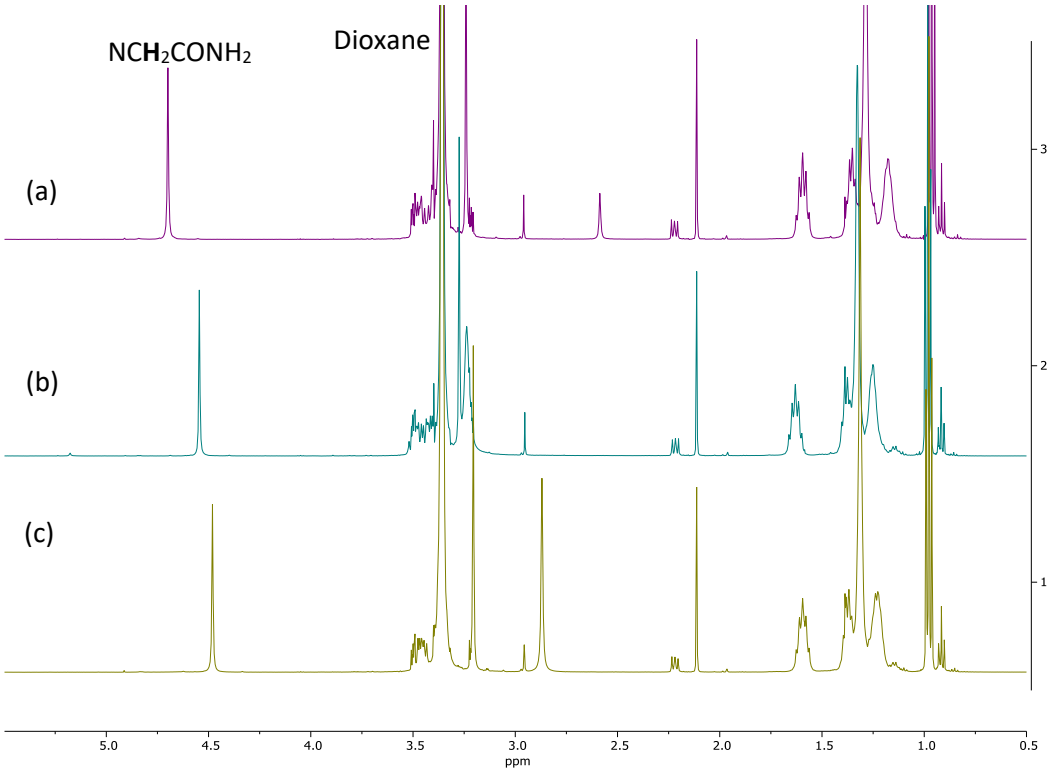

Figure 3.5.1.2 – A comparison of the ^{1}H NMR spectra of **1AA** (0.1 M) in deuterated benzene before contact (a), following contact with water (b) and following contact with a La (0.01 M) and $NaNO_3$ (7.0 M) aqueous phase (c).

The integrations across all three NMR spectra are equal indicating that **1AA** is not aqueous soluble to any significant degree (Figure 3.5.1.2) and instead remains in the organic phase. This is further supported by contacting **1AA** (0.1 M) in deuterated benzene with D_2O. The ^{1}H NMR spectrum of the resulting D_2O phase was recorded and did not show a significant presence of **1AA** (Figure 3.5.1.3); only water and dioxane chemical shift signals are observed.

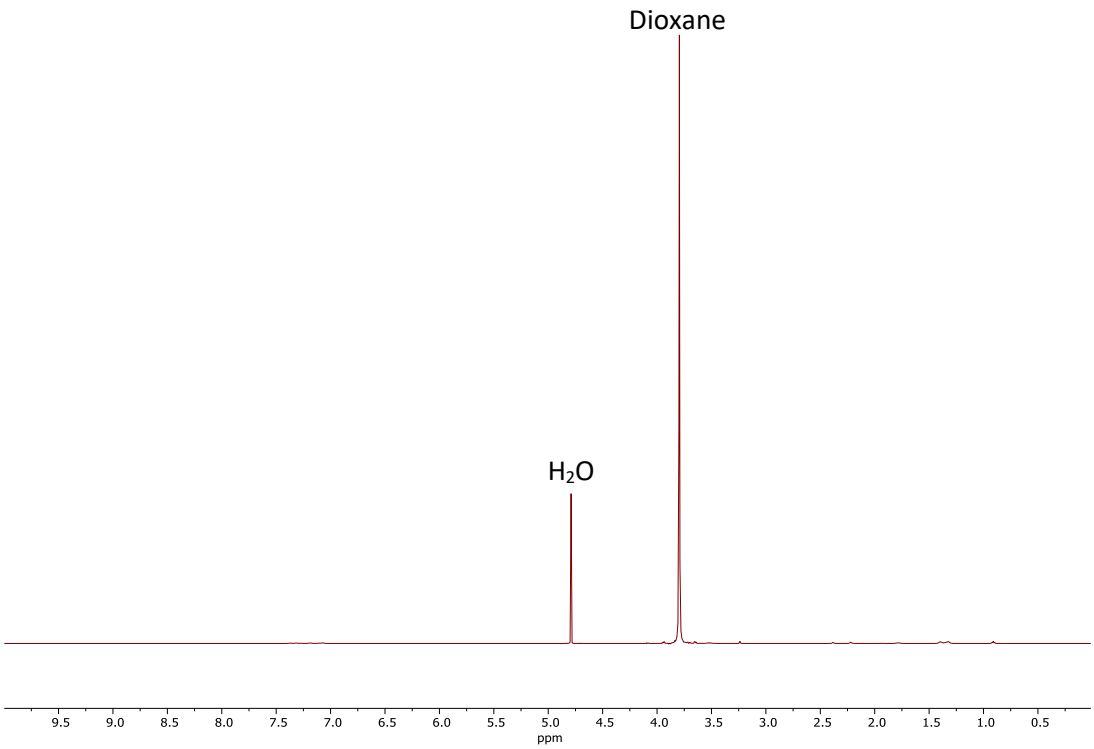

Figure 3.5.1.3 – The ^{1}H NMR spectrum of a D_2O phase following contact with **1AA** (0.1 M) in deuterated benzene.

3.5.2 Extraction of REEs using varying IL concentration

Varying the **1AA**, **2AA** and **3AA** concentration (0.005 – 0.2 M) with a constant aqueous $NaNO_3$ (7.0 M) concentration results in a similar trend to that of **IL0** (section 2.6.2) for the transport of La (0.01 M) from single metal aqueous solutions (Figure 3.5.2.1). An increasing concentration of the IL transports an increasing percentage of La into the organic phase with 65% (**1AA**), 94% (**2AA**) and 90% (**3AA**) of La transported at 0.2 M **IL0**. In contrast, only minimal amounts of La are extracted at 0.005 M IL – 3% (**1AA**), 6% (**2AA**) and 3% (**3AA**) respectively.

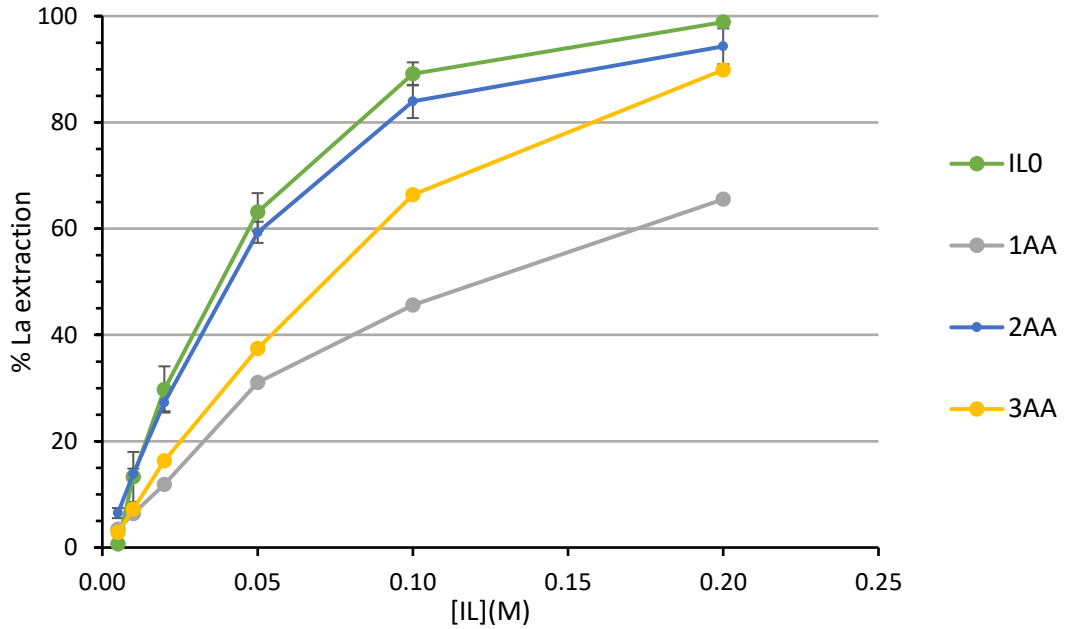

Figure 3.5.2.1 – The extraction of La (0.01 M) using **1AA, 2AA** or **3AA** (0.005 – 0.2 M) in toluene from $NaNO_3$ (7.0 M) aqueous solution. Interpolation used to aid the eye only.

While increasing the concentration of **IL0**, **2AA** and **3AA** has a positive effect on the transport of La, the percentage of La extracted with **1AA** remains comparatively poor. As such, few further studies using **1AA** were undertaken and **2AA**, due to its greater tolerance of acid (Figure 3.5.1.1) will be the chapter's main focus.

3.5.3 Extraction of REEs from HNO_3 acid solutions

Similar to **IL0** (section 2.6.5), the ability of amido-ammonium ILs to extract REEs is substantially reduced as the HNO_3 concentration increases beyond 0.1 M.[107, 114, 118] When **1AA** and **2AA** (0.10 M) are contacted with an acidic aqueous phase of $NaNO_3/HNO_3$ (5.0 M/0.01 – 2.00 M) and La (0.01 M), the extraction of La is highest (18% and 70%) at low HNO_3 concentrations (0.01 M) (Figure 3.5.3.1). While **IL0** does not extract La beyond HNO_3 (1.0 M), **2AA** still extracts La to a noticeable degree (38%) at this concentration of acid. The amido-ammonium IL, **2AA** is more tolerant of HNO_3, perhaps due to increased selectivity for La over HNO_3 transport.[123]

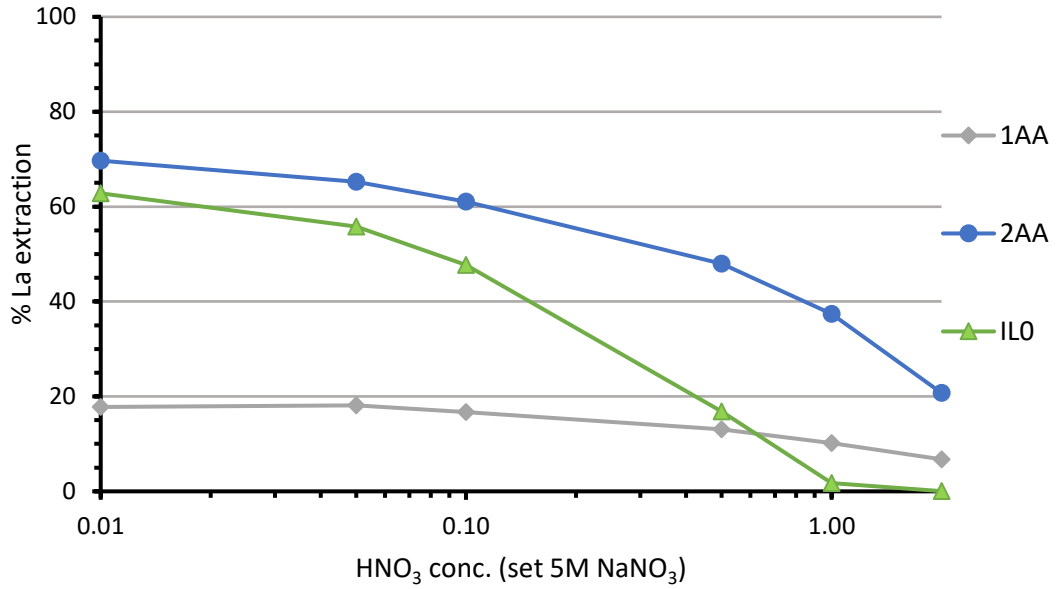

Figure 3.5.3.1 – The extraction of La (0.01 M) using **IL0**, **1AA**, or **2AA** (0.1 M) in toluene from a $NaNO_3/HNO_3$ (5.0 M/0.01 – 2.00 M) aqueous solution. Interpolation used to aid the eye only.

The amount of nitric acid extracted by **2AA** was quantified using ion-chromatography (IC) using the method previously described for **IL0** (section 2.7.4). From an aqueous phase of $NaNO_3/HNO_3$ (5.0 M/0.1 M) **IL0** transports 36 mM of nitrate while **2AA** only transports 30 mM. From an aqueous phase of $NaNO_3/HNO_3$ (5.0 M/1.0 M) **IL0** transports 67 mM of nitrate while **2AA** only transports 51 mM (Figure 3.5.3.2). These measurements reveal that the general trends of both **IL0** and **2AA** are the same although under all conditions investigated **2AA** transports a lower quantity of nitrate into the organic phase and supports the rationale that **2AA** is more selective for REEs over HNO_3 than **IL0.**

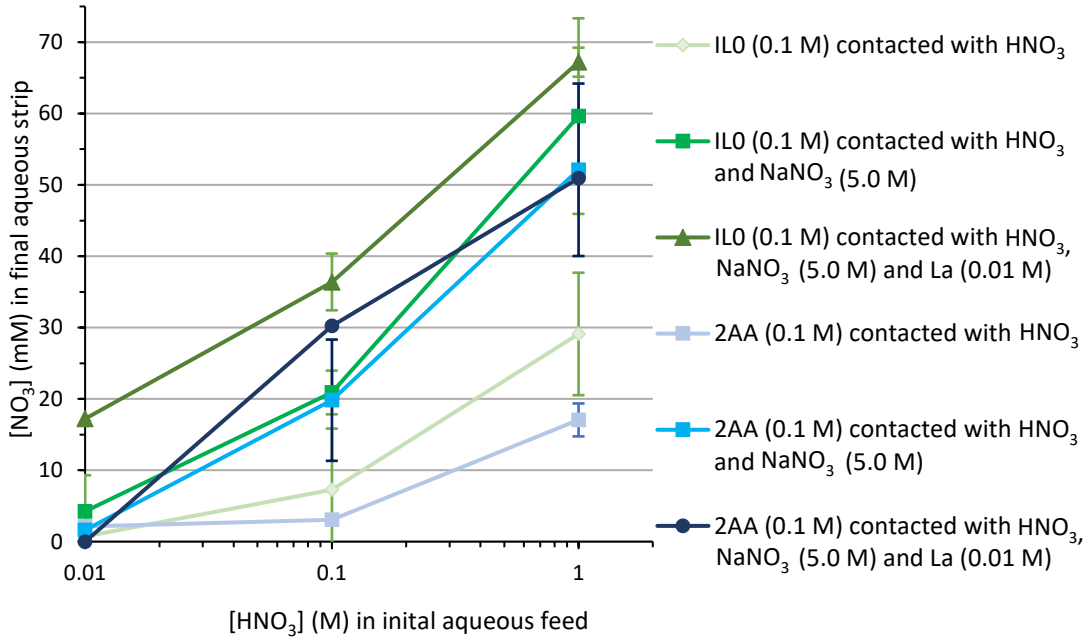

Figure 3.5.3.2 – The nitrate anion content of aqueous solutions following contact of **IL0** or **2AA** (0.1 M) in toluene with HNO_3 (0.01 – 1.00 M), $HNO_3/NaNO_3$ (0.01 – 1.00 M/5.0 M) and $HNO_3/NaNO_3/La$ (0.01 – 1.00 M/5.0 M/0.01 M). Interpolation used to aid the eye only.

The increased selectively for REEs and greater tolerance of acid by **2AA** could allow for REE recovery from HNO_3 only solutions, with no $NaNO_3$ salt present. Contacting an organic phase containing **IL0**, **2AA** and **3AA** (0.1 M) with an aqueous HNO_3 (0.0 – 8.0 M) solution containing La (0.01 M) shows some extraction of La (14% and 5% at 2.0 – 4.0 M HNO_3) with **2AA** and **3AA** but virtually none with **IL0** (Figure 3.5.3.3).[42, 134] Above 4.0 M HNO_3 the extraction of La gradually decreases, presumably due to competitive extraction of HNO_3 as discussed above (section 3.5.3).

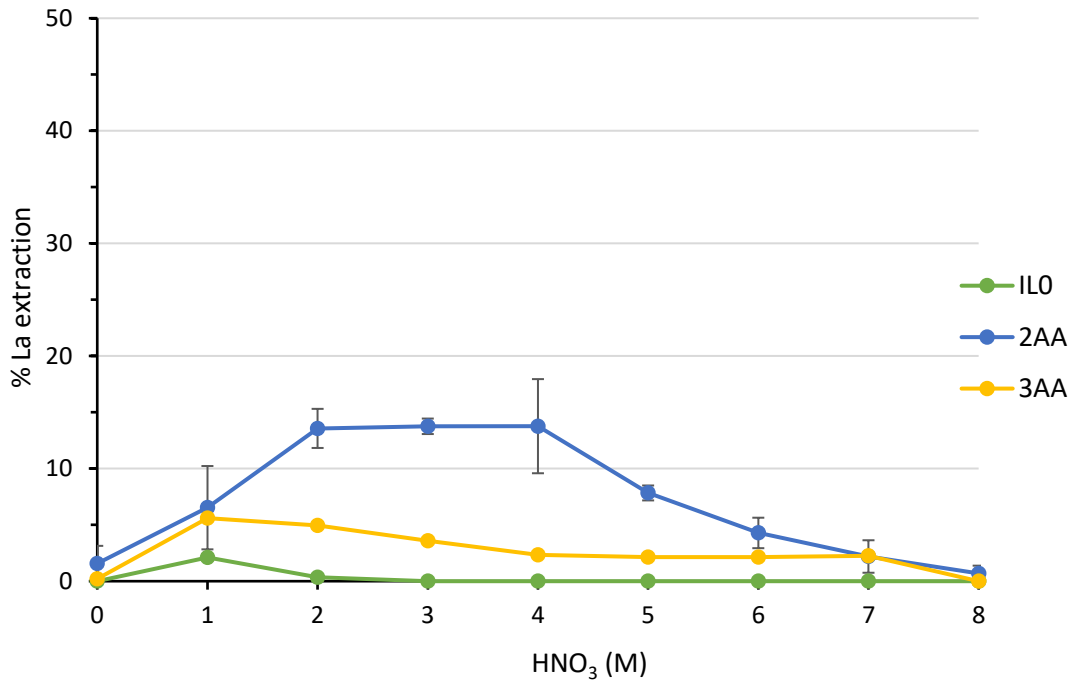

Figure 3.5.3.3 – The extraction of La (0.01 M) using **IL0, 2AA** or **3AA** (0.1 M) in toluene from a HNO_3 (0.0 – 8.0 M) solution. Interpolation used to aid the eye only.

3.5.4 Extraction from single REE solutions

IL0 displays modest selectivity for lighter REEs over heavier REEs (section 2.4).[88, 107, 108] To compare the selectivity of **IL0** against **2AA** and **3AA** single REE aqueous phases containing La – Dy were contacted with **IL0**, **2AA** and **3AA** (0.1 M) in toluene. While **IL0**, **2AA** and **3AA** all readily extract (>60%) the lighter REEs (La – Nd), only minimal extraction (<10%) of intermediate–heavier REEs (Eu – Dy) was attained with **2AA** indicating a high degree of selectivity for lighter REEs by **2AA** (Figure 3.5.4.1). In contrast, **IL0** still maintains moderate extraction (*ca.* 50%) of intermediate-heavier REEs.

These differences remain when extracting REEs from moderate $NaNO_3$ concentration (5.0 M), low HNO_3 concentration (0.1 M) aqueous solutions (Figure 3.5.4.2). **IL0**, **2AA** and **3AA** (0.1 M) in toluene were contacted with single REE aqueous phases containing La – Dy (0.01 M) and $NaNO_3$/HNO_3 (5.0 M/0.1 M). **IL0** and **2AA** both attain moderate extraction (>40%) of the lighter REEs (La – Nd) but **2AA** does not extract (<1%) the intermediate–heavier REEs (Eu – Dy). **IL0** still extracts a minor quantity (*ca.* 10%) of the intermediate–heavier REEs under the equivalent conditions.

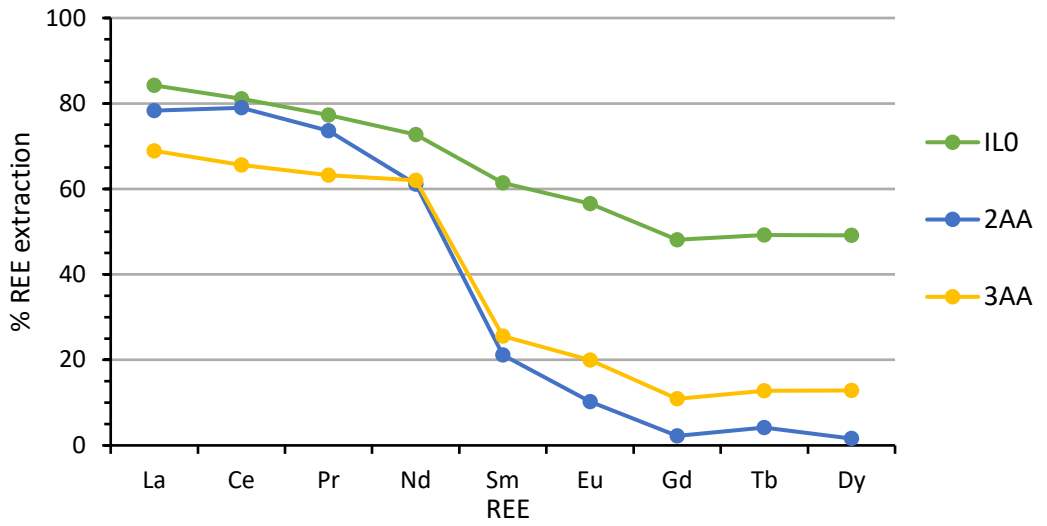

Figure 3.5.4.1 – The extraction of REEs (0.01 M) using **IL0**, **2AA** or **3AA** (0.1 M) in toluene from a single REE $NaNO_3$ (7.0 M) aqueous solution. Interpolation used to aid the eye only.

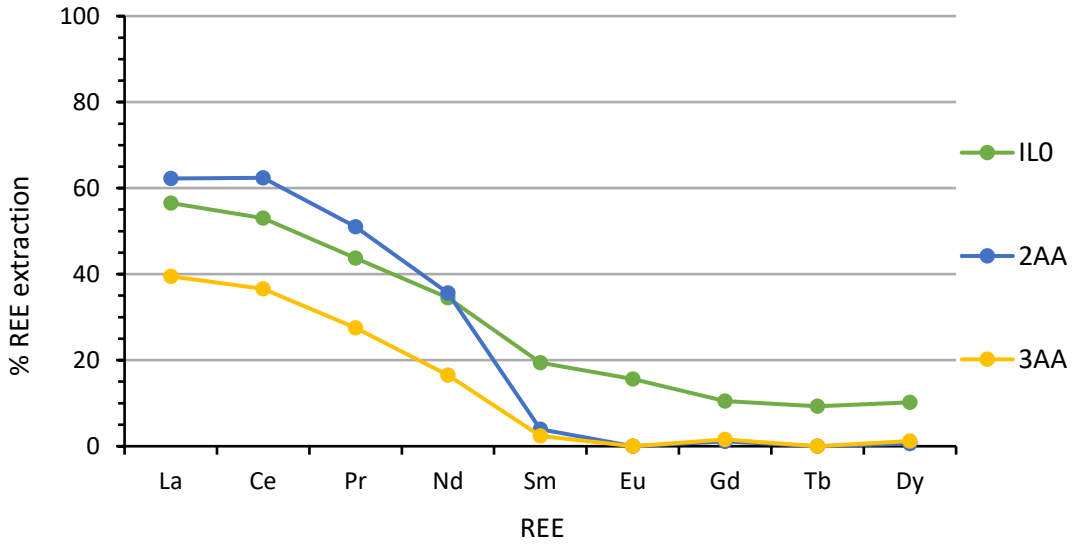

Figure 3.5.4.2 – The extraction of REEs (0.01 M) using **IL0, 2AA or 3AA** (0.1 M) in toluene from a single REE $NaNO_3/HNO_3$ (5.0 M/0.10 M) aqueous solution. Interpolation used to aid the eye only.

Under both of the aqueous conditions highlighted (Figure 3.5.4.1 and 3.5.4.2) there are large differences in % extraction between Ce/Tb abd Nd/Dy when using **2AA**. This is notable as the separations of Ce from Tb or Nd from Dy are of significant industrial importance and will be discussed later (section 3.5.6).[12, 28, 164, 165]

3.5.5 Extraction from mixed REE solutions

Aqueous solutions in reality often contain multiple REEs rather than one. To investigate the selective extraction of REEs from a multiple REE solution, **IL0** and **2AA** (0.25 M) in toluene were contacted with an aqueous phase containing 8 REEs (La – Dy) (0.01 M) and $NaNO_3$ (7.0 M). An increased IL concentration was chosen in order to compensate for the near magnitude increase (x8) in total aqueous REE concentration. The extraction trends across the f-block is found to be comparable to that observed with single REE aqueous solutions (Figure 3.5.5.1). While the extraction of Nd by **IL0** and **2AA** was found to be comparable (48 vs. 43 %) a greater difference in La extraction under these conditions is observed with **IL0** extracting 69% La while **2AA** extracts 85%. The arguably more significant difference though is that while **IL0** extracts approximately 25% of the heavier REEs (Gd–Dy), the extraction of heavier REEs with **2AA** is reduced to <3%.

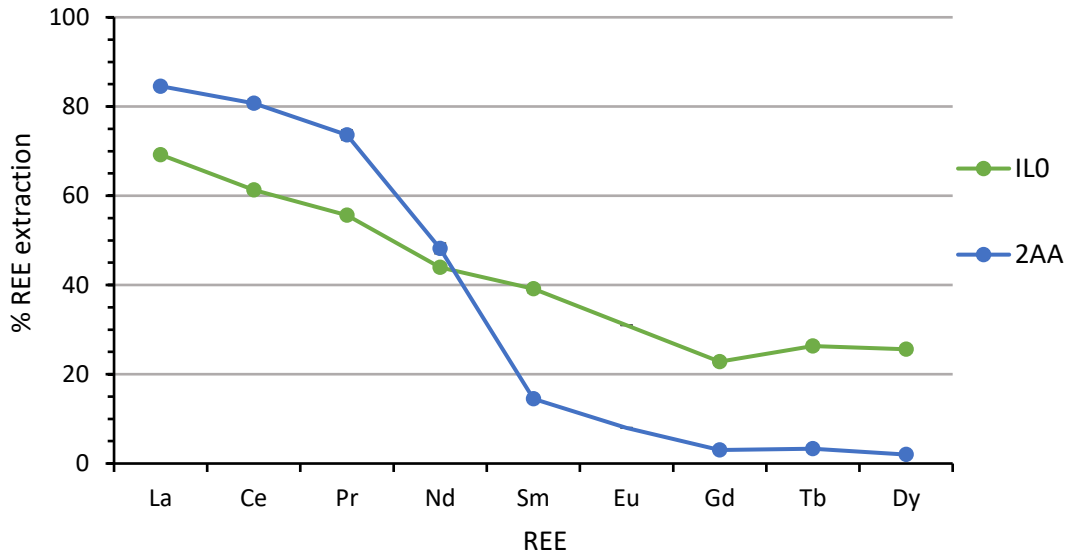

Figure 3.5.5.1 – The extraction of REEs (0.01 M) using **IL0 or 2AA** (0.25 M) in toluene from a mixed REE $NaNO_3$ (7.0 M) aqueous solution. Interpolation used to aid the eye only.

When extracting REEs from a $NaNO_3/HNO_3$ (5.0 M/0.1 M) aqueous phase containing multiple (9) REEs (La – Dy) instead, the extraction of each individual REE by either **IL0** or **2AA** decreases. **2AA** still modestly extracts (25 – 72%) the lighter REEs (La – Nd) but does not extract (<1%) the heavier REEs (Eu – Dy) (Figure 3.5.5.2). **IL0** retains some extraction (>5%) of heavier REEs.

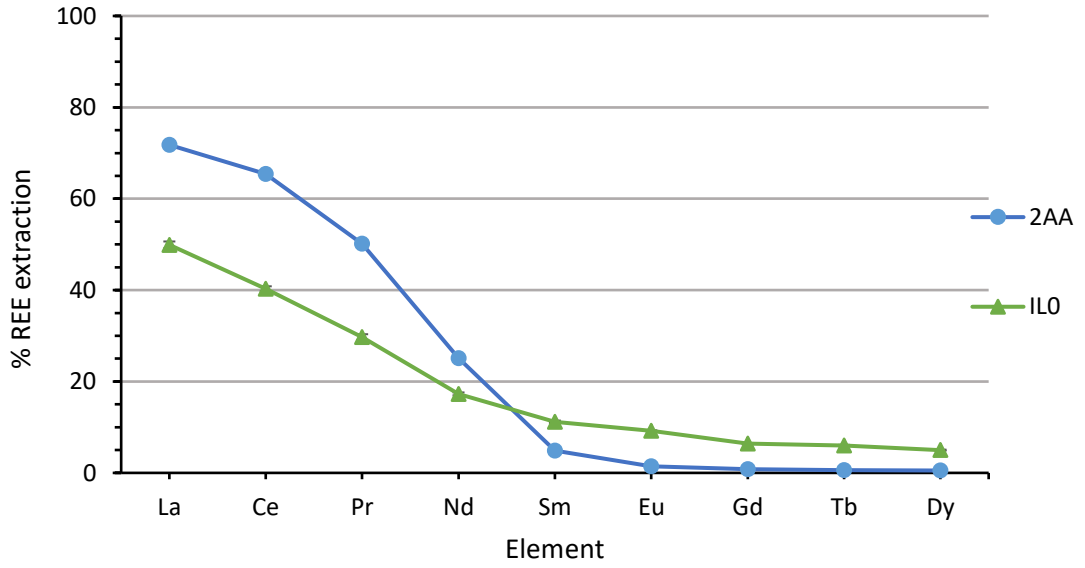

Figure 3.5.5.2 – The extraction of REEs (0.01 M) using **IL0** or **2AA** (0.25 M) in toluene from a mixed REE $NaNO_3/HNO_3$ (5.0 M/0.10 M) aqueous solution. Interpolation used to aid the eye only.

When a 1°, 2° or 3° amide (0.25 M) (Figure 3.5.5.3) is used in combination with **IL0** (0.25 M) to extract REEs (La-Dy) (0.01 M) from a $NaNO_3/HNO_3$ (5.0 M/0.1 M) aqueous phase the trend is similar to that observed with **IL0** alone (Figure 3.5.5.4). The % of REE extraction gradually decreases across the f-block from 41-59% (La) to 5-10% (Dy). The limited selectivity and separation when using an ammonium IL and an amide instead of an amido-ammonium IL suggests that the amido-ammonium functionality is crucial to selectivity.

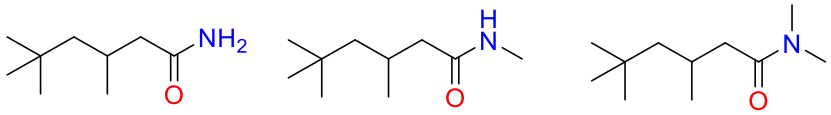

Figure 3.5.5.3 – A 1° (left), 2° (centre) and 3° (right) amide used in combination with **IL0** for REE extraction.

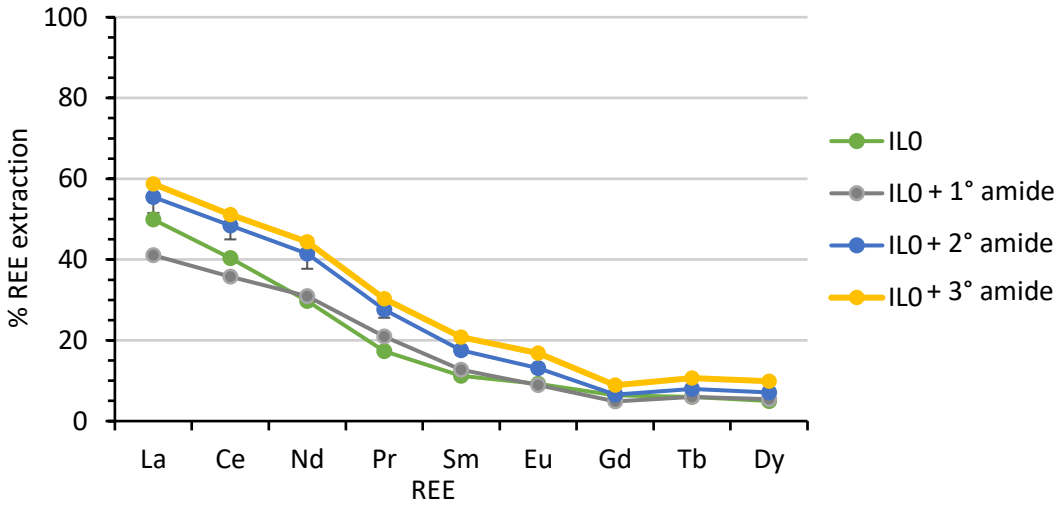

Figure 3.5.5.4 – The extraction of REEs (0.01 M) using **IL0** (0.25 M) and a 1°, 2° or 3° amide (0.25 M) in toluene from a mixed REE $NaNO_3/HNO_3$ (5.0 M/0.10 M) aqueous solution. Interpolation used to aid the eye only.

3.5.6 Separation of Ce/Tb and Nd/Dy

Examining earlier graphs (section 3.5.5) it can be seen that **2AA** effectively separates lighter REEs from heavier REEs. This is a promising alternative to typical industrial reagents (e.g. D2EHPA) that display the reverse selectivity and often only provide separation factors between adjacent REEs of about two (section 3.1).[74, 166-168]

With Ce and Tb being key constituents within fluorescent lighting, of which many are now approaching 'end-of-life' and are being succeeded by arguably more sustainable light-emitting diode (LED) lighting, there is an opportunity to recover Ce from Tb and other constituents within fluorescent lighting waste.[16, 28, 164, 165] Fluorescent lighting, once crushed and finely powdered, has an approximate composition of halophosphate (45 wt. %), silica (25 wt. %), alumina (12 wt. %) and a significant REE content present as REE phosphors (18 wt. %). It is estimated that there are 25,000 tons of REEs available within fluorescent lighting while the total quantity mined from ores each year is only five times greater (*ca.* 125,000 tonnes).[169, 170] There are five common REE phosphors in fluorescent lighting which are $Y_2O_3:Eu^{3+}$ (YOX), $LaPO_4:Ce^{3+}$, Tb^{3+} (LAP), $(Gd, Mg)B_5O_{10}:Ce^{3+},Tb^{3+}$ (CBT), $(Ce, Tb)MgAl_{11}O_{19}$ (CAT) and $BaMgAl_{10}O_{17}:Eu^{2+}$ (BAM). These REE phosphors are often combined in different ratios within lighting systems to provide the desired colour.[12, 16, 165]

In a previous study, >95% of Gd, Eu Tb and Y were extracted with D2EHPA (60% v/v) in xylene from powdered lighting waste that was leached into an HCl aqueous solution;[165] <5% of Ce and La was extracted under these conditions, corroborating the preferential extraction of heavier REEs by organophosphorus compounds discussed earlier (section 2.1).[67, 69] Another study explored using methanesulphonic acid to solubilise the REE phosphor – LAP from which >95% Tb was subsequently extracted using D2EHPA, and separated from the other REEs present (La and Ce).[171]

The graphs in section 3.5.5 suggest that **2AA** can successfully separate Ce from Tb and achieve the inverse separation to that of industrial reagents.[67, 69, 165] When contacting **2AA** (0.1 M) in toluene with a model binary REE aqueous phase containing Ce (0.01 M), Tb (0.01 M) and $NaNO_3/HNO_3$ (5.0 M/0.1 M), Ce is extracted (59%) but not Tb (<0.1%) (Figure 3.5.5.1). When using **IL0** under the comparable conditions, 46% of Ce is extracted and 3% Tb. While **IL0** yields a separation factor for Ce/Tb of 25.9 ± 0.4, **2AA** achieves a separation factor of 2670 ± 1340 (Table 3.5.5). It should be noted that the large variance is due to the difficulties in measuring the very trace concentrations of Tb (<0.01 ppm) in the organic phase. Accuracy and error is discussed later (section 7.3).

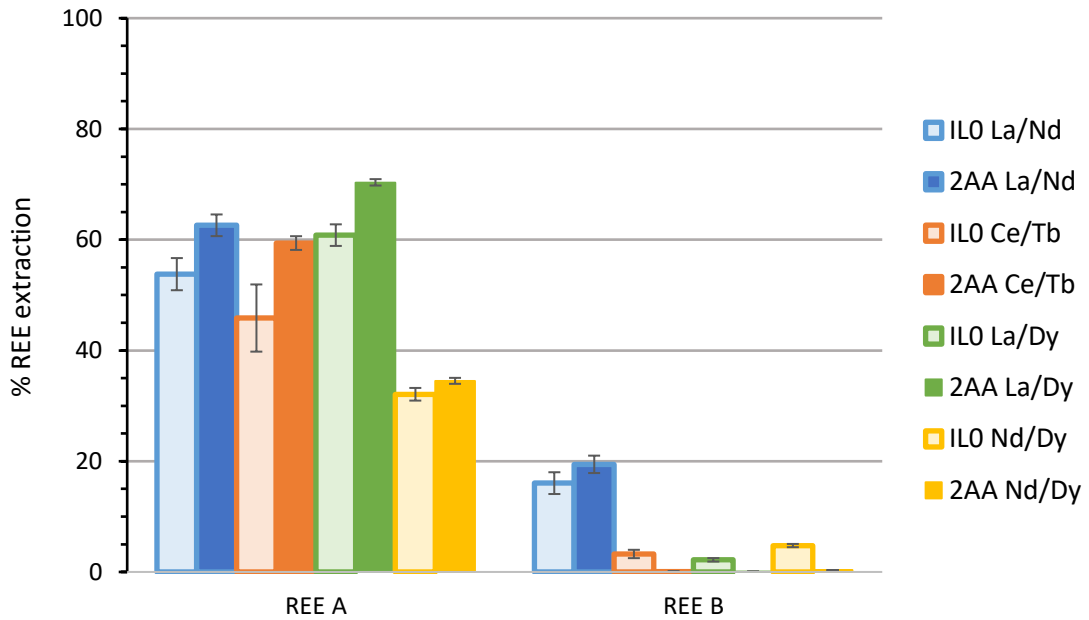

Figure 3.5.5.1 – The extraction of REEs (0.01 M) using **IL0 or 2AA** (0.10 M) in toluene from a binary REE (0.01 M and 0.01 M), $NaNO_3/HNO_3$ (5.0 M/0.10 M) aqueous solution.

The separation of Nd and Dy from one another is of interest as of their prominent use in high strength permanent magnets that are found in a range of applications including wind turbines, MRI machines, audio systems and hard disk drives.[8, 172] The composition of these permanent magnets is mainly, Fe (70%), trace B (<1%) and REEs (30%) in ratios between Nd:Dy 10-20:1.[2, 173-175]

The separation of Nd and Dy by solvent extraction from model solutions representative of solubilised permanent magnets has been reported. Using TODGA (Figure 2.2.4) (0.1 M) in an aliphatic solvent, preferential extraction of Dy was observed with a maximum separation factor of 39 ± 1.1 over Nd achieved.[172] Very little Fe, the main constituent within permanent magnets, was extracted. In another study, D2EHPA in a very low polarity solvent was used to extract Nd and Dy from magnet leachate with a maximum separation factor between Nd and Dy of 6.5 ± 0.4.[166] Little of the trace elements were extracted and the absolute extraction of Nd and Dy was significantly reduced in more polar solvents. Using a phosphonium ionic liquid, trihexyl(tetradecyl)phosphonium chloride (Figure 4.2.4), transition metals such as Fe and Co present within REE magnet waste have been extracted from HCl solutions.[176] REEs remained in the aqueous phase allowing for high separation values of 5.0×10^6 for Nd/Fe and 8.0×10^5 for Sm/Co to be attained.

In our case, contacting a model aqueous solution of equimolar Nd and Dy (0.01 M) in $NaNO_3/HNO_3$ (5.0 M/0.1 M) with **2AA** (0.1 M) in toluene results in the highly selective separation of Nd (35%) over Dy (<0.5%). Under the same conditions **IL0** extracts Nd (32%) but also Dy (5%) representing a separation factor for Nd/Dy of 9.46 ± 0.17, whereas for **2AA** the separation factor rises to 162 ± 2 (Table 3.5.5).

Table 3.5.5 – The separation of two REEs (0.01 M) using **IL0 or 2AA** (0.10 M) in toluene from a binary REE mixture (both 0.01 M), $NaNO_3/HNO_3$ (5.0 M/0.1 M) aqueous solution.

REEs in aqueous solution	**Separation factors e.g. $(La_{org}/La_{aq})/(Nd_{org}/Nd_{aq})$**	
	IL0	**2AA**
La/Nd	*6.14 ± 0.20*	*6.97 ± 0.12*
Ce/Tb	*25.9 ± 0.4*	*2670 ± 1340*

La/Dy	*70.2 ± 4.2*	*4280 ± 590*
Nd/Dy	*9.46 ± 0.17*	*162 ± 2*

The separation of La from Nd using either **IL0** (6.14 ± 0.20) or **2AA** (6.97 ± 0.12) is similar probably due to the fact that both reagents extract lighter REEs from single-metal solutions with comparable success (Figure 3.5.5.1 and Table 3.5.5). The difference is much more distinct when comparing the separation of La from Dy. **IL0** achieves a separation factor of 70.2 ± 4.2 but **2AA** achieves a separation factor of 4280 ± 590, a 60-fold increase.

The extraction of Nd can be maximised through multiple contacts of a Nd containing aqueous phase with the organic phase. Contacting **2AA** (0.25 M) with an aqueous $NaNO_3/HNO_3$ (5.0 M/0.10 M) phase containing Nd (0.05 M) and Dy (0.0025 M) (a concentration ratio representative of that obtained from the leaching of a permanent magnet) results in only 33% Nd extraction following the first contact. Repeatedly contacting the Nd–Dy aqueous phase with **2AA** (0.25 M) though results, by the 6th contact, in 99% Nd extraction, but <10% Dy extraction (Figure 3.5.6.2). This suggests that **2AA** can be effective at purifying Nd from 'end-of-life' magnets. The unfunctionalized IL **IL0**, under the same conditions equally extracts 99% Nd but also >70% of the Dy present by the 6th contact, reinforcing the comparative lack of selectivity of **IL0** for lighter REEs over heavier REEs.

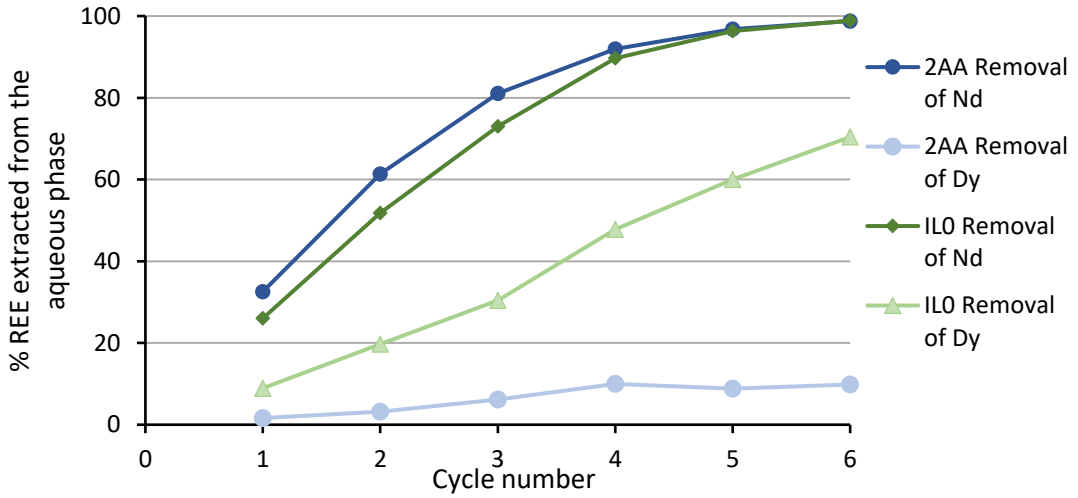

Figure 3.5.6.2 – The extraction of REEs using **IL0** or **2AA** (0.25 M) in toluene from a $NaNO_3/HNO_3$ (5.0 M/0.10 M) aqueous solution containing Nd (0.05 M) and Dy (0.0025 M). Multiple contacts of the same aqueous solution. Interpolation used to aid the eye only.

3.5.7 Summary of the use of amido-ammonium ILs to separate REEs

Incorporation of a 2° amide into the ammonium cation of a simple IL results in enhanced selectivity for the extraction of lighter REEs over heavier REEs by solvent extraction; this amido-functionalised IL is also more compatible with acidic solutions. Under the conditions and parameters tested, the lightest REEs (La, Ce) can be readily extracted (>80%) with **2AA**, while the heavier REEs (Tb, Dy) remain almost entirely (*ca*. 99%) in the aqueous phase. This leads to significant enhancement in the separation factors of Ce from Tb or Nd from Dy when compared to using non-functionalised **IL0**, suggesting that the amido-ammonium functionality is crucial to the mechanism of transport. This is reinforced by the fact that mixtures of **IL0** and a conventional 1°, 2° or 3° amide show no significant increase in performance. To help gain an insight into the differences in extraction between **IL0** and **2AA**, a series of analytical and computational studies were carried out.

3.6 Comparing the assemblies formed in the organic phases with IL0 and 2AA ILs

3.6.1 Karl-Fischer water content measurements

Similar to **IL0**, does not transport REEs through a reverse-micelle process. This was concluded through a similar series of experiments as those undertaken for **IL0** (section 2.7.1).

A linear increase in the volume of water transported as the concentration of **2AA** was increased (0.01 – 0.50 M) is observed (Figure 3.6.1.1), similar to **IL0**. Furthermore, contact of a solution of **2AA** with a $NaNO_3$/La (7.0 M/0.01 M) aqueous phase results in a lower volume of water being transported; at 0.1 M **2AA**, only 1016 ppm of water is transported compared with 1690 ppm for a water only contact. While **2AA** may be expected to transport more water than **IL0**, due to the secondary amide functional group having an increased propensity to form hydrogen bonds, 25% less water on average was transported with **2AA** than with **IL0**.

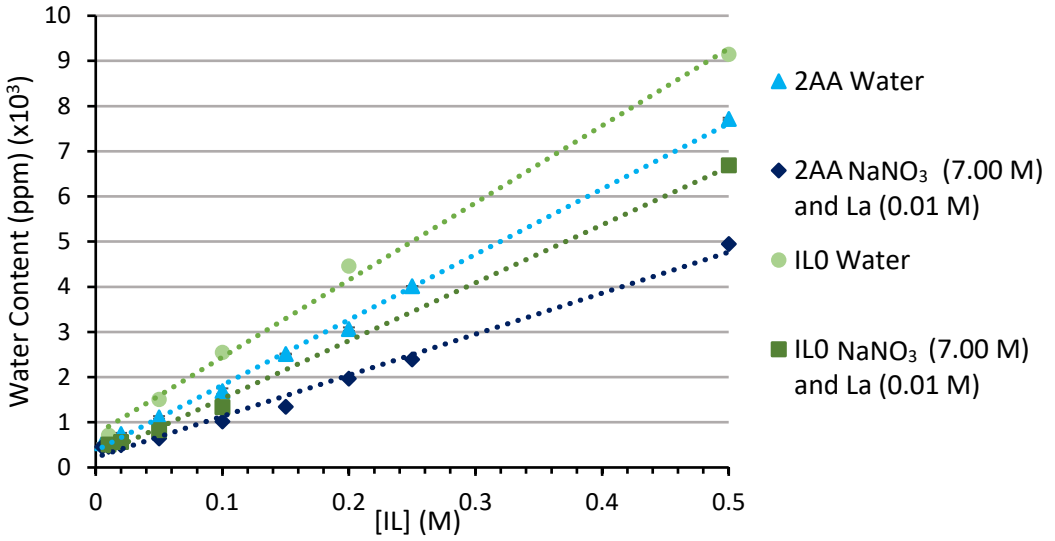

Figure 3.6.1.1 – Karl-Fischer measurements of the water content of solutions of **IL0** and **2AA** (0.01 - 0.50 M) in toluene after contact with water and a $NaNO_3$/La (7.0 M/0.01 M) aqueous phase.

When the REE (Nd) concentration (0.01 – 0.50 M) in the aqueous phase is varied but the **2AA** (0.25 M) concentration remains fixed, a decrease in water content (Figure 3.6.1.2) is observed in the organic phase, matching the trend of **IL0** (section 2.7.1); the water content in the loaded **2AA** organic phase was found to decrease from 2989 ppm to 1169 ppm. This indicates that the general mechanism of REE transport into the organic phase for both ILs is similar.

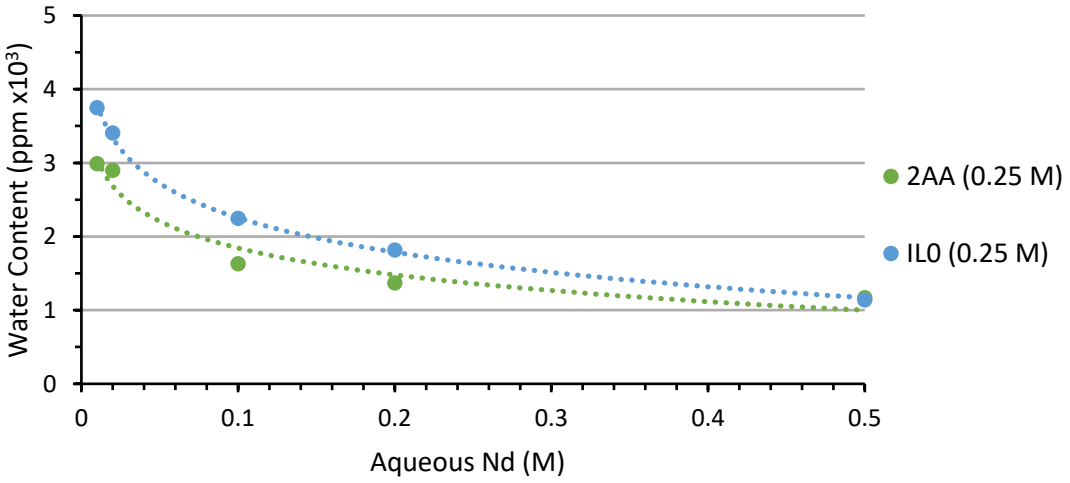

Figure 3.6.1.2 – Karl-Fischer measurements of the water content of solutions of **IL0** and **2AA** (0.25 M) organic phases after contact with an aqueous phase of varying Nd concentration ($NaNO_3$ 7.0 M, Nd 0.01-0.50 M).

3.6.2 Mass spectrometry of the 2AA organic phase

The similar pathway of REE extraction by **IL0** and **2AA** is additionally indicated by the mass spectrometry data. When the experimental procedure described previously for **IL0** (section 2.7.2) (where the organic phase content of La, Nd or Dy is maximised) is repeated with **2AA** instead, ions of the general formula $REE(NO_3)_4(\mathbf{2AA})_n^-$ (where n = 0 – 3) are identified in the –ve mode ESI-MS (Figure 3.6.2). A repeating unit of *m/z* 417.35 correlating to **2AA** is observed and no REE containing ions comprising more than three **2AA** were identified, although this may be due to the relatively harsh experimental mass spectrometry conditions, e.g. cone voltage, as previously discussed (section 2.7.2).[129, 130] Assemblies containing water molecules are not detected and the reasoning is previously discussed (section 2.7.2).

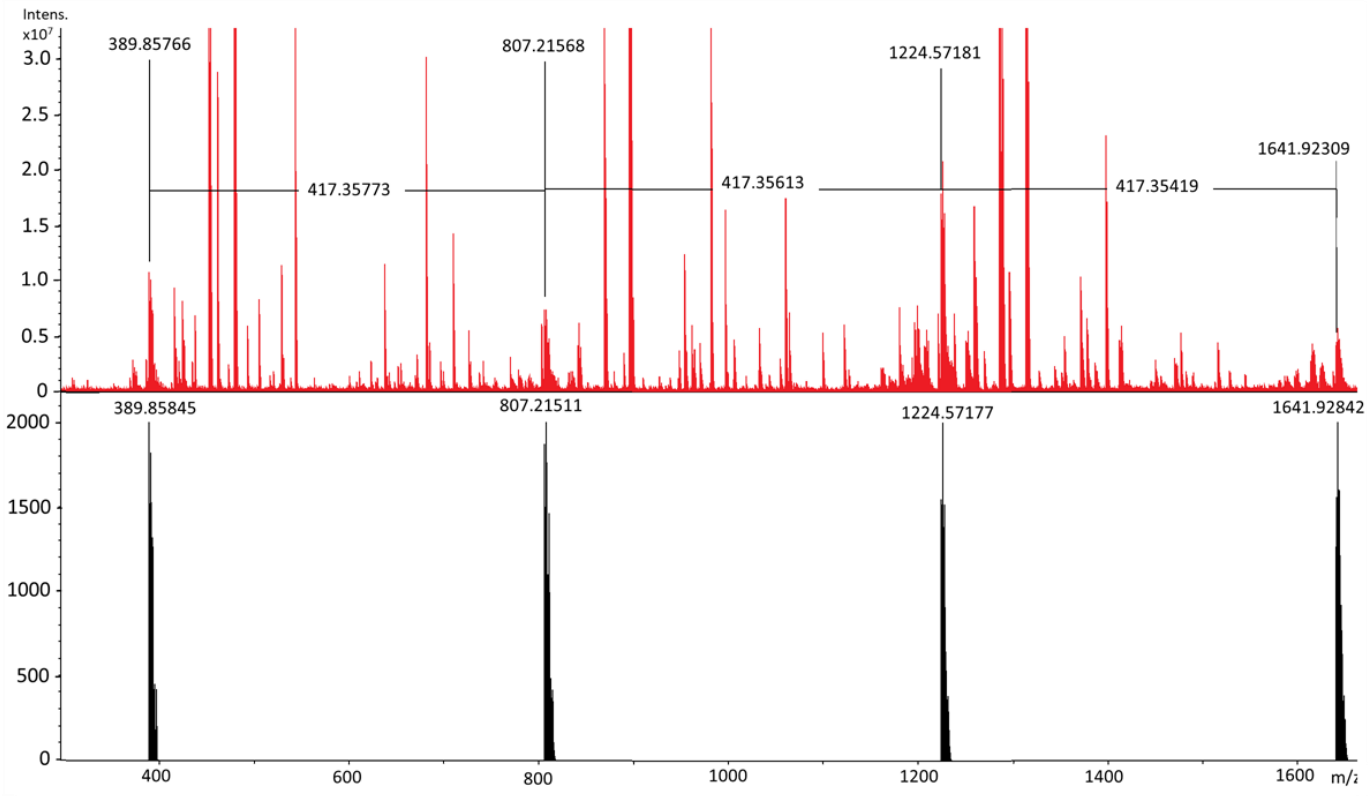

Figure 3.6.2 – Negative-ion mode ESI-MS of **2AA** (0.05 M) diluted with methanol (1:25,000) after contact with a $NaNO_3$ (7.0 M) aqueous phase containing Nd (0.05 M). Anions of the general formula $Nd(NO_3)_4(\mathbf{2AA})_n^-$ with *m/z* ratios of 389.8577 (n = 0, calc. 389.8585), 807.2157 (n = 1, calc. 807.2151), 1224.5718 (n = 2, calc. 1224.5718) and 1641.9231 (n = 3, calc. 1641.9284) are identified.

3.6.3 ^{1}H, ^{13}C and ^{15}N NMR studies

While the ammonium cation of **IL0** cannot coordinate directly to a REE, **2AA** could potentially coordinate directly to a REE centre through the amide group. REEs coordinated by neutral functional groups within overall positively charged ligands are known. These include a nine-coordinate Eu centre coordinated by a phosphine oxide donor group of an imidazolium ion (section 3.3) and a partially hydrated Y dimer complex bridged by two carboxylate groups of imidazolium cations.[160, 177] Currently, no crystalline complexes with a REE-amide-ammonium motif (Figure 3.6.3.1) are reported, or for any 3+ metal centre, but 2+ Mn,[178] Co,[179] Ni,[180] Cu,[181] and Zn[182] solid-state structures with a M-O=C-CH_2-NR_3^+ structural motif are known.

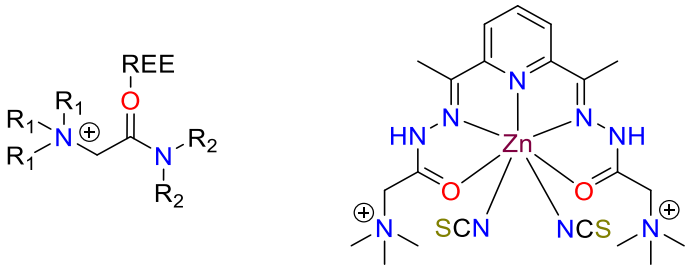

Figure 3.6.3.1 – Left: proposed inner-sphere coordination of an ammonium-amide ligand to a REE^{3+}. R_1 is any alkyl chain. R_2 is any alkyl chain or H. Right: A seven coordinate Zn^{2+} containing a Zn-amide-ammonium structural motif (CSD code: ADIROX).[182]

To investigate the potential inner-sphere binding of **2AA** to a REE centre, ^{1}H, ^{13}C, and ^{15}N NMR spectra of a solution of **2AA** (0.05 M) in deuterated benzene were recorded before and after contact with an aqueous solution of La (0.01 M) and $NaNO_3$ (7.0 M). If amide complexation to the La was to occur, a substantial chemical shift in the NMR spectra of nuclei associated with the amide functional group would be expected. A change in the chemical shift can also result from strong outer-sphere interactions between amide and anionic La nitratometalate.

The changes in the chemical shifts in the ^{1}H NMR spectra of **2AA** (Table 3.6.3) (Figure 3.6.3.2) are more significant than those seen for **IL0** (section 2.7.3). The largest proton chemical shifts correlate to those associated with the amide functional group. The amide proton (N**H**) shifts to a lower frequency (9.26 ppm to 8.56 ppm), indicating a large increase in shielding and electron density. The two neighbouring C$\mathbf{H}_2$ protons are also shifted, from 4.71 ppm and 3.32 ppm to 4.22 ppm and 2.91 ppm, respectively. These changes in proton chemical shifts are concurrent with previously reported chemical shift changes for these proton environments

following La-amide complex formation.[183, 184] Protons multiple bonds away from the amide functional group were only marginally shifted, with those furthest away (e.g. $OCNCH_2C\mathbf{H}_2$) actually becoming marginally more deshielded.

Table 2.7.3 – The change in ^{1}H NMR chemical shifts for **2AA** (0.05 M) after contact with a La (0.05 M), $NaNO_3$ (7.0 M) aqueous phase. NMR spectra were recorded in deuterated benzene.

Assigned Proton	^{1}H NMR shift before La (0.05 M) loading (ppm)	^{1}H NMR shift after La (0.05 M) loading (ppm)
N**H**CO	*9.26*	*8.56*
$NC\mathbf{H}_2N$	*4.71*	*4.22*
$OCNC\mathbf{H}_2$	*3.32*	*2.91*
$OCCH_2NC\mathbf{H}_2$	*3.29, 3.44*	*3.13, 3.43*
$NC\mathbf{H}_3$	*3.08*	*2.91*
$OCNCH_2C\mathbf{H}_2$	*1.64*	*1.69*

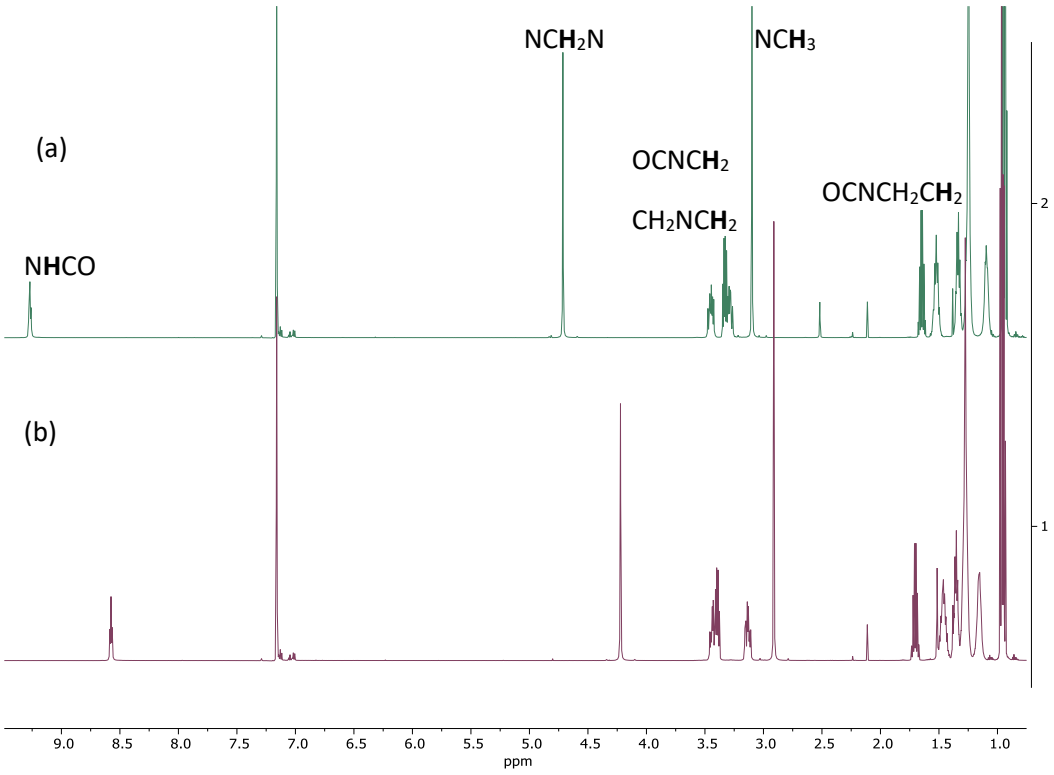

Figure 3.6.3.2 – A comparison of the ^{1}H NMR spectra of **2AA** (0.05 M) in deuterated benzene (a) before contact and (b) after contact with a $NaNO_3$/La (7.0 M/0.05 M) aqueous phase.

The $^{13}C[^{1}H]$ NMR spectra prior and post contact are very similar and almost unchanged, with the ^{13}C chemical shifts varying by less than 0.1 ppm (Figure 3.6.3.3) with one exception. The N**C**H_2CO carbon shifted to a lower frequency (60.9 ppm to 60.2 ppm), a 0.7 ppm shift suggesting a very minor increase of electron density.

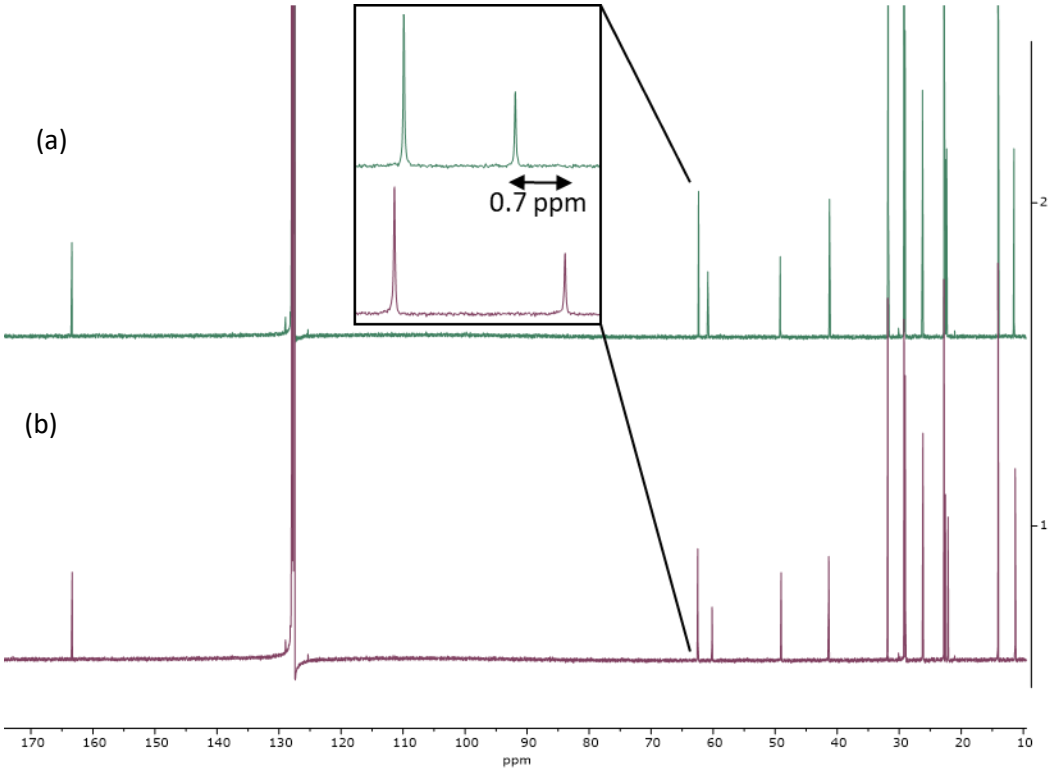

Figure 3.6.3.2 – A comparison of the carbon NMR spectra of **2AA** (0.05 M) in deuterated benzene (a) before contact and (b) after contact with a $NaNO_3$/La (7.0 M/0.05 M) aqueous phase.

Minor changes in the ^{15}N chemical shifts are observed in the HMBC long-range ^{1}H-^{15}N correlation NMR spectra (Figure 3.6.3.3). The amide nitrogen shifted to lower frequencies, from 127.3 ppm to 123.4 ppm and, to a lesser degree, the ammonium nitrogen shifted from 59.9 ppm to 59.0 ppm. The shifts for all nuclei are much less pronounced, if at all, when contacted with a $NaNO_3/HNO_3$ aqueous phase containing no REE. It should be emphasised that this is not evidence of an inner-sphere REE-amide-ammonium structural motif such as that illustrated (Figure 3.6.3.1) but merely that there is a significant change in the chemical environment of the atoms associated with the amide functional group. Considering that similar experiments using the paramagnetic REE (Ce) did not result in paramagnetically shifted and broadened resonances in the ^{1}H NMR spectrum after contact, it is highly doubtful

that there is any inner-sphere coordination of the amide to the REE, and instead only outer-sphere interactions exist.

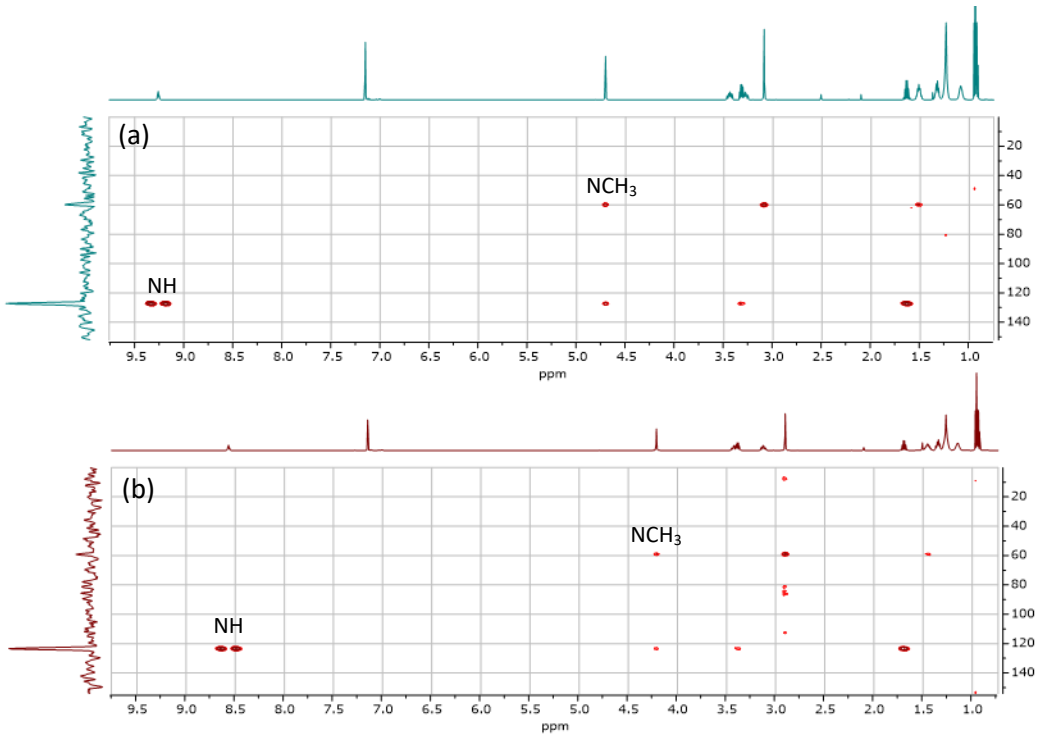

Figure 3.6.3.3 – A comparison of the HMBC long-range ^{1}H-^{15}N NMR spectra of **2AA** (0.05 M) in deuterated benzene (a) before contact and (b) after contact with a $NaNO_3$/La (7.0 M/0.05 M) aqueous phase.

3.6.4 Infrared spectroscopy

A weakening of the carbonyl C=O bond of **2AA** could be diagnostic of amide coordination to the Lewis acidic REE centre. Infrared spectrometry (IR) has, for example, been used to support the coordination of diglcyolamide ligands to REEs due to the observation of 25 cm^{-1} shifts in the carbonyl bond stretching frequency.[154, 185] The IR spectrum of **2AA** (0.05 M) in toluene was initially recorded against a toluene background. The amide carbonyl double bond stretch is observed as a distinct and sharp peak at 1683 cm^{-1} (Figure 3.6.4). The IR spectrum of **2AA** (0.05 M) acquired after multiple contacts with a $NaNO_3$/La (7.0 M/0.05 M) aqueous phase shows no shift of the carbonyl stretching frequency, suggesting that Lewis acid coordination does not occur, and is concurrent with only outer-sphere interactions between the amide and a La nitratometalate.

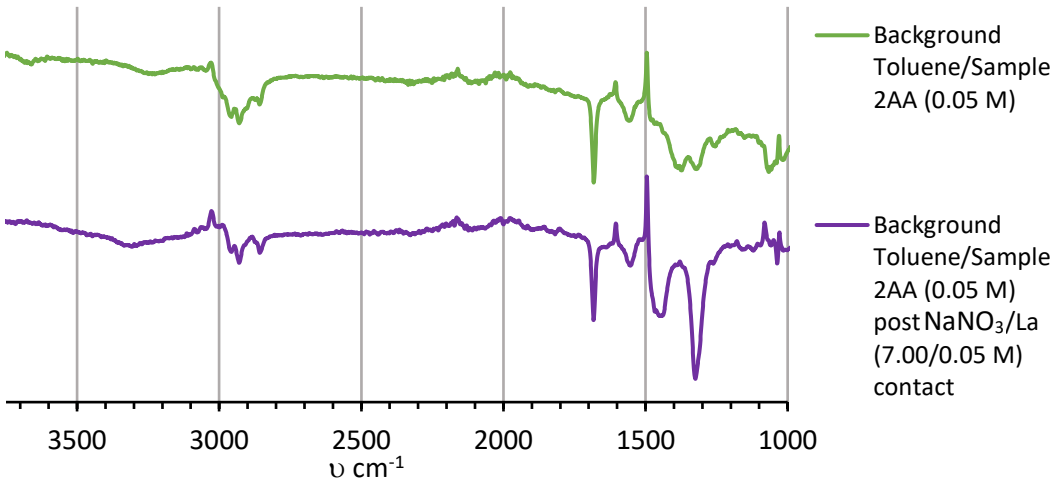

Figure 3.6.4 – The IR spectra of **IL0** (0.05 M), pre and post contact with a $NaNO_3$/La (7.0 M/ 0.05 M) aqueous phase. Compared against a toluene background.

3.6.5 Summary of the experimental analyses

The spectroscopic and analytical data show that **2AA** extracts REEs through the same general pathway as that of **IL0** where multiple NO_3^- anions are coordinated in the inner-sphere of a partially dehydrated REE to form the series of anions $REE(NO_3)_n(H_2O)_x^-$ (where n>3 and x>0). Given the notable shifts in the ^1H and ^{15}N NMR spectra, the improved REE extraction with **2AA** compared against **IL0** is plausibly a result of enhanced hydrogen-bonding interactions within the post REE extraction aggregates that are facilitated by the amide groups. To probe the potential of hydrogen-bonding interactions, and to help understand the differences between **IL0** and **2AA** computational studies comparing the two systems were undertaken.

3.7 Comparing the IL0 and 2AA organic phase assemblies computationally

3.7.1 Overview and introduction

The computational simulations undertaken for **IL0** (section 2.8) were replicated for **2AA** to allow comparison of the organic assemblies. Computational simulations modelling the formation of **2AA**-nitrate-water-La aggregates were run using classical molecular dynamics (MD) as described previously (section 2.8.1) and the starting geometry of the amido-ammonium cation (Figure 3.7.1) was optimised using DFT in the Gaussian 09 programme at

the B3LYP level of theory with the basis set 6-31+G* applied (Section 7.6)). Further details for sections 3.7.2 and 3.7.3 are provided in section 7.6.

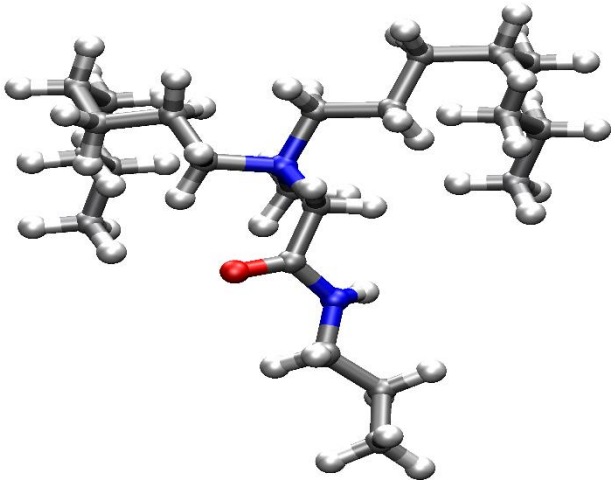

Figure 3.7.1 – The optimised starting geometry for the amido-ammonium cation of **2AA**.

3.7.2 Comparison of the classical MD simulated IL0-La and 2AA-La assemblies

A classical MD simulation of a 60 Å^3 randomly configured toluene solvent box comprising 1147 toluene molecules, three **2AA** extractants, three nitrate anions, three water molecules and one La^{3+} cation was allowed to proceed. Starting from a random configuration, a stable aggregate of ammonium cations, nitrate anions and water molecules is formed where multiple nitrate anions and water molecules are associated with a partially dehydrated La centre (Figure 3.7.2.1).

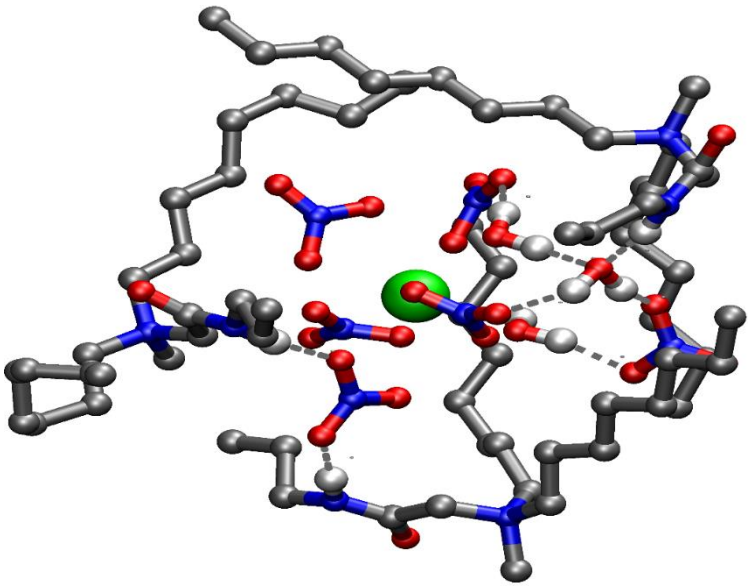

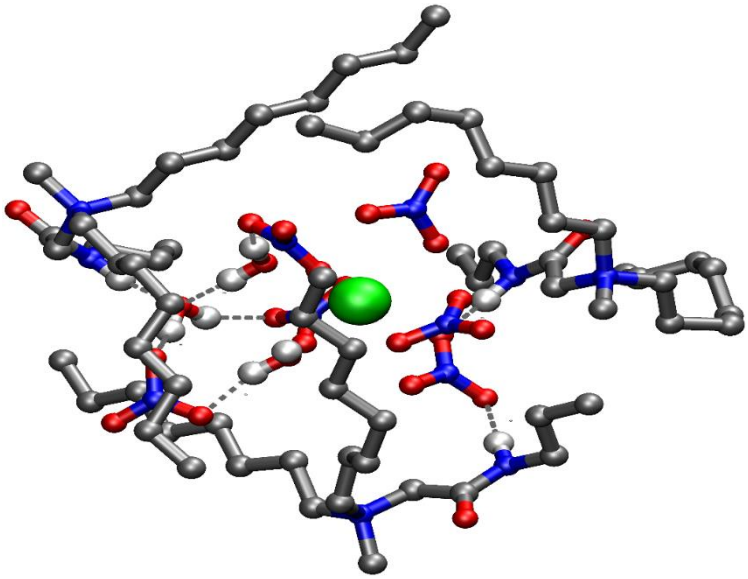

Figure 3.7.2.1 – The formation of a REE-**2AA**-water-nitrate aggregate following a classical MD simulation (top – front, bottom – reverse). Parameters for visualisation are described previously (section 2.8.2).

The aggregate initially appears remarkably similar to that of **IL0**-La although closer inspection reveals some structural differences. While the **IL0**-La aggregate (section 2.8.2) contained all three water molecules in the inner-coordination sphere of the La centre and were encapsulated well within the lipophilic alkyl carbon chains, the **2AA**-La aggregate only has two water molecules, with the third residing away from the La centre and interacting only with a nitrate anion and amide group (Figure 3.7.2.1).

By comparing the average number of water molecules and nitrate anions associated with La as the distance from the La centre increases, it is confirmed that only two water molecules interact with the La centre and are always with 2.75 Å (Figure 3.7.2.2). Five nitrate anions were found to always be within 3.65 Å while the final nitrate anion in the **2AA**-La simulation is always closer (<6.05 Å) than in the **IL0**-La simulation (>10.0 Å). The average distance of the amide group (oxygen and nitrogen atoms) to the La centre indicates that inner-sphere coordination of the amide does not occur (O-La distance >6.25 Å) comparing well with the FT-IR and NMR spectroscopic data. The absence of amide-REE coordination here represents a divergence from previous amide and REE MD modelling work that reports the presence of amide-REE coordination.[50, 52, 186, 187]

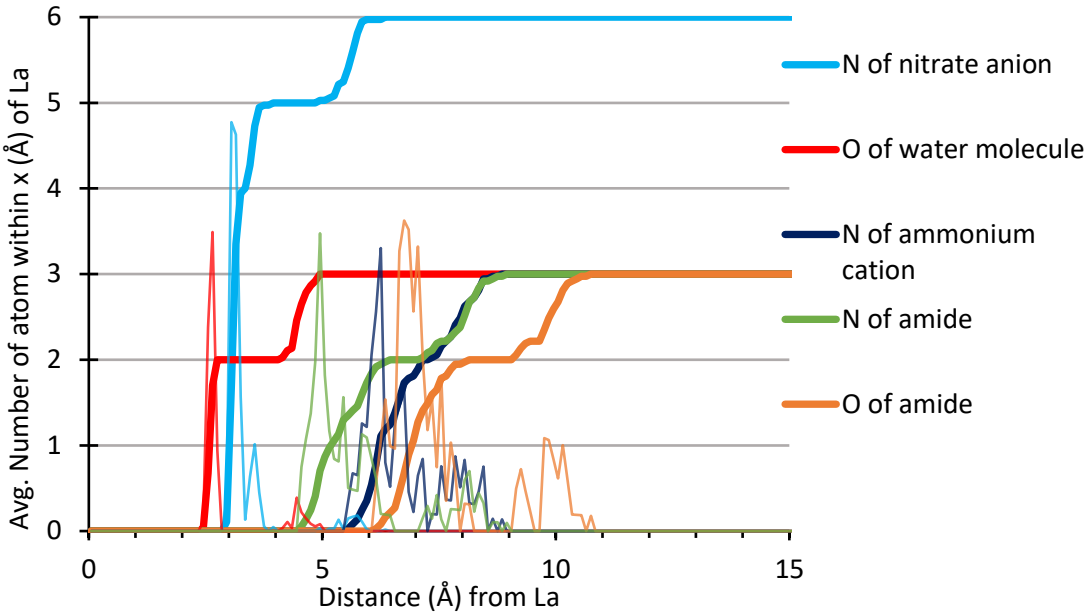

Figure 3.7.2.2 – Integrations obtained from the g(r) output plot from a classical MD simulation indicating how the average number of **2AA** extractants, water molecules and nitrate anions associated with La increases as a function of distance from La following the spontaneous formation of a La-containing aggregate. Averaged over 50 simulation frames (0.75 ns).

The amide functional groups of **2AA** contribute to a hydrogen-bonding network that is much more complex than that observed with **IL0**, providing hydrogen-bonding interactions similar to those reported previously within other amide-REE MD simulations.[188] The hydrogen-bonding interactions of the **2AA** amide groups, nitrate anions and water molecules (Figure 3.7.2.1) help provide a molecular scaffold for the more lipophilic alkyl chains and thus results in the components of the assembled aggregate residing closer to one another.[189, 190] As **IL0** can only form non-classical hydrogen bonds (Figure 2.8.2.1), the lipophilic alkyl chains in this case are more poorly templated leading to reduced encapsulation of the La centre and an aggregate of lower sphericity. In contrast, encapsulation measurements using a Monte Carlo script (section 7.6.2) for aggregates formed using **2AA** show a lower La core exposure (over 50 simulation frames) of 3.8 ± 0.5 % than that of **IL0** (4.9 ± 0.4%).[43] The more effective shielding and encapsulation of the La by **2AA** than **IL0** may help explain why **2AA** extracts La more readily from mildly acidic solutions.

Interestingly, when repeating the MD simulations using **1AA** or **3AA** (parameters provided and discussed in section 7.6) aggregation still occurs suggesting that under classical MD

conditions, all charged components within the non-polar solvent will, given enough time, aggregate (Figures 3.7.2.3 – 3.7.2.4). The stability of the aggregates studied thus appears to depend upon how effectively a molecular scaffold of comparatively polar constituents can promote the assembly of only weakly charged lipophilic groups.

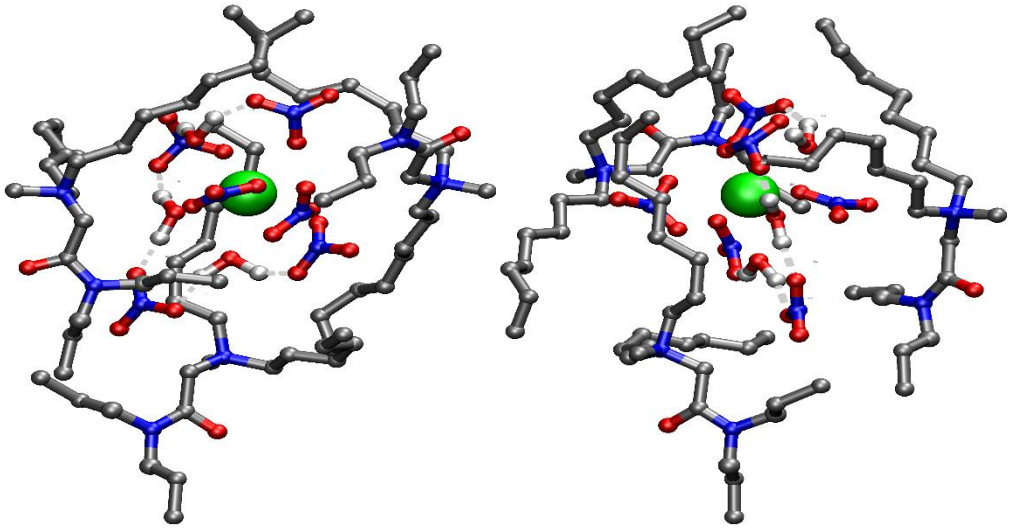

Figure 3.7.2.3 – The formation of a REE-**3AA**-water-nitrate aggregate following a classical MD simulation (left – front, right – reverse).

The amide groups of **3AA**, in contrast to **2AA**, are not involved in hydrogen-bonding (Figure 3.7.2.3) and instead have a tendency to be positioned on the periphery of the assembly, meaning only water molecules and nitrate anions are within the hydrogen-bonding network. Meanwhile, **1AA** creates an effective cavity for La with an extensive hydrogen-bonding network of multiple amide-nitrate, amide-water and water-nitrate interactions (Figure 3.7.2.4). This is somewhat surprising given that **1AA** is a relatively poor reagent for the recovery of REEs (section 3.5) which perhaps arises from the lipophilicity of **1AA** being insufficient to adequately shield the REE centre, limiting its ability to transport REEs into the organic phase.

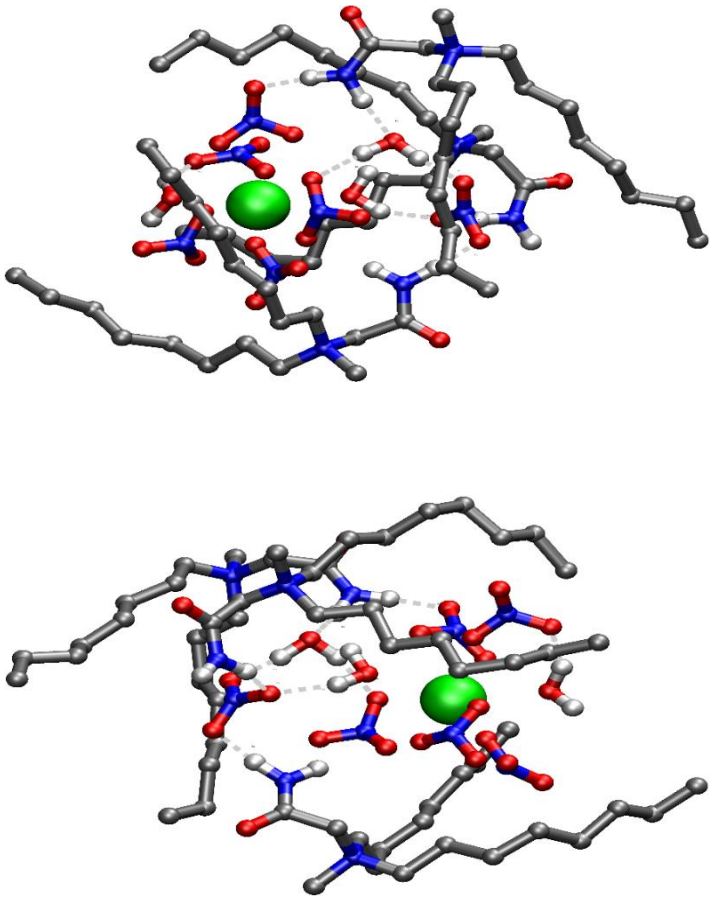

Figure 3.7.2.4 – The formation of a REE-**1AA**-water-nitrate aggregate following a classical MD simulation (top – front, bottom – reverse).

3.7.3 Comparison of the REE-IL0 and REE-2AA assemblies by DFT

Aggregation can be observed in all the MD simulations (section 3.7.2) indicating that classical MD simulations alone cannot fully explain the differences in REE extraction with **IL0** and **2AA**. The amide-REE aggregates seen by MD simulations suggest that small contributions to stability that manifest beyond the primary coordination sphere, such as hydrogen-bonding interactions, are essential.[189, 190] To quantify the subtle differences in stability of the La-**IL0** and La-**2AA** aggregates, a series of DFT calculations were undertaken. The stable La-**2AA** aggregation (Figure 3.7.2.1) from the MD simulations was optimised to allow comparison to the La-**IL0** structure (section 2.8.6). MD simulations with Nd and Dy, rather than La, were undertaken with both **IL0** and **2AA** and the resulting Nd-**IL0**, Dy-**IL0**, Nd-**IL0** and Dy-**2AA** assemblies were optimised to allow for comparison across the f-block. DFT calculations were

all undertaken at the M06 level of theory with the basis set 6-31+G* applied (section 7.6) and the distance cut-off for inner-sphere coordination was set at 3.0 Å.

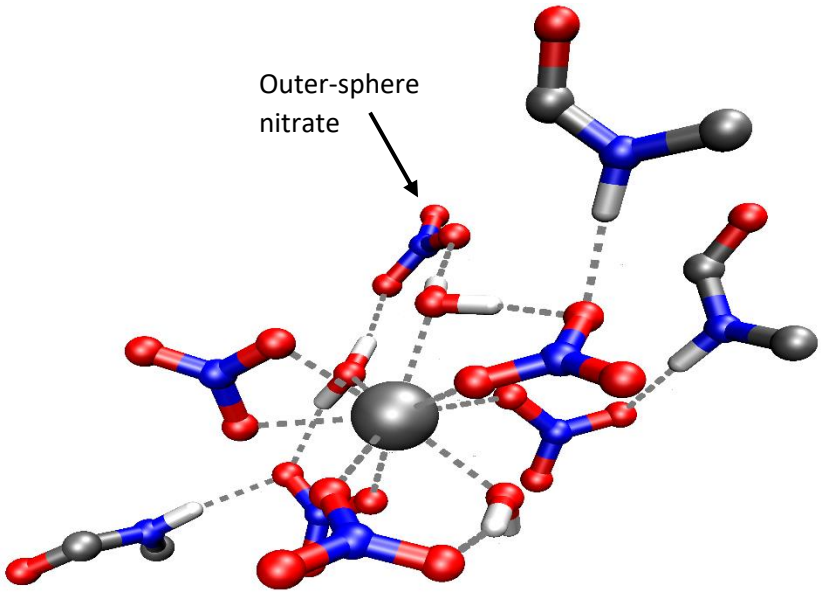

Figure 3.7.3.1 – A DFT optimised structure of a Dy-containing aggregate from an MD simulation comprising one Dy (black), three nitrate anions, three **2AA** extractants and three water molecules. Only the amide functional group of the ammonium cation is shown and depth visualisation is applied for clarity.

The six optimised structures consisted of a 9, 10 or 11 coordinate REE containing water molecules and a combination of mondentate and bidentate nitrate anions in the inner-coordination sphere. Results are summarised in the table below (Table 3.7.3.1). The coordination number trends downwards from La to Dy as expected.[4, 86, 88, 136] Dependant on REE, the coordinated water molecules resided at an average distance of between 2.43 – 2.70 Å and the coordinated nitrate anions between 2.47 – 2.70 Å. These compare well with solid phase crystallographic data for a La-nitrate complex (CSD code: MUQREW) with average La-O water bonds of 2.55 Å and average La-O nitrate bonds of 2.69 Å.[104] In both the **IL0** and **2AA** simulations, nitrate anions act as structural 'anchors' by donating electron density to hydrogen-donors such as water molecules (Figure 3.7.3.1). To a greater effect in the **2AA** simulations, amide groups are involved in hydrogen-bonding interactions and increase the molecular scaffolding.[48] Only hydrogen-bonding interactions where the H…X (where X is a Lewis-base) distance is shorter than 2.0 Å are illustrated.

Table 3.7.3.1 – A summary of the DFT optimised inner-coordination spheres of the La-**IL0**, Nd-**IL0**, Dy-**IL0**, La-**2AA**, Nd-**2AA** and Dy-**2AA** assemblies and their immediate outer-coordination spheres (approx. <5.0 Å). All distances in Å. Coordination number = CN.

Assembly	REE CN.	Water molecules		Nitrate anions			
		No. inner-sphere (avg. REE-O distance)	No. outer-sphere (REE-O distance)	No. inner-sphere (avg. REE-O distance)			No. outer-sphere (REE-O distance)
				Monodentate	Bidentate	Distance	
La-**IL0**	*11*	*3 (2.70)*	*N/A*	*2*	*3*	*(2.69)*	*0*
Nd-**IL0**	*11*	*1 (2.66)*	*1 (5.15)*	*0*	*5*	*(2.59)*	*0*
Dy-**IL0**	*10*	*1 (2.45)*	*1 (4.57)*	*1*	*4*	*(2.49)*	*0*
La-**2AA**	*11*	*2 (2.57)*	*1 (4.66)*	*1*	*4*	*(2.70)*	*1 (5.11)*
Nd-**2AA***	*10*	*2 (2.51)*	*1 (4.75)*	*3*	*2*	*(2.62)*	*0*
Dy-**2AA**	*9*	*3 (2.43)*	*N/A*	*4*	*1*	*(2.47)*	*1 (4.74)*

*The inner-coordination sphere of the Nd-**2AA** assembly also contains one coordinated ammonium-amide with a REE-O bond distance of 2.56 Å.

With the assemblies showing distinctly different inner-coordination spheres, a series of formation energy (ΔU_f) calculations (section 7.6.3) were undertaken to determine if the formation of the REE-**2AA** organic phase assemblies was more thermodynamically favourable than REE-**IL0** assembly formation and if formation of La assemblies was more favourable than Nd or Dy, to explain the selectivity seen experimentally. The formation energies of all the assemblies were calculated from the internal energies of all the individual components and of the REE-IL assemblies (Eq. 3.7.3).

Eq. 3.7.3 – $\Sigma\, U(\text{products}) - \Sigma\, U(\text{reactants})$

Where an REE-IL assembly is the product and water molecules, a REE cation, ammonium cations and nitrate anions are the reactants. The formation of all assemblies was determined to be favourable (Table 3.7.3.2). The formation energies of the **2AA** assemblies were more negative than those of **IL0** and this agrees with the experimental work that indicates that **2AA** forms more stable complexes with REEs than **IL0**. Formation energies of −37 KJ mol^{-1} for La-**IL0** and −157 KJ/mol^{-1} for La-**2AA** compare favourably with formation energies for other supramolecular assemblies formed following metal recovery processes.[84, 85]

Basis set superposition error (BBSE) has not been accounted for this work. BSSE manifests itself from the basis set used typically describing the orbitals within assemblies (products) more accurately than the individual components (reactants). This can result in a formation energy (ΔU_f) error of up to 30% for a basis set such as 6-31+G* (section 7.6.3).[191-193] This error can be somewhat mitigated by using a basis set that includes more Gaussian functions (e.g. 6-311+G*) but this increases computational demand which, in these simulations, is already very high. BSSE can be accounted for using the counterpoise correction method although as each REE-IL assembly in this work involves 13 reactants, this too was determined to be computationally unfeasible.[194] As BSSE is systematic of all the simulations discussed and the error in the formation energies (ΔU_f) should be comparable due to the structural similarity of the assemblies, BSSE has not been accounted for.

Table 3.7.3.2 – The formation energies of REE-IL assemblies.

Assembly	**Formation energies (ΔU_f) (KJ mol^{-1})**
La-**IL0**	*-37*
Nd-**IL0**	*-182*
Dy-**IL0**	*-273*
La-**2AA**	*-157*
Nd-**2AA**	*-295*
Dy-**2AA**	*-419*

In disagreement with the experimental trend, the Nd and Dy assemblies were calculated to form more readily than the La assemblies (Table 3.7.3.2). The formation energy calculations suggest that Dy should be the most readily extratced REE studied but experimentally this does not occur. The input geometries for these DFT calculations were very large assemblies from classical MD simulations, consisting of either 250 or 274 atoms and is nearing the limit of what is computationally feasible with QM. Associated with these large REE-IL assemblies will be complex potential energy surfaces with many local minimum and as such the global minimum is perhaps difficult to reach (section 7.6).[195] Therefore, it is possible that within the Dy classical MD simulations a more stable assembly was formed than in the La MD simulations, resulting in a local minimum of lower energy following DFT optimisation.

To investigate this, Dy was simply replaced with La or Nd in the DFT optimised structures of Dy-**IL0** and Dy-**2AA** and re-optimised. Conversely, La was replaced with Dy in the DFT optimised structures of La-**IL0** and La-**2AA**, and re-optimised. As hypothesised, the formation energies for the La-**IL0**, La-**2AA**, Nd-**IL0** and Nd-**2AA** assemblies, having started from the Dy-**IL0** and Dy-**2AA** scaffolds were more negative than those initially obtained, indicating that this geometry is overall a more stable assembly regardless of the REE. The formation energies for the Dy-**IL0** and Dy-**2AA** assemblies having started from the La-**IL0** and La-**2AA** scaffolds were less negative than those of the initial Dy-I**L0** and Dy-**2AA** assemblies (Table 3.7.3.3).

Table 3.7.3.3 – The formation energies of REE-IL assemblies.

Initial assembly	REE replacement	Formation energies (ΔU_f) (KJ mol^{-1})
La-**IL0**		*-37*
	When La is replaced with Dy	*-193*
Nd-**IL0**		*-182*
Dy-**IL0**	When Dy is replaced with La	*-79*
	When Dy is replaced with Nd	*-234*
		-273
La-**2AA**		*-157*
	When La is replaced with Dy	*-325*
Nd-**2AA**		*-295*
Dy-**2AA**	When Dy is replaced with La	*-245*
	When Dy is replaced with Nd	*-383*
		-419

Interestingly, the La assemblies, even when starting from the DFT optimised Dy assemblies (Dy-I**L0** and Dy-**2AA**), still remain the least stable and the Dy assemblies still remain the most stable. The lowest energy structure found for La-**IL0** has a formation energy of -79 KJ mol^{-1} compared against -234 KJ mol^{-1} for Nd-**IL0** and -273 KJ mol^{-1} for Dy-**IL0** (Table 3.7.3.3, Figure 3.7.3.2). The lowest energy structure found for La-**2AA** has a formation energy of -245 KJ mol^{-1} compared against -383 KJ mol^{-1} for Nd-**2AA** and -419 KJ mol^{-1} for Dy-**2AA** (Figure 3.7.3.3).

The calculated approximate 285 KJ mol^{-1} difference for $\Delta_{hyd}G^*$ between La and Dy is of a similar magnitude to the difference in assembly stability (ΔU_f).[85-88] The DFT modelling work

has attempted to account for hydration enthalpy by applying a polarizable continuum model (PCM) of water to the DFT optimisation of highly polar components although this consideration is perhaps insufficient to account for the stability differences resulting in the observed discrepancy between computational and experimental data. This discrepancy is discussed and considered further later in the chapter and within the conclusion.

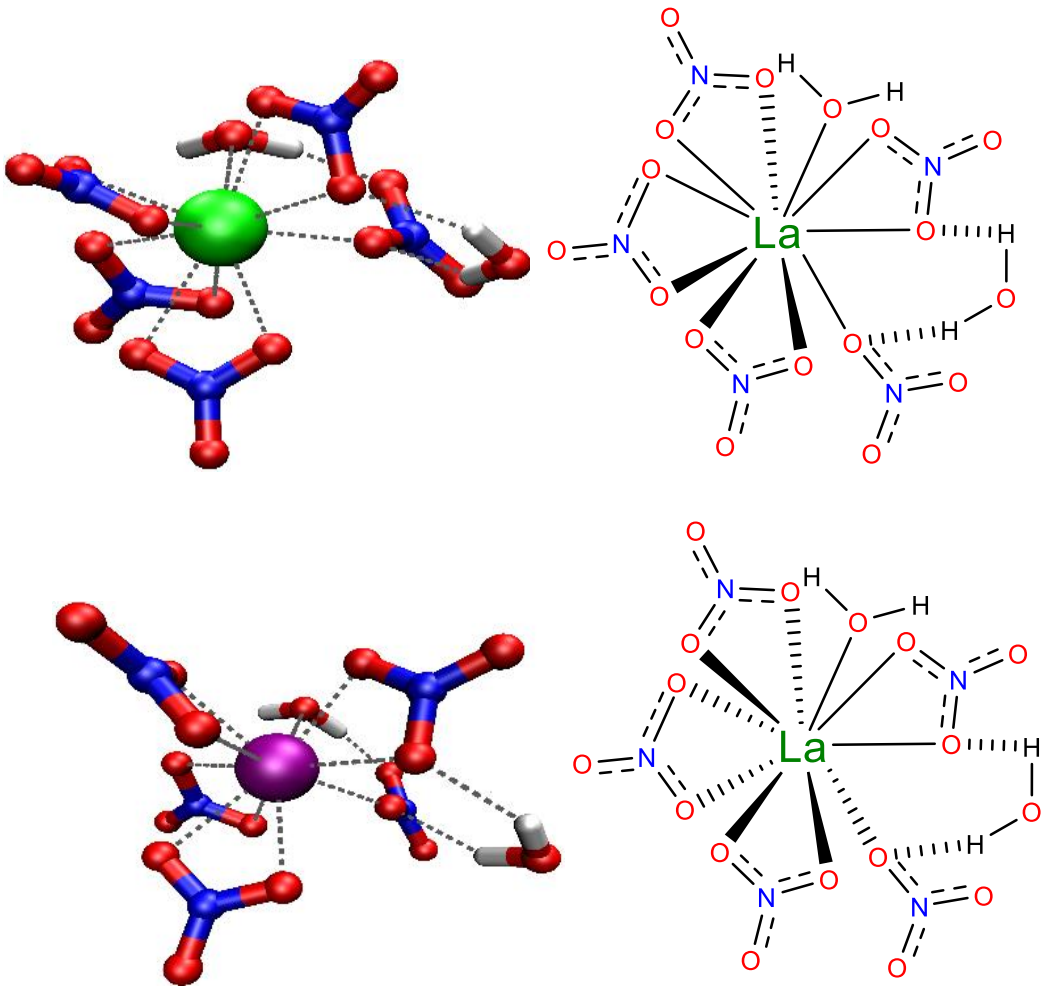

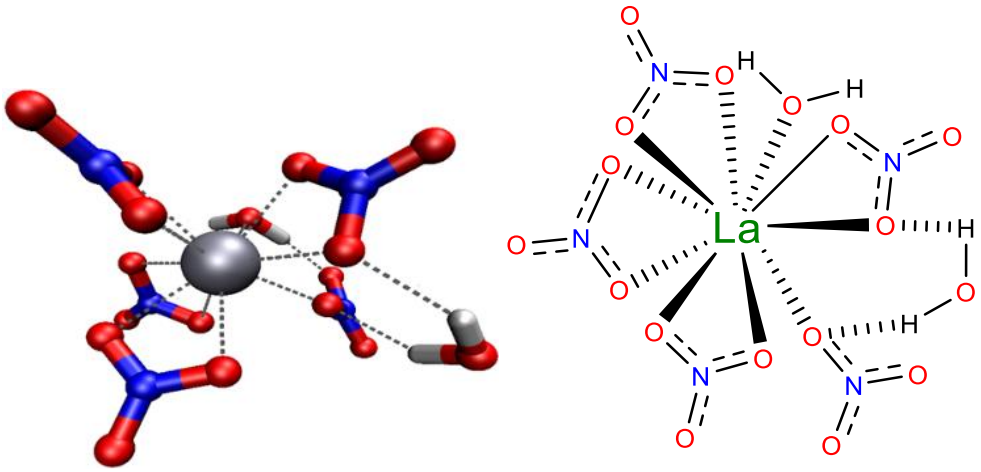

Figure 3.7.3.2 – The lowest energy structures found for DFT-optimised assemblies of La-**IL0** (top) Nd-**IL0** (centre) and Dy-**IL0** (bottom). La (green) and Nd (purple) assemblies have been optimised from the optimised Dy-**IL0** (black) structure. For clarity, the ammonium cations are hidden, depth visualisation is applied and ChemDraw representations provided.

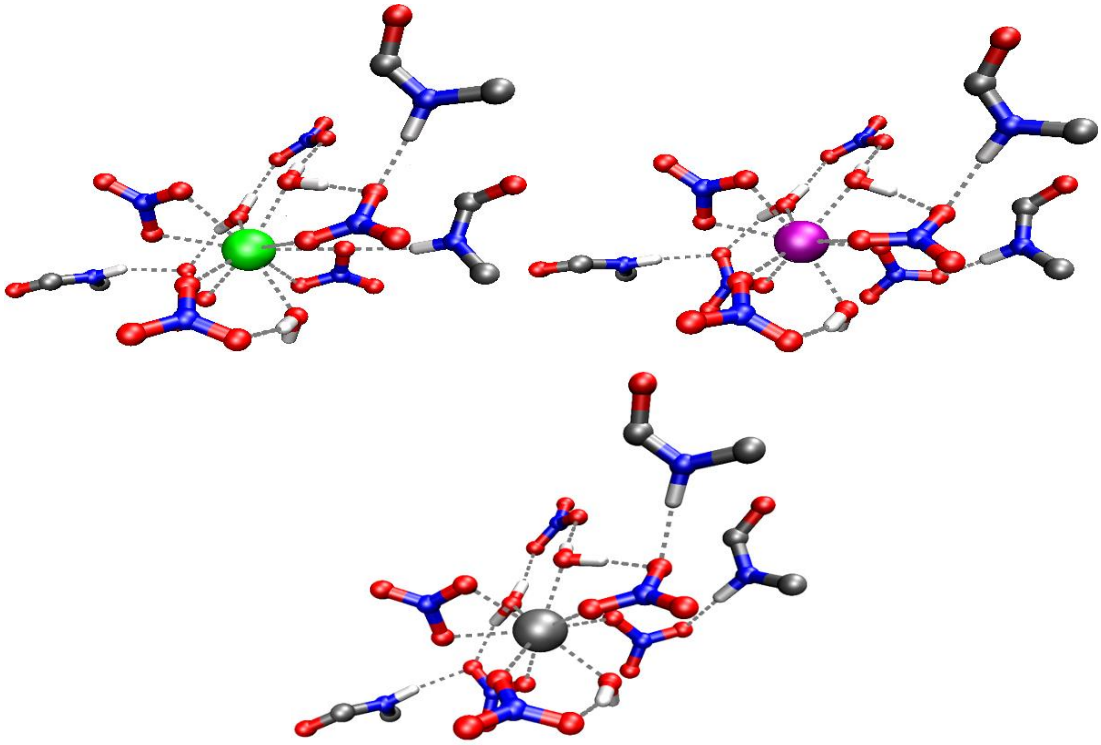

Figure 3.7.3.3 – The lowest energy structures found for DFT-optimised assemblies of La-**2AA** (top) Nd-**2AA** (centre) and Dy-**2AA** (bottom). La (green) and Nd (purple) assemblies have been optimised from the optimised Dy-**2AA** (black) structure**.** For clarity, only the amide functional group of the ammonium cation is shown and depth visualisation is applied.

In each DFT geometry optimisation, the inner- and outer-coordination shells remain broadly unchanged following replacement of one REE with another (Figures 3.7.3.2 – 3.7.3.3, Table 3.7.3.4). The exception to this is the replacement of Dy in the Dy-**2AA** assembly with La. The REE coordination number increased from nine to ten due to the bidentate coordination of two nitrates rather than one and can be attributed to the larger radii of La that is able to accommodate higher coordination numbers than Dy.[4, 5, 136] The only changes observed in the other DFT optimisations were either minor bond contractions (<0.2 Å) such as upon replacing La with Dy or minor bond elongations (<0.2 Å) such as upon replacing Dy with La and is predominately due to the different Lewis acidity of each REE. The coordinated water molecules resided at an average distance of between 2.43 – 2.63 Å and the coordinated nitrate anions between 2.47 – 2.66 Å dependant on REE.

Table 3.7.3.4 – A summary of the DFT optimised inner-coordination spheres of the lowest energy structures found for the La-**IL0**, Nd-**IL0**, Dy-**IL0**, La-**2AA**, Nd-**2AA** and Dy-**2AA** assemblies and their immediate outer-coordination spheres (approx. <5.0 Å) having started from DFT optimised Dy-**IL0** or Dy-**2AA**. All distances in Å. Coordination number = CN.

Assembly	**REE CN.**	**Water molecules**		**Nitrate anions**			
		No. inner-sphere (avg. REE-O distance)	**No. outer-sphere (REE-O distance)**	**No. inner-sphere (avg. REE-O distance)**			**No. outer-sphere (REE-O distance)**
				Monodentate	Bidentate	Distance	
La-**IL0**	*10*	*1 (2.63)*	*1 (4.59)*	*1*	*4*	*(2.62)*	*0*
Nd-**IL0**	*10*	*1 (2.56)*	*1 (4.60)*	*1*	*4*	*(2.57)*	*0*
Dy-**IL0**	*10*	*1 (2.45)*	*1 (4.57)*	*1*	*4*	*(2.49)*	*0*
La-**2AA**	*10*	*3 (2.57)*	*N/A*	*3*	*2*	*(2.66)*	*1 (4.89)*
Nd-**2AA**	*9*	*3 (2.51)*	*N/A*	*4*	*1*	*(2.54)*	*1 (4.80)*
Dy-**2AA**	*9*	*3 (2.43)*	*N/A*	*4*	*1*	*(2.47)*	*1 (4.74)*

While solid state structures of partially hydrated REE-nitrate complexes are rare, these bond distances are comparable those reported such as a $[Nd(NO_3)(H_2O)_6](NCS)_2(H_2O)$ compound (CSD code: QQQFQD) where Nd-water bond distances of 2.60 Å and a Nd-nitrate bond distance of 2.51 Å were reported. The ability for the amide groups to provide a molecular

scaffold is retained when Dy is replaced with La or Nd. The amide groups 'pull' the lipophilic ammonium cations closer to the REE nitratometalate through hydrogen-bonding interactions with nitrate oxygens. The increased thermodynamic stability of the **2AA** assemblies over the **IL0** assemblies can be attributed to the increased stability that these amide-nitrate hydrogen-bonding interactions provide. Hydrogen-bonding interactions between water molecules and nitrate anions are prominent in both the **IL0** and **2AA** assemblies and contribute towards the negative formation energies of the **IL0** and **2AA** assemblies. While a single hydrogen-bond only provides a relatively small stability gain, several hydrogen-bonding interactions collectively provide a significant gain to stability.[189]

While these (Figures 3.7.3.2 – 3.7.3.3) are the lowest energy structures found it should be stressed that they still may not be the global minimum energy structures, given that they fail to account for the selectively found experimentally, and are perhaps still only local minimum on a very complex potential energy surface.[195] Clear discrepancies remain between the experimental and computational trends which cannot be ignored.

The classical MD simulations and the DFT simulations only model the formation of one singular $REE(NO_3)_3(IL)_3(H_2O)_3$ assembly as it would be very computationally demanding to model the interactions of multiple REEs with a large number of ILs.

However, as strongly suggested by multiple analytical and spectroscopic techniques, the organic phase contains many REE nitratometalates at a maximum REE loading of approximately 40% (assuming 3:1 ratio of REE: **IL0** or **2AA**). This initially suggests that the remaining ammonium cations of **IL0** or **2AA** in the organic phase do not associate with REE nitratometalates. Despite this, multiple ammonium cation environments are not observed on the NMR timescale (Figure 2.7.3.2 and 3.6.3.2), perhaps due to ammonium cations associated with REE nitratometalates exchanging with non-associated ammonium cations. Therefore while $REE(NO_3)_3(IL)_3(H_2O)_3$ assemblies may be present in the organic phase, and the 3:1 ratio of REE: **IL0** upheld, these assemblies may be more dynamic and less discrete than those modelled.

Additionally, the formation of clusters consisting of multiple loosely associated REE-IL assemblies, akin to those known for REE-diglcolamide systems (section 3.2), has not been totally discounted experimentally.[52] If weakly associated REE-IL clusters were present in the

REE loaded organic phase their detection by FT-ICR ESI-MS would be unlikely due to fragmentation.

The explanations as to why Dy complexes are the most stable computationally are speculative. Further computational modelling work is required to fully understand why there is a discrepancy between the experimental and theoretical work. This may involve the modelling of much larger simulations to try and accountant for potential bulk organic phase effects and dynamic exchange. EXAFS measurements have previously been successful at characterising challenging solution phase species and may provide a vital insight into the inner-coordination spheres in these REE-IL assemblies.[53, 109, 120, 155]

3.8 Conclusions

The 2° amido-ammonium IL **2AA** extracts lighter REEs with a significantly higher selectivity over heavier REEs than **IL0**. The high degree of separation of Ce from Tb or Nd from Dy is particularly promising given the occurrence of these REE pairs in a range of waste electronic and electrical equipment.[7, 165, 172, 174] The separation factors for these element pairs comfortably exceed those reached using conventional organophosphorus reagents. The 1° or 3° amido-ammonium ILs do not exhibit comparable performance, and neither does a synergistic mixture of **IL0** and a 2° amide, highlighting that particular structural characteristics of **2AA** are key to its performance.

Analytical and computational evidence indicates that **2AA** extracts REEs through a similar mode of action to **IL0**, forming $REE(NO_3)_5(H_2O)_2^{2-}$ nitratometalates in the organic phase. DFT simulations indicate that the amide groups of **2AA**, in combination with nitrate anions and water molecules, provide an extensive outer-sphere hydrogen-bonding network that provides a molecular scaffold for the comparatively lipophilic alkyl chains to encapsulate the REE-metalate which ultimately results in stronger light REE extraction than **IL0**. The small differences in ionic radii between the REEs appear to be amplified by these outer-sphere interactions and provide the greater selectivity observed.[80] Unfortunately not all of the computational work corroborates the experimental work and requires more investigation, with EXAFS measurements likely to be of great benefit.

If the ability of **2AA** to separate lighter REEs from heavier REEs remains effective when starting from ‘real’ non-synthetic leach solutions, and can be combined with a more

environmentally friendly leaching process that does not use harsh acidic conditions, a sustainable process to purify REEs could be proposed. As such, the bioleaching of REEs from a zirconate mineral and their subsequent separation using **2AA** in a solvent extraction process will be explored in Chapter 4.

Chapter 4

Bioleaching of REEs

4 Bioleaching of REEs

4.1 Introduction

The leaching stage of a hydrometallurgical flowsheet (section 1.2) for REE purification usually involves a strong inorganic acid or base at elevated temperatures. As highlighted earlier (section 1.3), industrial leaching operations can have a significant negative environmental impact. Alternative REE leaching methods are known, including the leaching of REEs with organic acids rather than inorganic acids or the bioleaching of REEs with a bacteria or fungi strain that either accelerates acid production or produces an organic acid as a metabolic by-product.[196, 197]

4.2 Leaching of REEs with organic solutions

Few studies have reported non-aqueous leaching processes of REEs but several non-aqueous leaching processes have been reported for transition metals.[196, 198, 199] One REE leaching study using an IL (Figure 4.2.1) at elevated temperatures, reported that over 70% of the trace REEs within bauxite residue were leached but that minimal (<3%) Fe and negligible value elements such as Si were leached.[200]

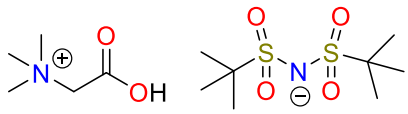

Figure 4.2.1 – An IL (betainium bistriflimide) used for the leaching of REEs from bauxite residue.[200]

At elevated temperatures (>55 °C), the IL (Figure 4.2.1) is water miscible allowing the leaching of REEs to proceed by the simplified equation:

Eq. 4.2.1 – $$6\ \mathbf{HIL} + REE_2O_3 \rightarrow 2\ REE(\mathbf{IL})_3 + 3\ H_2O$$

Where **HIL** is betainium bistriflimide and **IL** is deprotonated **HIL**.

Upon cooling, the water and IL phases disengaged and preferential leaching of REEs was observed. The ability to effectively leach REEs was attributed to the acidity of the ammonium cation which is reported to be more acidic (pK_a 1.83) than alkanoic acids such as acetic acid (pK_a 4.75) due to the inductive effect of the positive charge of the ammonium.[200, 201]

Earlier work showing limited solubility of Fe and Si in **HIL** explains why the leaching of REEs from bauxite residue is selective. Following leaching, bidentate coordination to the REE centre through the carboxylic acid groups of the betainium cation occured, and was confirmed by X-ray crystallography.[202] The REEs could be readily stripped from the IL organic phase with HCl (4.0 M), regenerating the IL.[200]

HIL in another study has been shown to preferentially leach the valuable red phosphor Y_2O_3:Eu^{3+} (YOX) while leaving other phosphors such as $LaPO_4$:Ce^{3+}, Tb^{3+} (LAP) and $BaMgAl_{10}O_{17}$:Eu^{2+} (BAM) undissolved.[203] Effectively complete leaching of the red phosphor was achieved by HIL and 5 wt% water at 90 °C over 96 hours. The researchers attributed the selective leaching to the inability of [Hbet][Tf2N] to solvate anions efficiently, meaning **HIL** almost exclusively dissolved only metal oxides such as Y_2O_3.

A mixture of choline chloride, urea and malonic acid (Figure 4.2.2) has been reported to leach Y, Sm and Nd selectively over La and Ce from bastnaesite, corroborating similar studies.[204, 205] Following leaching (1 week, 50 °C) >90% of Y, Sm and Nd was leached compared to <40% of Ce and La. Furthermore, negligible Ca, Mg and Fe were solubilised, minimising downstream process issues. Malonic acid reacted with the REE-carbonates producing H_2CO_3, accelerating the leaching process, although the processes resulted in consumption of malonic acid. Despite this drawback, the IL, choline chloride is naturally occurring, bolstering its environmentally friendly credentials.

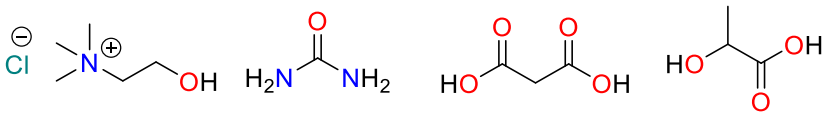

Figure 4.2.2 – Choline chloride (left). Urea (centre left). Malonic acid (centre right). Lactic acid (right).

Following ball-milling, the metallic elements (Fe, Co, Nd, Pr, Gd, and Dy) of a NdFeB magnet were effectively leached (>75%) with a choline chloride: lactic acid (1:2) (Figure 4.2.2) mixture (24 h, 70 °C).[206] Lactic acid reacted with the metal oxides present during leaching to produce water. Addition of water to the organic solution significantly decreased leaching (Figure 4.2.3), presumably due to water being a product of the leaching process. The leached transition metals (Fe and Co) were recovered using Aliquat 336 in toluene while REEs were recovered from the leach solution with D2EHPA.

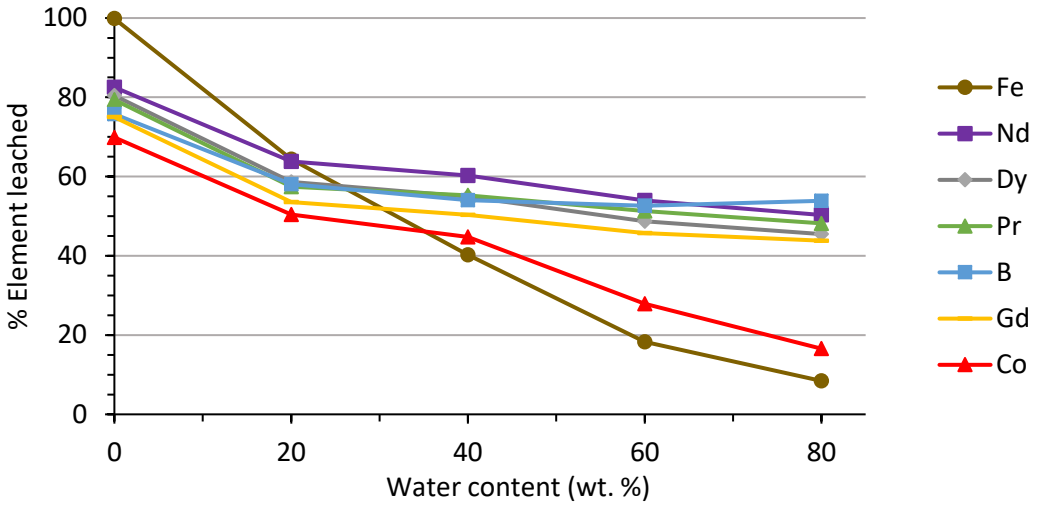

Figure 4.2.3 – The leaching of elements from waste NdFeB magnets with a choline chloride: lactic acid (1: 2) mixture with varying water content (wt. %).[206]

The effective solubilisation of REEs in these studies is due to the acidity of at least one component of the solutions.[161, 200, 204, 205] An alternative option is to use Cl_2 gas which is often used as oxidant in leaching processes despite its toxicity and lethality.[207, 208] Cl_2 gas can be safely stored by dissolving into a phosphonium chloride IL (Figure 4.2.4) resulting in phosphonium trichloride with no phosphonium cation degradation.[209]

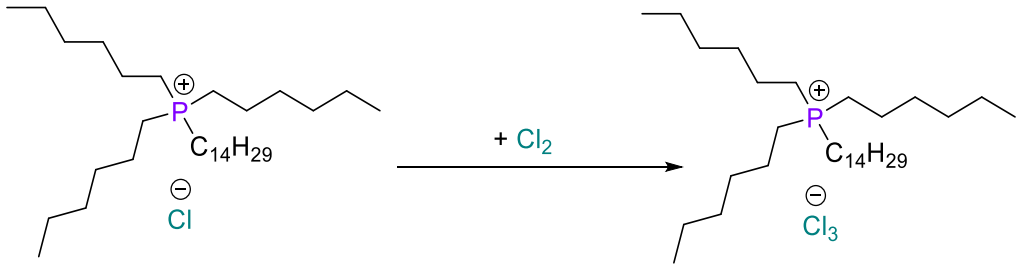

Figure 4.2.4 – The uptake of Cl_2 gas by the IL trihexyl(tetradecyl)phosphonium trichloride.[208]

The chlorinated phosphonium IL (Figure 4.2.4) leached Fe, Co, Cu and Sm from powdered SmCo magnets, forming the respective metalates of $FeCl_4^-$, $CoCl_4^{2-}$, $CuCl_4^{2-}$ and $SmCl_6^{3-}$. Due to the absence of excess water the Sm metalate was present, although upon water saturation of the organic IL phase, full aquation of Sm occured. The elements were sequentially stripped from the IL phase using NaCl (3.0 M) (Sm), water (Co), and NH_3 (1.0 M) (Cu, Fe) separating the metals effectively. While a typical hydrometallurgical process that uses solvent extraction may contain a leaching stage, an extraction stage and strip stage (sections 1.2 and 1.4), the

leaching of the metals using an IL removes the extraction stage, arguably streamlining the process.

4.3 Bioleaching of REEs

Bioleaching is extensively used within the Cu mining industry to recover Cu from low-grade ores and is effective due the ability of the bacteria strain A*cidithiobacillus ferrooxidans* to catalyse the oxidation of Fe^{2+} to Fe^{3+} (section 1.3).[36-38] In contrast, there is currently only one production scale REE bioleaching operation globally.[197] Despite minimal industrial uptake, the bioleaching of REEs has been investigated using bacterial and fungi strains. These have included, but not been limited to, P*enicillium tricolor* and A*spergillus terreus* which are fungi strains and the bacteria strains A*cetobacter sp.* and G*luconobacter oxydans*.[210-215] It can be postulated that any fungal or bacterial strain that metabolically produces an organic acid with a comparatively low pK_a value that can deprotonate and bind to a REE centre should promote the leaching of REEs into solution.

Penicillium tricol is a heterotrophic fungus that leaches REEs from bauxite residue despite the hostile environment of bauxite residue as of its low nutrient content, high NaOH content and toxicity.[210] The production of gluconic, oxalic and citric acid, determined by HPLC, by *Penicillium tricol* lowered the pH from >10.0 to <2.0 while simultaneously reducing the environment's toxicity towards the fungi strain by complexing toxic metal ions. A gradual increase in % leached was observed from the lighter (e.g. La and Ce) to heavier (e.g. Gd and Dy) REEs, increasing from around 30% (La) to 70% (Lu), which is a comparable trend to the leaching of REEs with ILs.[204, 205]

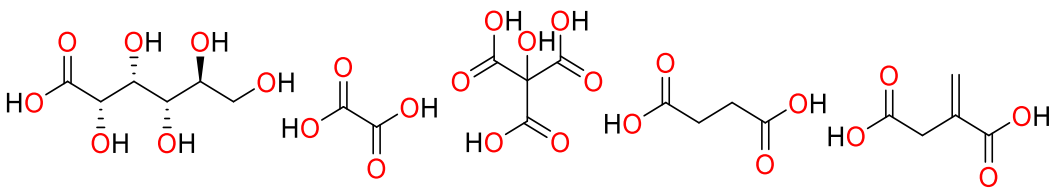

Figure 4.3.1 – Gluconic acid (left). Oxalic acid (centre left). Citric acid (centre). Succinic acid (centre right). Itaconic acid (right).

The bioleaching of monazite with a solution containing *Aspergillus terreus* is achieved by the production of the diprotic organic acids, succinic and itaconic acid, as metabolic by-products of the fungi growth.[211] Interestingly, when leaching with a synthetic solution of succinic and

itaconic acid at the equivalent pH and H^+ concentration the % of REEs leached was much lower. The ability of the heterotrophic fungus to provide enhanced REE dissolution over fungus absent conditions was not fully understood. It was hypothesised that consumption of phosphate anions by the heterotrophic fungus promoted additional REE dissolution as REE-phosphates are effectively insoluble ($<10^{-11}$ g/L) in water.

Heterotrophic fungi, such as *Penicillium tricol* and *Aspergillus terreus*, in contrast to autotrophic organisms, require an external energy input typically a sugar source (e.g. glucose) as heterotrophic fungi cannot generate their own energy.[216] Organic acids are produced as by-products from the enzymatic breakdown of sugars by amylase enzymes within fungi in aerobic processes.[213] Gluconic acid is formed from glucose through a two-step oxidative process *via* a lactone intermediate while citric acid is formed through a several step oxidative process named 'the Krebs cycle'. As glucose is essential to the growth of heterotrophic organisms, the cost of glucose needs to be considered in bioleaching operations. Cost analysis on the leaching of REEs from waste materials suggests that operational costs for a heterotrophic fungi leaching process would be lower than a traditional inorganic acid process.[213] The operational cost is expected to be even lower for autotrophic organisms such as *Acidithiobacillus ferrooxidans* that will be the focus of the research discussed in section 4.5.

4.4 Eudialyte

The leaching of eudialyte, a zirconosilicate mineral will be investigated in this chapter. Eudialyte is a comparatively rare, relatively low-grade ore mineral with significant deposits in Greenland, Sweden and Canada.[217] Eudialyte contains greater quantities of heavier REEs than more abundant REE minerals such as bastnaesite and, when compared against monazite, eudialyte contains very little Th or U. For these reasons, and due to the gradual depletion of these higher grade-REE deposits, eudialyte is potentially a future economically viable REE source.

The International Mineralogical Association (IMA) currently accepts $Na_{15}Ca_6Fe_3Si_{26}Zr_3O_{73}(O, OH, H_2O)_3(Cl, OH)_2$ as the formula for eudialyte with space within the complex framework filled by water molecules and anions (Cl^-, F^-, OH^- and SO_4^{2-}).[217] The crystal lattice typically has partial substitution of Fe by Mn and Si by Nb. EXAFS and XANES spectroscopy confirms that when present, all REEs, regardless of their radii, preferentially occupy the 6-coordinate

Ca sites.[217, 218] These Ca sites are of a distorted octahedral geometry with a slight contraction of z-axis M-O bonds (2.31 Å) and slight elongation of x- and y-axis M-O bonds (2.37 Å). The unit-cell structure of eudialyte is as below (Figure 4.4.1.1):

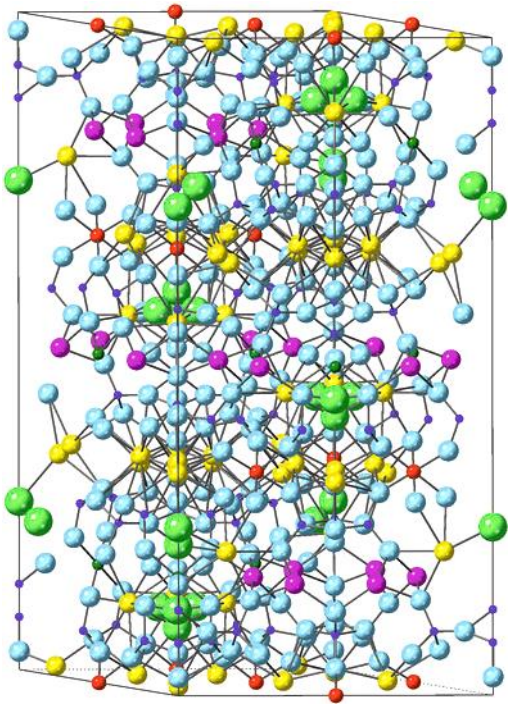

Figure 4.4.1 – Unit-cell crystal structure of eudialyte (CSD code: ICSD 9503).[217-219] Elements are coloured as Na (yellow), O (light blue), Ca/REE (magenta), Fe/Mn (dark green), Si/Nb (purple), Cl (light green) and Zr (red).

When Ca^{2+} ions are substituted by Y^{3+}, a contraction in all the metal–oxygen bonds distances is observed, decreasing from 2.31 Å and 2.37 Å to 2.24 Å and 2.30 Å respectively.[217] This can be attributed to the smaller ionic radius (1.0 Å vs. 0.9 Å) and a greater positive charge density. In contrast to eudialyte, where REE are present merely as a result of substitution into the regular crystal framework, REEs are integral to the repeating unit of more commonly mined monazite ($REEPO_4$) and bastnaesite ($REECO_3F$) which is why these minerals have traditionally been more economically viable REE sources.

Throughout the remainder of this chapter, the bioleaching assisted recovery of REEs from eudialyte will be investigated using *Acidithiobacillus ferrooxidans*.

4.5 REE bioleaching studies

4.5.1 Standard bacteria growth solution preparation

To H_2SO_4 (1 L, 2.5 mM), $(NH_4)_2SO_4$ (0.50 g), $MgSO_4.7H_2O$ (0.50 g) and KH_2PO_4 (0.50 g) were added.[220] The solution was then autoclaved (121 °C, 15 minutes). To H_2SO_4 (0.25 L, 25 mM), $FeSO_4.7H_2O$ (34.8 g, 0.125 M) was added and the solution then added to the autoclaved solution. In a laminar flow cabinet, the resulting $FeSO_4$ (0.1 M) and H_2SO_4 (6.9 mM) growth solution was filter sterilised (0.22 μm filter) and then stored in airtight vials (125 mL). This is the growth solution which will be referred to throughout this chapter.

4.5.2 Initial Bacteria growth

To assess the ability of *Acidithiobacillus ferrooxidans* (**ATs**) to promote the solubilisation of eudialyte, a series of leaching experiments were undertaken. In triplicate, flasks (with a membrane screw cap to allow inward O_2) containing **ATs** and the growth solution (125 mL) were allowed to agitate with the pH and oxidation of Fe^{2+} to Fe^{3+} measured over time. A control flask containing only growth solution was used as a reference.

An aliquot (5 mL) was acquired every 4 - 12 hours, filter sterilised (0.22 μm filter) and the pH measured for two weeks. Starting from an initial pH of 2.42, the solution containing **ATs** became more basic in the initial 36 hours, reaching a pH of 2.78 ± 0.02, before becoming gradually more acidic, stabilising at a pH of 2.16 ± 0.07 (Figure 4.5.2.1). In contrast, the pH of the flask without **ATs** remained almost unchanged, at a pH of 2.50-2.70 throughout.

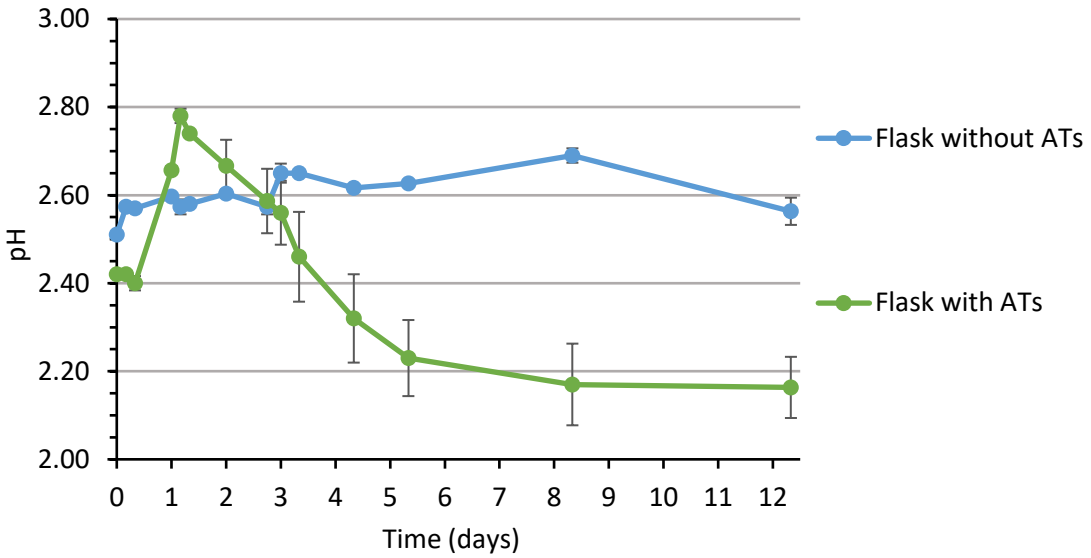

Figure 4.5.2.1 – The change in pH for a **ATs** solution compared against a solution without **ATs.** Interpolation used to aid the eye only.

The lowering of the pH in the flask containing **ATs** suggests that the **ATs** strain is growing and catalysing the oxidation process of Fe^{2+} to Fe^{3+}. Additionally, as the solution pH approaches 2.0, the environment is more suited towards **ATs**, promoting further growth and a greater catalytic effect. The catalytic benefit of **ATs** when the pH is above 3.0 is reported to be negligible.[221] The initial spike in pH can be attributed to early consumption of H^+ during the **ATs** catalysed oxidation of Fe^{2+} according to the equation:

Eq. 4.4.2.1 – $4\ Fe^{2+} + O_2 + 4\ H^+ \rightarrow 4\ Fe^{3+} + 2\ H_2O$ *(bacteria-catalysed reaction)*

Eq. 4.4.2.2 – $4\ Fe^{3+} + 12\ H_2O \rightarrow 4\ Fe(OH)_3 + 12\ H^+$

Eq. 4.4.2.3 – $4\ Fe^{2+} + O_2 + 10\ H_2O \rightarrow 4\ Fe(OH)_3 + 8\ H^+$ *(overall process)*

Initially H^+ is consumed during the bacteria-catalysed 1 e^- oxidation of Fe^{2+} although the overall process results in the generation of 2 H^+ for each Fe^{2+} ion oxidised.[222] A simplified scheme of the metabolic pathway by which **ATs** oxidise Fe^{2+} is given below (Figure 4.5.2.2).

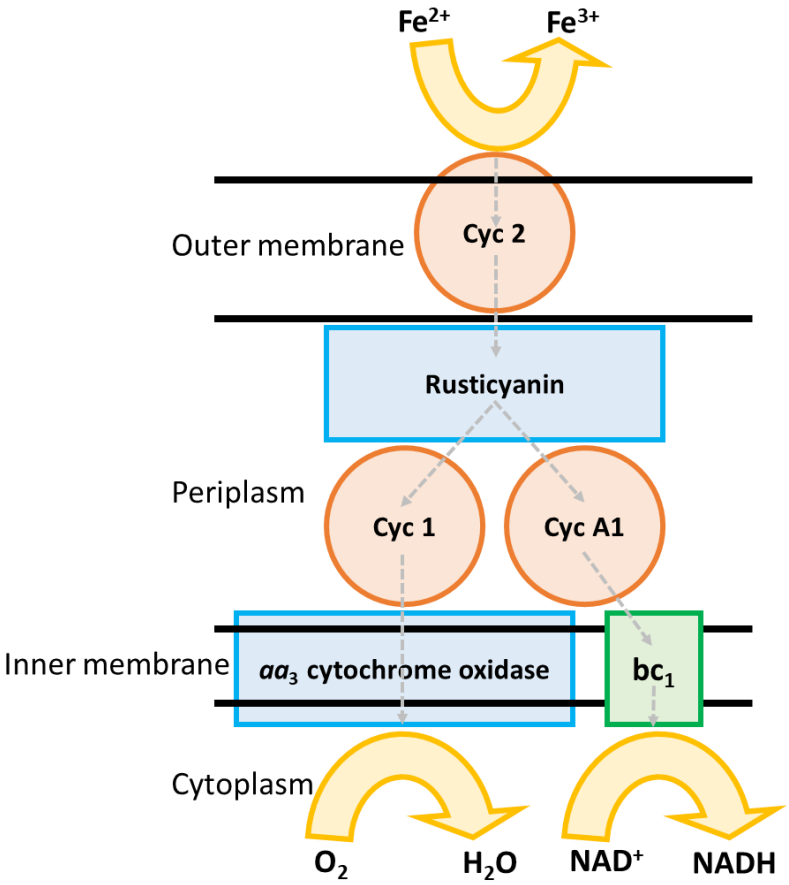

Figure 4.5.2.2 – A simplified schematic of the Fe^{2+} oxidation pathway within **ATs**.[222-224]

The metabolic pathway (Figure 4.5.2.2) begins with abstraction of 1 e^- from Fe^{2+} by 'cytochrome *c* Cyc 2' which is a Fe containing enzyme situated at the periphery of the bacteria cell within the 'outer membrane'.[224] The electron is then passed onto 'rusticyanin', a blue Cu enzyme that is located at the periplasm interface between the outer and inner-membranes of the bacteria cell and can generate 3 protons per Fe^{2+} oxidation.[222] From rusticyanin, the electron can then be passed onto 'cytochrome Cyc 1', another Fe containing protein, before passing onto 'aa_3 cytochrome oxidase', a Cu enzyme, within the inner membrane. This is the last enzyme in the electron transport chain. The enzyme, 'aa_3 cytochrome oxidase', reduces O_2 present in the cytoplasm of the cell to molecular water, through the transfer of 4 e^- per O_2 molecule and in doing so completes the equation above (Eq. 4.4.2.1).[223]

This is a thermodynamically favourable 'downhill' redox pathway but an alternative thermodynamically unfavourable 'uphill' pathway is possible, diverging from the above pathway at the rusticyanin enzyme (Figure 4.5.2.2).[222] The electrons can instead be passed

from rusticyanin to a different Fe containing cytochrome enzyme 'cytochrome Cyc A1', then onto the coenzyme 'cytochrome bc_1 complex' eventually reducing the cofactor NAD^+ to NADH present in the cytoplasm.[223, 224]

4.5.3 Time dependant leaching

As REE-oxides are readily soluble in mildly acidic solutions at room temperature (25 °C), the solubilisation of eudialyte and its component REEs should be possible under the conditions outlined (section 4.5.2). The set-up described (section 4.5.2) was repeated but now with the inclusion of eudialyte (0.50 g) in each flask. A flask without eudialyte was used as a reference. The eudialyte material was ground into a fine powder and autoclaved (121 °C, 15 minutes) prior to addition.

The pH of the flask without **ATs** remained almost unchanged throughout a three week leach process (Figure 4.5.3.1), while the flasks containing **ATs** became more acidic, stabilising at a pH of about 2.20 after two weeks, similar to the flasks without eudialyte present.

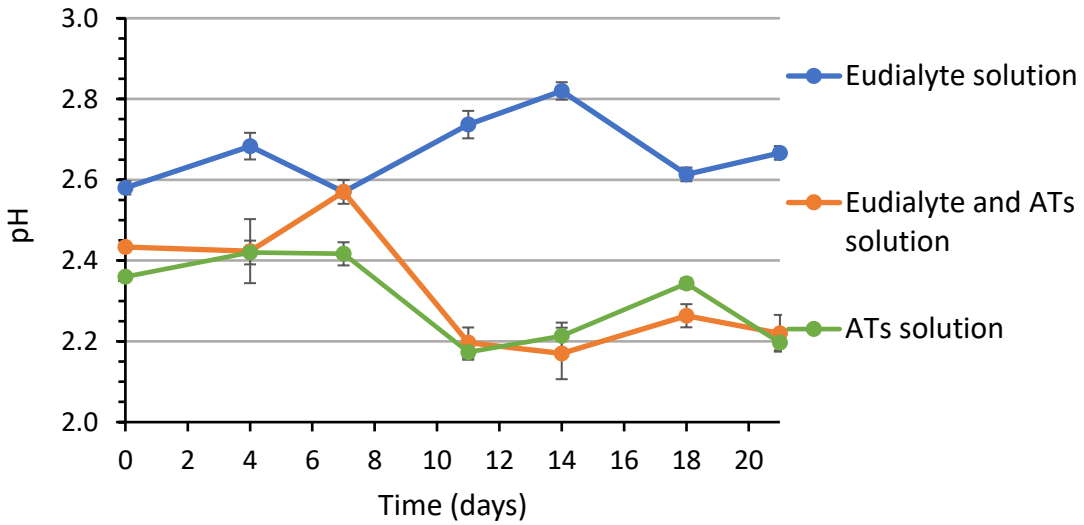

Figure 4.5.3.1 – The change in pH for a **ATs** solution containing eudialyte against time compared against a solution with no **ATs** bacteria and against a solution without eudialyte. Interpolation used to aid the eye only.

The oxidation of Fe^{2+} to Fe^{3+} can be studied by calculating the concentration of Fe^{2+} and Fe^{3+} from photometric measurements using 'the ferrozine method'.[225] This analytical technique is based upon the formation of a stable Fe^{2+}-ferrozine (Figure 4.5.3.2) complex that exhibits a deep magenta colour with a maximum absorbance at 562 nm.

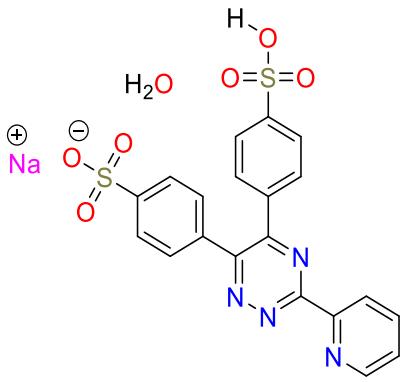

Figure 4.5.3.2 – Ferrozine is a reagent that can readily complex Fe^{2+} and form a stable magenta complex.[225]

The basis of the experiment is that a solution of ferrozine is added to a sample (or to a calibration standard) and the absorbance at 562 nm is recorded using a spectrophotometer. The resulting solution is then reduced and buffered to approximately pH 7 and the absorbance at 562 nm recorded again (chapter 7). If all Fe^{3+} is assumed to have been reduced to Fe^{2+} during the reduction step then the concentration of Fe^{3+} and Fe^{2+} can be determined from a constructed calibration curve.[225]

A calibration curve of pre-reduction and post-reduction of Fe^{2+} standards (0.0, 0.5, 1.0, 2.0 and 5.0 ppm) was constructed (Figure 4.5.3.3) with a linear trend observed up to 2 ppm for both pre and post reduction.

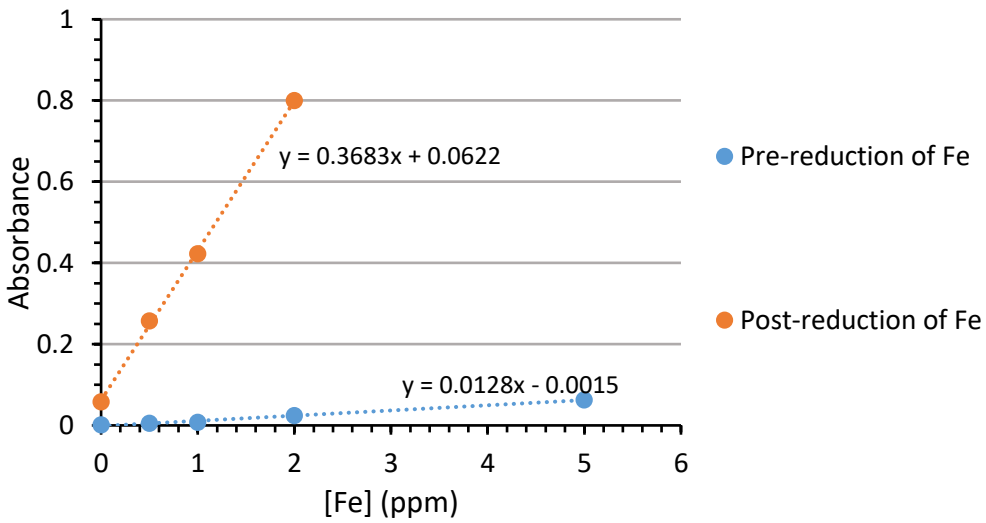

Figure 4.5.3.3 – The absorbance of a Fe^{2+}-ferrozine complex at 562 nm at varying Fe concentrations pre and post reduction.[225]

At 3 - 4 day intervals, leaching experiment aliquots (5 mL) were obtained, filter sterilised (0.22 μm filter), diluted 1:4000 with HCl (0.01 M) and then analysed using a spectrophotometer. The day zero aliquots displayed a comparably high absorbance for all pre- and post-reduction samples with values between 0.55 and 0.66 (Figure 4.5.3.4). Beyond day four, the absorbance recorded pre-reduction for **ATs** containing flasks was effectively zero but remained elevated at 0.67 in **ATs** absent flask samples.

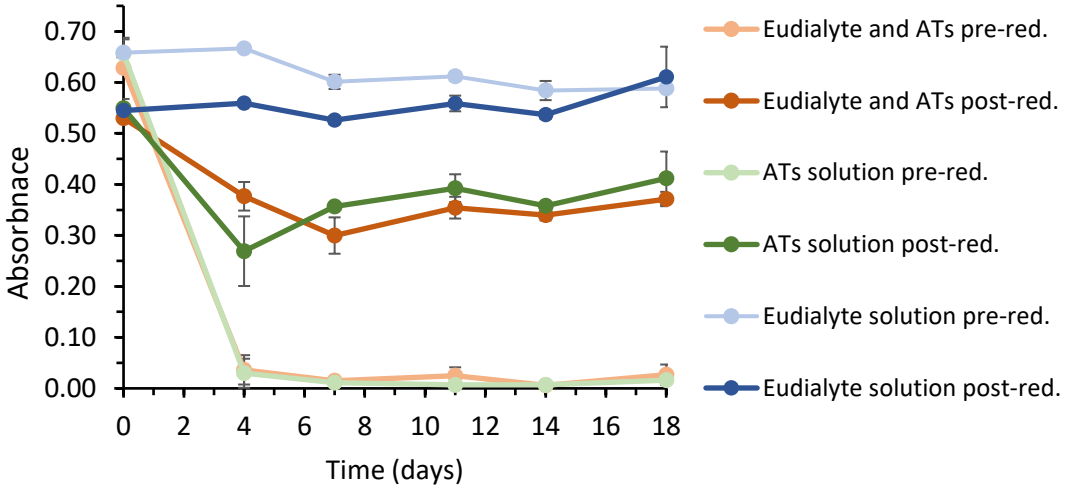

Figure 4.5.3.4 – A comparison of the absorbance values obtained pre- and post-reduction in the ferrozine assay as a function of time. Interpolation used to aid the eye only.

From absorbance values, the concentration of Fe^{2+} and Fe^{3+} can be determined through manipulation of the equations:

Eq. 4.4.2.1 – $[Fe^{2+}] = [(0.368A_A\text{-}0.013A_B)/(0.368*0.448)]*(4x10^3)$

Eq. 4.4.2.2 – $[Fe^{3+}] = [(A_B\text{-}A_A0.8)/0.358]*(4x10^3)$

Where A_A is the recorded absorbance pre-reduction, A_B the recorded absorbance post-reduction and [Fe] is the concentration in the leach flasks. Dilution factors are considered throughout. The numbers 0.368 and 0.013 are the line gradients obtained from the calibration lines.

Plotting the concentration of Fe^{2+} and Fe^{3+} in the flasks as a function of time (Figure 4.5.3.5) indicates that within four days all Fe^{2+} has been oxidised to Fe^{3+} when **ATs** are present. No Fe^{2+} remains and a substantial concentration of Fe^{3+} is present. The flasks absent of **ATs**

meanwhile have minimal Fe^{3+} after three weeks and predominantly consist of Fe^{2+} and strongly suggests that the oxidation of Fe^{2+} with O_2 alone is a relatively slow reaction.

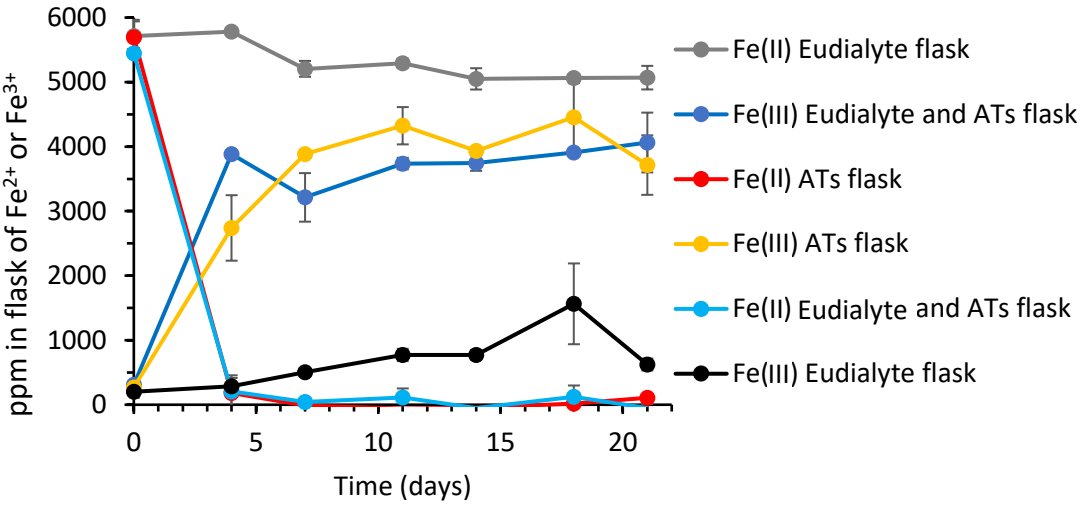

Figure 4.5.3.5 – The absolute concentration (ppm) of Fe^{2+} and Fe^{3+} in the leach flasks as a function of time. Interpolation used to aid the eye only.

The increased rate of Fe^{2+} oxidation and subsequent lowering of the pH when **ATs** are present increases the rate at which eudialyte is solubilised. The increased rate can be confirmed using ICP-OES. As eudialyte is a zirconosilicate mineral, Zr and Si are present in significant quantities so determining the aqueous concentration of these elements should accurately indicate dissolution rate.[226] Analysing the filter sterilised (0.22 μm filter) aliquots indicated that over time an increasing quantity of Si and Zr were leached when **ATs** were present, reaching 86 ppm (Si) and 9 ppm (Zr) within 21 days (Figure 4.5.3.6). Without **ATs** present, 53 pm (Si) and 0 ppm (Zr) are leached in the same time period. The dissolution rate of Si and Zr into the **ATs** solution is roughly constant, with the concentrations of Si and Zr in solution increasing by approximately 2.0 and 0.6 ppm per day, approximately a 3:1 difference. This does not agree with the eudialyte unit cell formula (section 4.4) which contains 26 Si for every 3 Zr, a ratio of approximately 9:1. The measured concentration of Si is far lower than what would be expected.

One explanation for the inconsistency in the Si:Zr ratio is that rather than remaining in the leachate following being leached, Si ions are being adsorbed onto Fe species that precipitate during the leaching process.[227] Fe oxide and hydroxide surfaces are known to adsorb Si and it has been determined that dimeric Si complexes can form on the Fe surface. Adsorption is

reported to occur over a wide aqueous phase pH range but is minimised under low pH conditions.[228]

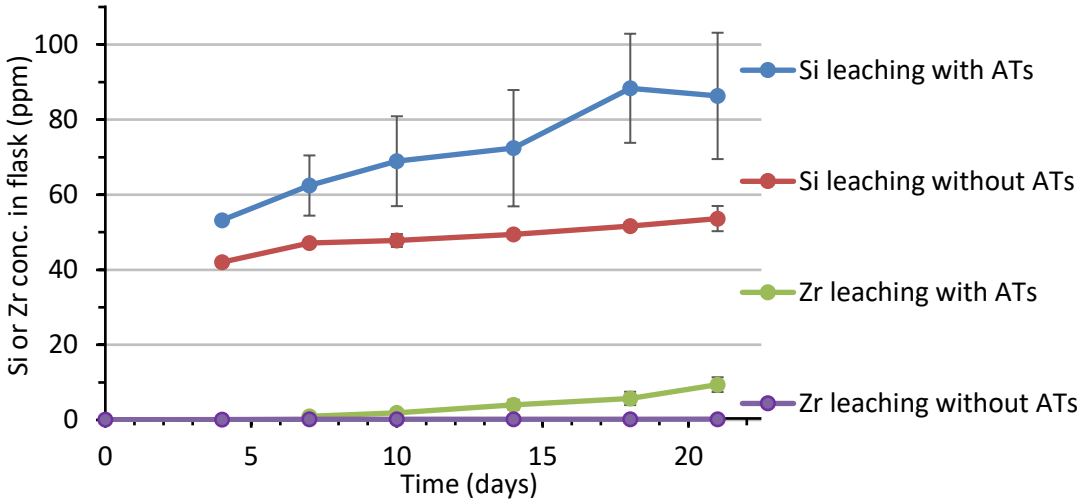

Figure 4.5.3.6 – The leaching of Si and Zr from eudialyte into solution as a function of time (days). Interpolation used to aid the eye only.

If the Si content of a solution exceeds 150 ppm (at pH 7) the formation of Si gel can occur which is a gelatinous and non-filterable phase.[226, 229] Si gel formation can be avoided until higher concentrations if the solution is acidic. The formation of a viscous gel is highly unfavourable in separation processes and significant research has been invested in how to avoid its formation. Inclusion of F^- ions into the leach solution prevents the formation of Si gel but typical F^- sources such as LiF and HF are toxic, dangerous and require highly specialist corrosion resistant equipment.[230] Alternatively, high temperature leaching with conc. HCl can limit Si gel formation but is energy intensive, costly and HCl is far more corroding than H_2SO_4.[229] No Si gel formation was observed during the leaching processes described in this chapter and can be attributed to the much lower eudialyte:leach solution ratio that is at least one order of magnitude lower than literature studies and a sufficiently low pH.

4.5.4 Comparison against HNO_3 and H_2SO_4 leaching

Comparing the leaching of REEs and other elements by the mildly acidic **ATs** solution against the leaching HNO_3 and H_2SO_4 (2.0 M) indicates that leaching is much more efficient with HNO_3 or H_2SO_4 (2.0 M) (Figure 4.5.4.1). This is to be expected though as the H^+ concentration is around 200 times greater, and the pH at least 2 units lower.

The set-up described earlier (sections 4.5.2 and 4.5.3) was repeated but with the inclusion of eudialyte (1.00 g) in each flask (125 mL). HNO_3 and H_2SO_4 (2.0 M) were found to leach around 10 times more REEs (when comparing the leaching of Y, La, Ce and Nd) than the **ATs** solution (Figure 4.5.4.1).

While leaching with **ATs** is inferior to HNO_3 or H_2SO_4, the presence of **ATs** still makes a noticeable difference when compared to their absence. The **ATs** solution leached several times more Y, La, Ce and Nd than the mildly acidic solution alone (Figure 4.5.4.1). This can be attributed to the pH difference of approximately 2.20 to 2.60 (section 4.5.2).

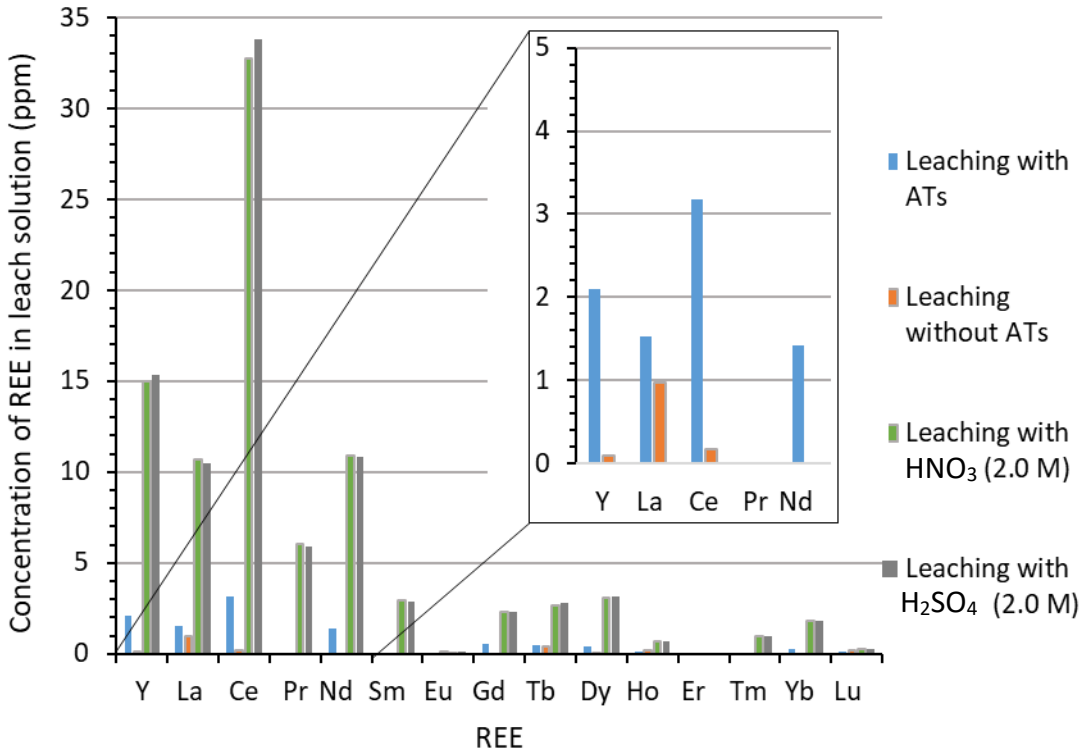

Figure 4.5.4.1 – The leaching of REEs (ppm) into solution using **ATs** in growth solution, growth solution without **ATs**, HNO_3 (2.0 M) or H_2SO_4 (2.0 M).

Despite a significant reduction in the leaching of REEs, the proportions of the elements within the **ATs** leach solution remains broadly similar to that of HNO_3 (2.0 M) or H_2SO_4 (2.0 M). The REE content of each solution was determined to consist of mainly of Y, La, Ce and Nd at approximately 75% by weight (Figure 4.5.4.2) and agrees with previous eudialyte leaching studies.[231] The remaining 25% consists of REEs that were only detected at very trace quantities by the ICP-OES and therefore significant variance in their quantities due to instrument limitations is a possibility.

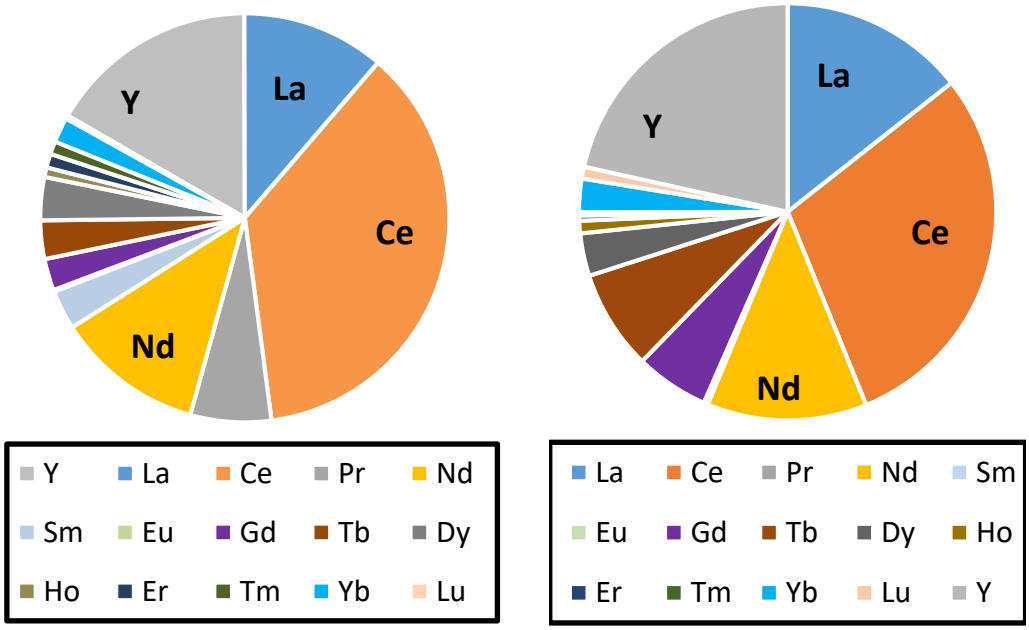

Figure 4.5.4.2 – The REE composition by weight % of a H_2SO_4 solution following leaching of eudialyte (left) compared against the equivalent **ATs** growth solution (right).

4.5.5 Separation of lighter REEs

To incorporate the bacteria assisted leaching of REEs using **ATs** into a REE separation and purification process, the ability to extract the lighter REEs (e.g. La, Ce and Nd) from the leach solution using the secondary amido-ammonium (**2AA**) ionic liquid (IL) introduced in chapter 3 was investigated.

A ratio representative model eudialyte solution (**MES**) containing the predominant REEs (Y, La, Ce and Nd) in the **ATs** leach solution was analysed to provide a proof of concept. As the **ATs** leach solution also contained substantial $Fe_2(SO_4)_3$, the **MES** reflected this. The **MES** contained $Fe_2(SO_4)_3$ (0.375 M) resulting in Fe^{3+} (0.75 M) and SO_4^{2-} (1.13 M). As discussed previously (chapters 2 and 3), ammonium ILs such as **2AA** effectively transport REEs from the aqueous phase to the organic under high salt conditions.[112] Therefore, the **MES** also contained either $NaNO_3$ (7.0 M) or $NaNO_3/HNO_3$ (5.0 M/0.1 M). **IL0** (chapter 2) was used as a comparison for the performance of **2AA**.

Contacting a water immiscible organic phase containing **2AA** (0.1 M) with the **MES** results in total extraction (>99%) of La (1 mM) and Ce (2 mM) from a $NaNO_3$ (7.0 M) **MES** and high extraction (>80%) from a $NaNO_3/HNO_3$ (5.0 M/0.1 M) **MES** (Figure 4.5.5.1). Nd (1.5 mM) is

modestly extracted (35% and 55%) from both solutions, while only trace amounts of the more Lewis acidic REE Y (2.5 mM) were extracted (2%). Meanwhile, **IL0** modestly extracts (<40%) La and Ce and a small amount of Nd (10%) from both solutions.

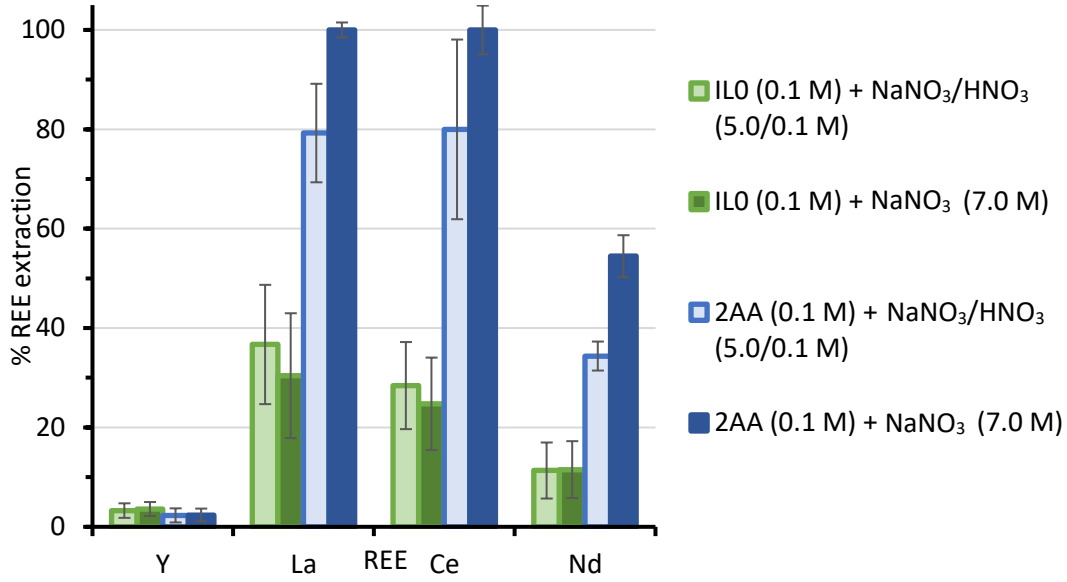

Figure 4.5.5.1 – The extraction of REEs (1 – 2.5 mM) using **IL0** or **2AA** (0.1 M) in toluene from an aqueous ratio representative model eudialyte solution (**MES**).

Interestingly, earlier experimental data for the extraction of REEs from mixed solutions (section 3.5.5) with **IL0** shows good extraction of lighter REEs. This suggests that the presence of $Fe_2(SO_4)_3$ in the **MES** supresses REE extraction despite competitive extraction of Fe not occurring. The extraction of the lighter REEs using **2AA**, despite the Fe concentration in the **MES** being almost 10^3 times that of REE indicates a remarkable degree of selectivity given that REEs and Fe are both present in solution as 3+ cations.

The extraction of REEs from the eudialyte leach solution was investigated. Due to the low concentrations in the **ATs** leach solution (section 4.5.4), following leaching of eudialyte (1.0 g) into the **ATs** leach solution (125 mL), the filter sterilised (gravity filtered, 0.45 μm syringe filtered and then 0.22 μm syringe filtered) mixture was concentrated under vacuum by a factor of five. The mixture was then adjusted to contain $NaNO_3/HNO_3$ (5.0 M/0.1 M) at a pH of 1.40. The resulting eudialyte concentrate was then contacted with **IL0** or **2AA** (0.1 M) in toluene. La, Ce and Nd were readily extracted (60 - 92 %) by **IL0** and **2AA** (Figure 4.5.5.2).

While **2AA** did not extract REEs heavier than Gd but some extraction of these heavier REEs was observed with **IL0**.

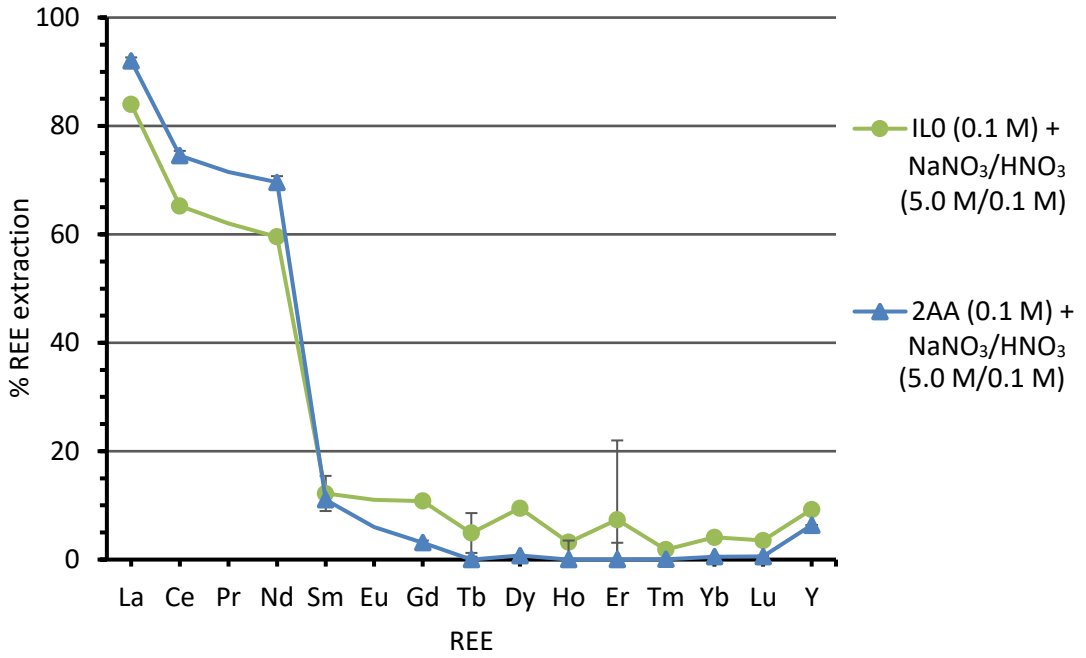

Figure 4.5.5.2 – The extraction of REEs (<0.1 mM) using **IL0** or **2AA** (0.1 M) in toluene from leached eudialyte. Interpolation used to aid the eye only.

It should be stressed though that with La, Ce, Nd and Y comprising >75% of the REE content in eudialyte leachate, the concentration of the remaining REEs was very low (<1 ppm) resulting in difficulties in accurately measuring their concentration by ICP-OES. Regardless, this experimental data consolidates the previously observed effective separation of lighter REEs from heavier REEs with a solution of **2AA** from synthetic REE solutions.

4.6 Conclusions

Acidithiobacillus ferrooxidans (**ATs**) effectively low the pH and increase the acidity of leach solutions by catalysing the oxidation of Fe^{2+}.[36, 37] This allows for a solution containing **ATs** to leach eudialyte, a REE containing zirconosilicate mineral, more effectively than a solution without **ATs**.

While the leaching with **ATs** is significantly less effective in terms of speed and efficiency than a highly acidic HNO_3 or H_2SO_4 solution, some advantages are present. The **ATs** solution is safer to handle, requires no post-leach pH adjustment or corrosion resistant apparatus.[229] These

traits are all advantageous and result in the proof of concept of a potentially environmentally friendlier eudialyte leaching process.

2AA preferentially extacts the lighter REEs over the heavier REEs in the eudialyte leach solution, corroborating the results observed with synthetic solutions (Chapter 3). Additionally, while the Fe concentration is approximately 10^3 times that if the REEs, no extraction of Fe is observed and **2AA** remains highly selective for the lighter REEs.

While the percentage of REEs leached from the eudialyte mineral using **ATs** is low, this could be significantly improved if the leach process proceeded for months, rather than only days or weeks, given that the concentration of Si and Zr in solution continually increased over time (section 4.5.3). As the Zr concentrations within the final leach solutions studied in this chapter are significant, the development and implementation of a process that separates and purifies Zr would bolster the materials balance and add value. Furthermore, the integration of a Fe extraction or a one electron Fe reduction step into the REE recovery and separation process could improve the atom economic credentials of the process.

Chapter 5

A brief exploration of amido-ammonium IL modifications for REE extraction

5 A brief exploration of amido-ammonium IL modifications for REE extraction

5.1 Introduction

5.1.1 Overview

The secondary amido-ammonium IL **2AA** introduced in Chapter 3 is a more effective IL for separating lighter REEs from heavier REEs than its non-functionalised analogue **IL0**. This has been attributed to the increased number of hydrogen-bonding interactions that **2AA** promotes that provide a molecular scaffold for lipophilic alkyl chains that sufficiently encapsulate lighter REEs over the heavier REEs. This chapter investigates if modest adaptations of **2AA** are possible and whether these variations can further improve selectivity.

5.1.2 Modified Diglycolamides

Diglycolamides such as TODGA (introduced in Chapters 2 and 3), readily extract REEs under appropriate conditions although 3rd phases tend to form at elevated concentrations.[52, 150, 151] The tridentate binding mode of diglycolamides to REEs through the two amide groups and the ether oxygen is evidently favourable.[128, 157] Therefore, previous studies have investigated how modifications to the diglycolamide structural motif can reduce 3rd phase formation while maintaining strong REE coordination. These modifications can include the combination of multiple diglycolamide structural motifs into one molecule (Figure 5.1.2.1). While this results in molecules with particularly high m/z ratios (>500) for the free ligand, the % extraction of REEs when using these ligands is often very high with in excess of 99% of the target REE extracted in some cases.

A ligand (0.1 M) (Figure 5.1.2.1) comprising two diglcyolamides substituted onto a benzene ring *meta* to one another extracted 99% of Eu from HNO_3 (3.0 M).[232, 233] The ligand to Eu ratio was determined to be 2:1 by slope analysis and suggested that assemblies of the formula $Eu(L)_2.(NO_3)_3$, where one coordinated L is orthogonal to the other, may reside in the organic phase following Eu transport. In the IR spectrum, a C=O stretch at 1651 cm^{-1} shifted to 1615 cm^{-1} following Eu transport indicated coordination of the amide groups to Eu.[233]

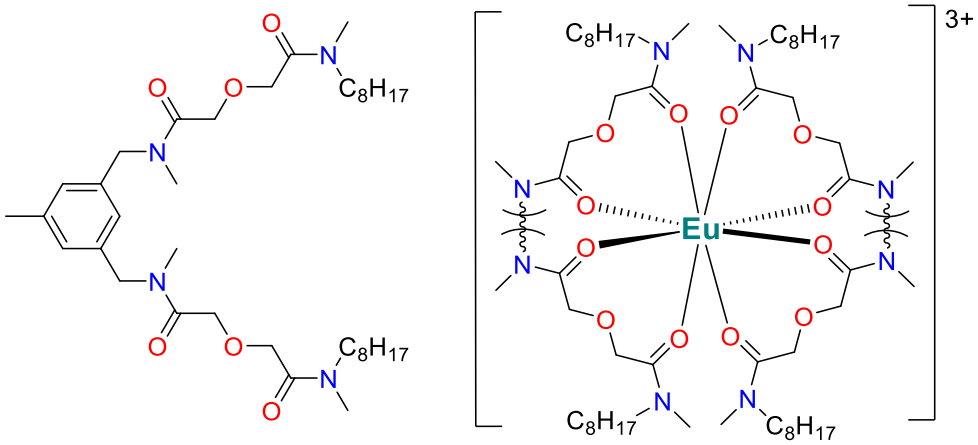

Figure 5.1.2.1 – A bis(diglycolamide) (left) and the potential coordination of two bis(diglycolamide) ligands to Eu where one bis(diglycolamide) ligand is orthogonal to the other (right).[232] For clarity, the alkyl chains are shortened.

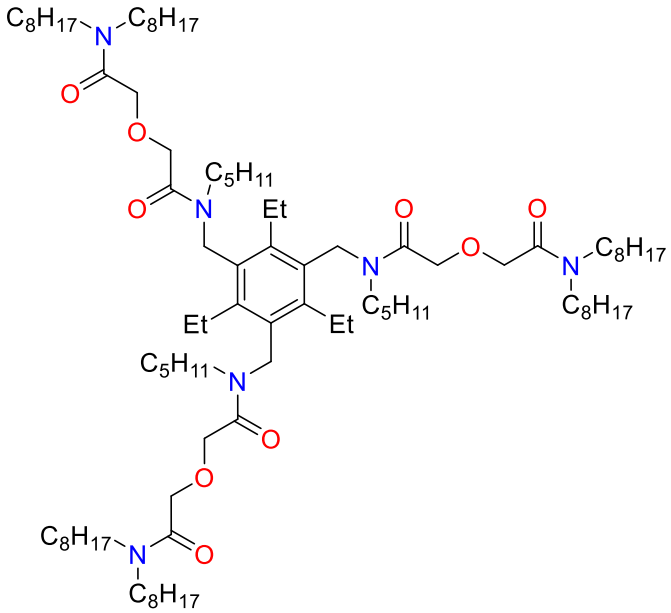

Figure 5.1.2.2 – A tripodal diglycolamide used for Eu extraction.[234]

Compounds comprising three diglycolamide substituents (Figure 5.1.2.2) follow a Eu extraction profile similar to that of bis(diglycolamide) analogues with Eu being successfully (>99%) extracted from 3.0 M HNO_3 but only very poorly recovered (<10%) from low HNO_3 (<1.0 M) concentrations.[234] Eu(L).$(NO_3)_3$ complexes were reported to be present in the organic phase following transport and suggest a nine coordinate Eu metal is encapsulated by the lipophilic ligand and agrees with earlier experimental and computational work on mono-

diglycolamide systems (e.g. TODGA – Chapter 3) at low ligand and metal concentrations.[52, 149, 152]

A ligand comprising eight diglycolamides functionalities was reported to complex to four Eu or Am ions when diluted in an imidazolium IL, achieving over 99% Eu extraction from HNO_3 (3.0 M).[235] Interestingly, dilution of the ligand into a non-polar solvent instead of an imidazolium IL, results in a M:L ratio of only 1:1 rather than 4:1.[236] DFT calculations (Figure 5.1.2.3) confirmed that four Am ions were coordinated to the ligand, with Am ions well separated by encapsulation within unique binding pockets formed by two diglycolamides with an average carbonyl oxygen to Am bond distance of 2.36 Å. Three nitrate anions were nearby the Am ions and increased the total Am coordination number to nine, through monodentate binding.

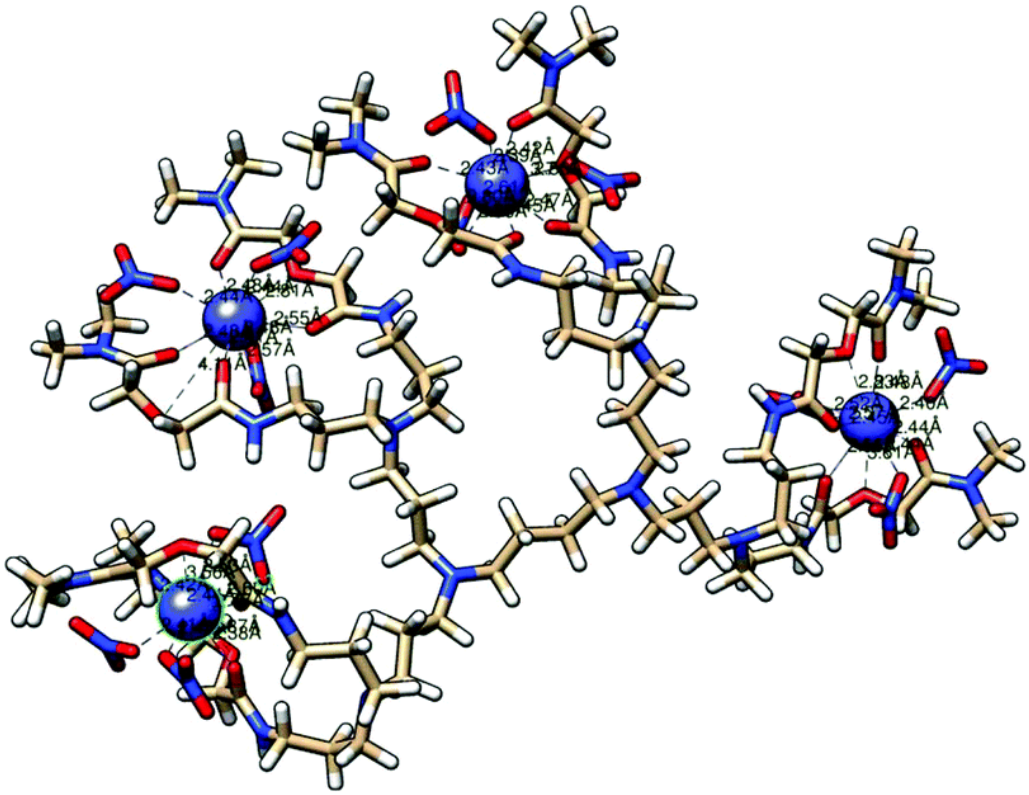

Figure 5.1.2.3 – The DFT optimised structure of an $Am_4(NO_3)_{12}L$ complex where the ligand L contains eight diglycolamide functionalities.[235] Elements are coloured as C (brown), N (blue), O (red) and Am (dark blue). The octyl substituents were shortened to methyl due to computational limitations.

Other modifications have included the tethering of diglycolamide functional groups to calix[4]arene macrocycles.[237-239] Even at low concentrations these macrocyclic structures comprising between four to eight diglycolamide functional groups have been found to readily extract Eu (>99%) from HNO_3 (3.0 M) solutions. The ability of these ligands to readily transport Eu into the organic phase can be attributed to the diglycolamide functional groups being pre-orientated by the calix[4]arene molecular scaffolds. In contrast, multiple mono-diglycolamide extractants such as TODGA must self-assemble during REE extraction.

While these diglycolamide modifications result in very effective REE extraction, the synthesis of these compounds is difficult and highly time-consuming meaning they are unlikely to be exploited industrially. Additionally, as the structures are so large, the molecular weight of the ligands relative to the REE is comparatively poor, even if a 1:1 REE to ligand ratio is achievable. Less extensive modifications to diglycolamides such as the replacement of the ether group with an amine group can still result in highly stable REE complexes (Figure 5.1.2.4).[240]

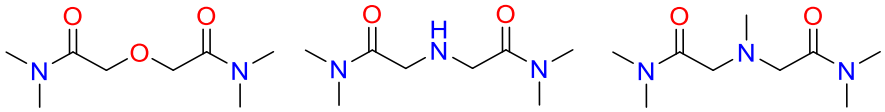

Figure 5.1.2.4 – Diglycolamide (left), a 2° amine-functionalised variation (centre) and a 3° amine-functionalised variation (right).[240]

The amine group allows for greater chemical and structural tuning of the electron density compared to an ether group and can result in greater REE binding ability or improved selectivity. The REE binding ability of an amine-functionalised ligand (Figure 5.1.2.4) can be increased by alkylating a 2° amine as the mild electron donating ability of alkyl substituents towards the nitrogen atom would increase its basicity.[240] This is supported by thermodynamic binding studies of Nd that show that amine-functionalised ligands form more stable Nd complexes than ether-functionalised analogues.[240, 241] Potentiometry, spectrophotometry, and calorimetry measurements determined that the ΔH values for the formation of $Nd(L)_3^{3+}$ complexes (where **L** is either a diglycolamide or amino-variant) (Eq. 5.1.3.1) were −19.3 ± 2.2 kJ mol^{-1} (ether), −39.4 ± 1.5 kJ mol^{-1} (2° amine) and −34.3 ± 1.5 kJ mol^{-1} (3° amine) (Figure 5.1.2.4).

Eq. 5.1.3.1 – $Nd^{3+} + 3\ \mathbf{L} = Nd\mathbf{L}_3^{3+}$

Eq. 5.1.3.2 – $H^+ + \mathbf{L} = H\mathbf{L}^+$

The non-alkylated 2° amine was calculated to interact the most favourably with Nd^{3+} but also the most favourably with H^+ (Eq. 5.1.3.2). A ΔH value of −37.2 ± 2.1 kJ mol^{-1} for the 2° amine in the formation of HL^+ was reported compared with −10.9 ± 0.9 kJ mol^{-1} for the ether and −33.5 ± 0.6 kJ mol^{-1} for the 3° amine.

5.1.3 IL modifications

Work presented earlier (Chapter 3) highlights that **2AA** extracts REEs more readily than **IL0** due to a more significant hydrogen-bonding network and that the amide functional group is a major component of this network. The modification of the amido-ammonium ILs **2AA** and **3AA** to contain additional amide groups should result in a greater number of potential hydrogen-bonding sites and a more complex hydrogen-bonding network. In turn, this should improve REE extraction. Synthesising diamido-ammonium ILs, similar structurally to the diamide-amines above (Figure 5.1.2.4) that strongly complex Nd, should be synthetically straightforward and will therefore be investigated later in this chapter.[240]

Synthesis of an amido-ammonium compound that replicates an effective structural motif used during Pt recovery should also be comparatively simple synthetically.[24, 49] Incorporation of an additional CH_2 linker between the ammonium and the amide functional groups (Figure 5.1.3.2) should increase the flexibility of the IL cations and alter the electron density on both the amide group and the ammonium nitrogen. An amino-amide version of this structural motif has resulted in highly effective proton chelation for Pt as a chloridometalate from HCl solutions (sections 1.5 and 2.2). While the methylation of the 3° amine removes the ability to chelate protons (or hypothetically the ability to chelate REE cations), the increased distance between the ammonium and amide groups may improve REE extraction due to the reduced degree of influence one group has over the other.

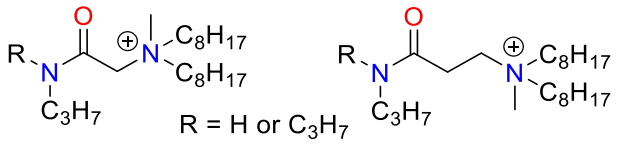

Figure 5.1.3.2 – The **2AA** or **3AA** cation (left) and the incorporation of an additional CH_2 linker (right)

Both modifications above will be explored for REE extraction as even relatively minor structural changes can cause large variations in complex stability.[240] Other structural changes

that could be considered include the replacement of amide functional groups with thioamide groups resulting in thioamido-ammonium ILs or sulfonium ILs rather than ammonium ILs (Figure 5.1.3.3).

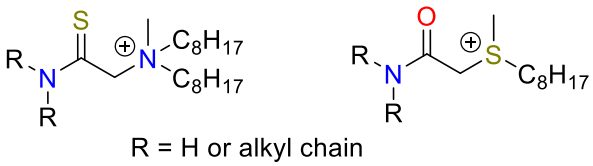

Figure 5.1.3.3 – Potential **2AA** and **3AA** modifications: a thioamido-ammonium IL (left) and an amido-sulfonium IL (right).

The replacement of N and O atoms that are highly electronegative and electron dense with S atoms that are less electronegative and more electron diffuse could drastically alter how the IL extracts REEs from aqueous solutions. This will not be explored though as earlier work (sections 3.6 and 3.7) with **IL0** and **2AA** suggests that strong hydrogen-bonding interactions are pivotal to the formation of stable organic-phase assemblies. It can be expected that the lower electronegativity of S would result in weaker hydrogen-bonding interactions, a less favourable assembly and poorer REE extraction. Furthermore, the inclusion of S atoms would signal a deviation away from CHON only compounds.

5.2 Diamido-ammonium ILs

5.2.1 Synthesis of diamido-ammonium (AdiA) ILs

Secondary (2°) and tertiary (3°) amido-ammonium ILs were synthesised using an adaptation of the preparative method for the amido-ammonium ILs **2AA** and **3AA** (Scheme 5.2.1). Previously prepared 2-chloroacetamides were reacted with 0.5 equivalents of octylamine to yield amido-amine intermediates, with HCl liberated.[240] The resulting amido-amine intermediates were then methylated using methyliodide as described prior for **IL0** (section 2.5), to yield 2° and 3° amido-ammonium compounds, herein referred to as **2AdiA** and **3AdiA**.[124, 134]

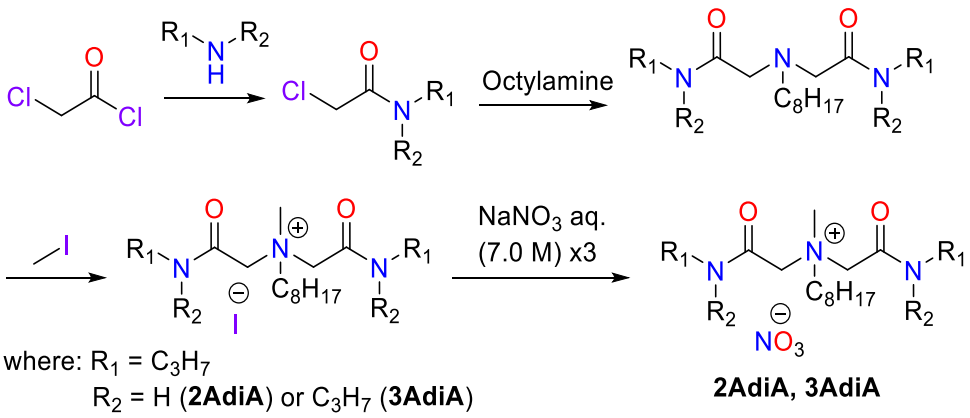

Scheme 5.2.1 – The synthesis of diamido-ammonium ILs **2AdiA** and **3AdiA** starting from 2-chloroacetyl chloride.[124, 134, 240]

5.2.2 REE extraction and separation studies

To assess the performance of **2AdiA** and **3AdiA** in relation to **IL0** and their monoamide variants (**2AA** and **3AA**), REE extraction tests were undertaken. Initially, organic solutions of **2AdiA** and **3AdiA** (0.1 M) were contacted with a series of aqueous phases containing La (0.01 M). The different compositions of the aqueous phases were: $NaNO_3$ (7.0 M); HNO_3/$NaNO_3$ (0.1 M/5.0 M); HNO_3 (2.0 M).

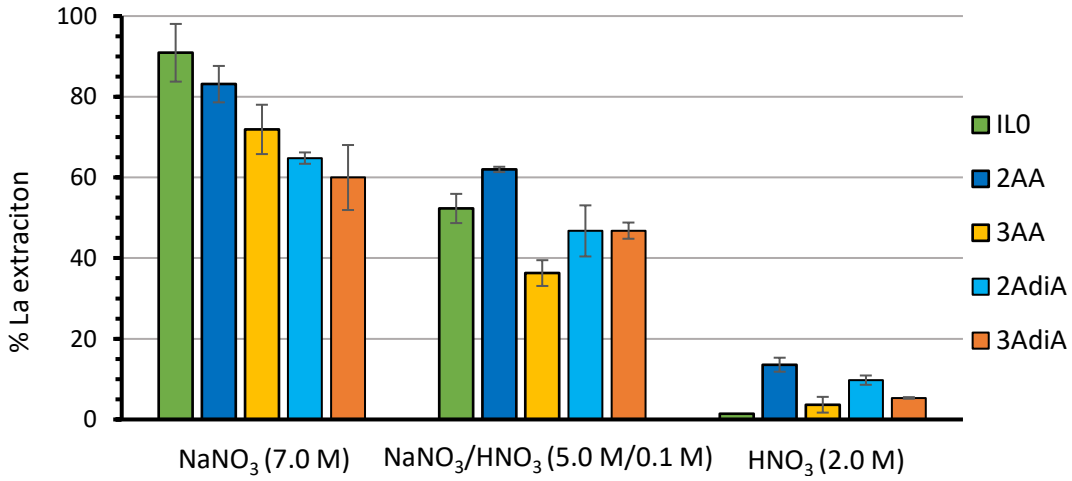

Figure 5.2.2.1 – Initial tests for the extraction of La (0.01 M) using **2AdiA** and **3AdiA** (0.1 M) in toluene from $NaNO_3$ (7.0 M), $NaNO_3$/HNO_3 (5.0 M/0.1 M) and HNO_3 (2.0 M), compared against the monoamido-ammonium analogues (**2AA** and **3AA**) and **IL0** (section 3.5.1).

From $NaNO_3$ (7.0 M), **2AdiA** and **3AdiA** extract 65% and 60% of La (0.01 M) respectively and although this is a noticeable decrease when compared with **2AA** (83%) and **3AA** (72%) (Figure 5.2.2.1). From $HNO_3/NaNO_3$ (0.1 M/5.0 M) solutions **2AdiA** extracts around 15% less La than **2AA**, while **3AdiA** extracts slightly (10%) more La than **3AA**. The ILs **2AdiA** and **3AdiA** only extract minor quantities (<10%) of La from HNO_3 (2.0 M) solutions indicating that diamido-ammonium ILs remain susceptible to the issue of competitive H^+/La^{3+} transport and that the 'salting-out' effect remains vital to REE extraction.[107, 118]

The effect of acid hindering La extraction is further supported by contacting **2AdiA** (0.1 M) in toluene with a $NaNO_3$ (5.0 M) and a La (0.01 M) aqueous phase containing varying HNO_3 concentration (0.01 - 2.0 M). **2AdiA** extracts La less readily than **2AA** at all HNO_3 concentrations, achieving on average 43% La extraction at 0.01 M HNO_3 (vs. 70% extraction with **2AA**) and 19% La extraction at 2.00 M HNO_3 (vs. 21 % extraction with **2AA**) (Figure 5.2.2.2). This indicates that the diamide-ammonium IL analogues are poorer reagents overall than the monoamido-ammonium analogues for La extraction. Speculatively, the ability of **2AdiA** to transport La into the organic phase may be limited as its lipophilicity is insufficient.

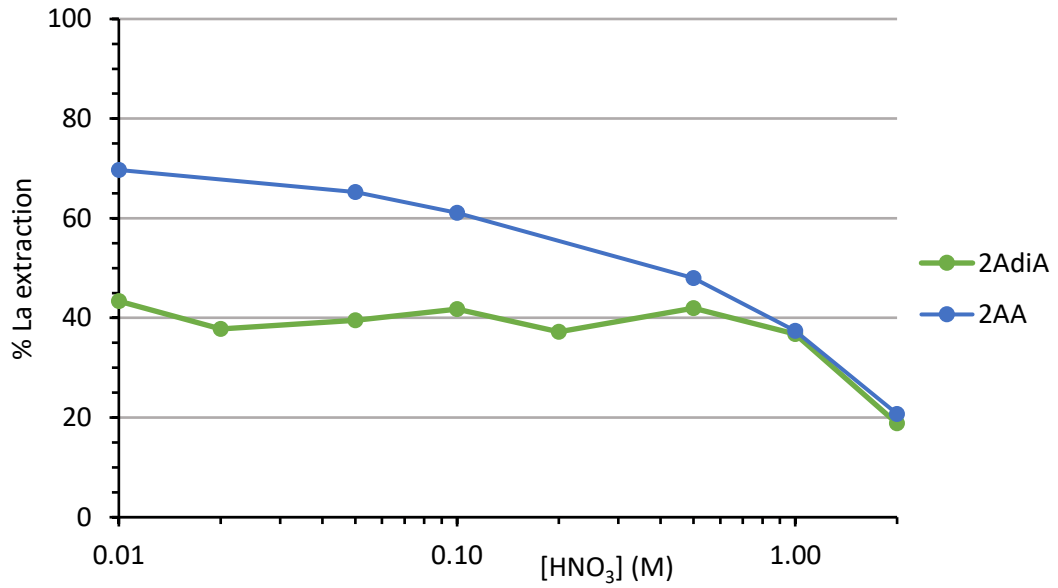

Figure 5.2.2.2 – The extraction of La (0.01 M) using **2AdiA** or **2AA** (0.1 M) in toluene from a $NaNO_3/HNO_3$ (5.0 M/0.01 – 2.00 M) aqueous solution. Interpolation used to aid the eye only.

To investigate if **2AdiA** and **3AdiA** can separate REEs, a solution of **2AdiA** and **3AdiA** (0.1 M) in toluene was contacted with an aqueous phase containing nine REEs (La – Dy) (0.01 M) and $NaNO_3$ (7.0 M). A gradual decrease in REE extraction across the f-block is observed for both

2AdiA and **3AdiA** with REE extraction decreasing from 43% and 45% of La to below 10% from (Sm, Eu, Gd, Tb and Dy) (Figure 5.2.2.3) and is comparable to the trend previously observed with **IL0** (Figure 3.5.5.1). While minimal extraction of heavier REEs by **2AdiA** and **3AdiA** from the mixed metal solution is observed, it is more than attained with **2AA**. Additionally, the extraction of the lighter REEs is lower with **2AdiA** and **3AdiA** than with **2AA**. These two factors result in **2AdiA** and **3AdiA** being poorer reagents overall for light REE extraction and separation than **2AA**.

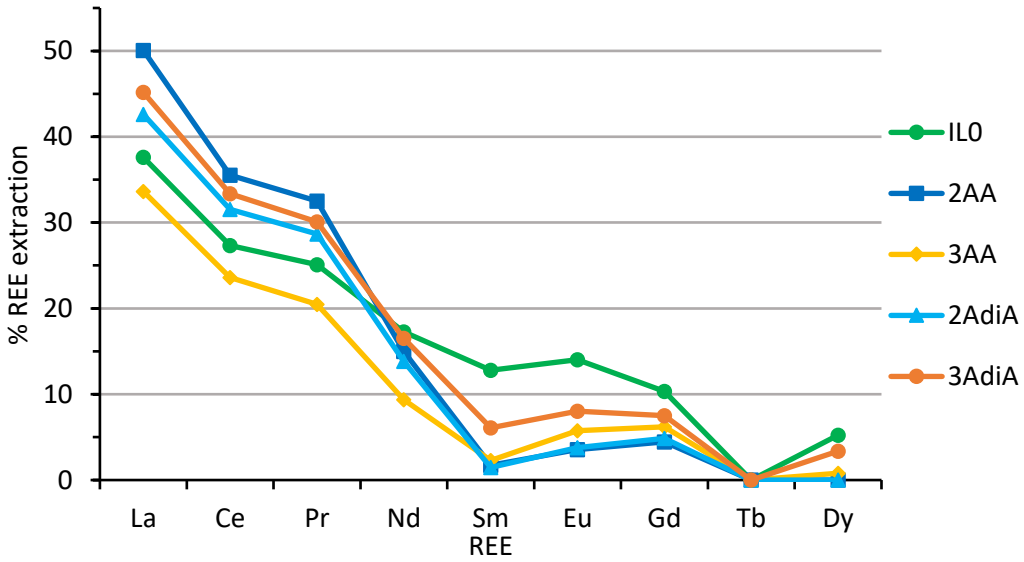

Figure 5.2.2.3 – The extraction of REEs (0.01 M) using **2AdiA**, **3AdiA**, **2AA**, **3AA** or **IL0** (0.10 M) in toluene from a mixed REE $NaNO_3$ (7.0 M) aqueous solution. Interpolation used to aid the eye only.

5.3 Extended amido-ammonium ILs

5.3.1 Synthesis of extended amido-ammonium (ACH_2A) ILs

The synthesis of 2° and 3° amido-ammonium ILs (herein referred to as **$2ACH_2A$** and **$3ACH_2A$**) whereby the ammonium and amide functional groups are separated by two CH_2 linkers rather than one CH_2 linker (e.g. **1AA**, **2AA** and **3AA**) is more challenging. Initially an adaptation of the synthesis of **2AA** and **3AA** starting from 3-chloropropionyl chloride (Scheme 5.3.1.1) was attempted. While the syntheses of the 3-chloro acetamides were straightforward, the subsequent reaction with dioctylamine under the conditions previously used (section 3.4) did not yield the target product as the major product.[240] Instead, the major products (>80%),

were dehydrated acrylamides, as of a base-catalysed elimination reaction (presumably *E2*) in which a proton is abstracted, a C=C bond formed and a Cl^- lost.

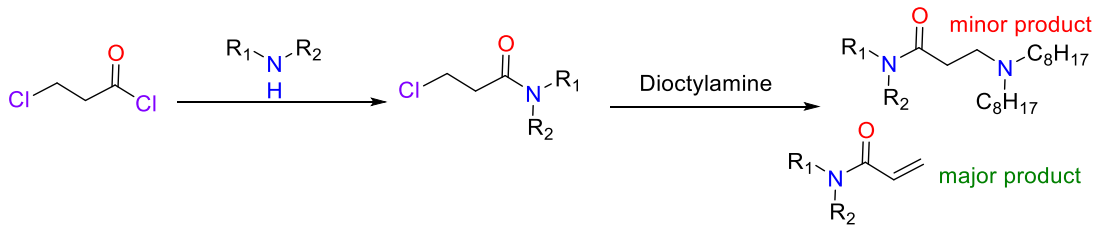

Scheme 5.3.1.1 – The synthesis of the **2ACH$_2$A** and **3ACH$_2$A** amido-amine intermediates starting from 3-chloropropionyl chloride.

This elimination reaction did not occur with 2-chloroacetamides due to the absence of a β-proton. The formation of acrylamides was identified in the ^{1}H NMR spectra with three distinct peaks at 5.65, 6.10, and 6.30 ppm corresponding to allylic protons in the crude reaction mixture (Figure 5.3.1.1), in agreement with previously reported NMR data.[242] The crude mixture also contained unreacted dioctylamine and the amido-amine target product. Dioctylamine and the acrylamide were removable from the crude reaction mixture through sustained heating under vacuum. While this is a valid route towards amido-amine isolation, the overall synthetic route is highly inefficient as it is only a minor product in reaction so alternative synthetic routes were investigated.

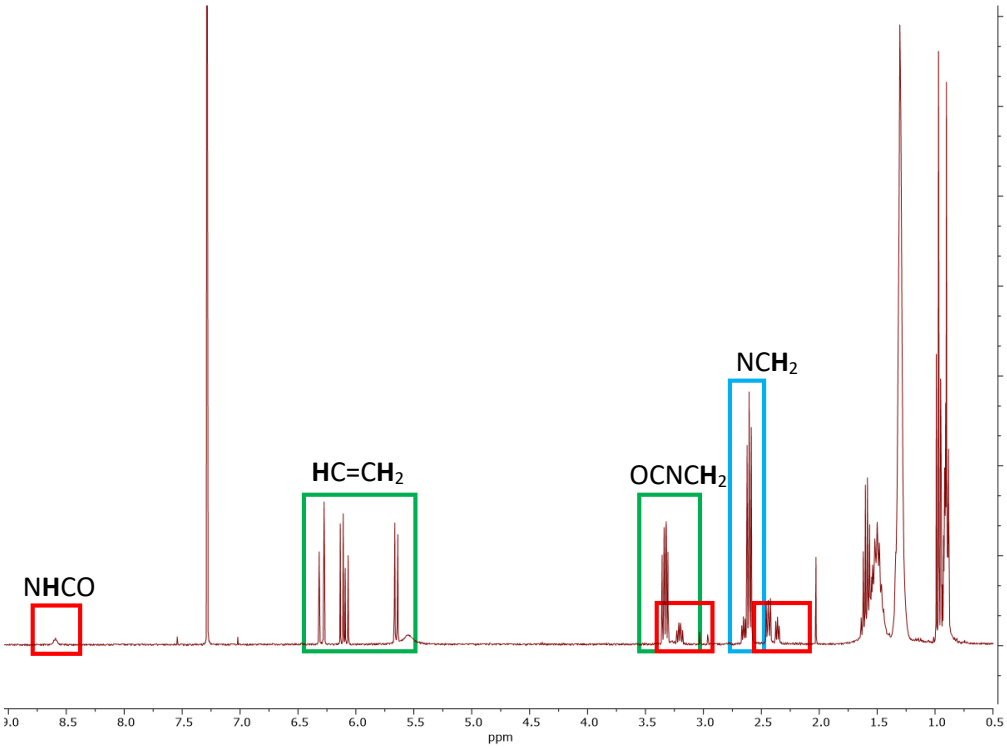

Figure 5.3.1.1 – The crude reaction mixture ^{1}H NMR of the synthesis of the **2ACH$_2$A** amido-amine intermediate. Distinctive acrylamide (green), amido-amine (red) and dioctylamine (blue) peaks are highlighted.

An alternative route towards **2ACH$_2$A** starting with the reaction of methyl acrylate with dioctylamine affords the amino-ester in 100% yield (Scheme 5.3.1.2).[49] Subsequent reaction of the amino-ester with propylamine resulted in synthesis of the target amido-amine intermediate in 75% yield.[243, 244] The amido-amine intermediate was then methylated using methyliodide to give **2ACH$_2$A** in 88% yield.[124, 134]

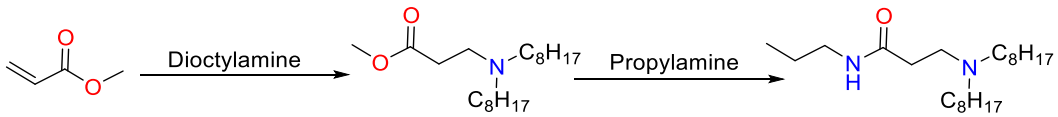

Scheme 5.3.1.2 – The synthesis of the **2CH$_2$A** amido-amine intermediate starting from methyl acrylate.[49, 243, 244]

Synthesis of the 3° analogue **3CH$_2$A** using this synthetic route was unsuccessful. Instead, acryloyl chloride was reacted with dipropylamine to cleanly yield the acrylamide (Scheme 5.3.1.3). The acrylamide was then reacted with dioctylamine in methanol to form, in modest

yield (25 %), the target amido-amine compound.[49] The amido-amine intermediate was then methylated using methyliodide to yield **3ACH$_2$A**.[124, 134]

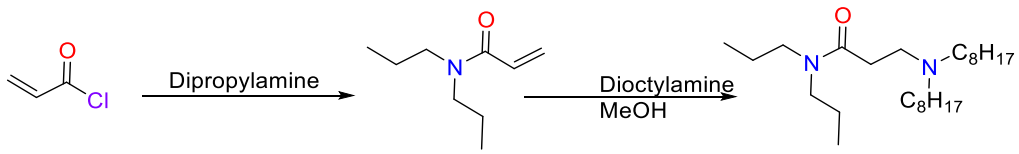

Scheme 5.3.1.3 – The synthesis of the **3ACH$_2$A** amido-amine intermediate starting from acryloyl chloride.[49]

5.3.2 REE extraction and separation studies

To assess the performance of **2ACH$_2$A** and **3ACH$_2$A** in relation to **IL0** and their single CH_2 linker analogues (**2AA** and **3AA**), REE solvent extraction experiments were undertaken. Initially, organic solutions of **2ACH$_2$A** and **3ACH$_2$A** (0.1 M) were contacted with a series of aqueous phases containing La (0.01 M). The different compositions of the aqueous phases were: $NaNO_3$ (7.0 M); HNO_3/$NaNO_3$ (0.1 M/5.0 M); HNO_3 (2.0 M).

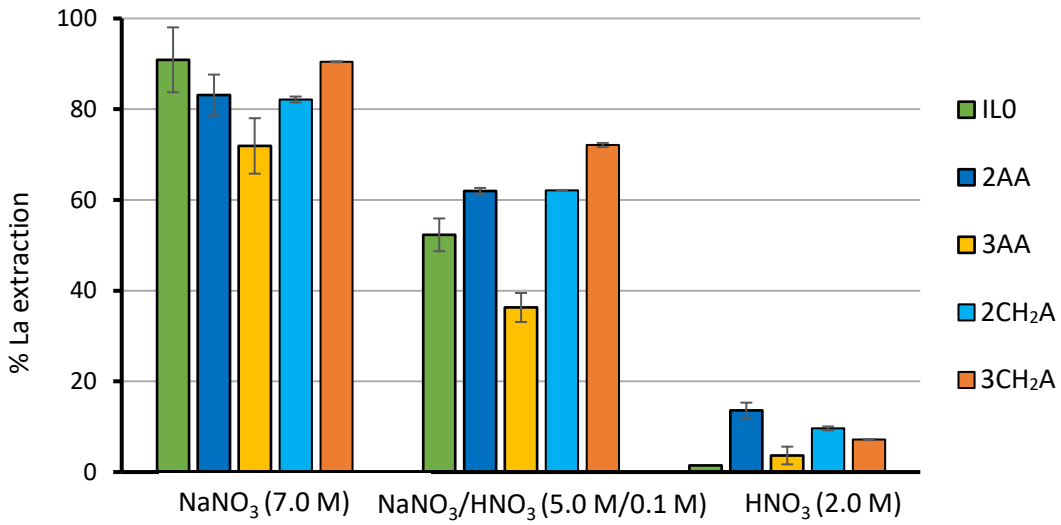

Figure 5.3.2.1 – Initial tests for the extraction of La (0.01 M) using **2ACH$_2$A** and **3ACH$_2$A** (0.1 M) in toluene from water, $NaNO_3$ (7.0 M), $NaNO_3$/HNO_3 (5.0 M/0.1 M) and HNO_3 (2.0 M), compared against **IL0**, **2AA** and **3AA** (section 3.5.1).

The modified ILs **2ACH$_2$A** and **3ACH$_2$A** (0.1 M) effectively extract La from a $NaNO_3$ (7.0 M) aqueous solution achieving 82% and 90% respectively but when the $NaNO_3$ concentration is reduced to 5.0 M and the HNO_3 concentration increased to 0.1 M La extraction is reduced to

62% and 72 % (Figure 5.2.2.1). While **2ACH$_2$A** and **2AA** exhibit essentially the same performance (62%), **3ACH$_2$A** interestingly extracts about twice as much La as **3AA** (72% vs. 36%). As expected La extraction from HNO_3 (2.0 M) with **2ACH$_2$A** or **3ACH$_2$A** was minimal (<10%).

The ability of **2CH$_2$A** to extract La from mildly (0.01 – 2.00 M) acidic HNO_3 solutions was examined. Broadly speaking, the extraction of La with **2CH$_2$A** (0.1 M) in toluene from a $NaNO_3$ (5.0 M) and La (0.01 M) containing aqueous phase of varying HNO_3 concentration (0.01 - 2.0 M) is comparable. **2AdiA** and **2AA** both extraction >60% of La at low HNO_3 concentrations (<0.1 M) but extract less than 20% of La at 2.00 M HNO_3 (Figure 5.3.2.2).

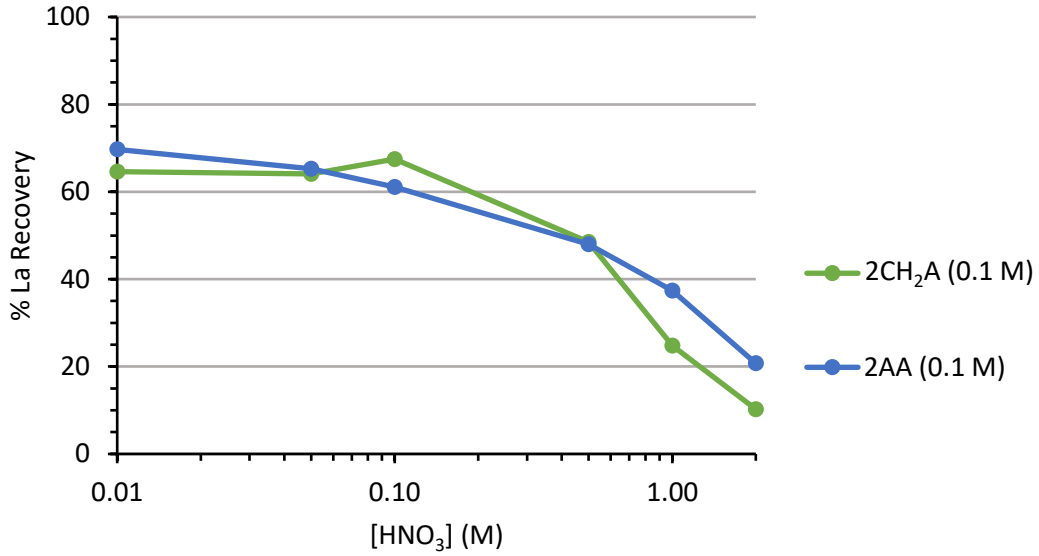

Figure 5.3.2.2 – The extraction of La (0.01 M) using **2ACH$_2$A** or **2AA** (0.1 M) in toluene from a $NaNO_3$/HNO_3 (5.0 M/0.01 – 2.00 M) aqueous solution. Interpolation used to aid the eye only.

5.4 Conclusions

This brief exploration into amido-ammonium IL modifications does not appear to have resulted in ILs that substantially exceed the ability of **2AA** to extract light REEs (e.g. La). However, **3CH$_2$A** in initial tests does appear to show a slight performance improvement (5-10 %) over **2AA** and may warrant further investigation.

The additional amide functional group in **2AdiA** and **3AdiA** may cause a minor increase in the stability of assemblies that form in the organic phase following REE extraction but this may be outweighed by the loss of a lipophilic C_8H_{17} alkyl chain. Computational modelling (section

3.7) for both **IL0** and **2AA** has suggested that effective encapsulation of REE-metalates by comparatively lipophilic alkyl chains is evident contributes to strong light REE extraction.[134]

The broad similarities between **2AA** and **2ACH$_2$A** for La extraction suggests that the assemblies formed in the organic phase are similar but structural characterisation is required to confirm this.

Despite the ILs studied not exceeding the ability of **2AA** to selectively extract lighter REEs, a valuable insight into understanding why **2AA** is an effective and selective extractant for lighter REEs has been gained and provides directionality for future structural modifications. Additionally, **2AdiA**, **3AdiA**, **2ACH$_2$A** and **3ACH$_2$A** are similar structurally to reagents that are effective during PGM recovery and so an exploration into PGM recovery may be of future interest.[23, 24, 245]

Chapter 6

Conclusions and future work

6 Conclusions and future work

The aim of this thesis, to develop and understand practices and reagents that can be more environmentally friendly and selective for rare earth element (REE) recovery, has been achieved. A new comparatively simple amido-ammonium ionic liquid (IL) **2AA** has been developed and is highly selective for the extraction of lighter REEs from aqueous leach solutions and those obtained from the bioleaching of REEs.

Chapter 2 focussed on increasing the chemical understanding of how an alkylammonium IL (**IL0**) rapidly (<1 minute) transports REEs from aqueous nitrate solutions of low acid (HNO_3) and high salt ($NaNO_3$) into an immiscible organic phase. Multiple analytical, spectroscopic and computational techniques strongly suggest that **IL0** extracts REEs through a microhydration mechanism pathway, resulting in partially hydrated REE-nitratometalates residing in the organic phase that are encapsulated and stabilised by multiple lipophilic **IL0** cations. The microhydration mechanism pathway avoids the comparatively high energetic cost associated of full REE dehydration and also allows for charge mediating water molecules to stabilise the assembly in the organic phase.[85, 86, 88] Similarly, in other work, microhydration has been reported to prevent the fragmentation of uracil and thymine by ionizing radiation and to stabilise aromatic amide cations through the formation of a hydrogen-bonding network.[246, 247]

Chapter 3 revealed that a 2° amido-ammonium IL (**2AA**) is a stronger, more selective extractant for the lighter REEs (e.g. Ce or Nd) than **IL0** and means **2AA** can effectively separate the lighter REEs from aqueous solutions containing heavier REEs (e.g. Tb or Dy). With **2AA**, the separation factors between Ce/Tb (2670 ± 1340) and Nd/Dy (162 ± 2), two common REE pairs in electronic waste, comfortably exceed those reported for organophosphorus reagents and for **IL0** (25.9 ± 0.4 and 9.46 ± 0.17).[67, 139] **2AA**, similar to **IL0**, extracts REEs through a microhydration pathway but a more extensive hydrogen-bonding network of amides, nitrate anions and water molecules enhances the stability of the formed organic phase assemblies.[188, 189] DFT calculations confirmed that the formation of a **2AA**-La assembly in the organic was more favourable than an **IL0**-La assembly. While the computational and experimental work agreed in this instance, further work is required to understand the differences in Nd and Dy extraction. Experimentally, Nd and Dy are less readily extracted than La but computationally they are calculated to form more stable assemblies with **IL0** and **2AA**.

A number of low energy structures were identified and the discrepancy may be arising as of this. Further investigation is required and EXAFS measurements that can probe the inner-coordination sphere of REEs are expected to be of great benefit, having previously been vital for understanding other systems.[52, 109, 155] Nevertheless, **2AA** conveniently provides effective separation of the lighter REEs from the heavier REEs and the mechanistic pathway of REE extraction is broadly understood.

Chapter 4 investigated the bioleaching of REEs from eudialyte, a zirconate REE mineral, with an *Acidithiobacillus ferrooxidans* (ATs) cell culture. It was found that the **ATs** could reduce the pH of the leach solution by approximately half a pH unit by catalysing the oxidation of Fe^{2+} resulting in greater quantities of REEs being leached. Despite the percentage of REEs leached using these mild conditions being significantly lower than with traditional, highly acidic conditions, the lighter REEs could be readily extracted from the **ATs** containing leach solution using **2AA** with no pH adjustment being required. Following the stripping of REEs with only water, **2AA** was regenerated. This work highlights a potentially more environmentally friendlier REE purification process that uses milder leaching conditions although further work is required to investigate whether the process is feasible on larger scales.

Chapter 5 briefly explores modifications to **2AA**. While initial screening of modifications did not indicate any substantial improvements, the results do help to solidify the effectiveness of the amido-ammonium structure for light REE extraction. Many further modifications are possible, including increasing the lipohilicity on diamido-ammonium ILs, the replacement of amide functional groups with thioamide functional groups or the replacement of the nitrate counter anion.

Chapter 7

Experimental and computational methods

7 Experimental and computational methods

7.1 Outline

This chapter outlines general procedures, treatment of data, sources of error, specific experimental details and computational parameters, methods and conditions.

7.2 Solvent extraction procedure

All solvent extractions were carried out in glass screw-top vials and mixed with magnetic stirrer bars on a stirrer plate (1000 rpm, 1 hour, RT unless otherwise stated). The solvent extractions consisted of an aqueous phase and an aqueous immiscible organic phase (usually toluene). Toluene was usually the solvent of choice as of its ease of use, comparability to typical industrial solvents and allowed for comparison to previous work at the University of Edinburgh in this field. Generally the ligand (or extractant) concentration in the organic phase was 0.1 M, the REE concentration in the aqueous phase was 0.01 M and the predominant anion in the aqueous phase was NO_3^-. Variations from the standard experimental set-up are explicitly highlighted where required. After stirring, the phases were allowed to disengage and the two phases were then physically separated (Figure 7.2.1).

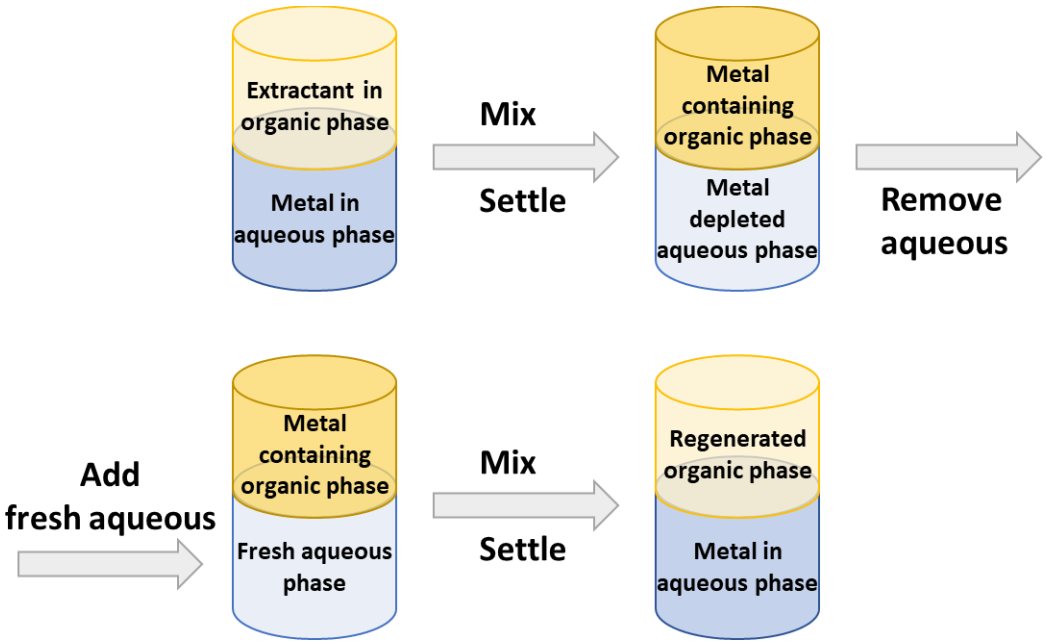

Figure 7.2.1 – The general method of a solvent extraction experiment.

The basic equations used to calculate percentage metal extracted and stripped are given:

Eq. 7.2.1 – %extraction = ([M conc. org]/[M conc. aq.])*100

Eq. 7.2.2 – %stripped = ([M conc. aq.])]/[M conc. org])*100

Separation factors (how preferentially one metal is extracted over another) are calculated by comparing the concentration of metal 'a' and metal 'b' in each phase according to the following equation:

Eq. 7.2.3 – ([M(b) conc. org]/[M(b) conc. aq.])/([M(a) conc. org]/[M(a) conc. aq.])

7.3 Sources of error

There are many sources of error associated with solvent extraction experiments. While some instrument and equipment errors can be determined (summarised in table 7.3.1), others are more difficult to quantify.

Table 7.3.1 – Quantifiable sources of error

Instrument/equipment	**Associated error**
Mass balance	*± 0.05 mg*
Manual pipettes#	
Gilson 0.1 mL	*± 0.5 μL*
Gilson 1 mL	*± 6 μL*
Gilson 5 mL	*± 27 μL*
Electronic Eppendorf Multipette E3x positive-displacement pipette#	*± 0.95 μL (dispensing 500 μL)* *± 0.38 μL (dispensing 2500 μL)* *± 0.23 μL (dispensing 5000 μL)*
Volumetric Flasks	
5 mL, 10 mL	*± 0.025 mL*
25 mL	*± 0.040 mL*
100 mL	*± 0.080 mL*
ICP-OES calibration line	$R^2 > 0.995$

ICP-OES sample data	$\sigma = \sqrt{(\sum(x-\mu)^2)/n}$ σ = *standard deviation* x = *value of sample* μ = *mean of samples* n = *number of samples*

 # Maximum uncertainty documented on 2019 calibration reports.

Uncertainties that are difficult to quantify that can result in artificially higher or lower metal concentrations include the rate of evaporation of solvents during experiment and ICP-OES (section 7.4.2) sample preparation, the entrainment of one phase into another and human error. To minimise these uncertainties, samples and experiments were prepared in the same manner each time and in a limited timeframe. Furthermore, most solvent extraction experiments were carried out in duplicate or triplicate with errors between independent but comparable samples being within ± 5%. Where experiments have been replicated error bars are present on the respective graphs. Where solvent extraction experiments have not been replicated a blanket ± 5% relative error can be assumed for extraction values.

7.4 Chemicals and Instrumentation

7.4.1 Solvents and reagents

All solvents and reagents were used as received from Sigma-Aldrich, Fisher Scientific UK, Alfa Aesar, Acros Organics, VWR International or Merck Millipore. Deionised water was obtained from a Milli-Q purification system. Column chromatography was carried out with 60 Å particle size 35-70 micron silica gel. The *Acidithiobacillus ferrooxidans* strain NCIMB 10435 was obtained from NCIMB. A eudialyte ore sample from the Ilimaussaq Complex in Greenland was manually crushed using a Jaw Crusher.[248]

7.4.2 Inductively Coupled Plasma Optical Emission Spectrometry (ICP-OES)

Inductively-coupled plasma optical emission spectroscopy (ICP-OES) is a spectroscopic technique used for elemental analysis. Liquid samples are introduced into a spray chamber by a peristaltic pump. The sample is then ionised by injection into argon plasma by a nebuliser. The plasma excites the electrons of the ions present to a higher atomic energy level. As the electrons decay back to the ground state, energy is emitted as photons of light.

The wavelength of this light is dependent on the electronic transition and is characteristic to the ion in question. These photons hit a detector where the number of 'counts per second' of a given wavelength is counted. With the 'counts per second' being proportional to the ion present, the concentration of an unknown sample can be determined by comparison to standards of known concentrations. A simplified representation of an ICP-OES is given (Figure 7.4.2.1).[249] This technique can be used to measure the metal concentration in both the aqueous and organic phases.

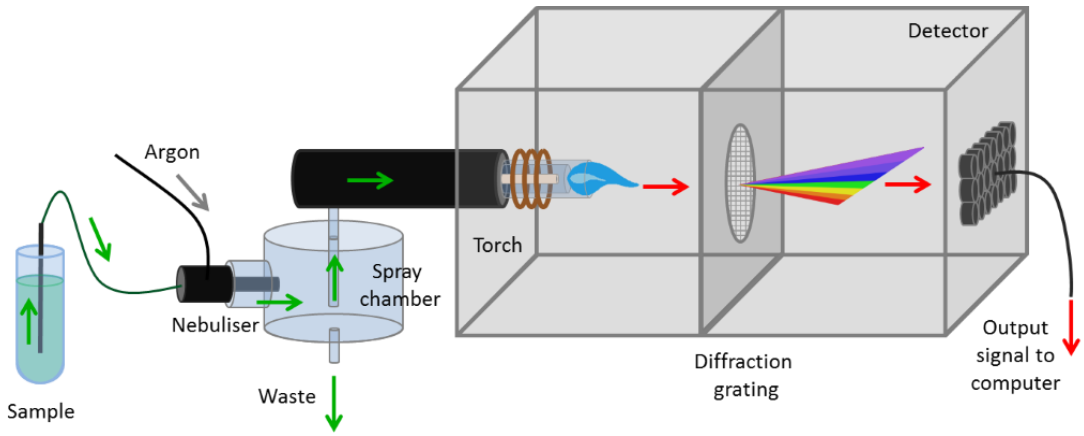

Figure 7.4.2.1 – A schematic representation of an ICP-OES.[249]

Samples were prepared for ICP-OES analysis by dilution of at least 1:10 in 1-methoxy-2-propanol or nitric acid (2% w/w, 0.45 M). Samples <25 ppm (mg/L) diluted in 1-methoxy-2-propanol were analysed using the 'organic' instrument conditions and set-up (table 7.4.2.1). Aqueous samples <100 ppm (mg/L) diluted in nitric acid (2% w/w, 0.45 M were analysed using the 'aqueous' instrument conditions and set-up (table 7.4.2.1). ICP-OES analysis was carried out on a Perkin Elmer Optima 8300 Inductively Coupled Plasma Optical Emission spectrometer. ICP-OES calibration standards were obtained from VWR International or Sigma-Aldrich and standards of appropriate concentrations were prepared by dilution. Y (10 ppm) (or Rh (10 ppm) where Y was a sample), was used as an internal standard with samples measured in triplicate. Unless explicitly stated otherwise, both aqueous and organic samples following solvent extraction experiments were diluted using 1-methoxy-2-propanol and ran under 'organic' conditions.

Table 7.4.2.1 – ICP-OES conditions and set-up

Parameters (units)	**'Organic'**	**'Aqueous'**
Spray chamber	*Glass cyclonic*	*Scotts*
Nebuliser	*Gem Tip cross-flow*	*Gem Tip cross-flow*
Radio frequency power (W)	*1500*	*1500*
Peristaltic Pump rate (mL min^{-1})	*1.00*	*1.30*
Argon gas flow rates (L min^{-1})		
Plasma	*17*	*10*
Auxiliary	*1.0*	*0.2*
Nebuliser	*0.5*	*0.6*

7.4.3 Karl-Fischer water content measurements

Karl-Fischer (KF) coulometric titrations were used to quantify the amount of water that was transported into the organic phase. Karl-Fischer (KF) coulometric titrations work on the basis of the electrochemical reaction of water with iodide and sulfur dioxide (equation 7.4.3.1).

Eq. 7.4.3.1 – $I_2 + SO_2 + 2\ H_2O \rightleftharpoons 2\ HI + H_2SO_4$

The iodine is generated electrochemically from iodide at an anode during the titration from a reagent present in the titration cell. The electrons liberated in this process react with H^+ at the cathode to form hydrogen gas. A platinum electrode monitors the potential of the solution by voltammetry allowing the endpoint to be determined. The amount of electrical current required to generate iodine is measured, calculated on 96485 C per mole of electrons and that two moles of electrons are involved in the oxidation of two moles of iodide to one mole of iodine. In doing so, the amount of water is therefore also determined.

Coulometric KF titrations were carried out using a C30S diaphragmless titrator, using a DM 143-SC electrode with HYDRANAL Coulomat AD as the titration reagent. A known mass of sample was injected into the titration vessel and the titrators gave the total mass of water contained within the sample.

7.4.4 pH measurements

Using a Mettler Toledo Excellence Titrator T5, pH measurements were carried with a DGi115-SC probe calibrated using aqueous buffers of pH 2.00, 4.01, 7.00 and 9.31 supplied by Mettler Toledo.

7.4.5 Ion-chromatography

Ion chromatography (IC) measurements were used to quantify the amount of nitrate that was transported into the organic phase (Figure 7.4.5.1). IC is a process that separates ions based on their affinity to an ion exchange resin within a pressurized column. As an eluent is passed through the column, different anions will remain retained upon the exchange resin for different lengths of time depending on their charge, radius and polarizability. At the end of the column is a detector that calculates ion concentrations using electrical conductivity measurements. Nitrate anion concentrations were determined using an ICS-110 RFIC ion chromatography system with AS22 110 diluent.

7.4.6 Electrospray ionisation mass spectrometry (ESI-MS)

Mass spectrometry (MS) measures the mass-to-charge ratio of ions. Electrospray ionisation (ESI) fourier-transform ion cyclotron resonance (FT-ICR) MS measurements were recorded in negative-ion mode using the standard Bruker ESI sprayer operated in “infusion” mode coupled to a SolariX FTICR mass spectrometer. Direct infusion spectra were a sum of 10 acquisitions. All mass spectra were analysed using DataAnalysis software version 5.0 SR1 build 203 (Bruker Daltonics) and ions were assigned manually.

ESI is considered a “soft” ionisation technique meaning that the fragmentation of the molecules in the sample is reduced.[250, 251] This means that the ionic fragments captured within the magnetic field of the instrument should be broadly representative of the complexes formed in the organic phase following REE extraction.

7.4.7 Infrared spectroscopy (IR)

Infrared (IR) spectroscopy measurements were carried out on a PerkinElmer Spectrum 65 FT-IR spectrometer with a PIKE MIRacle ATR sampling accessory with data collected using spectrum software version 10.02. Absorption peaks are reported in wavenumbers (υ) (cm^{-1}).

7.4.8 Nuclear magnetic resonance (NMR) spectroscopy

Nuclear magnetic resonance (NMR) spectra were recorded at 298 K (unless otherwise stated) on a Bruker AVA400, AVA500 or AVA600 spectrometer operating at 399.90, 500.12, or 599.95 MHz respectively for ^{1}H, and 100.55, 125.76, or 150.83 MHz, respectively, for ^{13}C. ^{139}La spectra were recorded on a Bruker AVA400 at 56.56 MHz and ^{15}N on a Bruker AVA600 at 60.94 MHz. Chemical shifts are reported in δ (ppm).

7.4.9 Ultraviolet-visible light (UV-Vis) spectrophotometry

Ultraviolet-visible light (UV-Vis) measurements to determine Fe^{2+} and Fe^{3+} concentrations were carried out on a Jenway 6300 spectrophotometer.[225] To 2 mL of a standard or unknown sample, 0.2 mL of sodium 3-(2-pyri-dyl)-5,6-diphenyl-1,2,4-triazine-p,p'-disulfonic acid (Ferrozine) (0.01 M) in ammonium acetate (0.1 M) was added and the absorbance recorded at 568 nm (section 4.5). 1.6 mL of the resulting solution was then added to 0.3 mL of a hydroxylamine.HCl (1.4 M) in HCl (2.0 M) solution and the mixture allowed to react (10 minutes). Then 0.1 mL of ammonium acetate (10.0 M) buffered to pH 9.5 with ammonium hydroxide was added and the absorbance of the mixture recorded at 568 nm.

7.5 Compound synthesis

7.5.1 IL0

IL0 – trioctyl methylammonium nitrate (IUPAC: *N*-methyl-*N*,*N*-dioctyloctan-1-aminium nitrate)

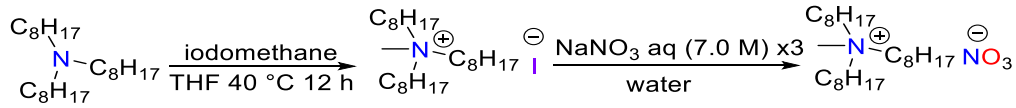

Iodomethane (4.44 g, 31 mmol) was added dropwise to a stirred solution of trioctylamine (8.85 g, 25 mmol) in THF (100 mL).[124, 134] The mixture was then allowed to react (12 h, 40 °C, N_2 flow). The crude mixture was concentrated under vacuum, diluted with chloroform (50 mL), and contacted with an aqueous solution of sodium nitrate (7.0 M, 50 mL, three times) (1 h, 25 °C) then washed with water (50 mL). The organic phase was separated, dried over sodium sulfate and concentrated under vacuum to yield a viscous orange oil (99 %). ^{1}H NMR (500 MHz, $CDCl_3$): δ_H 3.35–3.41 (m, 6H, NC**H**$_2$), 3.24 (s, 3H, NC**H**$_3$), 1.64–1.74 (m, 6H, C**H**$_2$),

1.23–1.43 (m, 30H, C**H**$_2$), 0.89 (t, 9H, C**H**$_3$). ^{13}C NMR (126 MHz, $CDCl_3$): δ_C 61.70, 48.83, 31.62, 29.10, 29.01, 26.30, 22.57, 22.43, 14.04. ESI-MS (m/z) $C_{25}H_{54}N$ [M^+] calculated 368.4251 found 368.4267.

7.5.2 Amido-ammonium ILs

1AA intermediate - (IUPAC: *N*,*N*-dioctylglycinamide)

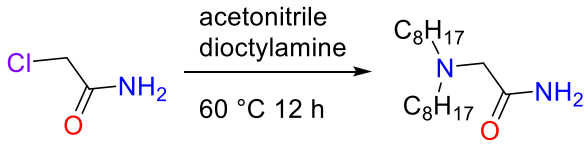

To a sealed, nitrogen-flushed round-bottom flask of acetonitrile (50 mL), 2-chloroacetamide (2.34 g, 25 mmol) was added dropwise. Dioctylamine (14.5 g, 60 mmol) was added dropwise and the reaction stirred (12 h, 60 °C, N_2 flow). The mixture was concentrated under vacuum and then re-dissolved in ethyl acetate (75 mL) and a water/brine (1:1) solution added (75 mL). A saturated solution of sodium hydrogen carbonate (25 mL) was added and the solution stirred (1 h, 20 °C). The organic phase was then separated and dried over sodium sulfate, concentrated under vacuum and purified using column chromatography (9:1 hexane:ethyl acetate) to yield a clear viscous liquid (95%). ^{1}H NMR ($CDCl_3$, 500 MHz): δ_H 7.22 (s, 1H, N**H**$_2$), 5.35 (s, 1H, N**H**$_2$), 3.04 (s, 2H, OCC**H**$_2$), 2.48 (t, 4H, NC**H**$_2$), 1.42-1.51 (m, 4H, C**H**$_2$), 1.24-1.36 (m, 20H, C**H**$_2$), 0.88-0.94 (tzz, 6H, C**H**$_3$); ^{13}C NMR ($CDCl_3$, 125 MHz) δ_C (ppm) 175.16, 58.61, 55.49, 31.83, 29.50, 29.29, 27.41, 27.34, 22.65, 14.09. ESI-MS (m/z) $C_{18}H_{36}N_2O$ [M+H]$^+$ calculated 299.307 found 299.305.

1AA – Primary amido-ammonium (IUPAC: *N*-(2-amino-2-oxoethyl)-*N*-methyl-*N*-octyloctan-1-aminium nitrate)

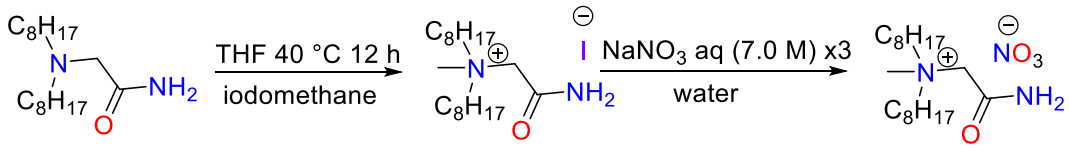

To a sealed, nitrogen flushed round bottom flask of THF (30 mL), 2-(dioctylamino) acetamide (1.09 g, 3.65 mmol) was added slowly. Iodomethane (0.57 g, 4 mmol) was added dropwise and the reaction stirred (12 h, 40 °C, N_2 flow). The general procedure for **IL0** was then followed to yield a clear viscous liquid (77%).[124, 134] ^{1}H NMR ($CDCl_3$, 500 MHz): δ_H 8.77 (s, 1H, N**H**$_2$), 5.67 (s, 1H, N**H**$_2$), 4.48 (s, 2H, OCC**H**$_2$), 3.43-3.63 (m, 4H, NC**H**$_2$), 3.26 (s, 3H, NC**H**$_3$), 1.69-1.81 (m, 4H, C**H**$_2$), 1.24-1.42 (m, 20H, C**H**$_2$), 0.88-0.94 (m, 6H, C**H**$_3$); ^{13}C NMR ($CDCl_3$, 125 MHz)

δ_C (ppm) 129.03, 128.22, 125.29, 62.95, 31.57, 28.96, 26.25, 22.55, 22.44, 21.66, 14.03. ESI-MS (m/z) $C_{19}H_{38}N_3O_4$ $[M–H]^-$ calculated 374.301 found 374.301.

(IUPAC: 2-chloro-*N*-propylacetamide)

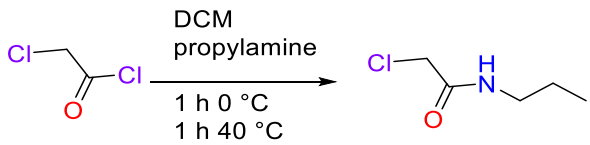

To a sealed, nitrogen flushed round bottom flask of DCM (100 mL), propylamine (3.0 g, 50 mmol) was added slowly. Chloroacetyl chloride (11.3 g, 0.1 M) was added dropwise over ice and with stirring. The mixture was allowed to proceed with stirring (1 h, 0 °C then 1 h, 40 °C, N_2 flow).[21] The reaction was quenched with DI water (10 mL) and the organic phase washed with saturated sodium hydrogen carbonate solution (30 mL, three times). The organic phase was dried over sodium sulfate and concentrated under vacuum to yield a faintly yellow liquid (94%). ^{1}H NMR ($CDCl_3$, 400 MHz): δ_H 6.61 (s, 1H, N**H**), 4.06 (s, 2H, OCC**H**$_2$), 3.25-3.32 (m, 2H, HNC**H**$_2$), 1.53-1.63 (m, 2H, C**H**$_2$), 0.96 (t, 3H, C**H**$_3$); ^{13}C NMR ($CDCl_3$, 100 MHz) δ_C (ppm) 165.76, 42.69, 41.52, 22.60, 11.25.

2AA intermediate - (IUPAC: *N*,*N*-dioctyl-*N*-propylglycinamide)

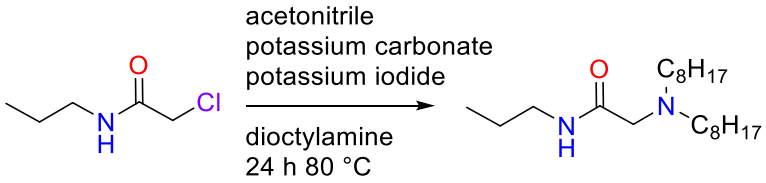

Potassium carbonate (10.1 g, 72.8 mmol), and potassium iodide (3.78 g, 22.8 mmol) were added to acetonitrile (150 mL). Then, 2-chloro-*N*-propylacetamide (2.47 g, 18.2 mmol) was added dropwise. Dioctylamine (4.60 g, 19.1 mmol) was then added dropwise. The mixture was then allowed to react with stirring (24 h, 80 °C, N_2 flow).[240] The mixture was cooled, gravity filtered and then concentrated. The mixture was then diluted with chloroform (150 mL) and filtered again. The crude product was concentrated then purified using column chromatography (8:2 hexane:ethyl acetate) to yield a faintly yellow liquid (95 %). ^{1}H NMR ($CDCl_3$, 400 MHz): δ_H 7.36 (t, 1H, N**H**), 3.18-3.25 (m, 2H, HNC**H**$_2$), 2.99 (s, 2H, OCC**H**$_2$), 2.42 (t, 4H, (NC**H**$_2$), 1.47-1.57 (m, 2H, C**H**$_2$), 1.36-1.44 (m, 4H, C**H**$_2$), 1.21-1.30 (m, 20H, C**H**$_2$) 0.92 (t, 3H, C**H**$_3$), 0.87 (t, 6H, C**H**$_3$); ^{13}C NMR ($CDCl_3$, 100 MHz) δ_C (ppm) 171.89, 58.75, 55.53, 40.52,

31.82, 29.49, 29.29, 27.45, 22.94, 22.65, 14.08, 11.42. ESI-MS (m/z) $C_{21}H_{44}N_2O$ $[M+H]^+$ calculated 341.353 found 341.352.

2AA – Secondary amido-ammonium (IUPAC: *N*-methyl-*N*-[2-oxo-2-(propylamino)ethyl]-*N*-octyl octan-1-aminium nitrate)

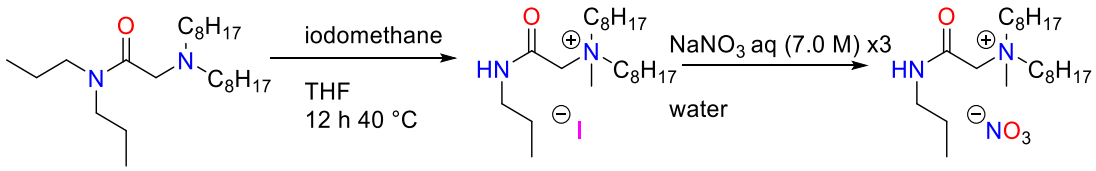

To a sealed, nitrogen flushed round bottom flask of THF (30 mL), 2-(dioctylamino) acetamide (1.09 g, 3.65 mmol) was added slowly. Iodomethane (0.57 g, 4 mmol) was added dropwise and the reaction stirred (12 h, 40 °C, N_2 flow). The general procedure for **IL0** was then followed to yield a yellow liquid (90%).[124, 134] ^{1}H NMR ($CDCl_3$, 500 MHz): δ_H 8.65 (t, 1H, N**H**), 4.43 (s, 2H, OCC**H**$_2$), 3.50-3.61 (m, 2H, NC**H**$_2$), 3.40-3.50 (m, 2H, NC**H**2), 3.25 (s, 3H NC**H**$_3$), 3.16-3.26 (m, 2H, NC**H**$_2$), 1.69-1.76 (m, 4H, C**H**$_2$), 1.54-1.61 (m, 2H, C**H**$_2$), 1.20-1.37 (m, 20H, C**H**$_2$), 0.91 (t, 3H, C**H**$_3$), 0.86 (t, 6H, C**H**$_3$); ^{13}C NMR ($CDCl_3$, 125 MHz) δ_C (ppm) 162.74, 62.92, 61.34, 53.44, 49.37, 41.53, 31.57, 28.98, 26.25, 22.54, 22.51, 22.22, 14.02, 11.53. ESI-MS (m/z) $C_{22}H_{46}N_3O_4$ $[M-H]^-$ calculated 416.348 found 416.348.

(IUPAC: 2-chloro-*N*,*N*-dipropylacetamide)

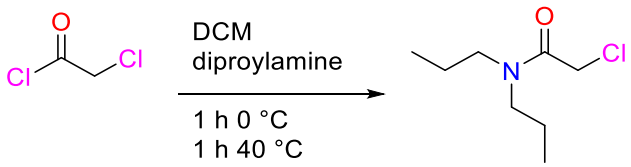

To a sealed, nitrogen flushed round bottom flask of DCM (100 mL), dipropylamine (5.05 g, 50 mmol) was added slowly. Chloroacetyl chloride (6.8 g, 60 mmol) was added dropwise over ice and with stirring (1 h, 0 °C then 1 h, 40 °C, N_2 flow). The reaction was quenched with DI water (10 mL) and the organic phase washed with saturated sodium hydrogen carbonate solution (30 mL, three times). The organic phase was dried over sodium sulfate and concentrated under vacuum to yield a yellow liquid (70%). ^{1}H NMR ($CDCl_3$, 600 MHz): δ_H 4.06 (s, 2H, OCC**H**$_2$), 3.23-3.32 (m, 4H, NC**H**$_2$), 1.54-1.67 (m, 4H, C**H**$_2$), 0.94 (t, 3H, C**H**$_3$), 0.90 (t, 3H, C**H**$_3$); ^{13}C NMR ($CDCl_3$, 150 MHz) δ_C (ppm) 166.19, 49.93, 47.78, 41.28, 22.31, 20.57, 11.27, 11.20.

3AA intermediate - (IUPAC: N,N-dioctyl-*N*,*N*-dipropylglycinamide)

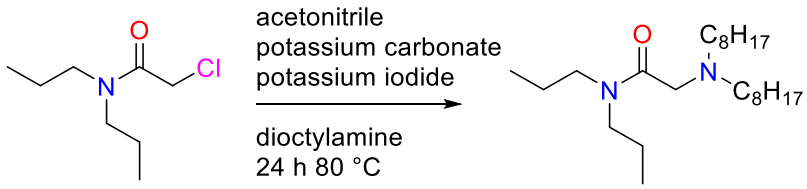

Potassium carbonate (10.1 g, 72.8 mmol), and potassium iodide (3.78 g, 22.8 mmol) were added to acetonitrile (150 mL).[240] Then, N, N-(dipropyl) chloroacetamide (3.55 g, 20 mmol) was added dropwise. Dioctylamine (4.82 g, 20 mmol) was then added dropwise. The mixture was then allowed to react with stirring (24 h, 80 °C, N_2 flow). The mixture was cooled, gravity filtered and then concentrated. The mixture was then diluted with chloroform (150 mL) and filtered again. The crude product was concentrated then purified using column chromatography (8:2 hexane:ethyl acetate) to yield a yellow liquid (90%). ^{1}H NMR ($CDCl_3$, 500 MHz): δ_H 3.35-3.39 (m, 2H, NC**H**$_2$), 3.20-3.25 (m, 2H, NC**H**$_2$), 3.20 (s, 2H, OCC**H**$_2$), 2.44 (t, 4H, (NC**H**$_2$), 1.49-1.59 (m, 4H, C**H**$_2$), 1.37-1.43 (m, 4H, C**H**$_2$), 1.21-1.29 (m, 20H, C**H**$_2$), 0.84-0.89 (m, 12H, C**H**$_3$); ^{13}C NMR ($CDCl_3$, 125 MHz) δ_C 170.50, 58.17, 54.48, 52.18, 50.12, 48.80, 47.24, 31.89, 30.14, 29.64, 29.54, 29.39, 29.29, 29.24, 27.63, 27.53, 27.40, 27.16, 27.08, 22.10, 20.70, 14.03, 11.38, 11.19. ESI-MS (m/z) $C_{24}H_{51}N_2O$ $[M+H]^+$ calculated 383.340 found 383.398.

3AA – Tertiary amido-ammonium (IUPAC: *N*-[2-(dipropylamino)-2-oxoethyl]-*N*-methyl-*N*-octyl octan-1-aminium nitrate)

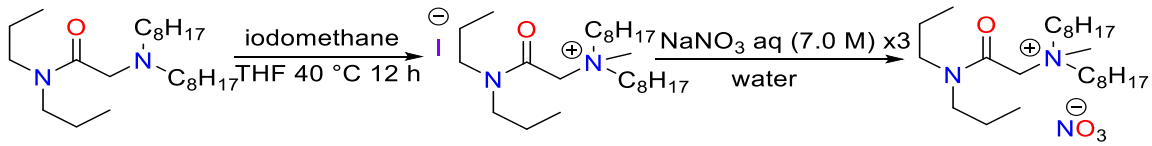

To a sealed, nitrogen flushed round bottom flask of THF (50 mL), 2-dioctylamino-N,N-dipropylacetamide (2.8 g, 7.3 mmol) was added slowly. Iodomethane (2.07 g, 14.6 mmol) was added dropwise and the reaction stirred. (12 h, 40 °C, N_2 flow). The general procedure for **IL0** was then followed to yield a yellow viscous liquid (78%).[124, 134] ^{1}H NMR ($CDCl_3$, 500 MHz): δH 4.60 (s, 2H, OCC**H**$_2$), 3.79-3.87 (m, 2H, NC**H**$_2$), 3.50-3.57 (m, 2H, NC**H**$_2$), 3.35 (s, 3H, NC**H**$_3$), 3.32-3.37 (m, 2H, NC**H**$_2$), 3.23-3.28 (m, 2H, NC**H**$_2$), 1.63-1.73 (m, 4H, C**H**$_2$), 1.50-1.63 (m, 4H, C**H**$_2$), 1.20-1.37 (m, 20H, C**H**$_2$), 0.96 (t, 3H, C**H**$_3$), 0.85-0.90 (m, 9H C**H**$_3$); ^{13}C NMR ($CDCl_3$, 125 MHz) δ_C 163.02, 62.93, 58.87, 49.95, 49.13, 47.99, 31.59, 28.99, 28.97, 26.25, 22.59,

22.55, 22.07, 20.70, 14.03, 11.31, 11.12. ESI-MS (m/z) $C_{25}H_{53}N_4O_7$ $[M+H]^+$ calculated 521.391 found 521.390.

7.5.3 Diamido-ammonium ILs

2AdiA intermediate - (IUPAC: 2,2'-(octylazanediyl)bis(*N*-propylacetamide))

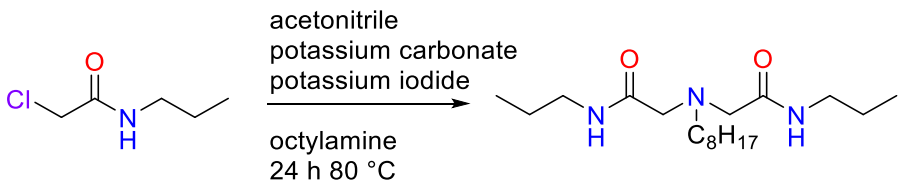

Potassium carbonate (13.6 g, 98 mmol), and potassium iodide (5.13 g, 31 mmol) were added to acetonitrile (150 mL).[240] Then, 2-chloro-*N*-propylacetamide (6.80 g, 50 mmol) was added dropwise. Octylamine (3.23 g, 25 mmol) was then added dropwise. The mixture was then allowed to react with stirring (24 h, 80 °C, N_2 flow). The mixture was cooled, gravity filtered and then concentrated. The mixture was then diluted with chloroform (150 mL) and filtered again. The crude product was concentrated then purified using columzn chromatography (ethyl acetate) to yield an orange oil (74%). ^{1}H NMR ($CDCl_3$, 400 MHz): δ_H 6.73 (t, 2H, CONH), 3.28 (td, 4H, HNC**H**$_2$), 3.17 (s, 4H, OCC**H**$_2$), 2.51 – 2.59 (m, 2H, NC**H**$_2$), 1.53 – 1.61 (qt, 4H, C**H**$_2$), 1.43 – 1.51 (m, 2H, C**H**$_2$), 1.24 – 1.36 (m, 10H, C**H**$_2$), 0.96 (t, 6H, C**H**$_3$), 0.90 (t, 3H, C**H**$_3$); ^{13}C NMR (126 MHz, $CDCl_3$) δ_C 170.42, 59.22, 56.32, 40.96, 31.79, 29.43, 29.22, 27.51, 27.28, 22.91, 22.63, 14.21, 14.08, 11.39. ESI-MS (m/z) $C_{18}H_{37}N_3O_2Cl$ $[M-H]^-$ calculated 362.258 found 362.261.

2AdiA – Secondary diamido-ammonium (IUPAC: *N*-methyl-*N*,*N*-bis[2-oxo-2-(propylamino) ethyl] octan-1-aminium nitrate)

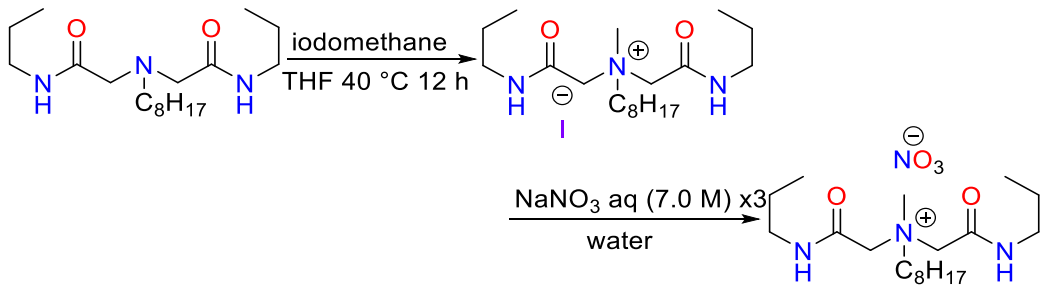

To a sealed, nitrogen flushed round bottom flask of THF (100 mL), 2,2'-(octylazanediyl)bis(N-propylacetamide (4.1 g, 12.5 mmol) was added slowly. Iodomethane (4.25 g, 30 mmol) was added dropwise and the reaction stirred. (12 h 40 °C, N2 flow). The general procedure for **IL0**

was then followed to yield a yellow viscous liquid (80%).[124, 134] ^{1}H NMR ($CDCl_3$, 600 MHz): δ_H 8.18 (t, 2H, CONH), 4.35 (s, 4H, OCC**H**$_2$), 3.85 – 3.89 (m, 2H, NC**H**$_2$), 3.45 (s, 3H, NC**H**$_3$), 3.22 (tdd, 4H, HNC**H**$_2$), 1.74-1.79 (m, 2H, C**H**$_2$), 1.57 (dt, 4H, C**H**$_2$), 1.22 – 1.36 (m, 10H, C**H**$_2$), 0.92 (t, 6H, C**H**$_3$), 0.87 (t, 3H, C**H**$_3$); ^{13}C NMR ($CDCl_3$, 150 MHz) δ_C 162.43, 63.29, 62.52, 49.97, 41.62, 31.57, 28.97, 28.91, 26.14, 22.69, 22.55, 22.27, 14.03, 11.39. ESI-MS (m/z) $C_{19}H_{40}N_3O_2$ $[M]^+$ calculated 342.312 found 342.312.

3AdiA intermediate - (IUPAC: 2,2'-(octylazanediyl)bis(*N*,*N*-dipropylacetamide))

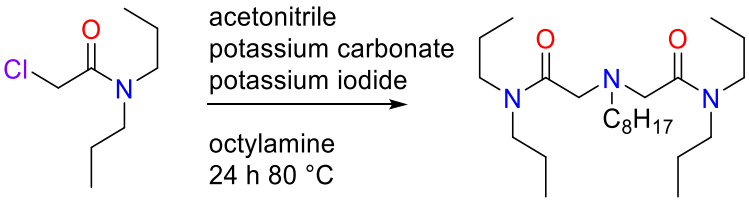

Potassium carbonate (13.6 g, 98 mmol), and potassium iodide (5.13 g, 31 mmol) were added to acetonitrile (150 mL).[240] Then, N, N-(dipropyl) chloroacetamide (8.89 g, 50 mmol) was added dropwise. Octylamine (3.23 g, 25 mmol) was then added dropwise. The mixture was then allowed to react with stirring (24 h, 80 °C, N_2 flow). The mixture was cooled, gravity filtered and then concentrated. The mixture was then diluted with chloroform (150 mL) and filtered again. The crude product was concentrated then purified using column chromatography (8:2 hexane:ethyl acetate) to yield an orange oil (74%). ^{1}H NMR ($CDCl_3$, 500 MHz): δ_H 3.52 (s, 4H, OCC**H**$_2$), 3.24 – 3.32 (m, 8H, NC**H**$_2$), 2.68 – 2.73 (t, 2H, NC**H**$_2$), 1.57 (qt, 8H, C**H**$_2$), 1.45 – 1.52 (m, 2H, C**H**$_2$), 1.22 – 1.33 (m, 10H, C**H**$_2$), 0.87 – 0.94 (m, 12H, C**H**$_3$); ^{13}C NMR ($CDCl_3$, 125 MHz) δ_C 170.22, 55.47, 55.20, 48.93, 47.46, 31.85, 29.58, 29.29, 27.75, 27.42, 22.66, 22.19, 20.89, 14.09, 11.42, 11.21. ESI-MS (m/z) $C_{24}H_{50}N_3O_2$ $[M+H]^+$ calculated 412.390 found 412.390.

3AdiA – Tertiary diamido-ammonium (IUPAC: *N*,*N*-bis[2-(dipropylamino)-2-oxoethyl]-*N*-methyl octan-1-aminium nitrate)

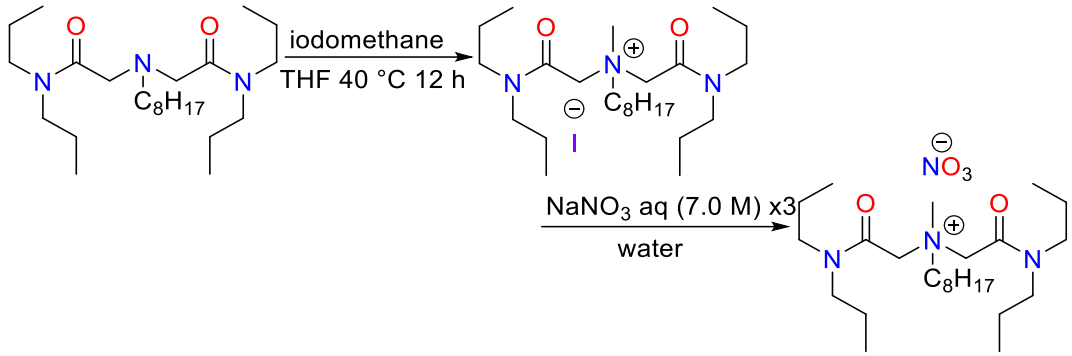

To a sealed, nitrogen flushed round bottom flask of THF (100 mL), 2,2'-(octylazanediyl)bis (N,N-dipropylacetamide (5.14 g, 12.5 mmol) was added slowly. Iodomethane (2.12 g, 15 mmol) was added dropwise and the reaction stirred. (12 h, 40 °C, N_2 flow). The general procedure for **IL0** was then followed to yield an orange viscous liquid (77%).[124, 134] ^{1}H NMR ($CDCl_3$, 500 MHz): δ_H 5.06 (d, 2H, OCC**H**$_2$), 4.85 (d, 2H, OCC**H**$_2$), 4.14 – 4.20 (m, 2H, NC**H**$_2$), 3.65 (s, 3H, NC**H**$_3$), 3.24 – 3.33 (m, 8H, C**H**$_2$), 1.62 – 1.71 (m, 2H, C**H**$_2$), 1.54 – 1.61 (m, 8H, C**H**$_2$), 1.24 – 1.40 (m, 10H, C**H**$_2$), 0.98 (t, 6H, C**H**$_3$), 0.90 (t, 6H, C**H**$_3$); ^{13}C NMR ($CDCl_3$, 125 MHz) δ_C 163.12, 67.98, 63.48, 60.01, 50.52, 49.34, 48.17, 31.58, 29.01, 28.95, 26.11, 25.62, 22.83, 22.57, 21.97, 20.74, 14.03, 11.30, 11.21. ESI-MS (m/z) $C_{25}H_{52}N_3O_2$ $[M]^+$ calculated 426.405 found 426.405.

7.5.4 Extended amido-ammonium ILs

(IUPAC: methyl *N*,*N*-dioctyl-β-alaninate)

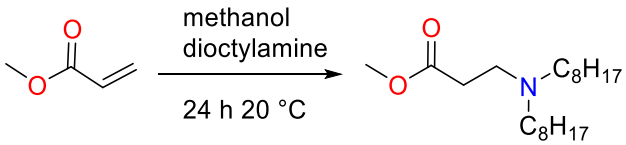

To methanol (40 mL), methyl acrylate (4.20g, 54 mmol) was slowly added. Dioctylamine (12.05g, 50 mmol) was than slowed added and the mixture allowed to stir (24 h, 20 °C).[49, 252] The reaction was then concentrated under vacuum to yield a colourless oil (99%). ^{1}H NMR (400 MHz, $CDCl_3$) δ_H 3.66 (s, 3H, OC**H**$_3$), 2.77 (dd, 2H, NC**H**$_2$), 2.43 (dd, 2H, OC**H**$_2$), 2.37 (t, 4H, NC**H**$_2$), 1.36 – 1.44 (m, 4H, C**H**$_2$), 1.21 – 1.32 (m, 20H, C**H**$_2$), 0.88 (t, 6H, C**H**$_3$); ^{13}C NMR (100 MHz, $CDCl_3$) δ_C 173.40, 54.01, 51.48, 49.41, 32.28, 31.87, 29.58, 29.34, 27.53, 27.19, 22.67, 14.10. ESI-MS (m/z) $C_{20}H_{42}NO_2$ $[M+H]^+$ calculated 328.321 found 328.321.

2ACH$_2$A intermediate (IUPAC: *N*,*N*-dioctyl-*N*-propyl-β-alaninamide)

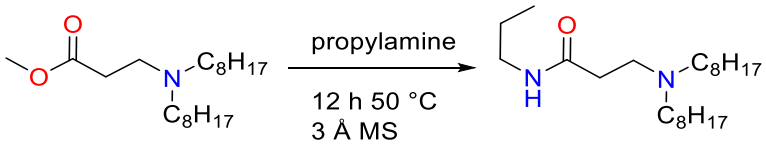

To propylamine (7.38g, 125 mmol) and 3 Å molecular sieves, methyl N,N-dioctyl-β-alaninate was slowly added and the mixture allowed to stir (12 h, 50 °C).[243, 244] The mixture was diluted with DCM (30 mL), filtered, washed with water (30 mL, two times) dried over sodium sulfate and concentrated under vacuum. The crude product was then purified using column chromatography (ethyl acetate) to yield a yellow viscous liquid (75%). ^{1}H NMR (500 MHz, $CDCl_3$) δ_H 8.58 (t, 1H, N**H**), 3.19 (td, 2H, HNC**H**$_2$), 2.64 (dd, 2H, HC**H**$_2$), 2.43 (t, 4H, NC**H**$_2$), 2.35 (dd, 2H, OCC**H**$_2$), 1.49 – 1.53 (m, 2H, C**H**$_2$), 1.42 – 1.48 (m, 4H, C**H**$_2$), 1.24 – 1.36 (m, 20H, C**H**$_2$), 0.94 (t, 3H, C**H**$_3$), 0.90 (t, 6H, C**H**$_3$); ^{13}C NMR (125 MHz, $CDCl_3$) δ_C 172.85, 53.30, 50.52, 40.69, 32.69, 31.82, 29.55, 29.30, 27.66, 26.66, 22.89, 22.65, 14.07, 11.59. ESI-MS (m/z) $C_{22}H_{46}N_2O$ $[M+Cl]^-$ calculated 389.330 found 389.335.

2ACH$_2$A (IUPAC: *N*-methyl-*N*-octyl-*N*-[3-oxo-3-(propylamino)propyl]octan-1-aminium nitrate)

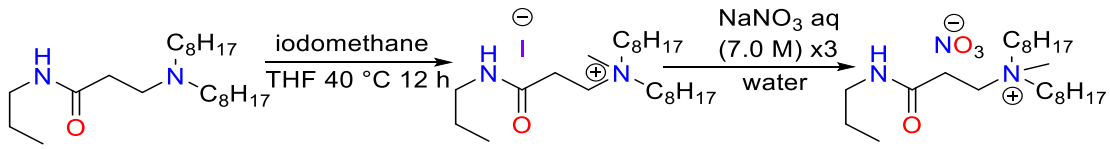

To a sealed, nitrogen flushed round bottom flask of THF (100 mL), N,N-dioctyl-N-propyl-β-alaninamide (2.66g, 7.5 mmol) was added slowly. Iodomethane (2.85g, 20 mmol) was added dropwise and the reaction stirred (12 h, 40 °C, N_2 flow). The general procedure for **IL0** was then followed to yield a yellow liquid (88%).[124, 134] ^{1}H NMR (600 MHz, $CDCl_3$) δ_H 7.97 (t, 1H, N**H**), 3.69 (t, 2H, NC**H**$_2$), 3.32 (t, 4H, NC**H**$_2$), 3.17 (t, 2H, HNC**H**$_2$), 3.15 (s, 3H, NC**H**$_3$), 2.98 (t, 2H, COC**H**$_2$), 1.63 – 1.70 (m, 4H, C**H**$_2$), 1.50 – 1.56 (m, 2H, C**H**$_2$), 1.19 – 1.36 (m, 20H, C**H**$_2$), 0.89 (t, 3H, C**H**$_3$), 0.85 (t, 6H, C**H**$_3$); ^{13}C NMR (150 MHz, $CDCl_3$) δ_C 168.52, 62.10, 58.43, 48.62, 41.62, 31.60, 29.47, 29.07, 28.99, 26.28, 22.55, 22.47, 14.02, 11.57. ESI-MS (m/z) $C_{23}H_{49}N_2O$ $[M]^+$ calculated 369.384 found 369.386.

(IUPAC: *N*,*N*-dipropylprop-2-enamide)

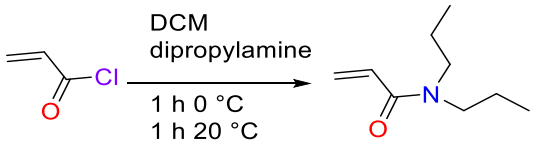

To a sealed, nitrogen flushed round bottom flask of DCM (100 mL), dipropylamine (5.05 g, 50 mmol) was added slowly. Acryloyl chloride (4.53 g, 50 mmol) was added dropwise over ice and with stirring (1 h, 0 °C then 1 h, 20 °C, N_2 flow). The reaction was quenched with DI water (10 mL) and the organic phase washed with saturated sodium hydrogen carbonate solution (30 mL, three times). The organic phase was dried over sodium sulfate and concentrated under vacuum to yield a yellow liquid (40%). ^{1}H NMR (500 MHz, $CDCl_3$) δ_H 6.56 (dd, 1H, C**H**), 6.36 (dd, 1H, C**H**), 5.67 (dd, 1H, C**H**), 3.26 – 3.40 (m, 4H, NC**H**$_2$), 1.56 – 1.66 (m, 4H, C**H**$_2$), 0.93 (t, 6H, C**H**$_3$). ^{13}C NMR (125 MHz, $CDCl_3$) δ_C 166.00, 127.96, 127.43, 49.78, 48.28, 22.84, 21.02, 11.43, 11.18.

3ACH$_2$A intermediate (IUPAC: *N*,*N*-dioctyl-*N*,*N*-dipropyl-β-alaninamide)

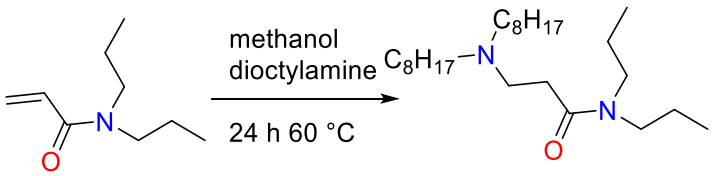

To methanol (125 mL), N,N-dipropylprop-2-enamide (3.20g, 20 mmol) was slowly added. Dioctylamine (5.45g, 22.5 mmol) was than slowed added and the mixture allowed to stir (24 h, 60 °C).[49] The reaction was then concentrated under vacuum to yield a colourless oil and purified using column chromotorgraphy (3:7) hexane:ethyl acetate to yield an orange oil (25%).^{1}H NMR (500 MHz, $CDCl_3$) δ_H 3.28 (t, 2H, NC**H**$_2$), 3.22 (t, 2H, NC**H**$_2$), 2.81 (t, 2H, OCC**H**$_2$), 2.47 (t, 2H, NC**H**$_2$), 2.43 (t, 4H, NC**H**$_2$), 1.65 – 1.58 (m, 2H, C**H**$_2$), 1.58 – 1.52 (m, 2H, C**H**$_2$), 1.49 – 1.42 (m, 4H, C**H**$_2$), 1.32 – 1.25 (m, 20H, C**H**$_2$), 0.94 (t, 4H, C**H**$_3$), 0.90 (t, 9H, C**H**$_3$); ^{13}C NMR (125 MHz, $CDCl_3$) δ_C 171.82, 54.38, 50.35, 49.76, 47.52, 31.87, 31.28, 29.59, 29.33, 27.65, 27.17, 22.67, 22.37, 21.00, 14.10, 11.43, 11.26. ESI-MS (m/z) $C_{25}H_{53}N_2O$ $[M+H]^+$ calculated 397.415 found 397.415.

3ACH$_2$A (IUPAC: 3-(dioctylamino)-*N*-methyl-*N*,*N*-dipropylpropanamidium nitrate)

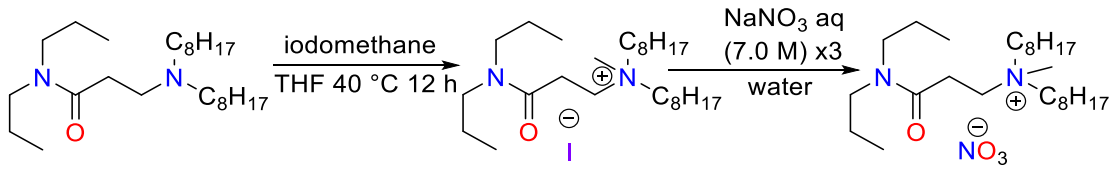

To a sealed, nitrogen flushed round bottom flask of THF (100 mL), N,N-dioctyl-N,N-dipropyl-β-alaninamide (2.98g, 7.5 mmol) was added slowly. Iodomethane (2.85g, 20 mmol) was added dropwise and the reaction stirred (12 h, 40 °C, N_2 flow). The general procedure for **IL0** was then followed to yield an orange oil (70%).[124, 134] ^{1}H NMR (500 MHz, $CDCl_3$) δ_H 3.67 (t, 2H, NC**H**$_2$), 3.39 – 3.47 (m, 6H, NC**H**$_2$), 3.26 – 3.32 (m, 2H, NC**H**$_2$), 3.22 (s, 3H, NC**H**$_3$), 3.12 (t, 2H, OCC**H**$_2$), 1.66 – 1.76 (m, 4H, C**H**$_2$), 1.52 – 1.61 (m, 2H, C**H**$_2$), 1.24 – 1.44 (m, 20H, C**H**$_2$), 1.00 (t, 3H, C**H**$_3$), 0.91 (m, 9H, C**H**$_3$); ^{13}C NMR (125 MHz, $CDCl_3$) δ_C 167.77, 62.44, 58.73, 49.33, 48.74, 47.81, 31.62, 29.13, 28.97, 26.69, 26.26, 22.57, 22.55, 22.08, 20.81, 14.04, 11.41, 11.16. ESI-MS (m/z) $C_{26}H_{55}N_2O$ $[M]^+$ calculated 411.431 found 411.431.

(IUPAC: 3-chloro-*N*-propylpropanamide)

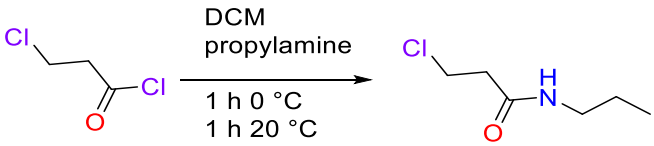

To a sealed, nitrogen flushed round bottom flask of DCM (125 mL), propylamine (2.96 g, 50 mmol) was added slowly. 3-chloropropionyl chloride (7.56 g, 60 mmol) was added dropwise over ice and with stirring (1 h, 0 °C then 1 h, 20 °C, N_2 flow). The reaction was quenched with DI water (15 mL) and the organic phase washed with saturated sodium hydrogen carbonate solution (30 mL, three times). The organic phase was dried over sodium sulfate and concentrated under vacuum to yield a colourless oil (77%). ^{1}H NMR (500 MHz, $CDCl_3$) δ_H 5.67 (s, 1H, N**H**), 3.83 (t, 2H, OCN**z**$_2$), 3.28 (td, 2H, HNC**H**$_2$), 2.64 (t, 2H, ClC**H**$_2$), 1.57 (tq, 2H, C**H**$_2$), 0.96 (t, 3H, C**H**$_3$); ^{13}C NMR (125 MHz, $CDCl_3$) δ 169.41, 41.43, 40.27, 39.75, 22.81, 11.32.

(IUPAC: 3-chloro-*N*,*N*-dipropylpropanamide)

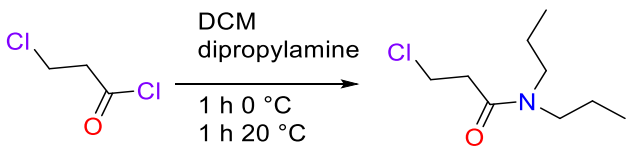

To a sealed, nitrogen flushed round bottom flask of DCM (125 mL), dipropylamine (5.05 g, 50 mmol) was added slowly. 3-chloropropionyl chloride (7.56 g, 60 mmol) was added dropwise over ice and with stirring (1 h, 0 °C then 1 h, 20 °C, N_2 flow). The reaction was quenched with DI water (15 mL) and the organic phase washed with saturated sodium hydrogen carbonate solution (30 mL, three times). The organic phase was dried over sodium sulfate and concentrated under vacuum to yield a colourless oil (68%). ^{1}H NMR (400 MHz, $CDCl_3$) δ_H 3.87 (td, 1H, OCC**H**$_2$), 3.78 (td, 1H, OCC**H**$_2$), 3.29 (dt, 4H, NC**H**$_2$), 2.85 (dt, 3H, ClC**H**$_2$), 1.52 – 1.71 (m, 4H, C**H**$_2$), 0.88 – 0.99 (m, 6H, C**H**$_3$). ^{13}C NMR (100 MHz, $CDCl_3$) δ_C 169.18, 49.55, 47.71, 40.33, 36.14, 22.26, 20.94, 11.37, 11.23.

7.6 Computational methods

7.6.1 Overview

Computational chemistry simulations can be broadly defined as classical or quantum mechanical (QM), depending on what approximations are involved. Classical mechanics (also known as molecular mechanics (MM)) (section 7.6.2) makes use of experimentally determined or quantum mechanically derived parameters to describe molecules as spherical atoms of fixed charge, connected by force constant dependent springs, whereas QM calculations describe matter through the multi-electron Schrodinger equation (section 7.6.3).

Both QM and MM simulations have their own advantages and disadvantages. MM simulations are much less computationally demanding, and as such are more suited towards studying large systems (>> 1000's atoms). Its strength lies in providing a general overview of the formation of large structures and assemblies, but due the absence of electrons in this model any property reliant on this information (e.g. bond energies or formation energies) cannot be determined. This simulation approach has successfully though been applied to study the formation of supramolecular reverse-micelle $PtCl_6$-TBP aggregations, gold-containing nanoclusters extracted using simple amide ligands, the complexation of ReO_4^- anions by the UO_2^{2+} cation and the extraction of Eu cations with a malonamide.[21, 43, 187, 253] In contrast, QM calculations are more suited towards studying smaller systems (1 - 100's atoms) and where knowledge of properties reliant on electrons such as bond energies and formation energies is required. QM calculations have been successfully used to understand selective

$RhCl_5(H_2O)^{2-}$ extraction from HCl solutions, the chelation of protons with an amino-amide during $PtCl_6^{2-}$ extraction and the binding of Am^{3+} to a diglcyolamide structural motif.[49, 235, 245]

Throughout this thesis both MM and QM simulations are used to gain an understanding of what assemblies reside in the organic phase following REE transport from the aqueous phase.[43, 49, 254] For the REE extraction work performed using ILs in this work (chapters 2 and 3), as the structure of the extractant species was too complex to be determined solely from the experimental data obtained, MM simulations were undertaken to create probable self-assembly aggregates. The geometries obtained were then pursed further with QM calculations to validate the models proposed, in particular to improve upon the ligand and counter ion binding motifs, and to determine complex formation energies. In this way the modelling work undertaken attempted to rationalise the differences in REE selectivity observed in the ligands employed in this work.

The following sections provide a brief overview of both modelling techniques employed in this work.

7.6.2 Classical molecular dynamics

Background

Classical MM simulations consider the entirety of the atom (electrons and nuclei) as a hard-sphere, of fixed mass, radius, valency and charge. Molecules are built from atoms using a ball and stick approach, with bonds being considered as springs according to a harmonic potential (Hooke's Law).

Molecular mechanics relies on the observation that the structural properties of functional groups (e.g. C=O, C-O) are transferable across and between molecules. For instance, all C=O bonds are approximately 1.2 Å in length and vibrate around 1750 cm^{-1}, regardless of the molecular environment.[254] From this an equilibrium geometry and a bond force constant can be derived. By extension, the same process applies to bond angles, torsional angles and non-bonding (electrostatics and van der Waal interactions) (Figure 7.6.2.1). Collecting information relating to these terms together creates a force field, and these terms are then used to describe the potential energy of the system, as denoted by equation 7.1.

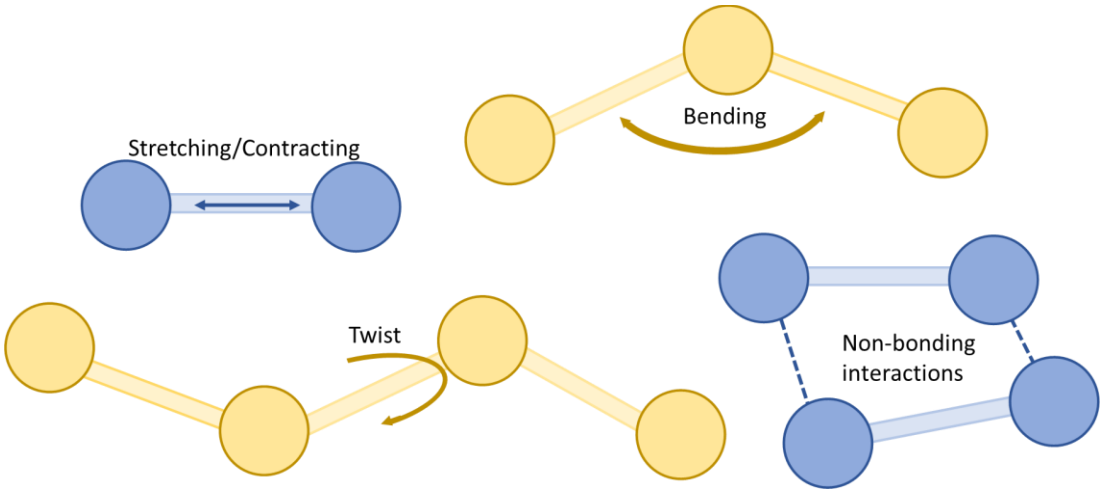

Figure 7.6.2.1 – An illustration of bond stretching, bending and twisting and of non-bonding interactions. Bonding and stretching can be account for by Hooke's Law, twisting through a series of cosine functions and non-bonding interactions through modelling Lennard-Jones potentials.[254]

Eq. 7.6.1 – $E_{total\ potential} = \Sigma(\text{bond stretching}) + \Sigma(\text{bond bending}) + \Sigma(\text{torsional angle}) + \Sigma(\text{non-bonding terms})$

This equation describes the total potential energy of the system as a linear combination of the total energy of bonds stretching and bending, torsional angles and the non-bonding terms, and in this way accounts for the energetic penalty associated with bending, twisting or stretching a molecule away from its lowest point energy or equilibrium state.[254] In this work the OPLS-AA force field (Optimised Potentials for Liquid Simulations – All Atoms) has been used, as it had previously been successfully benchmarked for related simulations such as the modelling of $PtCl_6$-TBP aggregations.[43, 255] With the equilibrium geometry reference values and force constants (denoted in equation 7.1) provided by the force field, the only remaining terms to account for are the atomic charges. These can also be provided by the force field, however in the case of unusual molecular species (such as protonated ligands) the user has to supplement the force field with this missing data.

In this work this was done by performing QM simulations (section 7.6.3). For all classical MD simulations within this work all atomic charges (excluding REEs and Cl^-) were obtained by performing QM simulations (section 7.6.3) with the Gaussian 09 programme at the B3LYP level of theory and the 6-31+G* basis set to generate mulliken atomic charges. Where identical atoms had small variations in Gaussian 09 generated atomic charges these atomic

charges were averaged (e.g. the charge on each O within NO_3^- was averaged). The atomic charges of C atoms situated on lipophilic C_8 chains of **IL0**, **1AA**, **2AA** and **3AA** cations were also averaged. La, Nd, Dy were manually assigned a charge of 3.00 and Cl manually assigned a charge of -1.00. The atomic charges for all molecules and ions used within classical MD simulations in this thesis are given below (Table 7.6.2.1)

Table 7.6.2.1 – The atomic charges for all molecules and ions used within classical MD simulations in this thesis.

Molecule or ion	**Atomic charges** (relevant atom is highlighted in bold)
La^{3+}, Nd^{3+} and Dy^{3+}	*3.000*
Cl^-	*–1.000*
H_2O	***O*** *= –0.834,* ***H*** *= 0.417*
H_3O^+	***H*** *= 0.548,* ***O*** *= –0.644*
NO_3^-	***N*** *= 0.661 ,* ***O*** *= –0.554*
$CHCl_3$	***C*** *= –0.657,* ***H*** *= 0.327,* ***Cl*** *= 0.110*
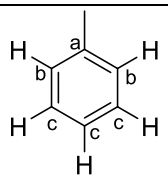	$H_3\mathbf{C}$ *= –0.040,* $C\mathbf{H}_3$ *= 0.028,* ***H*** *= 0.062,* $\mathbf{C}_a$ *= –0.050,* $\mathbf{C}_b$ *= –0.059,* $\mathbf{C}_c$ *= –0.062*
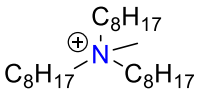 **IL0**	***N*** *= –0.388,* ***H*** *= 0.000,* ***C*** *= 0.056*
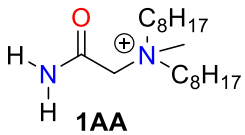 **1AA**	$H_3C\mathbf{N}$ *= –0.392,* $H_2\mathbf{N}$ *= –0.737,* $N\mathbf{H}_2$ *= 0.372,* $O\mathbf{C}$ *= 0.613,* $C\mathbf{O}$ *= –0.469,* $OC\mathbf{C}$ *= 0.181,* ***C*** *= 0.062,* ***H*** *= 0.000*
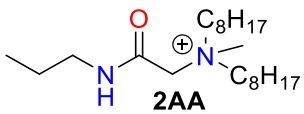 **2AA**	$H_3C\mathbf{N}$ *= –0.385,* $H\mathbf{N}$ *= –0.593,* $N\mathbf{H}$ *= 0.341,* $O\mathbf{C}$ *= 0.624,* $C\mathbf{O}$ *= –0.502,* $OC\mathbf{C}$ *= 0.164,* $HN\mathbf{C}$ *= 0.229,* ***C*** *= 0.059,* ***H*** *= 0.000*
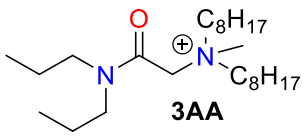 **3AA**	$H_3C\mathbf{N}$ *= –0.411,* $OC\mathbf{N}$ *= –0.393,* $O\mathbf{C}$ *= 0.613,* $C\mathbf{O}$ *= –0.518,* $OC\mathbf{C}$ *= 0.165,* $OCN\mathbf{C}$ *= 0.179,* ***C*** *= 0.056,* ***H*** *= 0.000*

MD simulation programmes such as LAMMPS, working from the force field conditions inputted by the user, predict where atoms, molecules and ions will be a certain time step into the future and move accordingly. The time step (the time between each frame of a simulation) chosen in all the MD simulations present within this thesis was 0.5 fs as a balance between length of total simulation and simulation reliability. The process is repeated for a desired length of time (number of steps) resulting in a 'molecular movie' where the frames of the movie are comprised of the changing positions of the components studied.[249] At each time step the forces (F) on the atoms are calculated. From the forces the acceleration (a) and velocity (v) of the atoms present can be calculated and used to predict the position (r) and velocities of the atoms at the next time step (Figure 7.6.2.2). This is then continued for a desired length of time.[256]

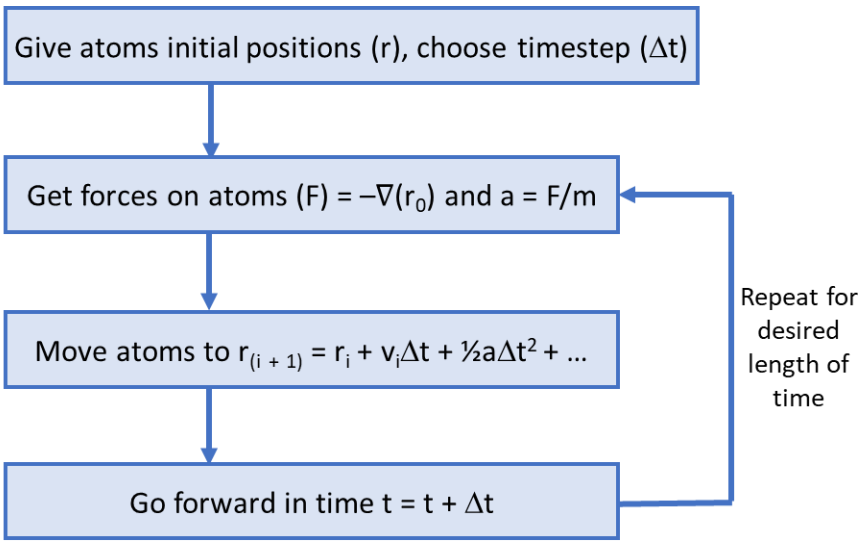

Figure 7.6.2.2 – MD simulation steps. F = force, a = acceleration, m = mass, t = time, v = velocity and i = iteration

Simulation set-up

All classical molecular dynamics simulations were carried out using the LAMMPS (Large-scale Atomic/Molecular Massively Parallel simulator) programme on the University of Edinburgh high-performance ECDF Linux Compute Cluster (Eddie Mark 3).[255] Each MD LAMMPS simulation started from an initial model that was constructed using Packmol and was comprised of the desired number of the respective components (e.g. IL, nitrate anions, water molecules, toluene molecules and La) randomly distributed in a cubic simulation cell of length 60 Å.[257] The QM optimised structures of the components packed in the cubic simulation cell

were obtained from geometry optimisation calculations with Gaussian 09 (section 7.6.3).[258] The Packmol generated xyz coordinate file was converted into a LAMMPS data file using the Visual molecular dynamics (VMD) Topo tools. Remaining parameters (atom masses, pair coefficients, bond, angle and dihedral parameters) were manually added to the data file.[259] Atomic charges were given as discussed above (Table 7.6.2.1).

LAMMPS simulations were then accrued for a minimum of 10.2 ns. This included 0.50 ns equilibration time under canonical (constant Number of atoms, Volume, and Temperature, NVT) ensemble conditions followed by a production run of 9.7 ns under isothermal-isobaric conditions (constant number of atoms, pressure, and temperature, NPT). NVT and NPT conditions were themostated at room temperature and pressure using the Nosé–Hoover thermostat-barostat system.[260, 261] An example input script is available in the electronic SI.

Data analysis and processing

Processing and analysis of the MD simulation outputs included the use of a number of scripts that were based on pre-existing scripts initially developed by Dr K. MacRuary, Dr. R. M. Nicholson and Dr I. Carson.[43, 249]

A Fortran 95 script titled **'Scale coordinate script'** was used to position an atom or ion of choice at the centre or corner of the cubic simulation cell and then adjust the coordinates of every other atom accordingly. This script was primarily used in conjunction with the **'Porosity script'** (below) and for generation of simulation 'snapshots' (sections 2.8 and 3.7).

A Fortran 95 script titled **'Porosity script'** was used to determine the degree of encapsulation of REE or hydronium cations by the lipophilic ammonium cations (Chapters 2 and 3). A probe point was fired 10,000 times from random positions on the surface of a sphere of radius 20 Å, with the REE cation (surrounded by associated ligands) positioned at the centre point (Figure 7.6.2.3). The number of probes that hit the centre point was totalled and compared as a proportion of the number that hit the surrounding ammonium cations, water molecules or nitrate anions, to provide a % REE exposure. Each atom in the model was represented as a solid sphere of the appropriate Van der Waals radii.

Visual molecular dynamics (VMD) was used to provide additional analysis tools, including g(r) analyses on the simulation outputs, and to access the Persistence of Vision Ray Tracer (POV-Ray) programme to render high resolution 'snapshot' images of the simulation outputs.

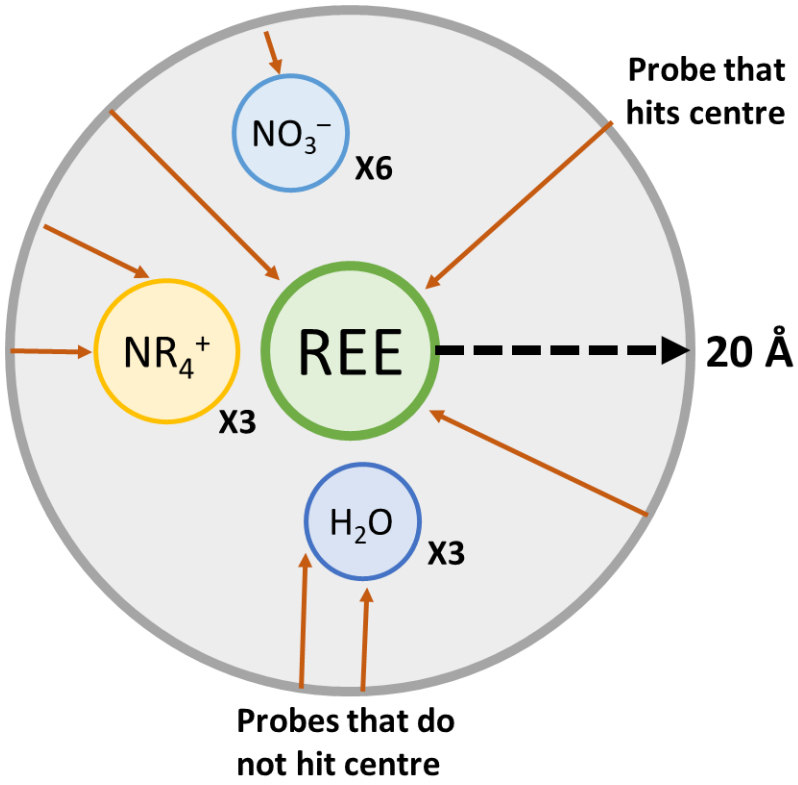

Figure 7.6.2.3 – The targeting of a centre point with a probe fired 10,000 times from 20 Å away to provide a % core exposure.

7.6.3 Quantum mechanical calculations

Background

QM calculations are based upon the Schrödinger equation to model the behaviour and interactions of electrons and nuclei.[195] It is shown in its simplest form below.

Eq. 7.6.3.1 – $\hat{H}\,\Psi = E\Psi$

The Schrödinger equation is an eigenfunction, where the Hamiltonian operator ($\hat{H}$) acts on the wavefunction (Ψ) to yield the permitted energy levels (E) of the molecule in consideration. The Schrödinger equation can only be solved exactly for a one-electron system. This arises due to the complex correlation between electrons, where the electrostatic field of each individual electron affects the position of every other electron present. [195] This creates a 'many body problem', for which an analytical, and exact, solution cannot be obtained.

It is for this reason that a series of approximations are required to allow for multi-electron and multi-atom calculations.[195] Hybrid DFT functionals, such as B3LYP and M06 that are present within this thesis, incorporate several theories and approximations including the Born-Oppenheimer approximation, Hartree-Fock theory (HF), local density approximation (LDA) and Generalised gradient approximation (GGA).[195] In brief:

- The Born-Oppenheimer approximation allows for the nuclei kinetic energy to be defined as zero and the nuclei-nuclei repulsion to be calculated classically.[195] This approximation is possible as heavy nuclei can be considered stationary as the far lighter electrons move several orders of magnitude faster. This step aids the geometry optimisation process, as it separates the complex process into two steps: nuclear positions will be frozen whilst the electronic structure (wavefunction optimisation) is computed; the nuclear positions can then be moved in small increments to lower the potential energy, re-frozen and a new wavefunction calculated. This process is repeated until the geometry optimisation criteria (on forces and atomic displacements) are fulfilled.
- Hartree theory simplifies the electron-electron correlation problem (how the motion of one electron effects the motion of another electron) by considering the movement of each electron individually in a uniform background field generated by all other electrons present.[195] This typically accounts for 95-99% of the total energy of the system. Attempts to recover the missing correlation energy are referred to as post-Hartree-Fock calculations.
- Fock theory provides an exact account of electron exchange (the pairing of electrons of opposite spin in one molecular orbital) in accordance with the Pauli Exclusion Principle, in effect insuring that no two electrons can have the same four quantum numbers.

Hybrid DFT is a semi-empirical blend of Hartree-Fock and density functional theory (DFT). The latter relies on calculation of the electron density, a variable that is experimentally observable, to calculate the energy of a system.[195] The relation between electron density and energy should result in an exact transformation, but in reality the equations required to perform this process (known as a functional – a function of a function) are unknown. Therefore, as with HF theory, approximations are used. Within DFT two of the most common

classes of functional are the local density approximation (LDA) and the generalised gradient approximation (GGA), the key points being:

- LDA is based on the assumption that electron density varies only very slowly over space, and therefore is most appropriate for metallic systems.[195]
- GGA includes a term to account for a more rapidly varying electron density profile, and as such is more appropriate for describing molecules.[195]

As DFT approximates both electron correlation and electron exchange, while HF theory ignores electron correlation (whilst providing an exact treatment of electron exchange), hybrid DFT model chemistry, by mixing HF and DFT together, provides a computationally efficient route to modelling the Hamiltonian operator that takes account of both electron correlation and exchange terms. The functional B3LYP, used in this work to generate atomic charges for MD LAMMPS simulations, is an example of a functional of this type. M06 is also a hybrid functional, and has been used in this work for the geometry optimisation of REE-IL assemblies formed following classical MD LAMMPS simulation and for the calculation of formation energies (ΔU_f).[262] M06 includes a correction to account for dispersion interactions and this is important when considering multi-component systems as the total energy associated with dispersion interactions in multi-component systems can become significant. The M06 hybrid functional is also more suited than B3LYP for modelling non-covalent or non-classical interactions such as those that may be present in molecular assemblies.[263]

Basis sets

The wavefunction (Eq. 7.6.3.1) is a mathematical description of the orbitals in a molecule, and can be constructed computationally using Gaussian basis sets.[195] These are linear combinations of Gaussian functions, to describe the size and shape of atomic orbitals, along with additional functions, such as a polarisation functions that allow orbitals to change shape, and diffuse functions that allows orbitals to occupy a greater space; the latter are critical to model anions, excited-state molecules and highly electronegative elements.[26]

The Gaussian basis set 6-31+G* has been used in this thesis, unless otherwise stated, for the elements C, H, O and N. In this basis set description, the '+' denotes a diffuse function, the '*' denotes a polarisation function (both applied to heavy (i.e. non hydrogen) atoms only), while the '-' denotes that the basis set is split-valence; this treats the core and valence

electrons separately, with the (computationally expensive) electron correlation calculation performed for the valence electrons only. The numbers denote that six Gaussian functions model the core electrons, while two sets of Gaussian functions (derived from three and one functions, respectively) model the valence electrons.

While increasing the level of basis set by increasing the number of Gaussian functions used would improve the accuracy of the calculation there will always be a trade-off against the computational demand. Provided the same basis set is used throughout when comparisons are made between analogous models, the calculation error will be constant throughout.

Pseudopotentials

Elements present in the 3rd row of the period table or higher (e.g. La, Nd and Dy) have a large number of core electrons. The core electrons of these heavier elements have a limited influence on the chemical properties and reactivity of these heavier elements but due to their sheer number require large computational resources to compute.[195] They are also subject to relativistic effects, which distort the orbits of the inner core orbitals, which in turn affects the valence distributions. To solve both problems simultaneously, a pseudopotential (or effective core potential) is used to represent the core electrons of heavy elements. By removing the core electrons from the simulation, and replacing with a pseudopotential (which mimics the core shielding and relativistic effects of the core electrons) the computational demand of the simulation is greatly reduced. For La, Nd and Dy in this thesis, the basis set/pseudopotentials used were MWB46, MWB49 and MWB55 respectively.

Geometry optimisation calculations

Geometry optimisation calculations allow the minimum energy structure of a molecular assembly, a molecule or ion to be determined. Once the minimum energy of structures is determined additional information such as formation energies can be calculated.

Geometry optimisation calculations require an initial input (a starting geometry). A starting geometry can be from a number of sources, such as coordinates derived from a crystal structure, constructed using a model builder or obtained from a classical simulation. The starting geometry should be close to the target minimum energy structure to avoid the minimisation process locating an undesirable stationary point on the potential energy surface (such as a local minimum or a transition state).[195] Once a stationary point has been

located, the gradient of the potential energy surface falls to zero and the pre-set convergence criteria are met, signalling that a minimum energy structure has been reached. A vibrational frequency calculation, which calculates the force constants, can be used to determine if the minimum energy structure obtained is a true minimum (all vibrational frequencies are real numbers) or a maximum (n vibrational frequencies are imaginary numbers, where n denotes the order of the transition state found). Differentiation between local and global minima are obtained through comparisons of energies obtained, with the latter representing the lowest energy point on the potential energy surface.

Simplified, a geometry optimisation calculation (Figure 7.6.3.1), begins with the fixing of the atoms and application of the Born-Oppenheimer approximation.[195] The wavefunction for the starting atoms configuration is then estimated and if it results in a lower energy structure than the previous structure, the forces on the atoms are calculated, and the force constants are estimated (these are computationally demanding calculations, and so an estimate only is usually obtained). The force constants provide knowledge of the curvature of the underlying potential energy surface, which upon lifting the Born-Oppenheimer approximation, guides the movement of the atoms to new, lower energy positions. A new wavefunction, for this updated geometry is then obtained. This cycle continues until the new energy matches that obtained on the previous cycle, and the convergence criteria (on forces and atomic displacements) are met.

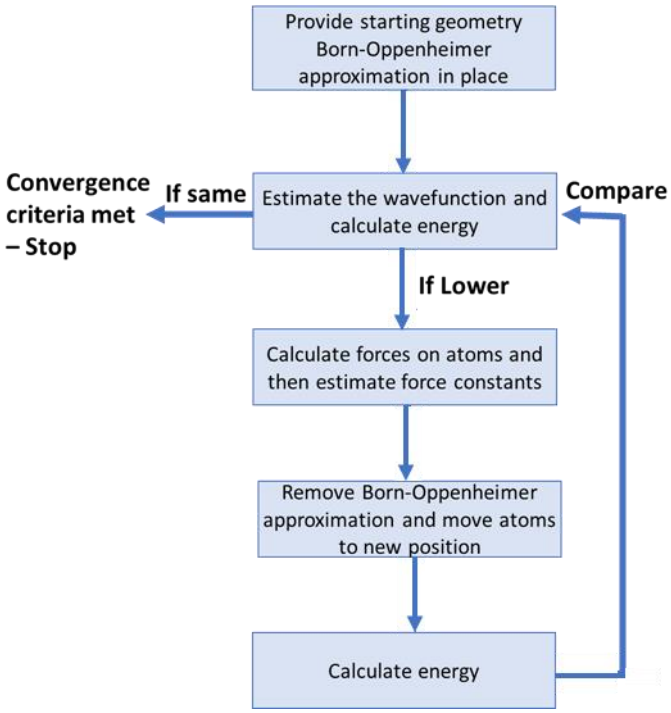

Figure 7.6.3.1 – The simplified flowsheet of a QM geometry optimisation.

In the work within this thesis structures were considered optimised when the preprogramed 'default' convergence criteria of the Gaussian 09 software package were met and a true minimum had been reached (confirmation by a vibrational frequency calculation), except for comparatively large input structures exceeding 100 atoms.[258] In these instances, structures were considered optimised when the 'loose' convergence criteria were met. Initial input structures for single molecules or ions were built using a model builder. For larger (REE-IL) assemblies containing multiple molecules and ions the initial input structures were obtained from classical MD simulations.

QM geometry optimisations were used in this thesis for two applications:

- To provide optimised starting structures for molecules and ions (Table 7.6.2.1) for classical MD LAMMPS simulations to understand what species form in the organic phase following REE extraction by ILs (Chapters 2 and 3).
- To calculate formation energies (ΔU_f) for REE-IL assemblies to try rationalise the differences in REE extraction observed experimentally between **IL0** and **2AA** (Chapters 2 and 3). The quoted formation energies within the thesis were obtained using the calculated values of internal energies (the equilibrium geometry energy – U) for each

component (e.g. nitrate anion, water molecule, REE-IL assembly) according to equation 7.6.3.1:

Eq. 7.6.3.1 – $\Sigma U(\text{products}) - \Sigma U(\text{reactants})$

Where an REE-IL assembly is the product while ammonium cations, a REE cation, water molecules and nitrate anions are the reactants.

These values were used to comparable the relative favourability of REE-IL assembly formation with a more negative value indicative of a more favourable assembly formation.

This can also be achieved by converting internal energy (*U*) values to Gibbs free energy (*G*) that allow for greater quantification of thermodynamic favourability. Converting from *U* values to *G* values requires vibrational frequency calculations for each optimised geometry though and these calculations are especially prohibitively computationally demanding for the large REE-IL assemblies of 250 or 274 atoms studied in this work. Therefore, all formation energies referred to and discussed in this thesis are as according to equation 7.6.3.1.

8 References

1. F. Xie, T. A. Zhang, D. Dreisinger and F. Doyle, *Minerals Engineering*, 2014, **56**, 10-28.
2. K. Binnemans, P. T. Jones, B. Blanpain, T. Van Gerven, Y. X. Yang, A. Walton and M. Buchert, *Journal of Cleaner Production*, 2013, **51**, 1-22.
3. C. E. Housecroft and A. G. Sharpe, *Inorganic Chemistry*, Pearson, 2012.
4. I. D. Hughes, M. Dane, A. Ernst, W. Hergert, M. Luders, J. Poulter, J. B. Staunton, A. Svane, Z. Szotek and W. M. Temmerman, *Nature*, 2007, **446**, 650-653.
5. T. Cheisson and E. J. Schelter, *Science*, 2019, **363**, 489-493.
6. S. Sugimoto, *Journal of Physics D-Applied Physics*, 2011, **44**, 11.
7. Y. X. Yang, A. Walton, R. Sheridan, K. Guth, R. Gauss, O. Gutfleisch, M. Buchert, B. M. Steenari, T. Van Gerven, P. T. Jones and K. Binnemans, *Journal of Sustainable Metallurgy*, 2017, **3**, 122-149.
8. M. Gergoric, A. Barrier and T. Retegan, *Journal of Sustainable Metallurgy*, 2019, **5**, 85-96.
9. D. Haskel, J. C. Lang, Z. Islam, A. Cady, G. Srajer, M. van Veenendaal and P. C. Canfield, *Physical Review Letters*, 2005, **95**, 4.
10. R. B. Lauffer, *Chemical Reviews*, 1987, **87**, 901-927.
11. J. C. G. Bunzli, *Coordination Chemistry Reviews*, 2015, **293**, 19-47.
12. T. Justel, H. Nikol and C. Ronda, *Angewandte Chemie-International Edition*, 1998, **37**, 3085-3103.
13. G. B. Haxel, J. B. Hedrick, G. J. Orris, P. H. Stauffer and J. W. Hendley Ii, *Rare earth elements: critical resources for high technology*, Report 087-02, 2002.
14. M. A. de Boer and K. Lammertsma, *Chemsuschem*, 2013, **6**, 2045-2055.
15. N. J. Beukes, J. Gutzmer and J. Mukhopadhyay, *Transactions of the Institutions of Mining and Metallurgy Section B-Applied Earth Science*, 2003, **112**, B18-B25.
16. K. Binnemans, P. T. Jones, B. Blanpain, T. Van Gerven, Y. Yang, A. Walton and M. Buchert, *Journal of Cleaner Production*, 2013, **51**, 1-22.
17. USGS, *Rare-Earths*, U. S. G. Survey, United States Geological Survey, United States, 2019.
18. M. H. Ting and J. Seaman, *Asian Studies Review*, 2013, **37**, 234-252.
19. A. M. Wilson, P. J. Bailey, P. A. Tasker, J. R. Turkington, R. A. Grant and J. B. Love, *Chemical Society Reviews*, 2014, **43**, 123-134.
20. J. R. Turkington, P. J. Bailey, J. B. Love, A. M. Wilson and P. A. Tasker, *Chemical Communications*, 2013, **49**, 1891-1899.
21. E. D. Doidge, I. Carson, P. A. Tasker, R. J. Ellis, C. A. Morrison and J. B. Love, *Angewandte Chemie-International Edition*, 2016, **55**, 12436-12439.
22. Y. Xiong, H. Kawakita, J. Inoue, M. Abe, K. Ohto, K. Inoue and H. Harada, *Solvent Extraction Research and Development-Japan*, 2010, **17**, 151-162.
23. R. J. Warr, A. N. Westra, K. J. Bell, J. Chartres, R. Ellis, C. Tong, T. G. Simmance, A. Gadzhieva, A. J. Blake, P. A. Tasker and M. Schroder, *Chemistry-a European Journal*, 2009, **15**, 4836-4850.

24. I. Carson, K. J. MacRuary, E. D. Doidge, R. J. Ellis, R. A. Grant, R. J. Gordon, J. B. Love, C. A. Morrison, G. S. Nichol, P. A. Tasker and A. M. Wilson, *Inorganic Chemistry*, 2015, **54**, 8685-8692.
25. M. A. R. Onal and Y. A. Topkaya, *Hydrometallurgy*, 2014, **142**, 98-107.
26. A. Majdi, M. Amini and A. A. Chermahini, *Journal of Hazardous Materials*, 2009, **165**, 1098-1108.
27. F. Sadri, A. M. Nazari and A. Ghahreman, *Journal of Rare Earths*, 2017, **35**, 739-752.
28. N. Swain and S. Mishra, *Journal of Cleaner Production*, 2019, **220**, 884-898.
29. M. A. R. Onal, C. R. Borra, M. Guo, B. Blanpain and T. Van Gerven, *Journal of Sustainable Metallurgy*, 2015, **1**, 199-215.
30. T. Vander Hoogerstraete, B. Blanpain, T. Van Gerven and K. Binnemans, *RSC Advances*, 2014, **4**, 64099-64111.
31. C. Tunsu, C. Ekberg and T. Retegan, *Hydrometallurgy*, 2014, **144**, 91-98.
32. S. G. Zhang, M. Yang, H. Liu, D. A. Pan and J. J. Tian, *Rare Metals*, 2013, **32**, 609-615.
33. D. Shin, J. Jeong, S. Lee, B. D. Pandey and J. C. Lee, *Minerals Engineering*, 2013, **48**, 20-24.
34. M. Motaghed, S. M. Mousavi, S. O. Rastegar and S. A. Shojaosadati, *Bioresource Technology*, 2014, **171**, 401-409.
35. C. Demergasso, F. Galleguillos, P. Soto, M. Seron and V. Iturriaga, *Hydrometallurgy*, 2010, **104**, 382-390.
36. H. R. Watling, *Hydrometallurgy*, 2006, **84**, 81-108.
37. J. C. Gentina and F. Acevedo, *Electronic Journal of Biotechnology*, 2013, **16**, 14.
38. E. R. Mejia, J. D. Ospina, M. A. Marquez and A. L. Morales, in *Biohydrometallurgy: A Meeting Point between Microbial Ecology, Metal Recovery Processes and Environmental Remediation*, eds. E. R. Donati, M. R. Viera, E. L. Tavani, M. A. Giaveno, T. L. Lavalle and P. A. Chiacchiarini, Trans Tech Publications Ltd, Durnten-Zurich, 2009, vol. 71-73, pp. 385.
39. M. K. Jha, A. Kumari, R. Panda, J. R. Kumar, K. Yoo and J. Y. Lee, *Hydrometallurgy*, 2016, **165**, 2-26.
40. D. S. Flett, *Journal of Chemical Technology and Biotechnology*, 1999, **74**, 99-105.
41. Y. Jing, J. Chen, L. Chen, W. R. Su, Y. Liu and D. Q. Li, *Journal of Physical Chemistry A*, 2017, **121**, 2531-2543.
42. E. D. Doidge, I. Carson, J. B. Love, C. A. Morrison and P. A. Tasker, *Solvent Extraction and Ion Exchange*, 2016, **34**, 579-593.
43. K. J. MacRuary, R. J. Gordon, R. A. Grant, S. Woollam, R. J. Ellis, P. A. Tasker, J. B. Love and C. A. Morrison, *Solvent Extraction and Ion Exchange*, 2017, **35**, 531-548.
44. G. A. Picayo and M. P. Jensen, in *Handbook on the Physics and Chemistry of Rare Earths*, eds. J.-C. G. Bünzli and V. K. Pecharsky, Elsevier, 2018, vol. 54, pp. 145-225.
45. J. Reedijk, *Platinum Metals Review*, 2008, **52**, 2-11.
46. S. K. Kim, V. M. Lynch, N. J. Young, B. P. Hay, C. H. Lee, J. S. Kim, B. A. Moyer and J. L. Sessler, *Journal of the American Chemical Society*, 2012, **134**, 20837-20843.

47. N. Busschaert, C. Caltagirone, W. Van Rossom and P. A. Gale, *Chemical Reviews*, 2015, **115**, 8038-8155.
48. P. A. Gale, E. N. W. Howe and X. Wu, *Chem*, 2016, **1**, 351-422.
49. R. J. Warr, K. J. Bell, A. Gadzhieva, R. Cabot, R. J. Ellis, J. Chartres, D. K. Henderson, E. Lykourina, A. M. Wilson, J. B. Love, P. A. Tasker and M. Schroder, *Inorganic Chemistry*, 2016, **55**, 6247-6260.
50. A. G. Baldwin, A. S. Ivanov, N. J. Williams, R. J. Ellis, B. A. Moyer, V. S. Bryantsev and J. C. Shafer, *Acs Central Science*, 2018, **4**, 739-747.
51. Z. C. Liu, M. Frasconi, J. Y. Lei, Z. J. Brown, Z. X. Zhu, D. Cao, J. Iehl, G. L. Liu, A. C. Fahrenbach, Y. Y. Botros, O. K. Farha, J. T. Hupp, C. A. Mirkin and J. F. Stoddart, *Nature Communications*, 2013, **4**, 9.
52. R. J. Ellis, Y. Meridiano, J. Muller, L. Berthon, P. Guilbaud, N. Zorz, M. R. Antonio, T. Demars and T. Zemb, *Chemistry-a European Journal*, 2014, **20**, 12796-12807.
53. R. J. Ellis, Y. Meridiano, R. Chiarizia, L. Berthon, J. Muller, L. Couston and M. R. Antonio, *Chemistry-a European Journal*, 2013, **19**, 2663-2675.
54. P. G. Plieger, P. A. Tasker and S. G. Galbraith, *Dalton Transactions*, 2004, 313-318.
55. S. G. Galbraith, Q. Wang, L. Li, A. J. Blake, C. Wilson, S. R. Collinson, L. F. Lindoy, P. G. Plieger, M. Schroder and P. A. Tasker, *Chemistry-a European Journal*, 2007, **13**, 6091-6107.
56. E. Dziwinski and J. Szymanowski, *Solvent Extraction and Ion Exchange*, 1998, **16**, 1515-1525.
57. W. Li, X. L. Wang, H. Zhang, S. L. Meng and D. Q. Li, *Journal of Chemical Technology and Biotechnology*, 2007, **82**, 376-381.
58. D. F. Peppard, G. W. Mason, W. J. Driscoll and R. J. Sironen, *Journal of Inorganic & Nuclear Chemistry*, 1958, **7**, 276-285.
59. C. Marie, B. Hiscox and K. L. Nash, *Dalton Transactions*, 2012, **41**, 1054-1064.
60. S. N. Bhattacharyya and B. Ganguly, *Journal of Colloid and Interface Science*, 1987, **118**, 15-19.
61. T. G. Lenz and M. Smutz, *Journal of Inorganic & Nuclear Chemistry*, 1966, **28**, 1119
62. A. Rout, J. Kotlarska, W. Dehaen and K. Binnemans, *Physical Chemistry Chemical Physics*, 2013, **15**, 16533-16541.
63. B. Gannaz, M. R. Antonio, R. Chiarizia, C. Hill and G. Cote, *Dalton Transactions*, 2006, 4553-4562.
64. E. Leclerc, D. Guillaumont, P. Guilbaud and L. Berthon, *Radiochimica Acta*, 2008, **96**, 85-92.
65. T. Harada, R. G. Bautista and M. Smutz, *Journal of Chemical and Engineering Data*, 1972, **17**, 203.
66. C. Scharf and A. Ditze, *Metallurgical Research & Technology*, 2017, **114**, 9.
67. S. Ganji, S. Z. Shafaie and N. Goudarzi, *Journal of Mining and Environment*, 2016, **7**, 143-148.
68. J. S. Preston and A. C. duPreez, *Journal of Chemical Technology and Biotechnology*, 1996, **65**, 93-101.

69. K. A. Rabie, *Hydrometallurgy*, 2007, **85**, 81-86.
70. F. Principe and G. P. Demopoulos, *Hydrometallurgy*, 2003, **68**, 115-124.
71. Y. Liu, J. Chen and D. Li, *Separation Science and Technology*, 2012, **47**, 223-232.
72. S. Acharya and A. Nayak, *Hydrometallurgy*, 1988, **19**, 309-320.
73. W. Su, J. Chen and Y. Jing, *Industrial & Engineering Chemistry Research*, 2016, **55**, 8424-8431.
74. Y. Koma, T. Koyama and Y. Tanaka, *Journal of Nuclear Science and Technology*, 1999, **36**, 934-939.
75. F. Hofmeister, *Archiv für experimentelle Pathologie und Pharmakologie*, 1888, **24**, 247-260.
76. K. D. Collins and M. W. Washabaugh, *Quarterly Reviews of Biophysics*, 1985, **18**, 323-422.
77. B. A. Moyer, P. V. Bonnesen, R. Custelcean, L. H. Delmau and B. P. Hay, *Kemija u industriji/Journal of Chemists and Chemical Engineers*, 2005, **54**, 65-87.
78. D. F. Parsons, M. Bostrom, P. Lo Nostro and B. W. Ninham, *Physical Chemistry Chemical Physics*, 2011, **13**, 12352-12367.
79. A. W. Omta, M. F. Kropman, S. Woutersen and H. J. Bakker, *Science*, 2003, **301**, 347-349.
80. Y. J. Zhang and P. S. Cremer, in *Annual Review of Physical Chemistry, Vol 61*, eds. S. R. Leone, P. S. Cremer, J. T. Groves, M. A. Johnson and G. Richmond, Annual Reviews, Palo Alto, 2010, vol. 61, pp. 63-83.
81. C. J. Fowler, T. J. Haverlock, B. A. Moyer, J. A. Shriver, D. E. Gross, M. Marquez, J. L. Sessler, M. A. Hossain and K. Bowman-James, *Journal of the American Chemical Society*, 2008, **130**, 14386.
82. D. Dupont, D. Depuydt and K. Binnemans, *The Journal of Physical Chemistry B*, 2015, **119**, 6747-6757.
83. N. R. Das and S. N. Bhattacharyya, *Talanta*, 1976, **23**, 535-540.
84. E. Benguerel, G. P. Demopoulos and G. B. Harris, *Hydrometallurgy*, 1996, **40**, 135-152.
85. Y. Marcus, *Journal of the Chemical Society-Faraday Transactions*, 1991, **87**, 2995-2999.
86. J. Ciupka, X. Cao-Dolg, J. Wiebke and M. Dolg, *Physical Chemistry Chemical Physics*, 2010, **12**, 13215-13223.
87. F. David, V. Vokhmin and G. Ionova, *Journal of Molecular Liquids*, 2001, **90**, 45-62.
88. F. Martelli, S. Abadie, J. P. Simonin, R. Vuilleumier and R. Spezia, *Pure and Applied Chemistry*, 2013, **85**, 237-246.
89. Y. Marcus, *Biophysical Chemistry*, 1994, **51**, 111-127.
90. K. Binnemans, *Chemical Reviews*, 2005, **105**, 4148-4204.
91. R. D. Rogers and K. R. Seddon, *Science*, 2003, **302**, 792-793.
92. N. V. Plechkova and K. R. Seddon, *Chemical Society Reviews*, 2008, **37**, 123-150.
93. P. G. Smith, *A S L E Transactions*, 1961, **4**, 263-274.

94. M. Armand, F. Endres, D. R. MacFarlane, H. Ohno and B. Scrosati, *Nature Materials*, 2009, **8**, 621-629.
95. M. Halpern, What Is Aliquat® 336 and Adogen® 464 HF? Let's Clear up the Confusion, http://phasetransfer.com/WhatisAliquat336andAdogen464.pdf
96. G. L. Lee, R. W. Cattrall, H. Daud and J. F. Smith, *Analytica Chimica Acta*, 1981, **123**, 213-220.
97. H. F. Aly, S. Elreefy and M. Elgarhy, *Microchemical Journal*, 1972, **17**, 431-&.
98. R. Pribil and V. Vesely, *Talanta*, 1970, **17**, 801-&.
99. A. S. R. Chesman, D. R. Turner, G. B. Deacon and S. R. Batten, *Acta Crystallographica Section E*, 2006, **62**, 1942-1943.
100. S. P. Ji, M. Tang, L. He and G. H. Tao, *Chemistry-a European Journal*, 2013, **19**, 4452-4461.
101. C. Yan, Y. Zhang, S. Gao, B. Li, C. Huang and G. Xu, *Journal of Alloys and Compounds*, 1995, **225**, 385-389.
102. S.-Y. Zhang, X. Shu, Y. Zeng, H.-R. Wen and Z.-Y. Du, *Inorganica Chimica Acta*, 2018, **482**, 878-883.
103. C. V. K. Sharma and R. D. Rogers, *Chemical Communications*, 1999, 83-84.
104. A. Trzesowska-Kruszynska, R. Kruszynski, M. Zalewicz and T. J. Bartczak, *Journal of Coordination Chemistry*, 2010, **63**, 1013-1028.
105. D. Zhang, X. R. Fan, Y. Lu and Y. Xu, *Chemical Research in Chinese Universities*, 2013, **29**, 10-14.
106. L. Zheng, X. M. Qiu, Z. B. Zhang, D. R. Zhu and Y. Xu, *Inorganic Chemistry Communications*, 2011, **14**, 906-909.
107. M. H. Zhu, J. M. Zhao, Y. B. Li, N. Mehio, Y. R. Qi, H. Z. Liu and S. Dai, *Green Chemistry*, 2015, **17**, 2981-2993.
108. S. Acharya and S. Mishra, *Separation Science and Technology*, 2017, **52**, 1660-1669.
109. T. Vander Hoogerstraete, E. R. Souza, B. Onghena, D. Banerjee and K. Binnemans, *Journal of Solution Chemistry*, 2018, **47**, 1351-1372.
110. L. Ma, Z. Y. Zhao, Y. M. Dong and X. Q. Sun, *Separation and Purification Technology*, 2017, **174**, 474-481.
111. H. L. Yang, W. Wang, H. M. Cui, D. L. Zhang, Y. Liu and J. Chen, *Journal of Chemical Technology and Biotechnology*, 2012, **87**, 198-205.
112. K. Y. Wang, H. Adidharma, M. Radosz, P. Y. Wan, X. Xu, C. K. Russell, H. J. Tian, M. H. Fan and J. Yu, *Green Chemistry*, 2017, **19**, 4469-4493.
113. P. Sun, K. Huang and H. Z. Liu, *Journal of Colloid and Interface Science*, 2019, **539**, 214-222.
114. Y. Xiong, W. Q. Kuang, J. M. Zhao and H. Z. Liu, *Separation and Purification Technology*, 2017, **179**, 349-356.
115. J. E. Quinn, K. H. Soldenhoff and G. W. Stevens, *Hydrometallurgy*, 2017, **169**, 621-628.
116. M. Cerna, E. Volaufova and V. Rod, *Hydrometallurgy*, 1992, **28**, 339-352.
117. K. Larsson and K. Binnemans, *Hydrometallurgy*, 2015, **156**, 206-214.

118. T. Vander Hoogerstraete and K. Binnemans, *Green Chemistry*, 2014, **16**, 1594-1606.
119. S. Acharya and S. Mishra, *Separation Science and Technology*, 2017, **52**, 1660-1669.
120. B. Onghena, E. Papagni, E. R. Souza, D. Banerjee, K. Binnemans and T. Vander Hoogerstraete, *RSC Advances*, 2018, **8**, 32044-32054.
121. P. G. Allen, J. J. Bucher, D. K. Shuh, N. M. Edelstein and I. Craig, *Inorganic Chemistry*, 2000, **39**, 595-601.
122. E. D. Doidge, L. M. M. Kinsman, Y. Ji, I. Carson, A. J. Duffy, I. A. Kordas, E. Shao, P. A. Tasker, B. T. Ngwenya, C. A. Morrison and J. B. Love, *ACS Sustainable Chemistry & Engineering*, 2019, **7**, 15019-15029.
123. M. Cerna, V. Bizek, J. Stastova and V. Rod, *Chemical Engineering Science*, 1993, **48**, 99-103.
124. M. A. Ab Rani, N. Borduas, V. Colquhoun, R. Hanley, H. Johnson, S. Larger, P. D. Lickiss, V. Llopis-Mestre, S. Luu, M. Mogstad, P. Oczipka, J. R. Sherwood, T. Welton and J.-Y. Xing, *Green Chemistry*, 2014, **16**, 1282-1296.
125. K. Larsson and K. Binnemans, *Journal of Sustainable Metallurgy*, 2017, **3**, 73-78.
126. J. E. Quinn, K. H. Soldenhoff, G. W. Stevens and N. A. Lengkeek, *Hydrometallurgy*, 2015, **157**, 298-305.
127. in *Solvents and Solvent Effects in Organic Chemistry*, pp. 389-469.
128. R. J. Ellis, L. D'Amico, R. Chiarizia and M. R. Antonio, *Separation Science and Technology*, 2012, **47**, 2007-2014.
129. S. Banerjee and S. Mazumdar, *International Journal of Analytical Chemistry*, 2012, 40.
130. L. W. McDonald, J. A. Campbell and S. B. Clark, *Analytical Chemistry*, 2014, **86**, 1023-1029.
131. E. E. Racow, J. J. Kreinbihl, A. G. Cosby, Y. Yang, A. Pandey, E. Boros and C. J. Johnson, *Journal of the American Chemical Society*, 2019, **141**, 14650-14660.
132. G. Gattuso, A. Pappalardo, M. F. Parisi, I. Pisagatti, F. Crea, R. Liantonio, P. Metrangolo, W. Navarrini, G. Resnati, T. Pilati and S. Pappalardo, *Tetrahedron*, 2007, **63**, 4951-4958.
133. D. F. Evans and P. H. Missen, *Journal of the Chemical Society-Dalton Transactions*, 1982, 1929-1932.
134. J. P. Hunter, S. Dolezalova, B. T. Ngwenya, C. A. Morrison and J. B. Love, *Metals*, 2018, **8**, 13.
135. R. Banda, F. Forte, B. Onghena and K. Binnemans, *RSC Advances*, 2019, **9**, 4876-4883.
136. S. Ishiguro, Y. Umebayashi and M. Komiya, *Coordination Chemistry Reviews*, 2002, **226**, 103-111.
137. R. K. Mishra, P. Rout, K. Sarangi and K. Nathsarma, *Hydrometallurgy*, 2011, **108**, 93-99.
138. J. C. G. Buenzli, B. Klein, G. O. Pradervand and P. Porcher, *Inorganic Chemistry*, 1983, **22**, 3763-3768.
139. A. Battsengel, A. Batnasan, A. Narankhuu, K. Haga, Y. Watanabe and A. Shibayama, *Hydrometallurgy*, 2018, **179**, 100-109.

140. A. Kumari, R. Panda, J. Y. Lee, T. Thriveni, M. K. Jha and D. D. Pathak, *Separation and Purification Technology*, 2019, **227**, 6.
141. O. V. Cheremisina, V. V. Sergeev, A. T. Fedorov and A. P. Il'ina, *Metallurgist*, 2019, **63**, 300-307.
142. V. V. Belova, M. M. Martynova and A. A. Erastov, *Russian Journal of Inorganic Chemistry*, 2018, **63**, 1651-1655.
143. D. Q. Li, *Journal of Rare Earths*, 2019, **37**, 468-486.
144. I. Rodriguez, C. Alvarez, J. Gomez-Lara, R. A. Toscano, N. Platzer, C. Mulheim and H. Rudler, *Journal of the Chemical Society, Chemical Communications*, 1987, 1502-1503.
145. O. Amri, S. Abid and M. Rzaigui, *Crystal Research and Technology*, 2007, **42**, 930-936.
146. B. E. Cole, I. B. Falcones, T. Cheisson, B. C. Manor, P. J. Carroll and E. J. Schelter, *Chemical Communications*, 2018, **54**, 10276-10279.
147. J. A. Bogart, C. A. Lippincott, P. J. Carroll and E. J. Schelter, *Angewandte Chemie-International Edition*, 2015, **54**, 8222-8225.
148. X. M. Yin, Y. X. Wang, X. J. Bai, Y. M. Wang, L. H. Chen, C. L. Xiao, J. Diwu, S. Y. Du, Z. F. Chai, T. E. Albrecht-Schmitt and S. Wang, *Nature Communications*, 2017, **8**, 8.
149. H. Narita, T. Yaita, K. Tamura and S. Tachimori, *Journal of Radioanalytical and Nuclear Chemistry*, 1999, **239**, 381-384.
150. G. J. Lumetta, B. M. Rapko, P. A. Garza, B. P. Hay, R. D. Gilbertson, T. J. R. Weakley and J. E. Hutchison, *Journal of the American Chemical Society*, 2002, **124**, 5644-5645.
151. M. R. Healy, A. S. Ivanov, Y. Karslyan, V. S. Bryantsev, B. A. Moyer and S. Jansone-Popova, *Chemistry-a European Journal*, 2019, **25**, 6326-6331.
152. L. F. Rao, P. Zanonato, P. Di Bernardo and A. Bismondo, *Journal of the Chemical Society-Dalton Transactions*, 2001, 1939-1944.
153. E. A. Mowafy and D. Mohamed, *Separation and Purification Technology*, 2014, **128**, 18-24.
154. K. R. Swami, A. S. Suneesh, R. Kumaresan, K. A. Venkatesan and M. P. Antony, *ChemistrySelect*, 2017, **2**, 11177-11186.
155. M. R. Antonio, D. R. McAlister and E. P. Horwitz, *Dalton Transactions*, 2015, **44**, 515-521.
156. Y. Sasaki, Y. Sugo, S. Suzuki and S. Tachimori, *Solvent Extraction and Ion Exchange*, 2001, **19**, 91-103.
157. S. Okumura, T. Kawasaki, Y. Sasaki and Y. Ikeda, *Bulletin of the Chemical Society of Japan*, 2014, **87**, 1133-1139.
158. H. Mehdi, K. Binnemans, K. Van Hecke, L. Van Meervelt and P. Nockemann, *Chemical Communications*, 2010, **46**, 234-236.
159. Y. M. Dong, X. Q. Sun, Y. L. Wang and Y. J. Chai, *Hydrometallurgy*, 2015, **157**, 256-260.
160. J. A. Vicente, A. Mlonka, H. Q. N. Gunaratne, M. Swadzba-Kwasny and P. Nockemann, *Chemical Communications*, 2012, **48**, 6115-6117.
161. A. Rout, K. A. Venkatesan and M. P. Antony, *Solvent Extraction and Ion Exchange*, 2018, **36**, 558-573.

162. D. R. Raut, S. Sharma, S. K. Ghosh and P. K. Mohapatra, *Separation Science and Technology*, 2017, **52**, 1430-1440.
163. R. Boyd, L. Jin, P. Nockemann, P. K. J. Robertson, L. Stella, R. Ruhela, K. R. Seddon and H. Q. N. Gunaratne, *Green Chemistry*, 2019, **21**, 2583-2588.
164. M. Sethurajan, E. D. van Hullebusch, D. Fontana, A. Akcil, H. Deveci, B. Batinic, J. P. Leal, T. A. Gasche, M. A. Kucuker, K. Kuchta, I. F. F. Neto, H. Soares and A. Chmielarz, *Critical Reviews in Environmental Science and Technology*, 2019, **49**, 212-275.
165. L. Yurramendi, L. Gijsemans, F. Forte, J. L. Aldana, C. del Rio and K. Binnemans, *Hydrometallurgy*, 2019, **187**, 38-44.
166. M. Gergoric, C. Ekberg, B. M. Steenari and T. Retegan, *Journal of Sustainable Metallurgy*, 2017, **3**, 601-610.
167. S. H. Yin, W. Y. Wu, B. Zhang, F. Y. Zhang, Y. Luo, S. W. Li and X. Bian, *Journal of Rare Earths*, 2010, **28**, 111-115.
168. A. Ferdowsi and H. Yoozbashizadeh, *Metallurgical and Materials Transactions B-Process Metallurgy and Materials Processing Science*, 2017, **48**, 3380-3387.
169. B. S. Van Gosen, P. L. Verplanck, R. R. Seal, K. R. Long and J. Gambogi, *Rare-earth elements*, Report 1802O, Reston, VA, 2017.
170. X. Du and T. E. Graedel, *Environmental Science & Technology*, 2011, **45**, 4096-4101.
171. L. Gijsemans, F. Forte, B. Onghena and K. Binnemans, *RSC Advances*, 2018, **8**, 26349-26355.
172. M. Gergoric, C. Ekberg, M. R. S. Foreman, B. M. Steenari and T. Retegan, *Journal of Sustainable Metallurgy*, 2017, **3**, 638-645.
173. M. A. R. Onal, C. Jonsson, W. Zhou, T. Van Gerven, M. X. Guo, A. Walton and B. Blanpain, *Journal of Alloys and Compounds*, 2017, **728**, 727-738.
174. C. Tunsu, M. Petranikova, M. Gergoric, C. Ekberg and T. Retegan, *Hydrometallurgy*, 2015, **156**, 239-258.
175. S. S. Behera and P. K. Parhi, *Separation and Purification Technology*, 2016, **160**, 59-66.
176. T. Vander Hoogerstraete, S. Wellens, K. Verachtert and K. Binnemans, *Green Chemistry*, 2013, **15**, 919-927.
177. I. Ling, Y. Alias, B. W. Skelton and C. L. Raston, *Dalton Transactions*, 2012, **41**, 4884-4889.
178. L. S. Vojinovic-Jesic, V. I. Cesljevic, G. A. Bogdanovic, V. M. Leovac, K. M. Szecsenyi, V. Divjakovic and M. D. Joksovic, *Inorganic Chemistry Communications*, 2010, **13**, 1085-1088.
179. L. S. Vojinovic, V. M. Leovac, S. B. Novakovic, G. A. Bogdanovic, J. J. Csanadi and V. I. Cesljevic, *Inorganic Chemistry Communications*, 2004, **7**, 1264-1268.
180. G. Bradan, B. Cobeljic, A. Pevec, I. Turel, M. Milenkovic, D. Radanovic, M. Sumar-Ristovic, K. Adaila, M. Milenkovic and K. Andelkovic, *Journal of Coordination Chemistry*, 2016, **69**, 801-811.
181. V. M. Leovac, G. A. Bogdanovic, V. I. Cesljevic, L. S. Jovanovic, S. B. Novakovic and L. S. Vojinovic-Jesic, *Structural Chemistry*, 2007, **18**, 113-119.

182. G. Bradan, A. Pevec, I. Turel, I. N. Shcherbakov, M. Milenkovic, M. Milenkovic, D. Radanovic, B. Cobeljic and K. Andelkovic, *Journal of Coordination Chemistry*, 2016, **69**, 2754-2765.
183. X. F. Li, W. S. Liu, Z. J. Guo and M. Y. Tan, *Inorganic Chemistry*, 2003, **42**, 8735-8738.
184. W. N. Wu, N. Tang and L. Yan, *Journal of Fluorescence*, 2008, **18**, 101-107.
185. E. Campbell, V. E. Holfeltz, G. B. Hall, K. L. Nash, G. J. Lumetta and T. G. Levitskaia, *Solvent Extraction and Ion Exchange*, 2018, **36**, 331-346.
186. Y. S. Chen, M. Duvail, P. Guilbaud and J. F. Dufreche, *Physical Chemistry Chemical Physics*, 2017, **19**, 7094-7100.
187. R. Diss and G. Wipff, *Physical Chemistry Chemical Physics*, 2005, **7**, 264-272.
188. B. Qiao, T. Demars, M. O. de la Cruz and R. J. Ellis, *Journal of Physical Chemistry Letters*, 2014, **5**, 1440-1444.
189. M. Dobler and M. Hirata, *Physical Chemistry Chemical Physics*, 2004, **6**, 1672-1678.
190. G. Ferru, B. Reinhart, M. K. Bera, M. O. de la Cruz, B. Qiao and R. J. Ellis, *Chemistry-a European Journal*, 2016, **22**, 6899-6904.
191. S. Simon, M. Duran and J. J. Dannenberg, *Journal of Chemical Physics*, 1996, **105**, 11024-11031.
192. F. M. Tao, *International Reviews in Physical Chemistry*, 2001, **20**, 617-643.
193. M. A. Spackman and A. S. Mitchell, *Physical Chemistry Chemical Physics*, 2001, **3**, 1518-1523.
194. S. F. Boys and F. Bernardi, *Molecular Physics*, 1970, **19**, 553-566.
195. F. Jensen, *Introduction to Computational Chemistry*, John Wiley & Sons, Inc., 2006.
196. K. Binnemans and P. T. Jones, *Journal of Sustainable Metallurgy*, 2017, **3**, 570-600.
197. A. Isildar, E. D. van Hullebusch, M. Lenz, G. Du Laing, A. Marra, A. Cesaro, S. Panda, A. Akcil, M. A. Kucuker and K. Kuchta, *Journal of Hazardous Materials*, 2019, **362**, 467-481.
198. M. Orefice, H. Audoor, Z. Li and K. Binnemans, *Separation and Purification Technology*, 2019, **219**, 281-289.
199. T. Palden, M. Regadio, B. Onghena and K. Binnemans, *ACS Sustainable Chemistry & Engineering*, 2019, **7**, 4239-4246.
200. P. Davris, E. Balomenos, D. Panias and I. Paspaliaris, *Hydrometallurgy*, 2016, **164**, 125-135.
201. P. Nockemann, B. Thijs, K. Van Hecke, L. Van Meervelt and K. Binnemans, *Crystal Growth & Design*, 2008, **8**, 1353-1363.
202. P. Nockemann, B. Thijs, S. Pittois, J. Thoen, C. Glorieux, K. Van Hecke, L. Van Meervelt, B. Kirchner and K. Binnemans, *Journal of Physical Chemistry B*, 2006, **110**, 20978-20992.
203. D. Dupont and K. Binnemans, *Green Chemistry*, 2015, **17**, 856-868.
204. A. Entezari-Zarandi and F. Larachi, *Journal of Rare Earths*, 2019, **37**, 528-533.
205. J. W. Freiderich, J. J. Stankovich, H. M. Luo, S. Dai and B. A. Moyer, *European Journal of Inorganic Chemistry*, 2015, 4354-4361.

206. S. Riano, M. Petranikova, B. Onghena, T. Vander Hoogerstraete, D. Banerjee, M. Foreman, C. Ekberg and K. Binnemans, *RSC Advances*, 2017, **7**, 32100-32113.
207. X. H. Li, A. Van den Bossche, T. Vander Hoogerstraete and K. Binnemans, *Chemical Communications*, 2018, **54**, 475-478.
208. X. H. Li, Z. Li, M. Orefice and K. Binnemans, *ACS Sustainable Chemistry & Engineering*, 2019, **7**, 2578-2584.
209. E. Y. Kim, M. S. Kim, J. C. Lee, J. Jeong and B. D. Pandey, *Hydrometallurgy*, 2011, **107**, 124-132.
210. Y. Qu and B. Lian, *Bioresource Technology*, 2013, **136**, 16-23.
211. V. L. Brisson, W. Q. Zhuang and L. Alvarez-Cohen, *Biotechnology and Bioengineering*, 2016, **113**, 339-348.
212. D. W. Reed, Y. Fujita, A. L. Daubaras, Y. Jiao and V. S. Thompson, *Hydrometallurgy*, 2016, **166**, 34-40.
213. V. S. Thompson, M. Gupta, H. Y. Jin, E. Vahidi, M. Yim, M. A. Jindra, V. Nguyen, Y. Fujita, J. W. Sutherland, Y. Q. Jiao and D. W. Reed, *ACS Sustainable Chemistry & Engineering*, 2018, **6**, 1602-1609.
214. H. Fathollahzadeh, J. J. Eksteen, A. H. Kaksonen and E. L. J. Watkin, *Applied Microbiology and Biotechnology*, 2019, **103**, 1043-1057.
215. Y. Qu, H. Li, X. Q. Wang, W. J. Tian, B. Shi, M. J. Yao and Y. Zhang, *Minerals*, 2019, **9**, 13.
216. H. S. Grewal and K. L. Kalra, *Biotechnology Advances*, 1995, **13**, 209-234.
217. A. M. Borst, A. A. Finch, H. Friis, N. J. Horsburgh, P. N. Gamaletsos, J. Goettlicher, R. Steininger and K. Geraki, *Mineralogical Magazine*, 2019, 1-16.
218. O. Johnsen, G. Ferraris, R. A. Gault, J. D. Grice, A. R. Kampf and I. V. Pekov, *Canadian Mineralogist*, 2003, **41**, 785-794.
219. V. M. Golyshev, V. I. Simonov and N. V. Belov, *Kristallografiya*, 1972, **17**, 1119-&.
220. NCIMB, *Journal*, 2012.
221. J. J. Plumb, R. Muddle and P. D. Franzmann, *Minerals Engineering*, 2008, **21**, 76-82.
222. L. J. Bird, V. Bonnefoy and D. K. Newman, *Trends in Microbiology*, 2011, **19**, 330-340.
223. M. Ilbert and V. Bonnefoy, *Biochimica Et Biophysica Acta-Bioenergetics*, 2013, **1827**, 161-175.
224. V. Bonnefoy and D. S. Holmes, *Environmental Microbiology*, 2012, **14**, 1597-1611.
225. E. Viollier, P. W. Inglett, K. Hunter, A. N. Roychoudhury and P. Van Cappellen, *Applied Geochemistry*, 2000, **15**, 785-790.
226. A. Balinski, P. Atanasova, O. Wiche, N. Kelly, M. A. Reuter and C. Scharf, *Hydrometallurgy*, 2019, **186**, 176-186.
227. C. C. Davis, H. W. Chen and M. Edwards, *Environmental Science & Technology*, 2002, **36**, 582-587.
228. P. Taylor, *Interactions of silica with iron oxides: Effects on oxide transformations and sorption properties*, Canada, 1995.
229. Y. Q. Ma, S. Stopic and B. Friedrich, *Johnson Matthey Technology Review*, 2019, **63**, 2-13.

230. I. A. Dibrov, D. E. Chirkst and T. E. Litvinova, *Russian Journal of Applied Chemistry*, 2002, **75**, 195-199.
231. P. Davris, S. Stopic, E. Balomenos, D. Panias, I. Paspaliaris and B. Friedrich, *Minerals Engineering*, 2017, **108**, 115-122.
232. M. T. Murillo, A. G. Espartero, J. Sanchez-Quesada, J. de Mendoza and P. Prados, *Solvent Extraction and Ion Exchange*, 2009, **27**, 107-131.
233. D. P. Su, H. Huang, S. Huang, N. Liu and S. D. Ding, *Separation Science and Technology*, 2015, **50**, 1384-1393.
234. S. A. Ansari, A. Leoncini, P. K. Mohapatra, J. Huskens and W. Verboom, *Dalton Transactions*, 2018, **47**, 13631-13640.
235. S. A. Ansari, P. K. Mohapatra, A. Leoncini, S. M. Ali, A. Singhadeb, J. Huskens and W. Verboom, *Dalton Transactions*, 2017, **46**, 16541-16550.
236. A. Leoncini, S. A. Ansari, P. K. Mohapatra, A. Sengupta, J. Huskens and W. Verboom, *Dalton Transactions*, 2017, **46**, 501-508.
237. P. K. Mohapatra, M. Iqbal, D. R. Raut, W. Verboom, J. Huskens and S. V. Godbole, *Dalton Transactions*, 2012, **41**, 360-363.
238. M. Iqbal, P. K. Mohapatra, S. A. Ansari, J. Huskens and W. Verboom, *Tetrahedron*, 2012, **68**, 7840-7847.
239. S. A. Ansari, P. K. Mohapatra, S. M. Ali, A. Sengupta, A. Bhattacharyya and W. Verboom, *Dalton Transactions*, 2016, **45**, 5425-5429.
240. P. V. Dau, Z. C. Zhang, P. D. Dau, J. K. Gibson and L. F. Rao, *Dalton Transactions*, 2016, **45**, 11968-11975.
241. G. X. Tian, S. J. Teat and L. F. Rao, *Inorganic Chemistry*, 2014, **53**, 9477-9485.
242. C. Pardin, S. Gillet and J. W. Keillor, *Bioorganic & Medicinal Chemistry*, 2006, **14**, 8379-8385.
243. A. Ojeda-Porras and D. Gamba-Sanchez, *Journal of Organic Chemistry*, 2016, **81**, 11548-11555.
244. M. A. Ali, S. Siddiki, K. Kon and K. Shimizu, *Chemcatchem*, 2015, **7**, 2705-2710.
245. H. Narita, R. M. Nicolson, R. Motokawa, F. Ito, K. Morisaku, M. Goto, M. Tanaka, W. T. Heller, H. Shiwaku, T. Yaita, R. J. Gordon, J. B. Love, P. A. Tasker, E. R. Schofield, M. R. Antonio and C. A. Morrison, *Inorganic Chemistry*, 2019, **58**, 8720-8734.
246. J. Kocisek, A. Pysanenko, M. Farnik and J. Fedor, *Journal of Physical Chemistry Letters*, 2016, **7**, 3401-3405.
247. J. Klyne, M. Schmies, M. Fujii and O. Dopfer, *Journal of Physical Chemistry B*, 2015, **119**, 1388-1406.
248. M. A. W. Marks and G. Markl, in *Layered Intrusions*, eds. B. Charlier, O. Namur, R. Latypov and C. Tegner, Springer Netherlands, Dordrecht, 2015, pp. 649-691.
249. R. M. Nicholson, Doctorate, University of Edinburgh, 2020.
250. A. G. Marshall, C. L. Hendrickson and G. S. Jackson, *Mass Spectrometry Reviews*, 1998, **17**, 1-35.
251. A. C. Stenson, W. M. Landing, A. G. Marshall and W. T. Cooper, *Analytical Chemistry*, 2002, **74**, 4397-4409.

252. R. J. Ellis, J. Chartres, P. A. Tasker and K. C. Sole, *Solvent Extraction and Ion Exchange*, 2011, **29**, 657-672.
253. A. Chaumont, O. Klimchuk, C. Gaillard, I. Billard, A. Ouadi, C. Hennig and G. Wipff, *Journal of Physical Chemistry B*, 2012, **116**, 3205-3219.
254. in *Ideas of Quantum Chemistry*, ed. L. Piela, Elsevier, Amsterdam, 2007, pp. 275-323.
255. W. L. Jorgensen, D. S. Maxwell and J. TiradoRives, *Journal of the American Chemical Society*, 1996, **118**, 11225-11236.
256. R. Schneider, A. R. Sharma and A. Rai, in *Computational Many-Particle Physics*, eds. H. Fehske, R. Schneider and A. Weiße, Springer Berlin Heidelberg, Berlin, Heidelberg, 2008, pp. 3-40.
257. L. Martinez, R. Andrade, E. G. Birgin and J. M. Martinez, *Journal of Computational Chemistry*, 2009, **30**, 2157-2164.
258. M. Frisch, G. W. Trucks, H. B. Schlegel, G. E. Scuseria, M. A. Robb, J. R. Cheeseman, G. Scalmani, V. Barone, B. Mennucci and G. e. Petersson, 2014.
259. W. Humphrey, A. Dalke and K. Schulten, *Journal of Molecular Graphics*, 1996, **14**, 33-38.
260. S. Nose, *Journal of Chemical Physics*, 1984, **81**, 511-519.
261. W. G. Hoover, *Physical Review A*, 1985, **31**, 1695-1697.
262. Y. Zhao and D. G. Truhlar, *Theoretical Chemistry Accounts*, 2008, **120**, 215-241.
263. M. Walker, A. J. A. Harvey, A. Sen and C. E. H. Dessent, *Journal of Physical Chemistry A*, 2013, **117**, 12590-12600.